STAR FORMATION HISTORIES OF SOUTHERN COMPACT GROUPS

JoEllen McBride

A dissertation submitted to the faculty at the University of North Carolina at Chapel Hill in partial fulfillment of the requirements for the degree of Doctor of Philosophy in the Department of Physics.

Chapel Hill
2016

Approved by:

Gerald Cecil

Chris Clemens

Fabian Heitsch

Christian Iliades

Dan Reichart

ABSTRACT

JoEllen McBride: Star Formation Histories of Southern Compact Groups
(Under the direction of Gerald Cecil)

Compact group galaxies are a common phase in galaxy evolution and provide insight into the process that transforms galaxies from isolated, star forming late-type galaxies to passive galaxies in high density environments. I mapped spectrally the central and middle regions of 40 galaxies in 10 Southern Compact Groups and established group membership by redshift. Of the eight groups with all members observed, I found that one galaxy is not in the group in four cases. I obtained ages and metallicities of the stellar populations using the STARLIGHT code to summarize past star formation and current activity. Galaxies that are part of a group showed both high-metallicity stellar populations, indicating rapid processing of gas through multiple star formation episodes, and low-metallicity star formation. Thus, Southern Compact Group galaxies have a wide range of stellar population properties, indicating that these groups are in different stages of evolution.

ACKNOWLEDGEMENTS

I would like to thank my family and friends for supporting me during this endeavor. Especially my parents, for encouraging me since day one to pursue this degree. I would also like to thank Dr. Chris Clemens and his graduate students Josh Fuchs, Erik Dennihy and Bart Dunlap for their assistance in commissioning the MOS on Goodman and acquiring data for my project. A huge amount of appreciation and gratitude is extended to the engineers and day crew at the SOAR Telescope (Eduardo Serrano, Eduardo Aguirre, Guillermo Dubo, Gerardo Gómez, Ian Ordenes) for their assistance in trouble shooting and installing CINDERS. I would also like to thank the telescope operators (Patricio Ugarte, Daniel Maturana, Juan Espinoza, Sergio Pizarro, Leonardo Paredes) for their assistance during observations. The parts for CINDERS were made by the shop at UNC, so Phil Thompson, Cliff Tysor, Joel Norris and Steve Medlin have much of my gratitude. I would like to thank the graduate students and staff (Justin Moore, Nathan Franks, Josh Haislip) at PROMPT for their assistance. And finally, I thank my adviser, Dr. Gerald Cecil, for his mentorship.

TABLE OF CONTENTS

LIST OF TABLES

LIST OF FIGURES

LIST OF ABBREVIATIONS AND SYMBOLS

2MASS	Two Micron All Sky Survey
a	All regions
AAT	Australia Astronomical Telescope
ADC	Atmospheric Dispersion Corrector
AGN	Active Galactic Nuclei
AMIGA	Analysis of the interstellar Medium of Isolated GAlaxies
APO	Apache Point Observatory
BPT	Baldwin, Phillips & Terlevich
c	Central region
cm	Central + Middle region
CALIFAS	Calar Alto Legacy Integral Field Area Survey
CCD	Charged Coupled Device
CIG	Catalog of Isolated Galaxies
CINDERS	Circularized IFUs Nearly Deployed using Economical Robots on SOAR
DM	Disturbed morphology
e	Edge region
FITS	Flexiable Image Transport System
FLAMES	Fibre Large Array Multi Element Spectrograph
FOV	Field of View
FWHM	Full Width at Half Maximum
GAMA	Galaxy And Mass Assembly
H	High metallicity
HCG	Hickson Compact Group
HR	High Resolution
HR	Hertzsprung-Russell
I	Intermediate age

IDS	Image Dissector Scanner
IFS	Integral Field Spectroscopy
IFU	Integral Field Unit
IMF	Initial Mass Function
L	Low metallicity
LLAGN	Low Luminosity Active Galactic Nuclei
LINERS	Low-Ionization Nuclear Emission-line Regions
LR	Low Resolution
M	Mid metallicity
m	Middle region
me	Middle+Edge region
MANGA	Mapping Nearby Galaxies at APO
MILES	Medium resolution Isaac Newton Telescope Library of Empirical Spectra
MOS	Multi-Object Spectroscopy
NGC	Nearby Galaxies Catalog
O	Old Age
POSS	Palomar Observatory Sky Survey
PPAK	Pmas fiber PAcK
PROMPT	Panchromatic Robotic Optical Monitoring and Polarimetry Telescopes
RSCG	Redshift Selected Compact Group
SAM	SOAR Adaptive optics Module
SAMI	Sydney-AAO Multi-object Integral field
SAURON	Spectrographic Areal Unit for Research on Optical Nebulae
SB	Starburst
SCG	Southern Compact Group
SDSS	Sloan Digital Sky Survey
SED	Spectral Energy Distribution

SF	Star Formation
SFH	Star Formation History
SFR	Star Formation Rate
S/N	Signal-to-Noise
SOAR	SOuthern Astrophysical Research
SP	Stellar Population
SSP	Simple Stellar Populations
UKST	United Kingdom Schmidt Telescope
VENGA	VIRUS-P Exploration of Nearby Galaxies
VLT	Very Large Telescope
Y	Young age
”	Arcsecond
’	Arcminute
Å	Angstrom
$[\frac{\alpha}{Fe}]$	Mass fraction of heavy elements (C...) compared to that of Fe
B_j	$3200-5500$Å filter of POSS plates used in Iovino, 2002.
$C = R90/R50$	Concentration index
dm	Incremental mass element
Δmag_{comp}	B_j magnitude difference between the faintest and brightest group member.
Δmag_{isol}	B_j magnitude difference between the brightest galaxy in the isolation ring (R_{isol}) and the brightest group member
$\Delta\mu_{gr}$	Difference between the mean surface brightness within the isolation ring (μ_{isol}) and the group (μ_{gr})
$Dn(4000)$	4000Å break
$F(\lambda)$	Flux (energy per second) per unit wavelength
$< Fe >$	Average of Fe_{5270} and Fe_{5335} absorption lines
Φ_m	IMF
$H\alpha$	Hydrogen α line at 656nm rest wavelength

$H\beta$	Hydrogen β line at 486nm rest wavelength
$H\gamma$	Hydrogen γ line at 434nm rest wavelength
$H\delta$	Hydrogen δ line at 410nm rest wavelength
$H\delta_A$	Hydrogen δ line equivalent width
j	Emission line intensity
$\frac{L_{FIR}}{L_{opt}}$	Far infrared luminosity over optical luminosity
λ	Wavelength
$< \log t_* >_L$	Light weighted average age
$< \log t_* >_M$	Mass weighted average age
m	Mass of stars born
M_B	Bolometric absolute magnitude
M_c	Neighbor galaxies $\delta z < 150$ km/s
M_n	Neighbor galaxies with $150 < \delta z < 3000$ km/s
$M_\odot$	Solar mass
Mg_2	Magnesium absorption line
$[Mg/Fe]$	Ratio of Type II supernova to Type Ia
$m_{brightest}$	Magnitude of the brightest galaxy in the group measured in the POSS B_j-band
$m_{faintest}$	Magnitude of the faintest galaxy in group measured in the POSS B_j-band
μ_G	Compact group surface brightness
μ_{gr}	Mean surface brightness within a circle of radius R_{gr}
μ_{isol}	Mean surface brightness within circle of radius R_{isol}
μ_j	Mass weighted contribution
μ_{limit}	Limiting surface brightness
μ_*	Surface mass density
$[NII]$	Singly ionized Nitrogen at 648 and 683 nm rest wavelength
N_*	SSP templates
$[OI]$	Neutral Oxygen at 630 nm rest wavelength

$[OIII]$	Doubly ionized Oxygen at 496 and 501 nm rest wavelength
R50	Radius containing 50% of galaxy light
R90	Radius containing 90% of galaxy light
R_{gr}	Group radius
R_{isol}	Distances from the center of the group to the nearest nonmember within 0.35 magnitudes of the faintest group member
SFR/M_*	Specific star formation rate
SP_c	Same SPs for neighbor galaxies with $\delta z < 150$ km/s
SP_n	Same SPs for neighbor galaxies with $150 < \delta z < 300$ km/s
SP_{yng}	Young SPs
σ	Velocity dispersion
σ_e	Emission errors
σ_m	Model errors
σ_o	Observation errors
$[SII]$	Singly ionized Sulfur at 672 and 673 nm rest wavelength
t/T	Age
θ_G	smallest circle on sky containing the centers of all group members
θ_N	Angular diameter of the largest circle on sky that contains no galaxies
x_j	Light weighted contribution
z	Redshift
Z	Metallicity
$< Z >_L$	Light weighted average metallicity
$< Z >_M$	Mass weighted average metallicity
$[Z/H]$	Ratio of metals to Hydrogen

1: Introduction

1.1: Motivation

The most notable observed property of galaxies is the dependence of morphology on environment. In hierarchical models, two mechanisms influence the formation of galaxies: the baryonic processes that occur within each galaxy's dark matter halo and the inevitable interactions and mergers between galaxies within a common dark matter halo. How these two processes produce the morphology-environment dependence seen today is one of the bigger questions in Astronomy.

Interactions and mergers have long been thought to influence star formation (SF) and the output of supermassive black holes at the centers of galaxies. As galaxies interact within their combined dark matter haloes, stellar orbits and gas are perturbed and often stripped from the parent galaxy. Gas can then be pulled into the center of the more massive galaxy to trigger a burst of circumnuclear star formation and often feed the central supermassive black hole to activate the nucleus of the galaxy [1, 2]. There have been numerous studies of the central regions of interacting galaxies with interesting results. Observations reveal two populations of active galaxies, those with enhanced nuclear activity and quiet outer regions and those with their outer regions showing activity enhancement compared to the center, implying a time scale to star formation and active nuclei (AGN) induced by interactions [3, 4].

The results of extensive galaxy surveys such as the Sloan Digital Sky Survey (SDSS) have enabled researchers to obtain large samples of galaxy properties and to establish correlations with both internal and external factors. Most properties of galaxies depend on their stellar mass[5, 6, 7]. High mass galaxies have old stars, high mass-to-light ratios, high central light concentrations (C), high stellar mass surface densities and high likelihood of hosting an AGN, but low star formation rates (SFR) and dust. Low mass galaxies have young stars, high SFR and dust content, but low mass-to-light ratios, low concentrations, low stellar mass surface densities and rarely host an AGN. The aforementioned authors also find a characteristic mass ($\sim 3 \times 10^{10} M_{\odot}$) at which the dependence of these properties on mass changes significantly.

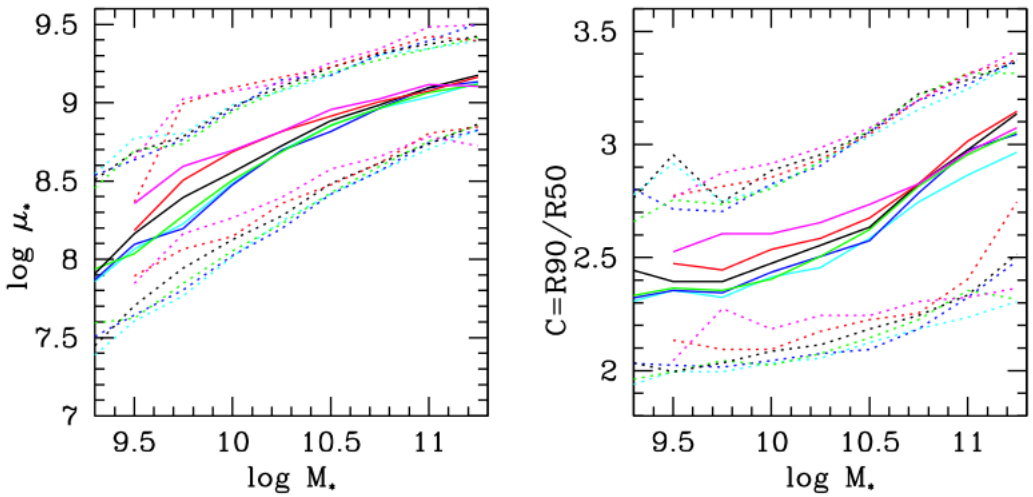

Figure 1.1: The relationship between surface mass density (μ_*) (left) and concentration index ($C = R90/R50$) (right) and stellar mass for galaxies in density bins of 0-1 neighbor (cyan), 2-3 neighbors (green), 4-6 neighbors (blue), 7-11 neighbors (black), 12-16 neighbors (red), > 17 neighbors (magenta). Neighbors are defined within a 2 Mpc projected radius and ± 500 km/s velocity difference of a target galaxy. The solid curves are the median values of surface mass density and concentration index for each mass bin and the dotted lines denote the 10th and 90th percentiles.[8]

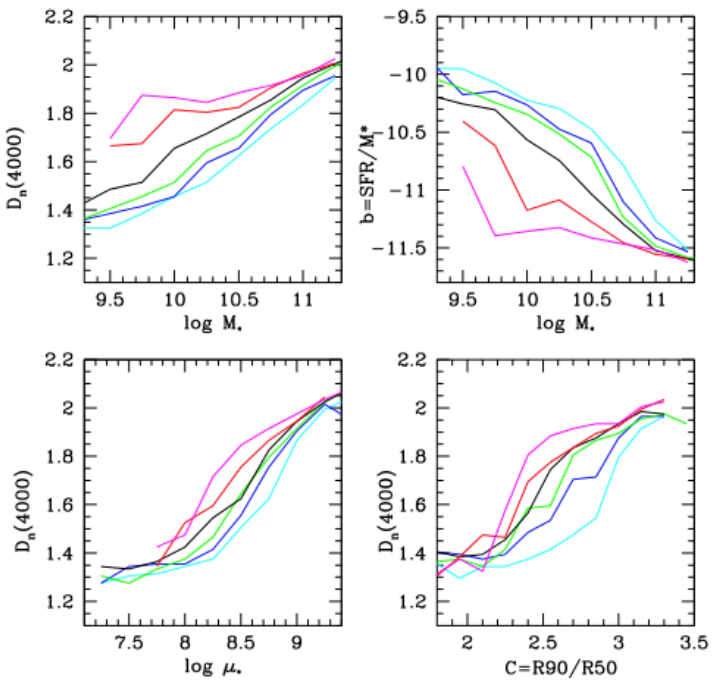

Figure 1.2: The relationship between the median values of $Dn(4000)$ (top left) and SFR/M_* (top right) and stellar mass for galaxies in previously defined density bins. Plots of the median value of $Dn(4000)$ and surface mass density (bottom left) and concentration index (bottom right) are also shown. [8]

The sample size of the SDSS allowed researchers to establish how these *relations* depend on environment[8]. The dependence on stellar mass of structural parameters (concentration and stellar mass surface density) does not vary significantly with environment (Figure 1.1), whereas that on environmental parameters does (Figure 1.2). Both a galaxy's stellar mass and the mass of the dark matter halo it resides in influences the amount of star formation that the galaxy will undergo. AGN do not show much dependence on environment except that the most powerful are found in the most massive galaxies (Figure 1.4).

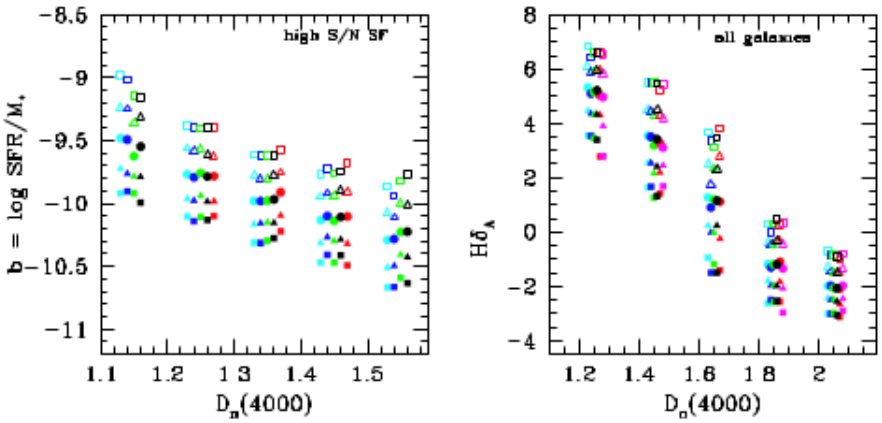

Figure 1.3: Relation between star formation history properties SFR/M_*, $Dn(4000)$ and $H\delta_A$. Solid circles are the median values, open and solid triangles are the 25th and 75th percentile and open and solid squares are the 10th and 90th percentiles respectively. [8]

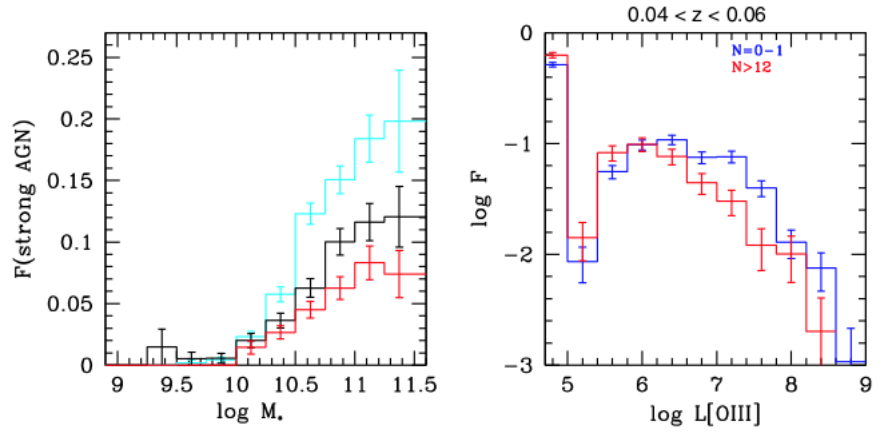

Figure 1.4: Left plot is of galaxies containing strong AGN with respect to stellar mass in three different density bins; 0-1 neighbor (cyan), 7-11 neighbors (black) and > 12 neighbors (red). The right plot shows the distribution of [OIII] luminous AGNs in low and high density environments. [8]

Two mechanisms create elliptical galaxies according to these findings: 1) mergers cause stars to form rapidly, which depletes the cold gas reservoir and suppresses its cooling and 2) the outer layer of cold gas is ram pressure stripped by the massive dark matter halos, causing star formation to decline gradually. How these two scenarios affect subsequent SF in the central and outer regions of galaxies could also explain the two observed populations of active galaxies. Whether the merger scenario or the high mass halo scenario plays a more important role at the transition from low to intermediate density environments is an important question to address. This density transition stage is also where a significant change in the characteristic stellar mass of galaxies occurs. To probe this transition, I chose compact groups of galaxies that lie in the density regimes represented by the blue and green curves in the Kauffman et al. 2003 plots shown in Figures 1.1 and 1.2.

1.2: Compact Groups

The first study of a compact group of galaxies, Stephan's Quintet, was published in 1877[9]. More than 70 years passed before another was found[10]. The focus then shifted to the compilation of atlases of galaxy images showing peculiar shapes and interactions [11, 12, 13]. Compact groups did not re-enter the scene until 1973 when 30 compact groups were found by searching 200 Palomar Observatory Sky Survey (POSS)[14] prints[15]. There are now over 350 Shakhbazian fields [16] and their properties are discussed in section 1.1.3. A survey of 205 compact groups obtained from 69 POSS plates and 23 Yale-Columbia southern proper motion survey plates[17] was published in 1977[18]. Groups were chosen if three or more galaxies had blue magnitudes brighter than 17.5 and a density enhancement with respect to the surrounding field of over 1000. A later study of these groups, searching for diffuse light indicative of tidally stripped material from interactions, turned up few examples, leading to the conclusion that these groups are transient configurations forming within loose groups[19]. In 1982, Hickson published a sample of 100 compact groups found by searching red POSS prints[20]. The selection criteria used in his search aimed to reduce biases in the Rose (1977) groups whose magnitude limits[18] created a distance dependent bias while surface density limits caused geometric and kinematic biases (i.e. transient compact configurations or oblate structures viewed so that only a small cross section is observed). The details of Hickson Compact Groups (HCGs) will be discussed in the next section.

A major bias of the Rose and Hickson groups is that group members with large magnitude differences are more difficult to detect when searching by eye, and faint groups are missed completely. Prandoni et al. 1994 used an algorithm with the same selection criteria as Hickson, 1982[20, 21]. Their search of the

digitized COSMOS/United Kingdom Schmidt Telescope (COSMOS/UKST) Southern Galaxy Catalog found 59 groups[22]. This algorithm was later altered to probe to fainter magnitudes and resulted in the 121 groups found in the Southern Compact Groups (SCGs) by Iovino, 2002 discussed in section 1.1.2[23].

Another issue with compact groups is the high frequency of putative members with discordant redshifts. Both Stephen's Quintet and Seyfert's Sextant have one as do 43 of 100 HCGs. To address this issue, Barton et al. 1996 used a friends of friends algorithm to search a magnitude limited three dimensional angle-redshift volume for compact groups[24]. Their algorithm discovered 89 groups known as the Redshift Selected Compact Groups (RSCGs). These groups overlap with the HCGs in a few cases and have similar physical properties. There are redshift dependent biases in this magnitude limited survey, but those are easily quantified.

Recent large all sky surveys have provided a huge database in which to apply many different group-finding algorithms to compact groups [25, 26, 27]. These algorithms tend to find more early-type galaxies than the Hickson samples but still use his criteria to find groups.

The HCGs are by far the most studied compact group catalog and I summarize what has been learned about them below. I then summarize work done on other compact group surveys. Finally, I focus on the SCGs of Iovino, 2002[23] because this survey covers the southern hemisphere and the groups fit into the field of the Goodman Spectrograph on the SOuthern Astrophysical Research (SOAR) Telescope[28].

1.2.1: Hickson Compact Groups

Hickson, 1982 used a hand lens to search POSS E-band (red wavelengths) prints and found 100 compact groups of galaxies using the following criteria[20]:

1. $N \geq 4$ - number of galaxies within 3 mag of brightest group member in the POSS E-band. (Richness constraint)

2. $\theta_N \geq 3\theta_G$ - the angular diameter of the largest circle that contains no galaxies in the magnitude range set by 1, θ_N, must be at least three times the smallest circle containing the centers of all group members, θ_G (Isolation constraint)

3. $\mu_G < 26\, mag/arcsec^2$ - total group surface brightness within θ_G (Compactness constraint)

Galaxies in each group were classified as spiral (S), elliptical (E) or other. Spiral classification includes irregular and blue compact dwarf galaxies. S0 galaxies were classified as other. The fraction of spiral galaxies in these compact groups is less than in the field and spirals appear to be preferentially in groups near the compactness constraint. He found that there are fewer faint galaxies in groups and even fewer in

groups with a dominant elliptical galaxy. Many groups have a spiral as the dominant galaxy, which makes them unlikely merger remnants. Group compactness does not correlate with the brightness of the dominant galaxy.

By measuring redshifts, Hickson et al. 1992[29] found 92 groups with three accordant members and 69 groups with four. Later studies found 57 then 61 groups with four accordant members that still satisfy the original criteria [30, 31]. Observationally, the physical characteristics of the discordant galaxies are consistent with chance alignments [32] and discordant galaxies do not show a preferential projected location within the originally defined group [33].

Kinematic and structural studies of group members show a wide range of interaction stages in most HCGs [34, 35, 36, 37, 38, 39]. Ribeiro et al. 1998 categorized 17 groups into three dynamical stages with distinct surface density profiles[35].

- loose groups
- core + halo
- compact groups

The core radius of groups decreases from loose to compact groups. There is also evidence that velocity dispersion (σ) plays an important role in group dynamics. Groups show clear trends between morphology and velocity dispersion with late-type galaxies residing mostly in groups with low velocity dispersions and early-types in groups with high velocity dispersions [40, 41]. However, this trend is not apparent in the Ribeiro et al. 1998 data of 17 HCGs[35].

Authors also classify groups based on velocity dispersion, morphology and activity [38, 37, 41, 42, 43].

- low σ, lots of late-type, active SF or AGN
- intermediate σ, lots of interacting/merging galaxies, some activity
- high σ, lots of early-type, not active

These classifications are thought to be evolutionary stages of groups from low σ to high σ. Coziol et al. 1998 I and II[44, 45] studied the brightest galaxies in HCGs and found that most show some activity. AGN tend to reside in the most luminous elliptical galaxies in the cores of groups. Half are actually low luminosity AGNs (LLAGNs). When only group members are included in the study, the number of starburst (SB) galaxies drops significantly and are found in the outer regions or halos of the groups. SB galaxies in HCGs are found in mostly late-type spiral galaxies and have stronger activity than normal spirals ($M_B \leq -19$) [45]. They also have lower metallicities than the other galaxies in the group, implying that they are in a less advanced

stage of evolution than the early-types. This suggested to the authors that early-type HCGs formed first and more quickly because they reside in the center of the group and the late-type galaxies are pulled in from the surrounding environment [44, 45, 43]. This scenario is also supported by reports that within HCGs low σ galaxies are younger [46], ellipticals have older stellar populations [47, 48] and older groups (i.e. more early-type galaxies) have higher σ and are more compact [49].

The AGN fraction in the nucleus of HCGs is higher than the SF fraction and what SF is present is not enhanced compared to field galaxies [50]. This supports the idea that gas is processed rapidly at the beginning of group formation, quickly turning late-type galaxies into quiescent early-types. Mid-infrared and X-ray properties of HCGs show a strong bimodality between gas rich and gas poor compact group systems [51, 39, 52].

Evidence of interactions have been uncovered in infrared and X-ray wavelengths. There is evidence of enhanced warm H_2 emission in HCGs due to shock excitations from group member collisions [53]. Diffuse X-ray emission has been linked to individual members of HCGs, emanating from star formation activity, AGN or tidal tails [54].

The spectra of Mendes de Oliviera et al. 2005 find that ellipticals in HCGs have similar mean metallicity and $\left[\frac{\alpha}{Fe}\right]$ as field galaxies[47], and many authors have noted that star formation activity in HCG spirals is comparable to field spirals [45, 55, 56, 57, 50]. Many papers contradict the findings of Hickson et al. 1989[58] that the $\frac{L_{FIR}}{L_{opt}}$ is more enhanced in HCGs due to interactions than in isolated galaxies [59, 60, 61, 62, 63, 64, 49, 65].

There is ongoing discussion as to the reality of the HCGs. Many simulations have been run to predict the frequency of chance alignments [66, 40, 67, 68, 69] and the lifetime of gravitationally bound groups [70, 71, 72, 73, 74, 75, 76, 77]. Mamon, 1986 estimated that roughly half of the HCGs are chance alignments in loose groups[66]. Hickson, Kindle and Huchra, 1988 simulations produced 35% of quintets with a single discordant redshift[40] and Hickson and Rood, 1988[67] found the probability of chance occurrence in HCGs to be 1% that found by Mamon, 1986. Walke and Mamon, 1989 ran semi-analytic models and confirmed the high frequency of chance alignments in the Nearby Galaxy Catalog but only in groups less compact than HCGs[68]. They also showed that although the chance alignments are a small effect, they can explain the high number of discordant redshifts found in the HCGs. Using the Millenium simulation and the Hickson criteria, Diaz-Gimenez and Mamon, 2010[69] found only half of indentified compact groups contain at least four accordant redshifts compared to Hickson, Kindl and Huchra's $\sim 70\%$.

If compact groups are formed in the early universe, they would quickly virialize according to hierarchical models of dynamical evolution [70]. Other mechanisms, such as the mass of group members, must play a significant role in the merging process. Having a wide range of masses within a group can delay merging

up to 9 Gyrs [71]. It has also been shown that as the mass of the merging galaxies decreases, the merging time is increased [72]. Many authors have suggested that compact groups are an on-going and frequent process where secondary infall of new galaxies plays an important role[73, 75]. Aceves & Velazquez, 2002 ran simulations where groups are virialized but do not share a common primordial dark matter halo and found that $\sim 40\%$ of groups can survive up to 10 Gyrs[77].

To verify group isolation, the environment surrounding the HCGs has been studied. A visual inspection of the regions around all 100 HCGs returned a third of the groups having galaxies in their immediate neighborhoods[78]. Ramella et al. 1994 found that 29/38 groups were actually part of looser, rich systems of galaxies[79] and Rood and Struble, 1994 found HCGs associated with 36 loose groups and seven Abell clusters[80]. In contrast, Palumbo et al. 1995 looked within $1.0h^{-1}$Mpc of 91 HCGs and found only 18% of groups have concentrations within $0.5h^{-1}$Mpc[81] and Palumbo et al. 1993 found no alignments between HCGs and Abell[82]. Evidence has also been presented indicating that HCGs are actually the compact core of an elongated, loose group of galaxies [43, 83].

From the above studies, the following explanations have been proposed for the arrangement of compact groups of galaxies [84].

- Transient, dense configurations
- Isolated, bound, dense configurations
- Chance alignments in loose groups
- Filaments seen end on [74]
- Bound, dense configurations in loose groups

There is still much work to be done to understand the role that interactions play in the evolution of galaxies in HCGs and how HCGs are related to their surrounding environments.

1.2.2: Recent Compact Group Surveys

The advent of large all-sky surveys has greatly advanced the study of compact groups. Two notable catalogs of compact groups have come from the SDSS[25, 27]. The survey by McConnachie et al. 2009 has been used to compare the properties of compact groups to loose groups and the field. Compact group galaxies are redder, smaller, more concentrated and have higher surface brightnesses than galaxies in loose group or the field [85, 86]. Compact groups embedded in larger clusters contain galaxies that are distinct from field galaxies while more isolated compact groups contain galaxies that are similar [87]. These findings

further support HCG studies that gas rich galaxies are very quickly transformed into early-type galaxies in compact group environments. A survey of compact groups with complete spectroscopic redshifts was released recently[27].

A compact group survey in the infrared, using the 2 Micron All Sky Survey (2MASS)[88], showed a group's proximity to larger systems affects the properties of the group's galaxies [26]. Galaxies in embedded compact groups are smaller and brighter than those that are isolated[89].

The majority of the surveys discussed thus far focus on compact groups in the Northern Hemisphere. To utilize the facilities accessible at UNC-Chapel Hill, my study focuses on compact groups that are easily observable by the SOAR Telescope.

1.2.3: Southern Compact Groups

To overcome the incompleteness and bias introduced by the visual selection of groups in HCGs, Iovino, 2002[23] applied an automated algorithm and altered the selection criteria of Hickson, 1982. This algorithm searched through galaxies in the COSMOS plate scans of the UKST SuperCOSMOS Sky Survey [22] and probed one magnitude deeper than the Hickson survey. As discussed, the Hickson selection criteria reject many possible groups due to projection effects but also include many that are actually part of a larger structure. The new selection criteria are similar to the Hickson criteria because HCGs probe an interesting class of galaxies at the brighter magnitudes of the survey and the changes are aimed at making the algorithm less restrictive by modifying the definition of the isolation ring.

1. Richness: $n \geq 4$ in magnitude interval $\Delta mag_{comp} = m_{faintest} - m_{brightest} \leq 3\, mag$ in B_j filter
2. Isolation: $R_{isol} \geq 3R_{gr}$ where R_{isol} is the distances from the center of the group to the nearest nonmember within 0.35 magnitudes of the faintest group member.
3. Compactness: $\mu_{gr} < \mu_{limit} = 27.7\, mag/arcsec^2$

Modifying the isolation criteria results in 60% of rejections being part of a larger substructure and only 25% of those groups satisfying the isolation criteria are within 15' of known clusters. Out of the 121 SCGs found, 4 are also found in the HCGs (HCG 4, 21, 90, 91). The SCG reports for each group n the number of galaxies in the group, $m_{brightest}$ the magnitude of the brightest galaxy in the group, Δmag_{comp} the difference between the faintest and brightest group member, $\Delta mag_{isol} = m_{isol} - m_{brightest}$ the difference between the brightest galaxy in the isolation ring and the brightest group member, μ_{gr} mean surface brightness within a circle of radius R_{gr} and $\Delta\mu_{gr} = \mu_{ext} - \mu_{int}$ the difference between the mean surface brightness within the isolation ring and the group. Searching with both the Hickson and Iovino criteria and dividing the

results into three categories allowed them to compare the contamination rates (background and foreground galaxies being included) of the SCGs with the HCGs. These three categories are defined by Δmag_{comp} and Δmag_{isol}. Category A groups are found in both the HCGs and SCGs and have $\Delta mag_{comp} \leq 2.65$ and $\Delta mag_{isol} \geq 3$. Category B groups are found in the SCGs but not in the HCGs and have $\Delta mag_{comp} < 2.65$ and $\Delta mag_{isol} < 3$. Finally, category C groups are found in the HCGs but not in the SCGs and have $\Delta mag_{comp} > 2.65$ and $\Delta mag_{isol} = 3$. The results show that category C groups have the highest contamination rate (˜50%) compared to categories A and B which have contamination rates of 25%. The density contrast between the density of galaxies within R_{gr} and those outside the isolation ring reveal that the majority of the groups reside in environments that are more than 10 times as dense as outside the isolation ring, with half being in environments that are more than 20 times as dense.

The most extensive study of SCGs is that of Coziol, Iovino and de Carvalho, 2000[90]. They spectroscopically classify the types of emission-line acitivty of 193 galaxies located in 49 of the compact groups. They did not examine stellar populations. Galaxies with and with out emission are identified and galaxies with emission are further divided into AGNs, low-ionization nuclear emission-line regions (LINERS), SF and LLAGN. They reported that $\sim 31\%$ of the SCGs observed could not be classified using the diagnostic diagrams but of those that could be classified, 41% had characteristics of LINERS and Seyfert 2 galaxies. The ambiguity in classifying the SCGs is attributed to an intermediate phase of activity where star formation and AGNs coexist, known as HII nucleus galaxies[91]. When compared to the HCGs, the authors see similar trends in activity with luminosity (LLAGN and AGNs are in the most luminous galaxies, non-emission and SF galaxies are less luminous) and activity with morphology (non-emission, LLAGN and AGNs are in early-type galaxies, SF galaxies in late-type). The SCGs have more SF galaxies and LLAGN than the HCGs and less galaxies without emission lines. More of the LLAGN SCGs are located in early-type spiral galaxies. They also found variation in activity type with number of galaxies in the group. The number of star forming galaxies decreases as the number of group members increases. These results show that the SCGs comprise an interesting phase in galaxy formation and evolution.

A few SCGs, along with HCGs, were included in the HI content survey completed by Stevens et al. 2004[92]. The SCGs were not included in any plots because their optical properties were not confirmed. The plots of HCGs revealed that galaxies with high masses tend to be HI deficient while galaxies with low mass are not. The survey was not sensitive enough to probe the low mass compact groups. However, Pompei, Dahlem and Iovino, 2007 completed a preliminary HI survey of 6 SCGs and found an average group mass of $9.2 \times 10^{12} M_{\odot}$, which is similar to that of the HCGs[93]. The mean HI deficiency of the groups was found to be 0.80 which is higher than for field galaxies; HI deficiency is defined as $Def(HI) = log[M(HI)_{pred}] - log[M(HI)_{ob}]$. The predicted HI mass is determined by summing the HI mass of field

galaxies with the same morphology as group members. Four galaxies with no observed HI are late-types. The authors also note that HI is a good tracer of interaction effects.

If these galaxies are gravitationally bound, they will eventually merge to form an elliptical galaxy. My goal is to study stellar populations and emission-line activity to uncover the process that removes gas as the SCGs form.

1.3: Multi-object Spectroscopy

Long-slit spectroscopy restricts light from extended objects to a rectangular area to focus on specific regions of nebulae and galaxies. To improve the efficiency of observations, it is possible to cut multiple slits in a single mask and arrange them so the spectra do not overlap on the detector. If multiple galaxies are in the field of view (FOV), one exposure can obtain simultaneous observations with careful alignment. Most productive astronomical spectrographs have multi-object capabilities. This project used the multi-object capabilities recently added to the Goodman Spectrograph[28] on the SOAR Telescope as an upgrade.

1.4: Integral Field Spectroscopy

Spatially detailed spectra are usually obtained through multiple long-slits. Recently, single fiber optic cables have been employed for multi-object spectra but provide no spatial information within each target. Monolithic integral field spectroscopy (IFS) systems comprised of either lenslets or fiber optics have also been successfully used but only for nearby galaxies that fill the FOV. Lightly fusing multiple fibers into bundles allows for full spatial sampling of multiple targets in the FOV to map spectrally more than one galaxy at a time.

Here I describe two set-ups of the Goodman Spectrograph. The first involves CINDERS, which mounts four bundles in actuators that can move in three dimensions around a $5' \times 9'$ FOV. A table of previous and current IFS systems is listed below along with the CINDERS set-up for comparison. The second set-up is the multi-slit addition to the Goodman Spectrograph. This has a $3' \times 5'$ FOV, which is still adequate for the SCGs. Many questions concerning galaxy evolution can be addressed using these set-ups as outlined below.

	SAURON[94] (HR/LR)	VENGA[95]	DiskMass[96]	PINGS[97]	SDSS[98]
Fiber properties	lenslets	fiber optics	fiber optics/ lenslets	lenslets	fiber optics
instrument	SAURON	VIRUS-P	SparsePak/ PPAK	PPAK	
# of fibers	1577	246	82/382	382	640
fiber diameter (")	0.27/0.94	4.3	4.7/2.7	2.7	3
telescope aperture (m)	4.2	2.7	3.5	3.5	2.5
wavelength range (nm)	450-700	360-580 460-680	500-900	370-710	380-920
FOV	$9'' \times 11''$/ $33'' \times 41''$	$1.7' \times 1.7'$	$74'' \times 65''$	$74'' \times 65''$	$7^o \times 7^o$
redshift range	< 0.01	low z	low z	$z < 0.005$	median=0.1
spectral sampling (Å/pixel)	1.1	2.2	0.13-0.28/ 0.2	3.2	1.5
spatial sampling (")	0.27/0.94	4.3	4.7/2.7	2.7	3
spectral resolution (Å)	2.8/3.6	5	3.3/3.8	10.7	˜3
velocity dispersion (km/s)	90/105	120	148/220	600	70
grating	514		316/1200	V300	
# galaxies	72 early	32 spiral	146 spiral	17 disk	˜930,000

Table 1.1: Prior IFU Survey Properties

	CINDERS	CALIFAS [99]	SAMI [100]	HECTOR [101]	HERMES [102]	GIRAFFE [103]	MANGA [104]
Fiber properties	fiber optics	lenslets	fiber optics	fiber optics	fiber optics	lenslets	fiber optics
instrument	CINDERS	PPAK	SAMI	HECTOR	HERMES	VLT+ FLAMES	SDSS
# of fibers	244	382	793 + 26 sky plug plate	100*# fibers in bundles	392 positioners	20	
fiber diameter (")	0.7-fiber 6.3-bundles	2.7	13 bundles		2	0.52	
telescope aperture (m)	4.2	3.5	3.9	3.9	3.9	8.2	2.5
wavelength range (nm)	350-700	430-700 370-500	370-950		471-490 565-587 648-674 759-789		
FOV	$4.1' \times 9'$	$74'' \times 65''$	1°	2°-3°	2°	$3'' \times 2''$	
redshift range	$0.01 - 0.2$	$0.005 - 0.03$				< 1.2	
spectral sampling (Å/pixel)	0.87	1.3/0.64	1.03/0.57				
spatial sampling (")	0.7	2.7	1.6		2	0.52	
spectral resolution (Å)	4.5-blue 8.4-red	5.4/2.7	2.8/1.5			0.55/0.45	
velocity dispersion (km/s)	150	300/200	173/67			30/22	
grating	400	V600/ V1200	580V/ 1000R			L04/L05	
# galaxies		942 all	$10^4 - 10^5$	10^5			

Table 1.2: Current and Future IFS systems

The SDSS used a single fiber to obtain spectra of the central regions of millions of galaxies. The spectral signatures of low luminosity AGNs are easily lost in the integrated light within the half light radius of a galaxy and any small star forming regions would blend in too. The Sydney-AAO Multi-object Integral field feed for the dual-beam AAO-OMEGA spectrograph (SAMI) uses 13 bundles of fiber optic cables each with 61 fibers of 1.6" diameter to cover 15" diameter of a galaxy. The wide FOV of the Australia Astronomical

Telescope (AAT) is enabling spectral maps of 3500 galaxies to reveal spatially detailed stellar population and activity across the central 15" of each. The SDSS Mapping Nearby Galaxies at APO (MANGA) survey is also deploying IFUs. The spatial variation of star formation history properties and stellar populations can better constrain the timescales of the suppression of star formation and whether SF occurs throughout the galaxy simultaneously or starts in the outer regions and moves inward.

1.5: Dissertation Outline

Chapter 2 describes the design of the dissertation program by detailing the history of the field and my observing and data analysis strategy. Chapter 3 discusses the instrumentation process that I developed for both CINDERS and the MOS on the Goodman Spectrograph. Chapter 4 presents the results of my observations and analysis. Chapter 5 summarizes my conclusions and future work.

2: Dissertation Design

2.1: Science Questions

My aim was to obtain spatially detailed spectra of the inner 7 arcsecond diameter of up to 44 SCG galaxies in 10 groups using the deployable IFU module, CINDERS[105], with the Goodman Spectrograph on the SOAR telescope to answer the questions of how SF and AGN activity are affected by intermediate density environments.

The clustering of the SCG galaxies on the sky is optimal for the narrow FOV spanned by CINDERS and the minimum spacing of the probes (100 arcseconds). CINDERS spectra could provide a two dimensional distribution of age, metallicity, SF and AGN emission in the central regions of these galaxies. The Lick indices Mg_2 and $< Fe >$ could map the age and metallicity of the stellar populations that fall in our fibers. When combined with the Balmer absorption lines ($H\delta$, $H\gamma$, $H\beta$) which trace star formation in the last Gyr, tighter constraints could be put on the ages of the populations and the SFH of the galaxy. Older ages show that SF has ceased in a galaxy but high metallicities would indicate rapid processing of elements via enhanced SF due to an abrupt compression of cold gas. Any current or recent SF in the last 10^7 yrs could be traced by $H\alpha$ emission in our maps. Strong emission line ratios ([OIII]5007/$H\beta$ vs [NII]6583/$H\alpha$) can classify the type of activity occurring in each fiber. If group membership influences central activity, the central regions SCG galaxies should cluster in areas of a Baldwin, Phillips & Terlevich (BPT) diagram distinct from field galaxies. Central regions showing enhanced SF compared to field galaxies could indicate that the groups are undergoing a merger scenario as described by Kauffmann et al. 2004. Measured SF that is lower than in field galaxies could indicate diminishing of SF in the massive halo scenario. If SF is the same then either the dark matter halos of the galaxies in the compact groups have not merged yet or we are seeing an intermediate stage following a period of enhanced SF.

The observations would also map kinematics of gas in the central regions. This could determine how much external factors perturb gas motions in the central regions. Gas funneled into the center of the galaxy would trigger circum-nuclear SF, which would show up in $H\alpha$ emission maps.

The control sample would use the data from galaxies in the observed SCGs that have discordant redshifts. By comparing activity and stellar populations of these field galaxies with our intermediate density groups, I can begin to unravel the effects dynamics play in the evolution of groups members.

2.2: Extra-galactic Stellar Populations

2.2.1: History of Stellar Population Analysis

Within the Milky Way, astronomers can study the spectra of individual stars to uncover the chemical signatures of past star formation. For galaxies outside the Local Group, it is impossible to see individual stars. Astronomers must use evolutionary population synthesis techniques to unmix stellar populations in a galaxy's spectrum. This method requires theoretical stellar evolution tracks that populate a Hertzsprung-Russell (HR) diagram with a simple stellar population (SSP). An SSP is a population of stars that were all born at the same time with the same initial chemical composition. A series of SSPs can be used to approximate a galaxy's star formation history.

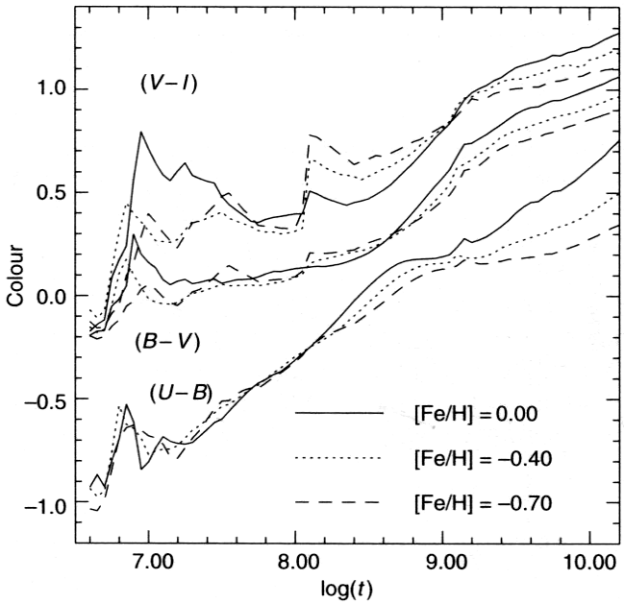

Figure 2.1: Color versus age for three types of metallicity[106]. Higher $V-I$ values correspond to redder colors.

Population synthesis aims to mitigate the age/metallicity degeneracy that affects star colors with ages > 1 Gyr. Older stars have redder colors but these colors can also be generated by increasing the metallicity of a younger star. In Figure 2.1, the broad-band colors of stars are plotted against age for various metallicities. As age increases, the stars get redder. As the metallicity is increased, the colors also become redder. Using evolutionary population synthesis techniques avoids this issue by fitting a galaxy's spectrum instead of relying solely on colors.

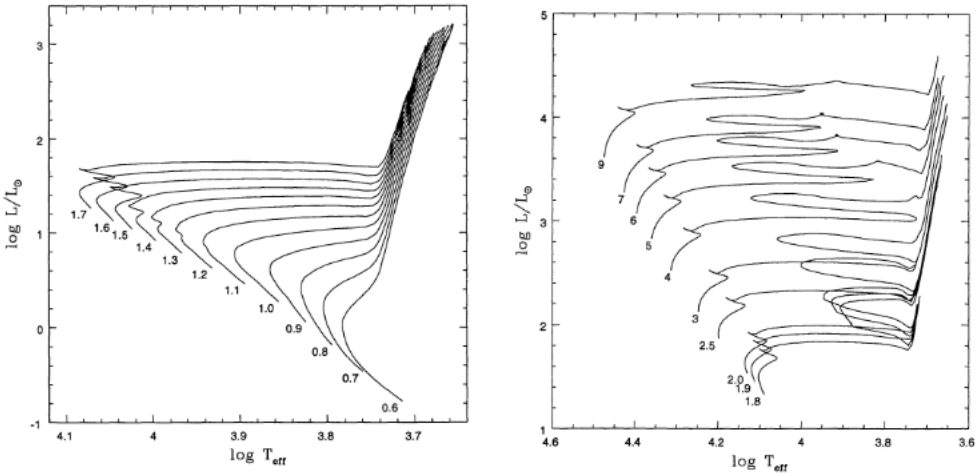

Figure 2.2: Theoretical HR diagrams from [107]. Tracks follow how the luminosity and temperature of a star at a given mass changes throughout its lifetime. The plot on the left is for low mass stars and the plot on the right is for intermediate mass and massive stars. Stars in both plots have composition $Y = 0.230$ and $Z = 0.0001$. The mass of each star is indicated in solar masses next to each curve.

Stellar evolution tracks for our own Galaxy have been widely studied and can be altered to non-solar values of metallicity using known relations between stellar parameters[108, 109, 110, 111, 112, 107, 113, 114, 115]. Figure 2.2 shows the tracks a star of a given mass will follow on the diagram throughout its life. From these theoretical HR diagrams, an isochrone can be traced for stars of different masses at a single age. At each point on an isochrone, stellar mass differs with the star moving through different stellar evolution phases on the HR diagram. An example of isochrones from theoretical HR diagrams is shown in Figure 2.3.

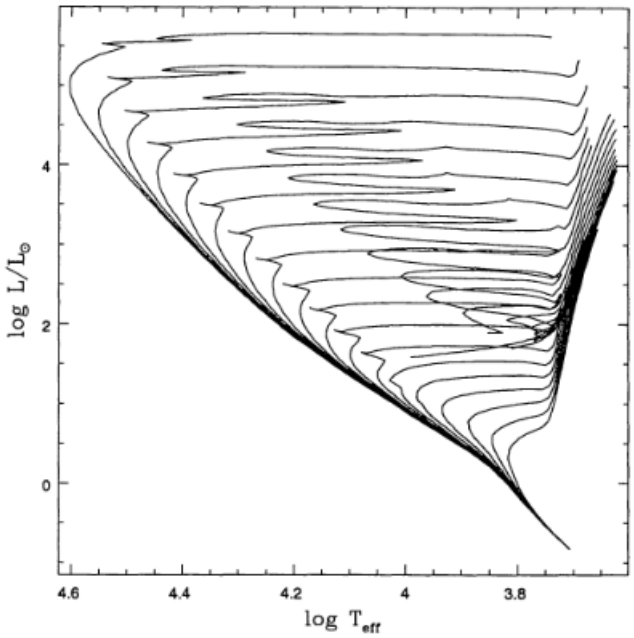

Figure 2.3: Isochrones derived from theoretical HR diagrams by [107]. Ages span from $log(age/yr) = 6.8 - 10.2$ in intervals of 0.2.

The initial mass function (IMF), defines the number of stars born with masses between $m + dm$. There are four commonly used IMFs[116]. The first two are the unimodal and bimodal IMFs. The unimodal is a simple power law where $\alpha = 1.35$ is the Salpeter IMF[117] defined for the solar neighborhood.

$$\Phi(m) = \beta m^{-\alpha} \qquad 0.4 < \frac{m}{M_\odot} < 10 \tag{2.1}$$

The bimodal IMF is based on observations of Scalo, 1986 and theoretical work of Kroupa et al. 1993[118, 119]. It combines different power laws for different mass ranges. The α values for the mass ranges are

$$\Phi(m) = \begin{cases} 0.035m^{-1.3} & 0.08 \leq \frac{m}{M_\odot} < 0.5 \\ 0.019m^{-2.2} & 0.5 \leq \frac{m}{M_\odot} < 1.0 \\ 0.019m^{-2.7} & 1.0 \leq \frac{m}{M_\odot} \end{cases} \tag{2.2}$$

Finally, work has been done to create a universal IMF. These are known as the Kroupa IMFs and the original and revised versions are stated below[120, 121].

Original:

$$\Phi(m) \propto \begin{cases} m^{-0.3} & 0.01 \leq \frac{m}{M_\odot} < 0.08 \\ m^{-1.3} & 0.08 \leq \frac{m}{M_\odot} < 0.5 \\ m^{-2.3} & 0.5 \leq \frac{m}{M_\odot} \end{cases} \tag{2.3}$$

Revised:

$$\Phi(m) \propto \begin{cases} m^{-0.3} & 0.01 \leq \frac{m}{M_\odot} < 0.08 \\ m^{-1.8} & 0.08 \leq \frac{m}{M_\odot} < 0.5 \\ m^{-2.7} & 0.5 \leq \frac{m}{M_\odot} < 1.0 \\ m^{-2.3} & 1.0 \leq \frac{m}{M_\odot} \end{cases} \tag{2.4}$$

The final piece is observed template stellar spectra at various determined effective temperatures, surface gravities, and metallicites, which are used to assign spectra to stars at the different evolutionary stages on the HR diagram. The integrated flux of all of these stars mimics the spectral energy distribution (SED) of this stellar population and is given by

$$F_\lambda(t, Z) = \int_{M_l}^{M_u} f_\lambda(M, t, Z)\Phi(M)dM \tag{2.5}$$

where F_λ is the flux per wavelength of a population of age t and metallicity Z, the limits of the integration are over the range of masses defined by the IMF ($\Phi(M)$) and f_λ is the flux per wavelength of a given spectrum for a star of mass M, age t and metallicity Z. The result is a library of SSPs at various stellar ages and metallicities that can be fit to an observed galaxy spectrum[122, 106]. We list the properties of some of the most common template stellar spectra used currently from [123].

Reference	Resolution FWHM (Å)	Spectral range (Å)	Number of stars	Comments
Spinrad (1962)				Spectrophotometry
Spinrad & Taylor (1971)				Spectrophotometry
Gunn & Stryker (1983)	20–40	3130–10 800	175	
Kitt Peak (Jacoby, Hunter & Christian 1984)	4.5	3510–7427	161	Only solar metallicity
Pickles (1985)	10–17	3600–1000	200	Solar metallicity except G-K giants
Lick/IDS (Worthey et al. 1994)	9–11	4100–6300	425	Not flux calibrated, variable resolution
Kirkpatrick, Henry & McCarthy (1991)	8/18	6300–9000	39	No atmospheric correction
Silva & Cornell (1992)	11	3510–8930	72 groups	Poor metallicity coverage
Serote Roos, Boisson & Joly (1996)	1.25	4800–9000	21	
Pickles (1998)		1150–10 620	131 groups	Flux calibrated
Jones (1999)	1.8	3856–4476 4795–5465	684	Flux calibrated
ELODIE (Prugniel & Soubiran 2001)	0.1	4100–6800	709	Echelle
STELIB (Le Borgne et al. 2003)	3.0	3200–9500	249	Flux calibrated
INDO-US (Valdes et al. 2004)	1.0	3460–9464	1273	Poor flux calibrated
MILES	2.3	3525–7500	985	

Figure 2.4: Table 1 from [123] which lists the properties of the most commonly used stellar templates.

From these SSPs one can measure expected values of strong absorption lines to obtain model predictions. These predictions are then compared to the measured indices in an observed spectrum. The lines used most often for this are the 25 Lick/IDS lines, which use as models 460 stars with a wide range of atmospheric parameters but at low resolution and signal to noise[124, 125, 126, 127, 128]. There are few young, hot stars in this library, so these lines are adequate for early-type galaxies with older populations[122]. The observed spectrum must be broadened to the Lick/IDS resolution, which degrades the original high resolution spectrum considerably.

Evolutionary population synthesis techniques allow observers to retain high resolution spectra by using the SSP libraries to fit an entire observed SED for a given galaxy. There are now extensive libraries of SSPs [122, 116] and many codes that search parameter space for the best combination of SSPs that match the observed spectrum[129, 130, 131, 132, 133]. These techniques have been applied to galaxies in a wide range of environments. I focus on the results of stellar population analysis of compact group galaxies.

2.2.2: Compact Group Stellar Populations

Stellar population analysis of compact groups has largely focused on the HCGs. The first studies found that HCG galaxies have a larger fraction of intermediate aged stars than their field counterparts[45, 134]. HCG galaxies that are not undergoing a star burst have metallicity values that compare to field galaxies but tend to be higher than expected for their luminosity. The absorption lines caused by metals are narrower than expected and the Balmer absorption is strong in HCG galaxies [45]. These observations led to the conclusion that compact groups show enhanced processing due to their denser environments.

More recent studies show that HCGs have higher rates of old and intermediate stellar populations than field galaxies, especially those galaxies classified as early-type[135]. Galaxies classified as late-type are more likely to have similar ages to field galaxies, again, pointing to enhanced processing of cold gas in more evolved galaxies[136, 48, 135, 137]. The elliptical galaxies in HCGs have enhanced $[Mg/Fe]$ ratios and depleted $[Z/H]$, suggesting that the cold gas was quenched to truncate the star formation[48].

2.2.3: STARLIGHT

My stellar population analysis used the STARLIGHT routine[130]. STARLIGHT fits a spectrum synthesized from many template stars to an observed spectrum, to constrain properties of the SP; it uses a combination of simulated annealing, Metropolis and Markov Chain Monte Carlo techniques. There are four steps to the fit. The first explores the parameter space. The second removes pixels that cannot be fit. The third attempts a fit using all the bases provided. The final step tweaks the fit after discarding bases that do not make a significant contribution.

The many parameters to set are discussed in the manual available on the STARLIGHT website. I used the suggested values for my fits. STARLIGHT outputs a very detailed file that includes the normalized input spectrum, the model, and the percent light and stellar mass contributed from each base.

Fit Analysis

For my base spectra I use the MILES (Medium Resolution Isaac Newton Telescope Library of Empirical Spectra) of observed stellar spectra that range from $0.06-14.2$ Gyr in age and $-2.32-0.2$ [M/H] in metallicity [123]. The SSPs are created as described in Vazdekis et al. 2010, 1996[138, 116]. In summary, the models determine the light distribution of stars from the isochrones of Girardi et al 2002[115] and use both power law and multi-part power law IMFs to weight the light. Figure 2.12 shows the age coverage of MILES spectra for different metallicities. I also include a plot of the metallicity properties of MILES[139].

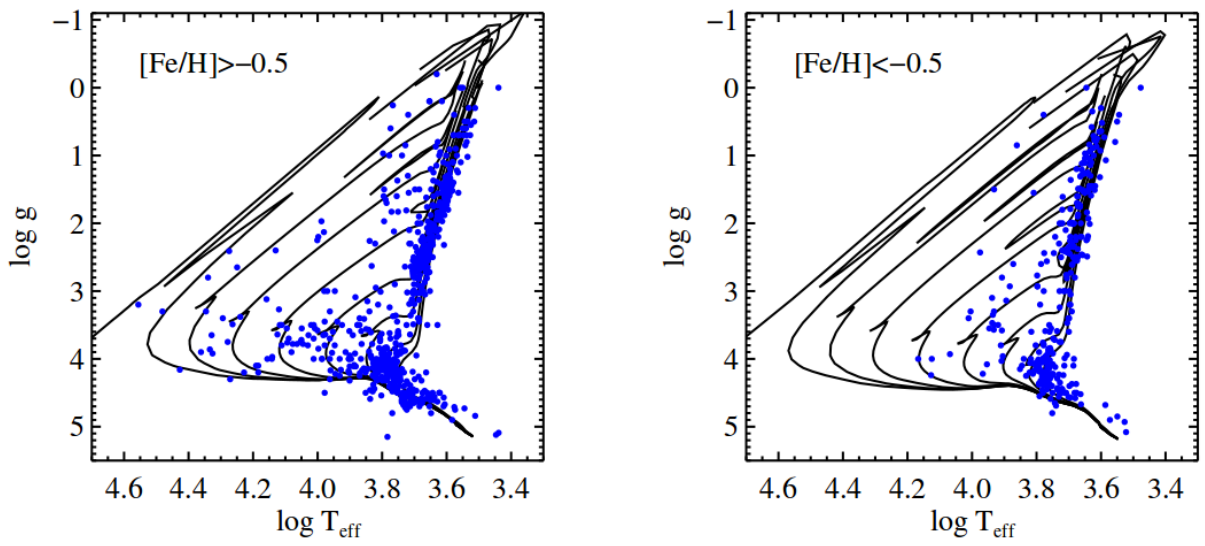

Figure 2.5: MILES metallicity properties plotted over the Padova isochrones. MILES covers the lower main sequence and RGB phases at both metallicities.[139]

There are complications in using the MILES (and other spectral libraries) that are extensively covered in Conroy (2013), and mentioned briefly here. Coverage of the spectra in age, metallicity and regions of the HR diagram, while better, are still not sufficient. The lack of hot, low-metallicity stars makes young ages difficult to fit. There are issues when assigning stellar physical parameters to the stars in the libraries. The errors associated with $log\,g$, T_{eff} and $[Fe/H]$ propagate into the SSP models in a significant way. Finally, there are known patterns in stellar abundances that are not usually corrected for in the SSPs[139].

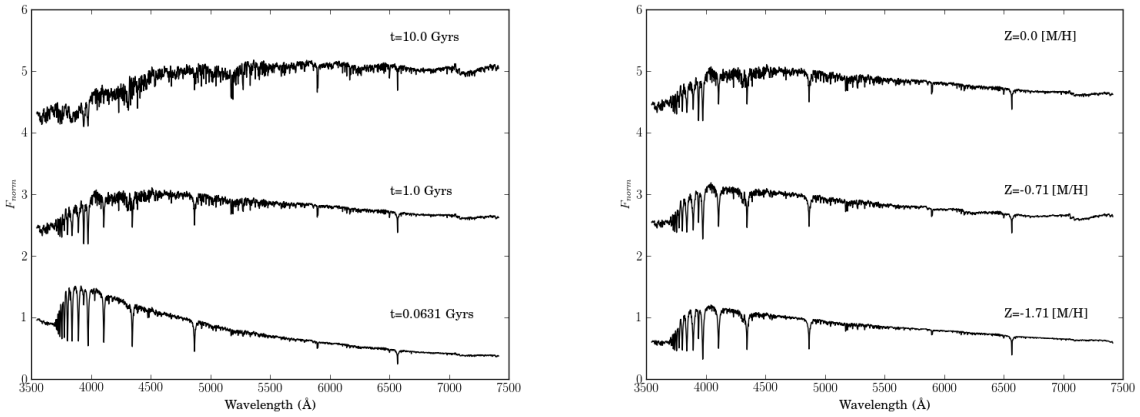

Figure 2.6: Examples of MILES template spectra with normalized flux. The plot on the left shows spectra for different ages with solar metallicity. The plot on the right shows spectra for different metallicities at 1.0 Gyrs. Spectra are offset by a constant flux so spectral features can be seen.

Figure 2.6 shows examples of the MILES spectra used as base templates in STARLIGHT. Because these spectra are flux calibrated, for each template I took 10%, 30%, 50%, 70% and 100% of the light and added Poisson noise of 10, 20 and 30. This procedure is similar to that of Fernandes et al. 2005[130] hereafter referred to as F05. As my priors, I combined two populations, an old+intermediate population and an old+young population. Each population was taken at 50% and added to the other along with the noises applied to the single population. Finally, I combined an old, intermediate and young population each taken at 33% and added the noise. The populations all had the same metallicity, and the ages were chosen at random.

Age and Metallicity Bins

I first used the fits to the single population templates to define my output age and metallicity bins. To explore where the age and metallicity ranges might fall, I plotted the template ages and metallicities against some commonly used Lick indices measured by MILES.

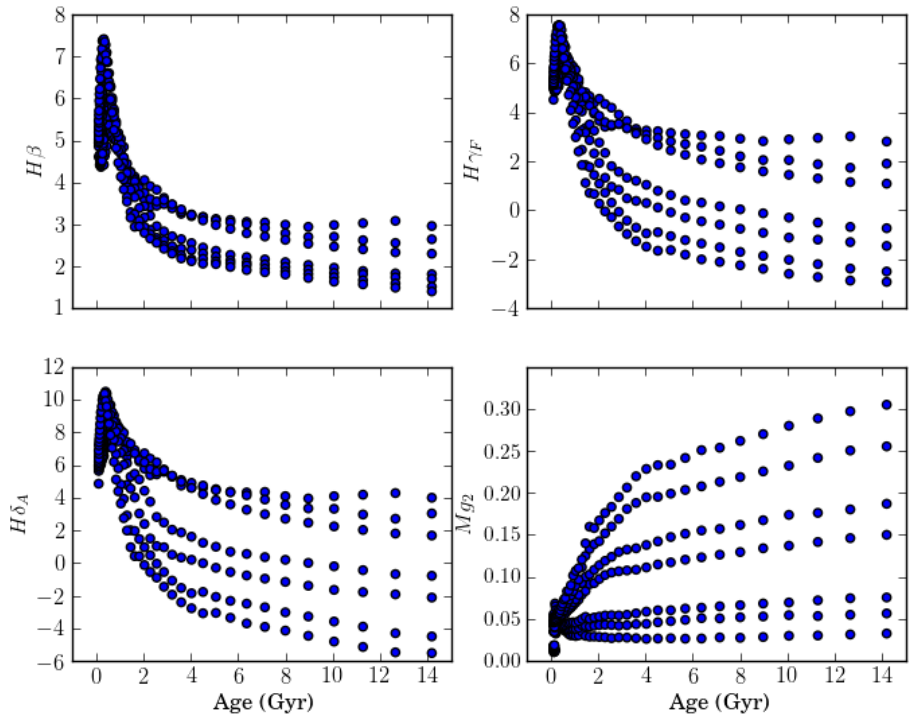

Figure 2.7: Age vs Lick indice for 294 MILES templates.

From this plot, I decided to vary the maximum value for the young SP range from 0.1 to 1.5 Gyrs. The output ages and percent light values were averaged for all templates that fell in the young age ranges. I then calculated the light weighted (x_j) and mass weighted (μ_j) ages and metallicities as suggested by F05.

$$< \log t_* >_L = \sum_j x_j \log_{10} t_j \tag{2.6}$$

$$< \log t_* >_M = \sum_j \mu_j \log_{10} t_j \tag{2.7}$$

$$< Z >_L = \sum_j x_j Z_j \tag{2.8}$$

$$< Z >_M = \sum_j \mu_j Z_j \tag{2.9}$$

Light weighted ages are expected to represent the younger populations because a galaxy's light will be dominated by younger stars. Mass weighted ages trace the older stars. I subtracted these averaged values from the input values and determined which maximum value for the range returned the smallest deviation from the input value. This analysis determined that the young range should run from $Age < 0.1$ Gyrs. I then used this age as the lower end of the intermediate age bracket and varied the maximum value from 1.7 to 4 Gyrs. From this analysis, the intermediate age was found to range from $0.1 \leq age \leq 4.0$ Gyrs. The old age range was found to be $age > 4.0$ Gyrs.

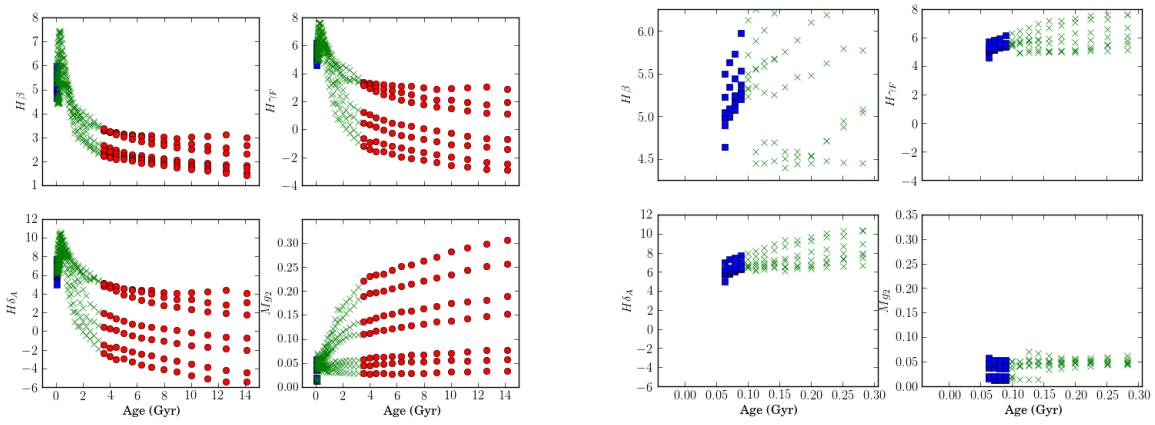

Figure 2.8: Age vs Lick indice plots showing young (blue squares), intermediate (green x) and old (red circle) ranges for templates.

I followed a similar procedure for the metallicity bins. The plots of the Lick indices revealed that the values were already separated into three distinct ranges.

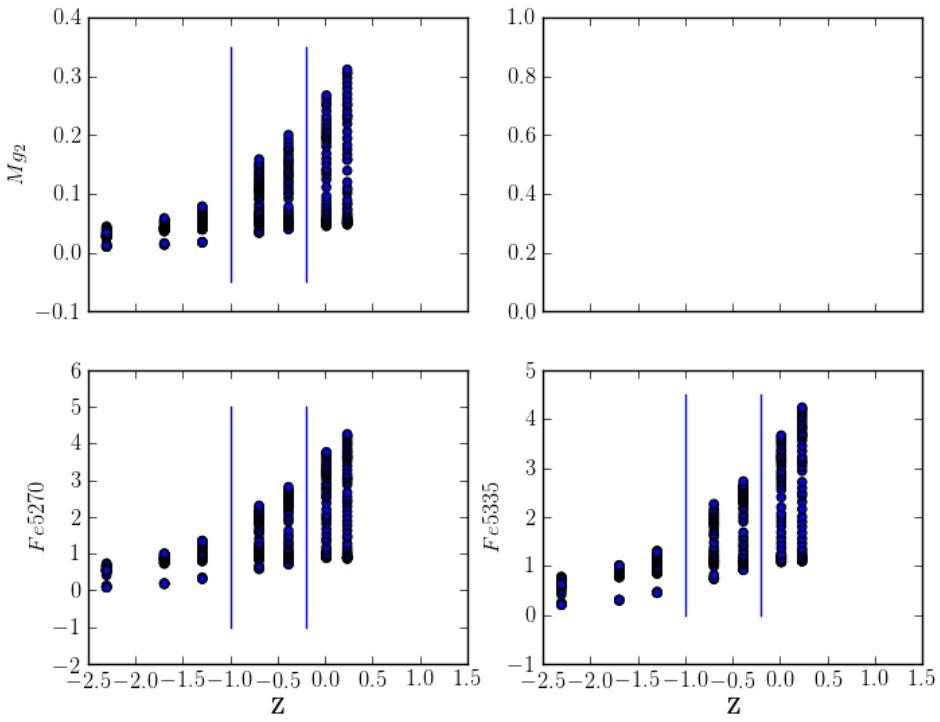

Figure 2.9: Z vs Lick indice for 294 MILES templates. Blue vertical lines indicate where the low, mid and high Z bins are located.

When running the analysis, I varied the maximum of the low and mid ranges. Metallicities did not separate into brackets as cleanly as ages, most likely due to the large spacing between the different metallicity values. A more continuous distribution would allow for better testing. Here I used the visually apparent bins. My results are tabulated in Appendix A.1.

STARLIGHT Fits

F05 suggest that STARLIGHT be used to obtain a robust idea of the stellar populations. Binning by age and metallicity is the best way to achieve this. Template choice is important. Redundancy is not useful for exploring parameter space. Because the ages have a pretty continuous distribution, I chose a few templates from each bracket to span a range of index values. I then chose one of the metallicity values in each metallicity

bin (in bold) and also kept the templates for the other metallicities. The following templates were used in my analysis.

Age (Gyr)	0.0631, 0.0794, 0.1995, 0.5012, 1, 2.5119, 6.3096, 10
Z [M/H]	,-2.32, **-1.71**,-1.31,-0.7, **-0.4**, 0.00, **0.22**

Table 2.1: Templates used for analysis.

I used these templates to fit the one, two and three population spectra. I then compared the different population fits with all 294 templates, the bolded 24 templates and the full 56 templates. When looking at the residuals ($age_{in} - age_{out}$; $Z_{in} - Z_{out}$) there is not a substantial difference between the single population fits and the mixed population fits. This is noted by the tables in Appendix A.2, which list the average and standard deviations of the residuals for each template fit. I also included tables of the residuals over all the files, only separated by number of templates and noise in Appendix A.3.

For the young populations ($t_j < 0.1$ Gyrs), the light weighted output ages were on average 0.07 dex younger than the input ages and did not vary with noise or templates used. For the old populations ($t_j > 4.0$ Gyrs), the mass weighted output ages were older than the input ages by 0.06 dex for the 294 template fits. The difference was 0.13 dex for the 24 and 56 template fits.

The intermediate populations ($0.1 \leq t_j \leq 4.0$ Gyrs) presented a challenge. My fits were showing very high residuals. This turned out to be due to more than half of the models being fit with a combination of young and old populations instead of an intermediate one. This pushed the overall light weighted average age toward the input age. Over all population mixtures, it occurred in 78% of the fits. To account for this in the analysis, I noted when a fit returned only young and old populations. I then used the total light weighted and mass weighted average to calculate the residual age. When this was done, residuals were more reasonable. I also determined how often this occurred in my templates with respect to the number of base templates used, the percent light of the input population and the input noise added to the templates. I found that only the number of base templates had substantial effect. When using the 24 or 56 base templates, all were fit with young and old populations instead of an intermediate one.

	Number Fit	Number Not Fit
Total	2878	9956
% Total	22%	78%
% Light		
10%	439	1577
30%	876	3093
50%	649	2168
70%	452	1564
100%	462	1554
Number of Templates		
24	5	4273
56	7	4343
294	2866	1340
Input Noise		
10	1117	3161
20	964	3314
30	797	3481

Table 2.2: Total templates fit and not fit by intermediate populations.

My data analysis had to take this into account. There are a few ways to do this: 1) I noted which fits only return young and old populations and calculated the total light weighted average age, 2) I noted which fits only return young and old populations and re-fit the spectrum with a base of only intermediate populations, and 3) I added more intermediate population templates to my base to see if this resulted in more intermediate templates being used.

For the Z analysis, the results were similar for the metallicity brackets and populations. I did not create as many different mixed populations as with the age templates. This could have affected the mixed population residuals. The residuals were similar between the single population Z residuals and the mixed populations that had more than a few files in that Z bracket. I created the same tables as for the age analysis in the Appendix.

From this analysis, I decided to use the 56 templates when running STARLIGHT on my observations.

Comparison With Other Data

I carried out long slit observations of an early and a late-type galaxy whose central 1" regions were fit with STARLIGHT by Cid Fernandes et al. [140] (hereafter CF04). They used galaxies with known stellar population properties as their templates. They had four different classifications for their templates:

- NGC 3367 and NGC 6217 are galaxies with young ($< 10^7 Gyr$) populations. Their spectra have weak metal absorption lines and the continuum is blue dominated.
- NGC 205 is a galaxy in the intermediate age range ($10^8 - 10^9 Gyr$). High order Balmer absorption lines (HOBLs) dominate the spectrum.
- NGC 221 and NGC 628 are galaxies with a mix of intermediate and old populations. The spectra show a mix of HOBLs and strong metal lines.
- NGC 224, NGC 1023, NGC 2950 and NGC 6654 are dominated by old populations and show strong metal lines.

After fitting the central 1" of NGC 660 and NGC 1052, they determined the percentage of light each population contributed to the observed spectrum. Their analysis revealed that NGC 660 is mostly comprised of intermediate (59.4%) and old (40.6%) populations. While NGC 1052 is dominated by older populations (83%) but has a small population of young stars (16.5%) in its central regions. My observations used the age bins described previously and the MILES templates. I fit using 56 and 294 templates to see if that had a significant effect on the outcome. Because I used different templates as my bases, I expected to match their percentages only broadly. As evident in the table below, my fits generally matched those of CF04 in stellar population characteristics.

Galaxy	NGC 660			NGC 1052		
Templates	CF04	56	294	CF04	56	294
% Young	0.0	7.8	5.9	16.5	8.6	7.1
% Intermediate	59.4	75.3	76.5	0.0	0.0	1.0
% Old	40.6	11.3	13.1	83.0	98.0	97.3

Table 2.3: Fraction of light due to young, intermediate and old template components.

In these two examples, it appears that using more templates recovers a slightly higher percentage of intermediate aged populations. This should be analyzed in future work to determine how sensitive the intermediate aged fits are to the number of templates used.

Future Work

More analysis should be done to ensure that STARLIGHT is accurately recovering the intermediate aged populations. This would require galaxy spectra with known stellar population properties to find the best combination of templates, then cycle through various combinations of templates to find the best match.

2.3: Emission Line Fitting

2.3.1: History of Emission Line Measurements

Emission lines in the optical spectra of galaxies are caused by two phenomena. When gas is photoionized by young stars, Balmer lines are visible. The nucleus of a galaxy will show signs of activity when gas is funneled into the supermassive black hole at the center to cause forbidden lines such as [OI], [OII], [OIII], [NII] and [SII] to appear at differing intensities depending on the nature and orientation of the nucleus. AGN can be further divided into Seyfert and LINER nuclei. LINERS have lower luminosities than Seyferts and are believed to be caused by shock heating due to star formation outside the nucleus or a heavily extinguished AGN[141].

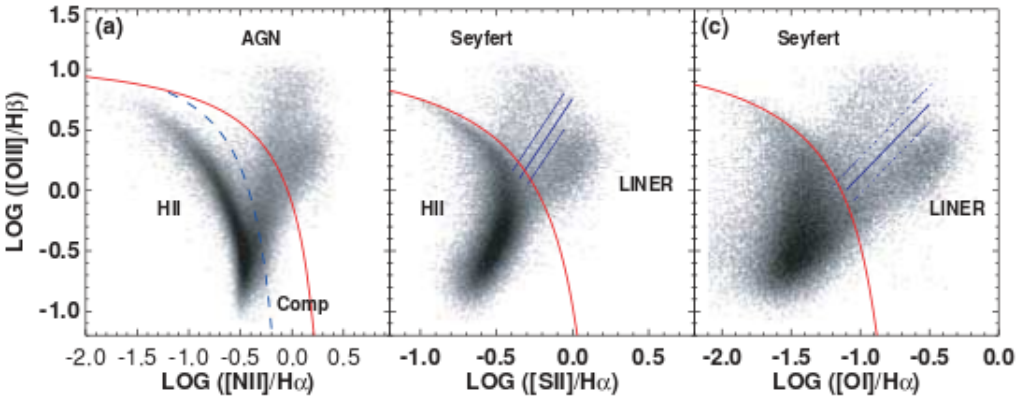

Figure 2.10: BPT diagram classifications defined by [141]

Galaxies tend to fall into three categories of activity - star forming, AGN, or neither. BPT diagrams can divide galaxies by their activity[142]. These diagrams utilize the ratio of emission from forbidden line phenomena and star forming, most commonly $[OI]/H\alpha$, $[SII]/H\alpha$, $[NII]/H\alpha$ and $[OIII]/H\beta$. These diagrams were revised by Osterbrock & Pogge, 1985 and Veilleux & Osterbrock, 1987 to further constrain the activity types[143, 144]. Diagram divisions based on theoretical models were first proposed by Kewley et al. 2001 with further modification to include composite galaxies in Kauffman et al. 2003[145, 7]. The division between Seyfert and LINER activity is best defined by the classifications in Kewley et al. 2006[141]. We present the definitions of Kewley et al. 2006 here.

Star forming:

$$log(\frac{[OIII]}{H\beta}) < \begin{cases} \frac{0.61}{log(\frac{[NII]}{H\alpha})-0.05}+1.3 \\ \frac{0.72}{log(\frac{[SII]}{H\alpha})-0.32}+1.30 \\ \frac{0.73}{log(\frac{[OI]}{H\alpha})+0.59}+1.33 \end{cases} \tag{2.10}$$

Composite/Transition:

$$\frac{0.61}{log(\frac{[NII]}{H\alpha})-0.05}+1.3 < log(\frac{[OIII]}{H\beta}) < \frac{0.61}{log(\frac{[NII]}{H\alpha})-0.47}+1.19 \tag{2.11}$$

Seyfert:

$$log(\frac{[OIII]}{H\beta}) > \begin{cases} \frac{0.61}{log(\frac{[NII]}{H\alpha})-0.47}+1.19 \\ \frac{0.72}{log(\frac{[SII]}{H\alpha})-0.32}+1.30 \\ \frac{0.73}{log(\frac{[OI]}{H\alpha})+0.59}+1.33 \end{cases} \tag{2.12}$$

or

$$log(\frac{[OI]}{H\alpha}) > -0.59 \tag{2.13}$$

and

$$log(\frac{[OIII]}{H\beta}) > \begin{cases} 1.89log(\frac{[SII]}{H\alpha})+0.76 \\ 1.18log(\frac{[OI]}{H\alpha})+1.30 \end{cases} \tag{2.14}$$

LINER:

$$log(\frac{[OIII]}{H\beta}) > \begin{cases} \frac{0.61}{log(\frac{[NII]}{H\alpha})-0.47}+1.19 \\ \frac{0.73}{log(\frac{[OI]}{H\alpha})+0.59}+1.33 \end{cases} \tag{2.15}$$

$$1.89log(\frac{[SII]}{H\alpha})+0.76 < log(\frac{[OIII]}{H\beta}) < \frac{0.72}{log(\frac{[SII]}{H\alpha})-0.32}+1.30 \tag{2.16}$$

or

$$log(\frac{[OI]}{H\alpha}) > -0.59 \tag{2.17}$$

$$log(\frac{[OIII]}{H\beta}) < 1.18log(\frac{[OI]}{H\alpha})+1.30 \tag{2.18}$$

Emission lines can also measure abundances of elements such as Oxygen, measure the temperature and density of the gas being excited, and estimate internal reddening from the ratio of the recombination lines $H\alpha/H\beta$. Temperatures can be measured in the low density regime if an element is structured such that it emits from different excitation energies in the same wavelength region. In our wavelength range, the following lines could be observed

$$\frac{j_{4959}+j_{5007}}{j_{4363}} = \frac{7.9exp(3.29\times10^4/T)}{1+4.5x10^{-4}n_e/T^{1/2}} \tag{2.19}$$

$$\frac{j_{6548}+j_{6583}}{j_{5755}} = \frac{8.23exp(2.50\times10^4/T)}{1+4.4x10^{-3}n_e/T^{1/2}} \tag{2.20}$$

Electron densities are measured by looking for the effects of collisional deexcitation, by looking at emission lines from the same ion that occur at similar excitation energies. This means that the excitation rates of the levels only depend on collision strengths. Examples of lines that satisfy this in our wavelength range are [OII]3729/3727 and [SII]6716/6731. The [OII] lines are too close together to be distinguished at my spectral resolution[146].

While the majority of SF studies of compact groups have been made at radio and infrared wavelengths [92, 39, 51, 52], $H\alpha$ emission can estimate the current SFR in the galaxy. This line provides the number of photons that are ionizing the gas surrounding newly formed O stars. Because these stars have short life spans ($\sim 10^6$yrs), their present number divided by their life span is their formation rate. The IMF provides us with the number of O-A hydrogen ionizing stars to derive the star formation rate using a Salpeter IMF

$$SFR(M_\odot yr^{-1}) = 7.9\times10^{-42}L(H\alpha) \tag{2.21}$$

with $H\alpha$ in units of $(ergs^{-1})$[146]. If one knows the stellar masses of the galaxies involved, the specific star formation rate (sSFR) can be calculated for a galaxy by dividing the SFR by the stellar mass (M_*).

2.3.2: Compact Group Emission Line Results

HCG studies have shown that compact groups tend to have more AGN activity than SF activity[84]. HCG 16 is composed of 5 galaxies with one classified as Seyfert, two as LINERs and three are starbursting[147]. HCG 31 has five galaxies with recent star formation activity[148, 57]. HCG 77, 92, 93 and 96 all have Seyferts[84].

SCGs are spectrally classified as SF more often than the HCGs and the SF is concentrated in the nuclear regions[90]. All SF galaxies have AGN activity and pure AGN galaxies are generally the more luminous galaxies in the group[90]. One of the most studied compact groups, Stephan's Quintet, has evidence for a starburst in the intragroup medium [149]. Another study found a compact group at high redshift falling into a larger cluster with higher than expected $H\alpha$ emission, implying enhanced SF activity[150].

2.3.3: PYSPECKIT

I fit emission lines using the *pyspeckit* Python package[151]. This package allows both interactive and automated fitting of emission and absorption lines. I fit all emission lines three times higher than the rms noise in the wavelength region $4789 - 4839$Å. A list of the lines are in the table below.

Element	Wavelength(Å)	Measures
$H\delta$	4102.92	SF-F stars,reddening
$H\gamma$	4341.69	SF-A stars,reddening
$[OIII]$	4364.44	AGN,O abundance,T
$H\beta$	4862.69	SF-B stars,reddening
$[OIII]$	4960.30	AGN,O abundance,T
$[OIII]$	5008.24	AGN,O abundance,T
$[OI]$	5577.0	AGN,O abundance
$[NII]$	5756.24	AGN,T
$[OI]$	6300.0	AGN,O abundance
$[NII]$	6549.84	AGN,T
$H\alpha$	6564.61	SF-O stars,reddening
$[NII]$	6585.23	AGN,T
$[SII]$	6718.32	AGN,n_e
$[SII]$	6732.71	AGN,n_e

Table 2.4: Emission lines potentially present in my spectra.

2.4: CINDERS Experiment Design

2.4.1: Observing set-up

Due to fringing on the CCD, I could not trust line measurements at $\lambda > 720nm$ on the Goodman Spectrograph. A 400 lines/mm grating was fabricated by the Goodman Lab at UNC to take advantage of the CCD's exceptional blue sensitivity. This grating covers the wavelength range 320-725nm and avoids the fringing region of the CCD. Because the CCD is $4k \times 4k$ and there are 244 fibers total, I allowed 14 pixels per fiber along the spatial axis and each spectrum to span the majority of the 4000 pixels along the wavelength axis. Below is a table of possible observation set-ups.

Table 2.5: Observation set-up

Telescope	SOAR 4.1m
Instrument	Goodman
FOV	$9' \times 4.5'$
spatial sampling	0.77”
bundle diameter	7.2”
min bundle separation	100”
grating	400 lines/mm VPH
spectral sampling	58 Å/mm ($\sim$ 52 km/s)
spectral resolution	4.2Å @ 3650Å and 8.3Å @ 7250Å
instrument dispersion	$\sim$ 150 km/s
wavelength coverage	3650 - 7200 Å

Below are plots of the diagnostics lines of interest versus redshift. The black horizontal lines enclose our wavelength range of interest. Many of these lines are necessary for absorption line indices measurements (i.e. LICK/IDS or ROSE systems) and emission line diagnostics.

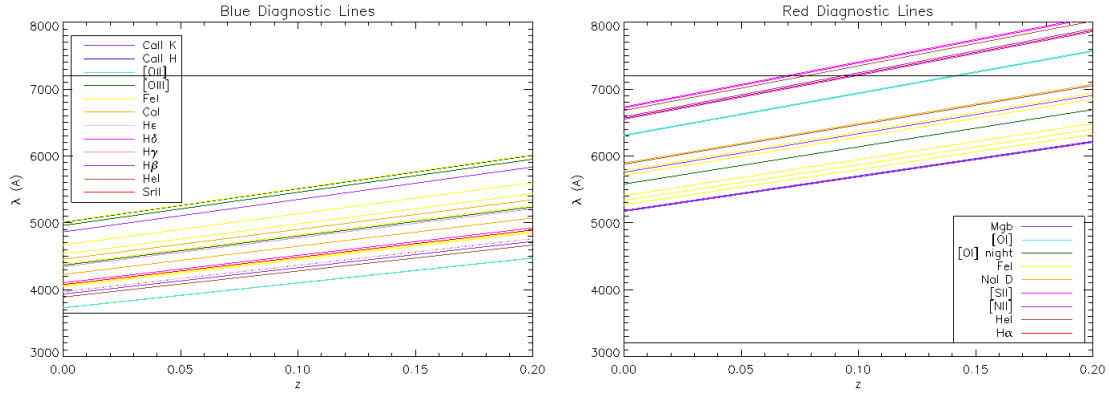

Figure 2.11: Diagnostic Lines

2.4.2: Sensitivity Analysis/Simulations

I downloaded many template spectra from the MILES Tune SSP Web Interface [116]. I assumed that these spectra have infinite S/N and re-sampled them to the SOAR spectral resolution, then applied atmo-

spheric corrections, SOAR+GS transmission functions and reddening. The MILES template spectra span the wavelength range $3540.5 - 7409.6$Å and have a spectral dispersion of 0.9Å$/pixel$ with FWHM=2.5Å. The downloaded spectra assumed a Kroupa revised IMF with a slope of 1.30 for a range of metallicities and ages, and have a spectral dispersion of 0.87 Å/pixel and instrument dispersion of 150 km/s. The spectra are reported in units of $F_\lambda L_\odot^{-1}$Å$^{-1} M_\odot^{-1}$.

For the signal-to-noise (S/N) predictions, I needed to choose which SSP best describes the flux through the fibers from a particular area of a galaxy in our sample. Vazdekis et al. 2010[116] have plotted the B-V color of their SSPs against their age for different metallicities. Below is a plot similar to Figure 19 in Vazdekis et al. 2010 with g-r substituted for B-V.

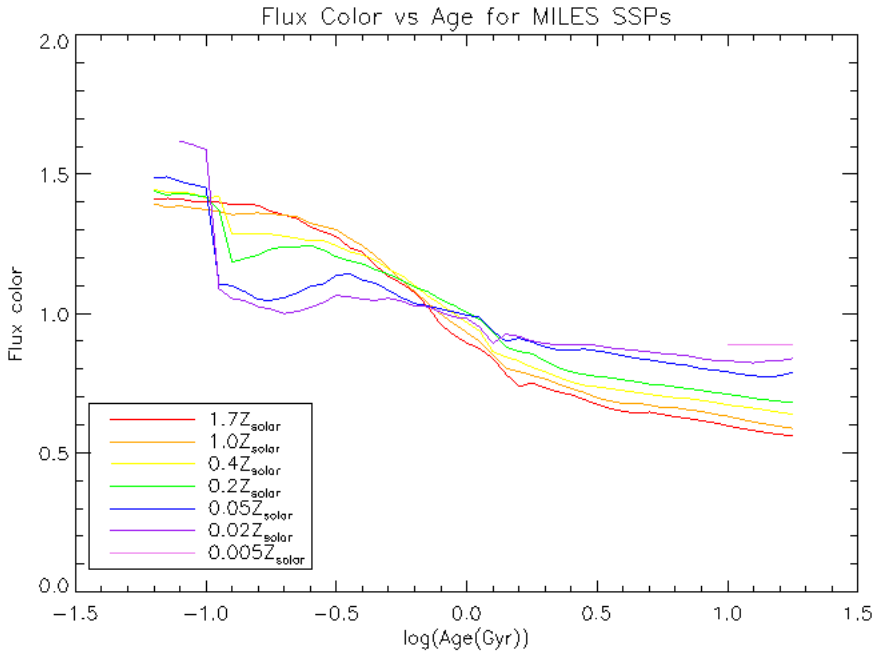

Figure 2.12: Color vs Age for SSPs with different metallicities.

I downloaded B_J ($\lambda = 3950 - 5400$Å, IIIa-J + GG395) and SERC-R ($\lambda = 5900 - 6900$Å, IIIa-F + OG590) filter images from the COSMOS UKST plate survey[22]. I measured the intensity within circular apertures of the same size as our fiber diameters. I measured the surface brightness per arcsecond^2 along the semi-major and semi-minor axis in two dithered positions each offset 2 arcseconds from the center of the galaxy. The FITS files report density within each pixel because these are photographic scans of plates. I used a look up table to determine the measured transmission in each pixel contained in each fiber (N. Hambly, private communication). $I = \left(\frac{1}{T}\right)^{0.3}$ converted this measured transmission into an intensity that is multiplied by 30

photons/darkened grain [152]. I multiplied the intensity by the ratio of the collecting areas of the SOAR telescope (410 cm) and the UKST (124 cm), the ratio of the B_j and g ($\Delta\lambda = 1379$Å) bandpass or the R_2 and r ($\Delta\lambda = 1382$Å) bandpass, the ratio of the SOAR (0.15 arcsec/pixel) and UKST (0.67 arcsec/pixel) pixel areas and divided by the exposure time listed in the header. The g-r color within each fiber is represented as a ratio of the g and r fluxes and used to choose the SSP spectrum that best represents the stellar population. The g and r band fluxes for each SSP model were calculated from the template spectra after being multiplied by their respective filter band passes. After choosing a template spectrum, I calibrated the flux in the g and r filters to match the flux in each fiber. The corresponding regions of the spectrum were multiplied by the g and r filter band passes to obtain a total flux for each filter. This flux was scaled to the flux within a fiber by a constant determined from the ratio of the fiber flux and the template spectrum flux in each filter. This converted the template spectrum flux from $L_{\odot}^{-1} M_{\odot}^{-1} \text{Å}^{-1}$ to counts/s. The scale factor was applied to the spectrum after it was reddened ($e^{-(\frac{A_\lambda}{0.77*R} f(\lambda))}$) to account for Galactic extinction. A_g and A_r were obtained from NED for each group field and I used the R=3.1 curve to estimate $f(\lambda)$.

Finally, I applied an atmospheric extinction to the spectra, using the Gemini telescope atmospheric extinction curves given on their website and in Table 2.6 below. I converted these magnitudes into fluxes for an average airmass of 1.5 and applied them to the template spectra. I interpolated to determine the values for the atmospheric extinction at each re-sampled wavelengths.

wavelength (nm)	extinction (mag/airmass)
310	1.37
320	0.82
340	0.51
360	0.37
380	0.30
400	0.25
450	0.17
500	0.13
550	0.12
600	0.11
650	0.11
700	0.10
800	0.07
900	0.05

Table 2.6: Atmospheric Extinction over Mauna Kea

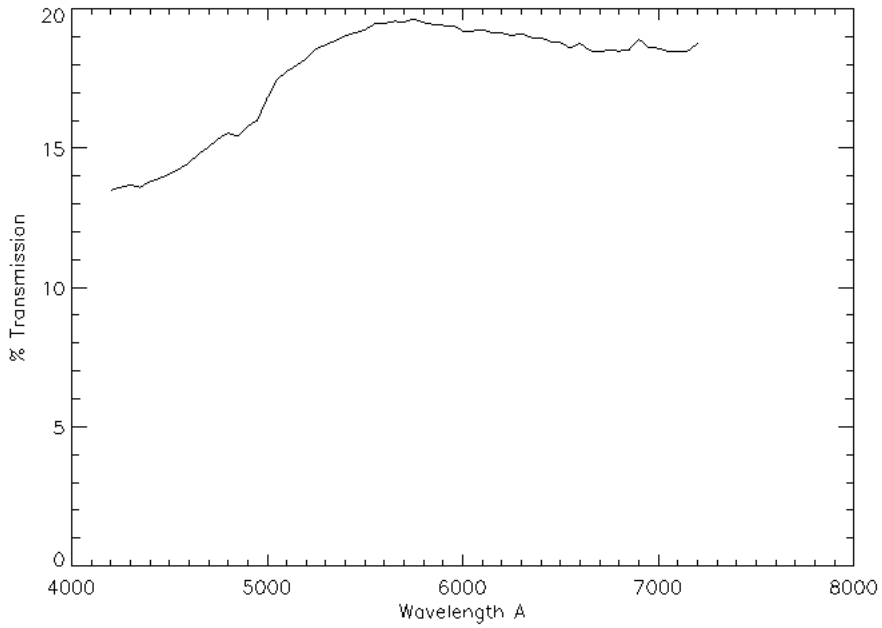

Figure 2.13: SOAR throughput.

I applied the SOAR telescope+Goodman Spectrograph+detector+grating transmission function. I planned to measure the throughput of the SOAR telescope+new collimator+bundles+grating+GS when CINDERS was on the telescope, but for this calculation I estimated that the bundles had 50% throughput so the transmission function reduced by half. The predicted resolution of the spectra was 0.87Å/pixel and the expected FWHM was 4.2Å at the extreme blue end and 8.3Å at the extreme red. I downloaded spectra from the MILES database with a constant velocity dispersion of 150 km/s, which corresponds to the change in FWHM I expected.

I only measured the flux along the semi-major and semi-minor axis for my initial analysis. Because I am focusing on the galaxy centers, the S/N should be adequate for the analysis. The final step before any S/N analysis was to add Poisson noise to the spectrum to simulate the CCD noise during an observation. I needed to know the amount of time that I will be observing the galaxy because signal variance goes as $\sqrt{flux * time}$. I added the $\sqrt{flux * time}$ to the total flux to account for Poisson variation. I calculated the exposure time necessary to reach a S/N of 3 in the faintest fiber of the faintest galaxy in each field using

$$\frac{\mathrm{S}}{\mathrm{N}} = \frac{\text{total flux in central bandpass} * \text{time}}{\sqrt{\text{total flux in central bandpass*time + sky flux} * A_{eff} * A_{fib} * \text{bandpass} * \text{time} + \text{dark} * \text{time} + \text{readnoise}^2}} \tag{2.22}$$

A_{eff} is the effective area of the telescope in cm^2, A_{fib} is the area of the fiber in $arcsec^2$, bandpass is the width of the central bandpass for each indice and the sky flux is the average sky flux for either the g or r filter within that bandpass obtained from Gemini South sky brightness measurements. All fluxes are in counts/s. I chose the faintest member of each group based on the Iovino, 2002 classifications[23]. The faintest fiber was determined from the faintest total spectral flux predicted from the described color matching.

I calculated the S/N for some of the various line indices I can measure, listed below, along with their central band passes. If these indices were observable within the 2 hour observing time, I could easily attain much higher S/N for any emission lines because emission lines are generally much brighter than absorption lines.

Indice	Bandpass
Mg_2	5154.125-5196.625
$H\beta$	4847.875-4876.625
Fe5270	5245.650-5285.650
Fe5335	5312.125-5352.125
$H\delta_A$	4083.500-4122.250
$H\gamma_A$	4319.750-4363.500

2.4.3: Target Selection

My dissertation focuses on groups where all galaxy members can be observed by CINDERS. The above analysis returned 45 groups containing 189 galaxies. Images of the groups from Iovino, 2002 are in the following table[23]. The black bar represents one arcsecond. I discuss their properties below.

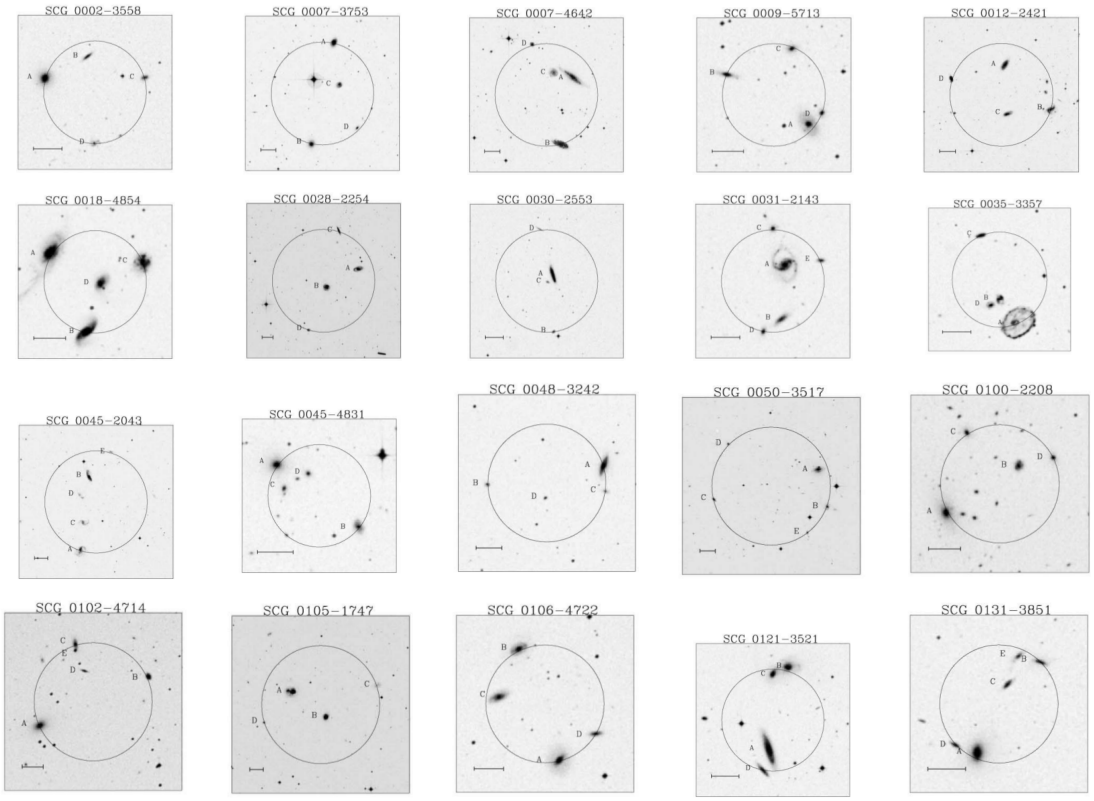

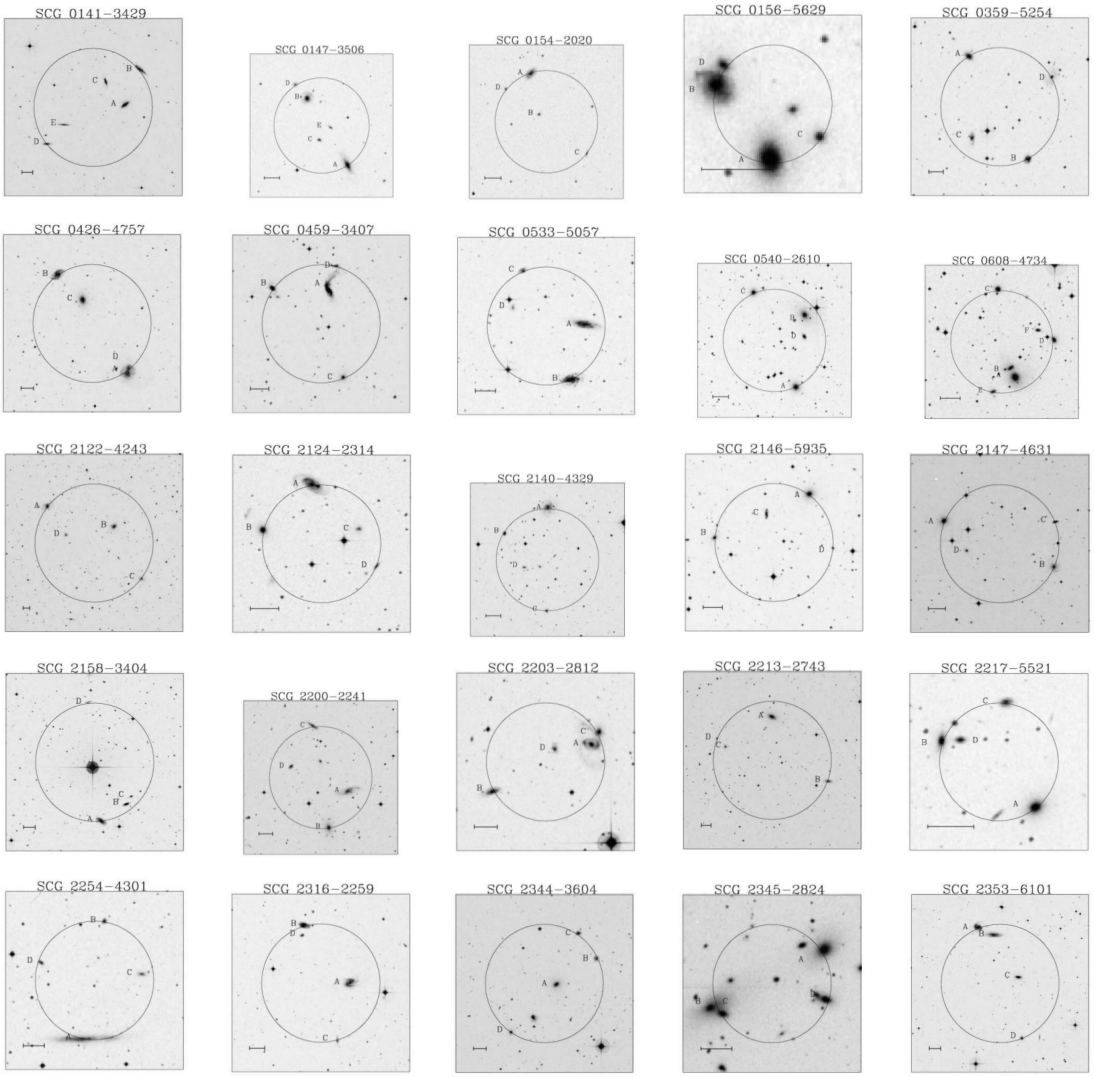

Table 2.7: Images of SCGs where all group members are observable.

Below is a plot of the environmental parameters of the groups where all members are observable with CINDERS. The 45 SCGs appear to span the same range of parameters as the total SCG catalog. Each parameter is described below.

- $m_{brightest}$- Magnitude of the brightest group member.
- μ_{gr}- Total magnitude of the groups members averaged over the circle defining the group.
- $\Delta\mu_{gr}$- Difference between the mean surface brightness within the group and the mean surface brightness within the isolation ring.

- Δmag_{isol}- Magnitude interval between the brightest group member and the brightest galaxy in the isolation ring.
- Δmag_{comp}- Magnitude interval between brightest and faintest group member.
- $R_{isol} = 3 * R_{gr}$- Definition of isolation ring.

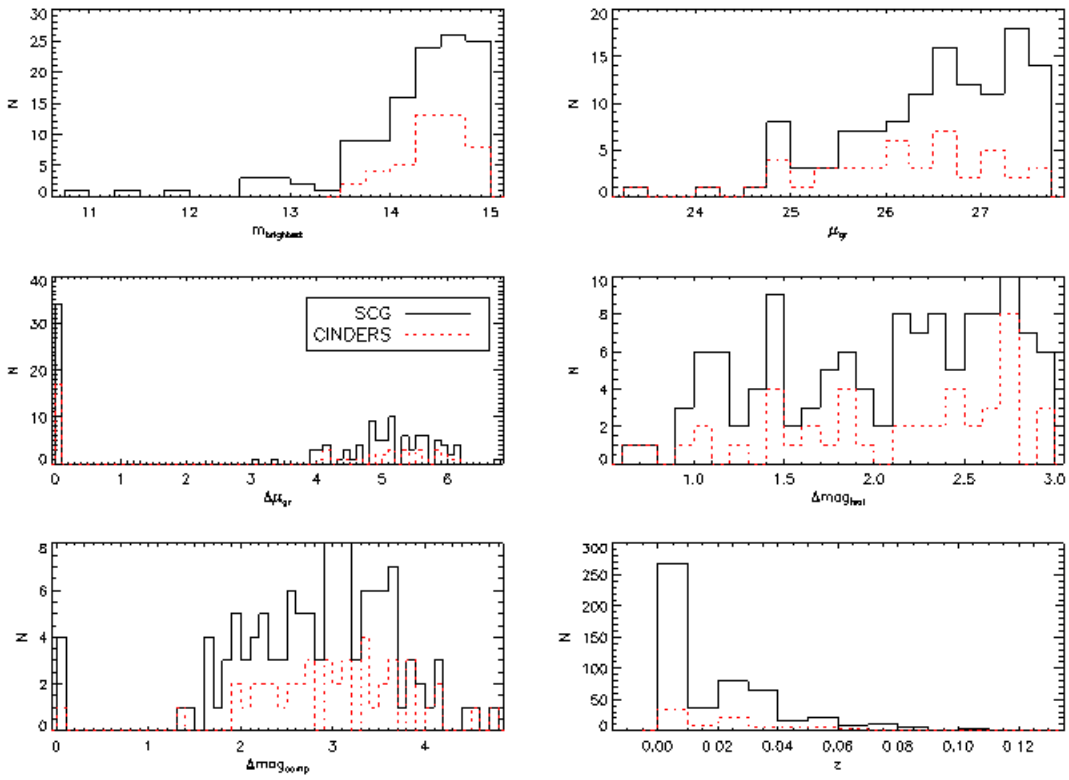

Figure 2.14: Environmental parameters.

I also plot luminosities and absolute magnitudes for the 10 brightest groups with redshift measurements along with their colors.

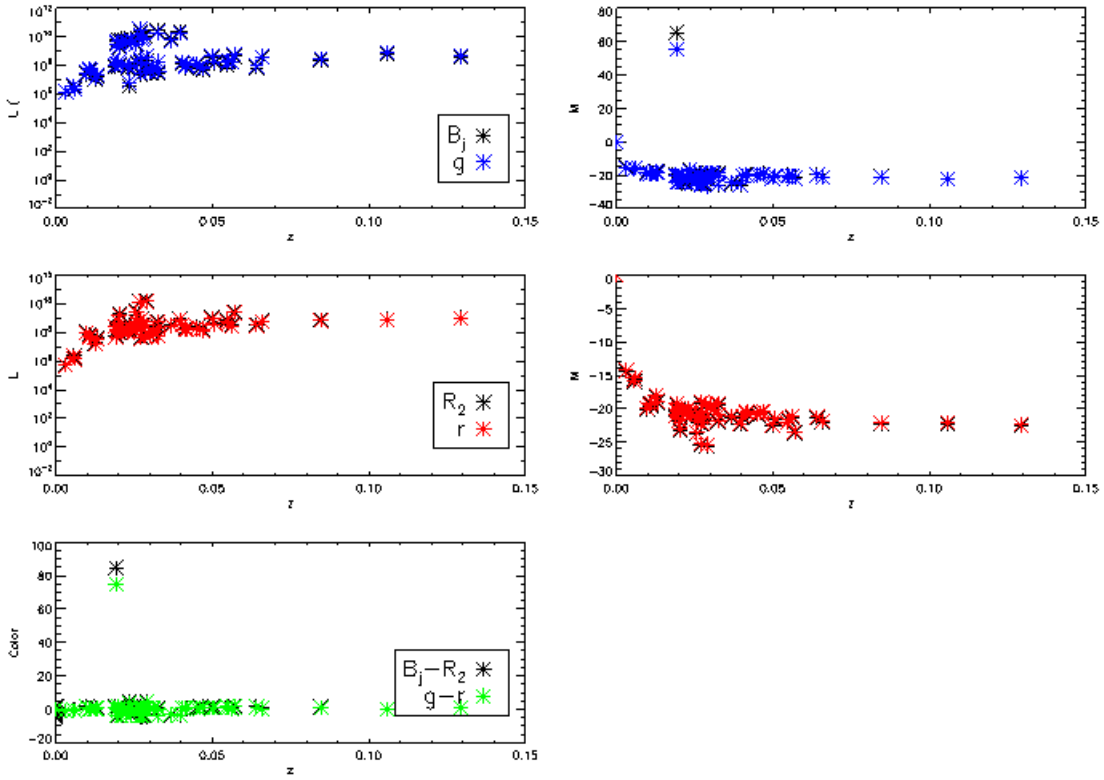

Figure 2.15: Group luminosity and color parameters.

In Appendix B, I list the times when all group members are observable with my set-up and the total hours and exposures necessary to complete observations assuming two to three dithers and 20 minutes of overhead. I take the maximum exposure time for each dither. If the results of the S/N calculations require each dithered observation to be carried out under different brightness conditions, I use the less bright condition for the observations. Bolded times are the ones I planned to use.

From these 45 groups, I chose to focus on 10 of the brightest groups to test the capabilities of CINDERS and increase the likelihood of finding previously collected data. Those 10 groups are listed in the table below.

Field	moon	RA	DEC	hours
SCG2114-2301ACF	dark	21:17:41.9	-22:47:12.7	2.7
SCG2114-2301EDB	dark	21:17:49.1	-22:49:20.1	2.7
SCG2128-4614CAB	dark	21:31:56.2	-46:02:5.16	4
SCG2128-4614CED	dark	21:31:54.1	-46:01:53.5	4
SCG2316-2259DAC	dark	23:19:8.48	-22:43:7.44	3.4
SCG2316-2259BA	dark	23:19:9.10	-22:40:59.3	2.3
SCG0007-4642DAB	dark	00:10:26.7	-46:25:52.1	4
SCG0007-4642DCB	dark	00:10:29.2	-46:25:45.1	4
SCG0030-2553DAB	grey	00:32:41.1	-25:36:42.1	3.7, 2.4
SCG0030-2553DCB	grey	00:32:41.5	-25:36:50.1	3.7, 2.4
SCG0031-2143AB	dark	00:34:13.8	-21:27:14.7	3.5
SCG0031-2143CD	dark	00:34:16.0	-21:27:0.79	2.6
SCG0031-2143ED	dark	00:34:12.4	-21:27:22.3	3.5
SCG0301-5041ACB	dark	03:03:16.3	-50:29:46.6	2.2
SCG0301-5041CD	dark	03:03:17.0	-50:29:36.8	3
SCG0316-5433ABC	dark	03:17:43.1	-54:22:42.3	3.8
SCG0316-5433ADC	dark	03:17:42.7	-54:22:54.0	3.8
SCG0537-2925DAB	grey	05:39:22.5	-29:23:38.5	3.4, 2.2
SCG0537-2925DCB	grey	05:39:22.7	-29:23:52.5	3.4, 2.2
SCG0540-2610CBA	grey	05:42:10.1	-26:8:21.6	3.2, 2.1
SCG0540-2610CDA	grey	05:42:10.2	-26:8:48.9	1.4, 1

2.5: MOS Procedure

Following tests on the telescope to be described, it became clear that CINDERS would not be debugged adequately for this dissertation. Therefore science observations were conducted using conventional but novel for SOAR multi-slits. Multi-object spectroscopy capabilities were added to the Goodman Spectrograph in the fall of 2013. The user has the ability to control the placement, size and orientation of slits for many objects within a 3×5 arcminute field. My observing set-up remained mostly unchanged. I used the same grating, only the slit width was 1" to allow more light to enter the camera, and I binned along the slit spatial axis in 1", 3", 5" and 10" bins to recover some spatial information. With a larger hence more sensitive slit aperture, it was possible to observe more groups with this set-up. Because the FOV is smaller with the

MOS, some of my target fields changed.

3: Instrumentation Results

My dissertation has two components, a science goal and an instrumentation project. I outlined my science goals in Chapter 2. In this chapter, I focus on the instrumentation projects I worked on to answer my science questions.

3.1: CINDERS

We attempted to add a robotic fiber feed to the Goodman Spectrograph on the SOAR telescope called CINDERS. This novel instrument is capable of positioning up to four fiber optic bundles each containing 61 fibers within a $9' \times 5'$ FOV. The bundles can be placed within 100" of each other and span a total diameter of 7" with 0.77" individual fiber diameters. The user interface to position the bundles was developed in Python. Additionally, a visualization aid was designed using Python so the user could see in real time where the bundles were positioned on sky. Calibration and reduction of spectra obtained from CINDERS used a script written in Python and Pyraf. CINDERS could not remain on the telescope due to significant hardware issues but I include the process here for completeness.

3.1.1: CINDERS Design

The concept of adding fiber optic cables to spectrographs is not new, but assembling them into an IFU is. SAMI, installed on the 4-meter Anglo-Australian Telescope at Siding Spring Observatory currently uses 13 fiber optic bundles [100]. The bundles are positioned before each observation using a plug-plate. This means that plates must be designed and cut before each run. To bypass the lengthy process of designing and cutting new plates every time a user needs to observe targets, these bundles could be placed on robotic positioners that allow the user to position the bundles in real time during observations. This was the motivation for CINDERS and will be implemented in the HECTOR instrument under design at the AAO.

Using SolidWorks, the majority of the parts can be designed and added to the SolidWorks rendering of the Goodman Spectrograph. The Goodman Spectrograph utilizes volume-phase holographic gratings [153] with $0.15"/pixel$ scaling over a wavelength range of $320 - 850nm$. The spectroscopic FOV of the Goodman is $3' \times 5'$ and the imagining FOV is $7.2'$ in diameter. Currently, light from the 4-meter telescope is routed into the $f/16$ collimator where it is collimated and passed through a grating, filter wheel and finally the

camera. The fiber bundles for CINDERS would sit at the end of the collimator farthest from the camera. The output end of the fibers route above the collimator and drop down into our own $f/5$ collimator, which feeds light through the grating, filter wheel and camera as before. The custom f/5 collimator is necessary because optical fibers must be fed by a fast telescope beam.

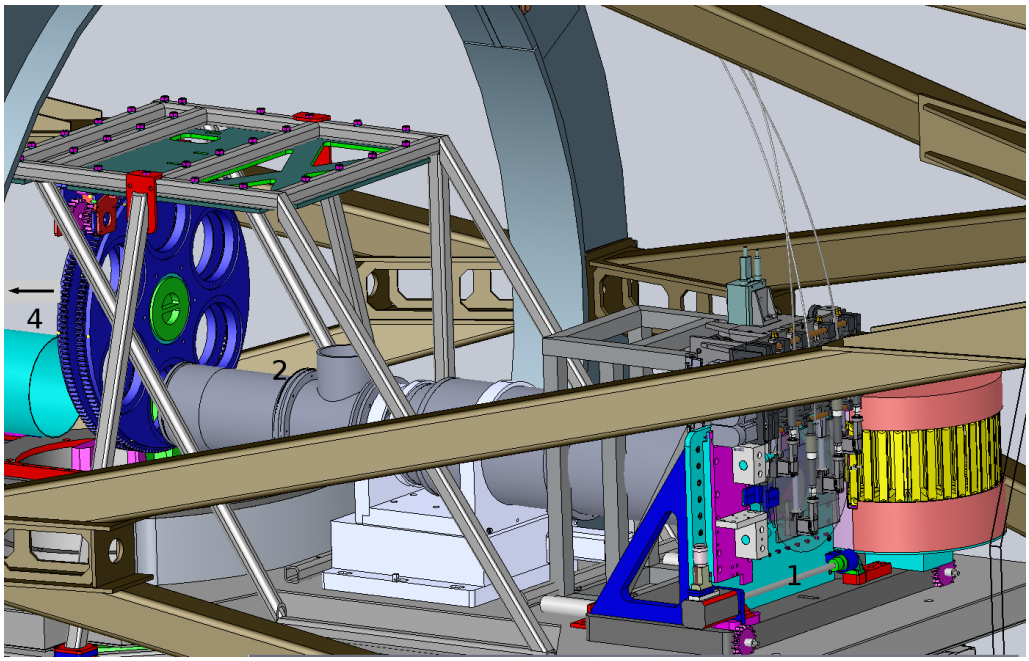

Figure 3.1: CINDERS positioning on the Goodman apparatus. 1) shows the CINDERS probes placed in front of the slit mask assembly. The region to the right off the image is where the light input from the primary telescope mirror is fed. 2) shows our $f/5$ collimator attached to the end of the current Goodman collimator. The protruding cylinder is where the output ends of the bundles are placed. Our collimator is fed through the grating, blue filter wheel and on into the camera, which is located to the left of the image.

The bundles have three dimensional motion via two types of actuators. The x-axis motion is controlled by NEMA 11 Quicksilver Controls motors that power a linear ball-screw with < 0.15" on sky errors. There are four rails mounted parallel to one another with $193mm$ range of motion. The IFU support and rail positioner were designed and fabricated in-house. The y and z axis motions are handled by Firgelli actuator models L12 and PQ12 respectively. The y motors have a $10cm$ range of motion and the z motors have a $2cm$ range of motion.

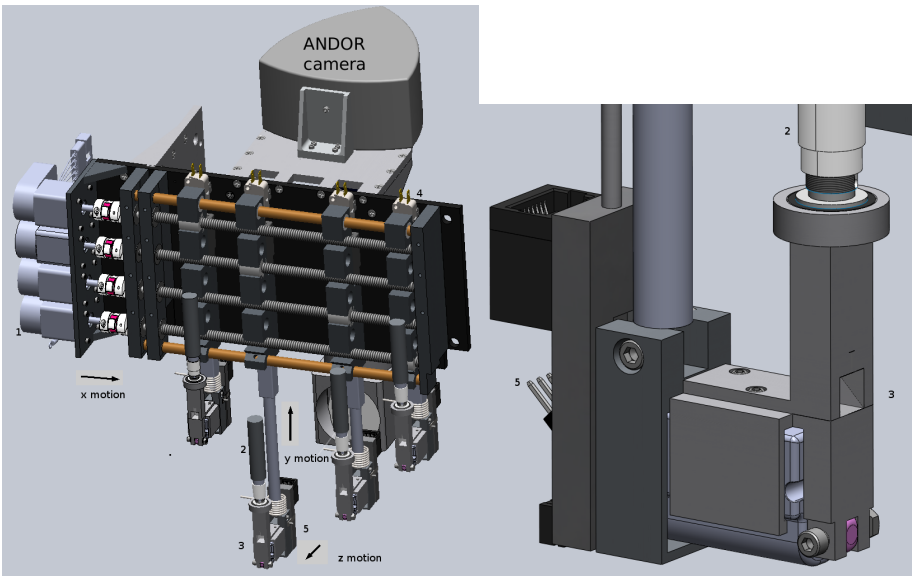

Figure 3.2: Left image: SolidWorks rendering of the x, y and z motion apparatus. The ANDOR camera and its field mirror are shown behind the rail positioner. Right image: Zoomed in on the z motion probe.

Mounted on top of the z-axis actuators is a probe, designed in-house, that attaches to each bundle. Because the bundle faces point towards the floor of the Goodman spectrograph, within each probe sits a 6.25mm right angle mirror to redirect the light from the primary telescope mirror up into each bundle. Before passing through the bundle the light hits a 6.5mm Edmund Optic achromatic doublet which reduces the focal ratio of the light from $f/16.63$ to $f/5$.

The other end of the bundles is unfused and the fibers are arranged linearly in a glass block. After the 4-m long bundles are routed up over the support they hang down into a slit block holds each glass block linearly with the short sides adjacent to one another. This slit block, designed in-house, sits on an opening in our $f/5$ collimator to be switched with the current Goodman collimator. Inside our collimator, a fold mirror redirects the light from the bundles into the collimator path where it passes through a super apochromat flouride triplet from William Optics. After the light is collimated, it passes through the grating, filter wheel and camera of the Goodman Spectrograph.

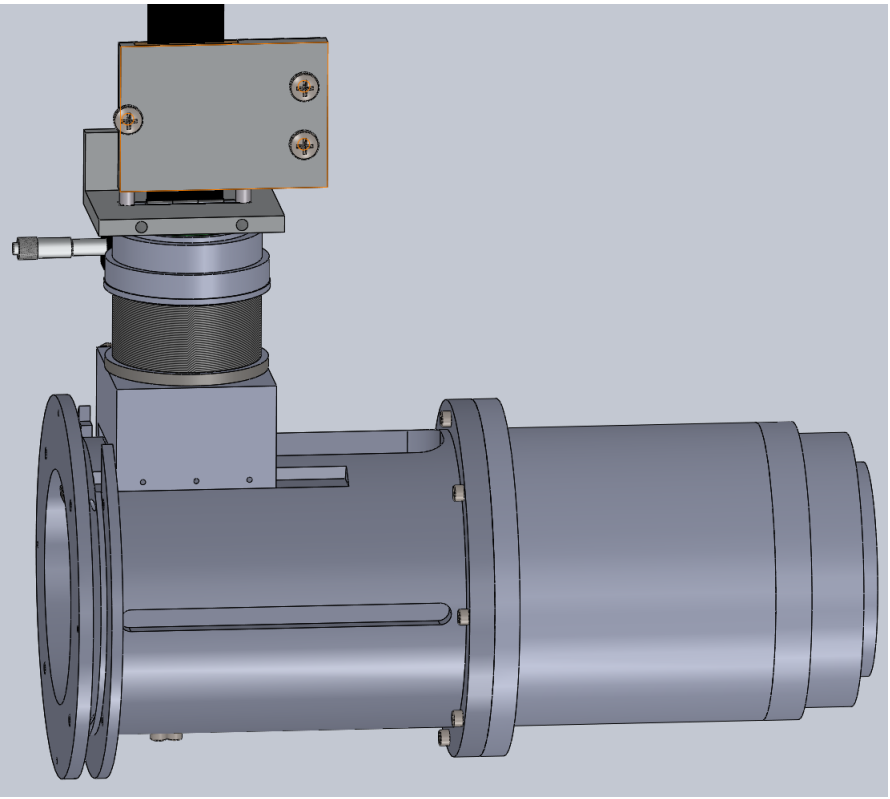

Figure 3.3: SolidWorks rendering of the slit block attached to the collimator.

Because the collimator has to be replaced, the imaging mode of the Goodman Spectrograph is lost when CINDERS is in use. Behind the IFU support, we attach an Andor EM-CCD camera which points down towards an Edmund Optics 0.25x telecentric lens fed by a right angle Aluminum enhanced coated mirror. The mirror peers between the probes and accesses a $1.7' \times 1.7'$ FOV which is used to help position each probe. The camera and mirror are shown in the SolidWorks rendering of the x, y and z motion apparatus.

3.1.2: CINDERS Construction

We include here images of the completed parts described in the previous section.

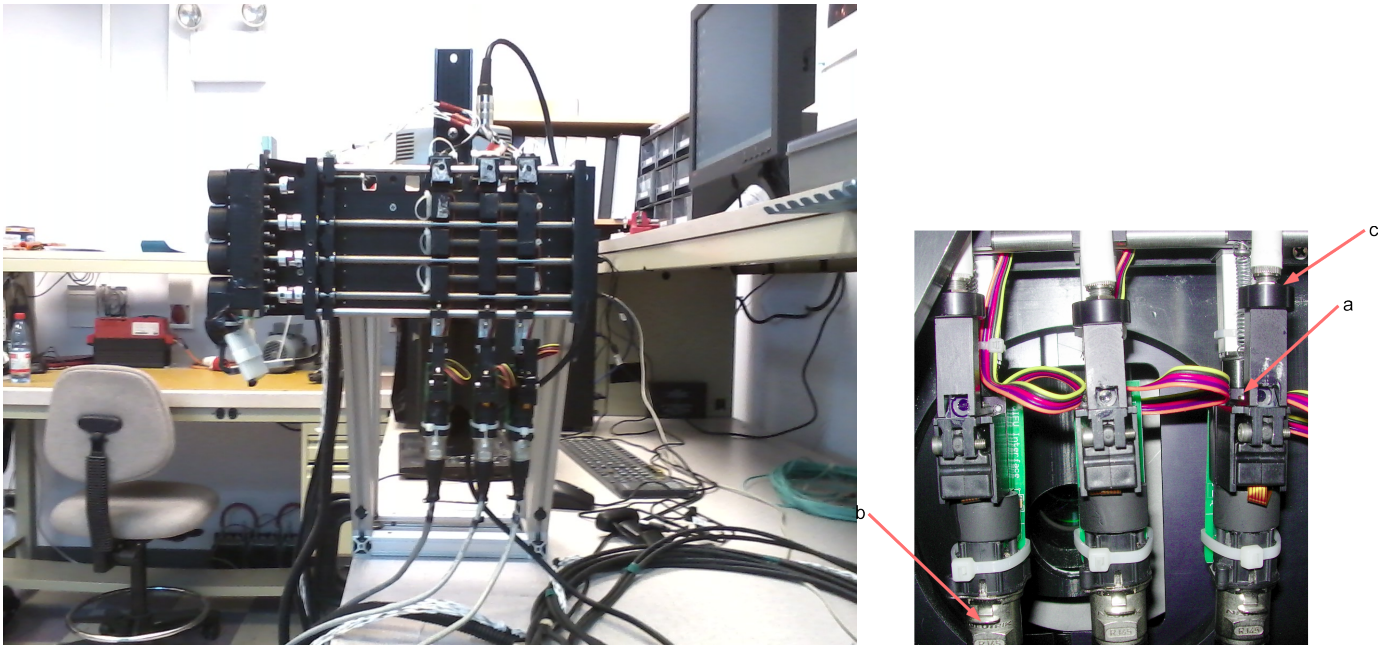

Figure 3.4: Left image: Front view of CINDERS. Right image: Front view of probes with prisms and lenses installed.

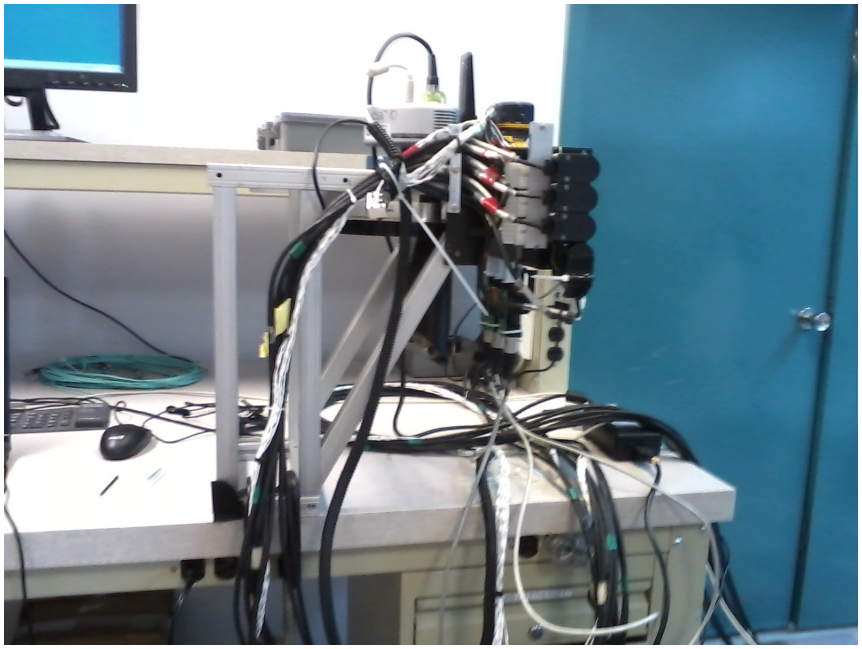

Figure 3.5: Side view of CINDERS to show ANDOR camera and field mirror.

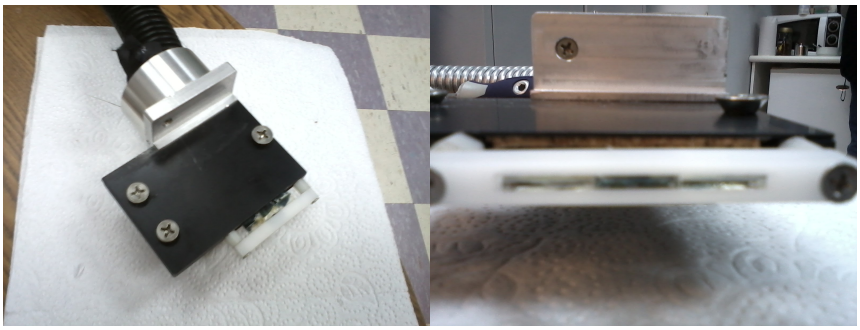

Figure 3.6: Left image: Slit block assemble that attaches to collimator. Right image: Showing glass block alignment.

Once parts were fabricated and assembled, we had to protect the exposed fibers at the slit block end of the bundles. We purchased silk fabric into which I sewed four parallel sheaths that each bundle could be carefully passed through. Once the fibers were safely covered, we passed the entire fabric protection sheath through a flexible, incompressible metal tube. The ends of each tube were dipped in black Plasti Dip^{TM} to cover sharp edges.

Figure 3.7: Left image: Top end of silk sheath with bundles. Right image: Sheath and bundles inside incompressible tube.

Once the bundles were protected, we epoxied the ends attached to the glass blocks to increase their stregth.

Figure 3.8: Left image: Glass block ends of fibers epoxied to increase strength and help prevent breakage. Right image: Bundle support for routing bundle and incompressible tube over gantry and collimator.

We developed a user interface to control the probes and ANDOR camera. We used Python software that can move the probes in x, y and z and control the filter wheel and ANDOR camera. The upper left of the GUI controls the exposure time and filter of the ANDOR camera. The resulting images are shown in the large box at the bottom of the GUI. The probe motions are controlled in the white text box above the position grid. The position grid tells you the probe's current positions and the grid to the right tells you if a probe is at its x-limit. I also developed a user interface for visualizing the positioning of probes on sky. This program shows a box that represents the FOV of CINDERS overlaid onto a DSS image which takes into account the rotation of the Goodman Spectrograph. Small $1.7' \times 1.7'$ boxes are also drawn on the center field and over targets to represent the ANDOR FOV. The program takes the x, y and z distances moved by the probes and draws circles representing the bundle diameters at the correct on-sky positions.

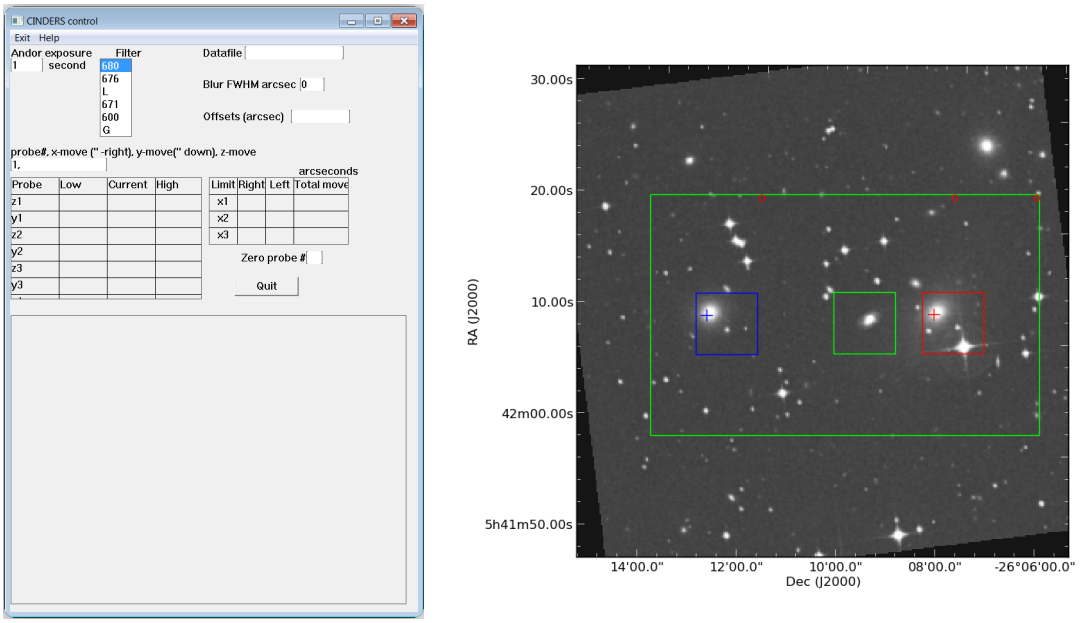

Figure 3.9: Left image: Image of probe control GUI. Right image: Output of CINDERS Field Viewer.

3.1.3: CINDERS Commissioning

Two commissioning runs were completed during October and November of 2013. During the October engineering run, our goals were to

1. Set-up CINDERS in the SOAR lab for testing and assembly
2. Attach the metal fiber feed to the slit end of the incompressible tube
3. Put apoxied fiber blocks into manufactured slit block
4. Attach ANDOR camera and tension mount to IFU gantry
5. Attach fiber support block to gantry
6. Make sure probe and camera control software work on computer at SOAR
7. Test positional accuracy of x, y and z motors
8. Test focus of fibers on CCD

All of this had to be done before my observing runs on the 24th and 25th of October. I completed all tasks except the last two. When CINDERS was put on Goodman, one of the probes fell off its y-axis motor. The

tension screws were worn and untrustworthy. So we removed CINDERS from Goodman and figured out a new way to hold probes on motors. The new pieces could not be fabricated and installed by my observing runs so I gave up that time. Eduardo Serrano, the head engineer at SOAR, fabricated and installed the pieces in the following weeks. I returned to SOAR in November to continue commissioning.

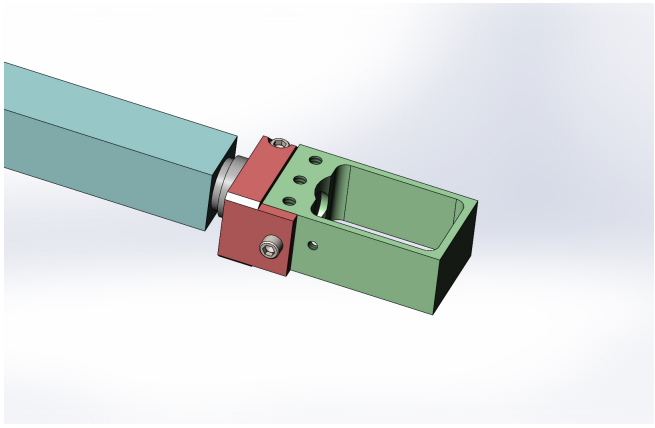

Figure 3.10: Solid Works rendering of attachment to reliably hold probe onto y-motion assembly.

During the November engineering run, we compiled a list of tasks to complete before my November 29th and December 8, 9 observing runs. Now that the probes were reliably attached we could pin down the focus on the CCD camera and better understand probe motions. While testing the accuracy of the motor positioning, it became apparent that the motions were not reliable. In many instances, the y and z motors would not return to their starting positions at first command but would register that they had moved in the control GUI. The x motions had additional movement after hitting their limit switches that needed to be quantified. The tools necessary to do this were not available at SOAR. After placing CINDERS on Goodman and making sure the motor control worked, we worked on pinning down the focus. This required adjusting the distance between the collimator lens at the filter wheel end and the height of the fibers above the collimator. The best focus achieved, unfortunately, required the fibers at the upper and lower edges of the image to be out of focus due to a slight field curvature in the optics used in the collimator.

Despite all this, I attempted to observe on November 29. I discovered that the ANDOR camera field was not aligned with the SOAR field. This meant that the camera had to be raised by placing pieces of cork board under the camera. The screw that attached the camera to the gantry was no longer aligned so the camera had to be clamped in place. This meant we could not rotate the spectrograph so had to observe stars for the night. When looking at a standard, I realized that the probes were not facing straight down the light path so were not uniformly illuminated. The only fix was to take CINDERS off the spectrograph,

again, and use lasers and mirrors to properly align them. The tools needed to do this were not available at SOAR. I also did not have a way to reliably align the probes onto their targets, because I did not know where the center of the prism was in relation to the circuit board on the back. To fix this, I determined the size of the probe entrance and painted a square on the circuit board with white out.

Figure 3.11: Probe entrance indicated on back of circuit board with white out.

I made one final attempt to observe remotely from UNC-Chapel Hill on December 8 and 9, 2013. I spent both nights trying to align the probes on the brightest galaxies in group SCG0540-2610. The mis-alignment of the probes made it difficult to tell if I was actually on the centers of my targets. There was considerable glint in the spectra, perhaps due to the collimator cap not being on, before the grating. The ANDOR camera was also off center by 10" East and 24" North. The engineers had raised the camera by 11 inches and attached it to the gantry but this was apparently not enough.

Initial throughput measurements for the observed standard star are inadequate to do science. A plot of the throughput for bundle 3 is shown. Clearly, the probes are not aligned to the light path. The reconstructed image shows that we are pointed on the star, but the throughput estimates are significantly lower than expected.

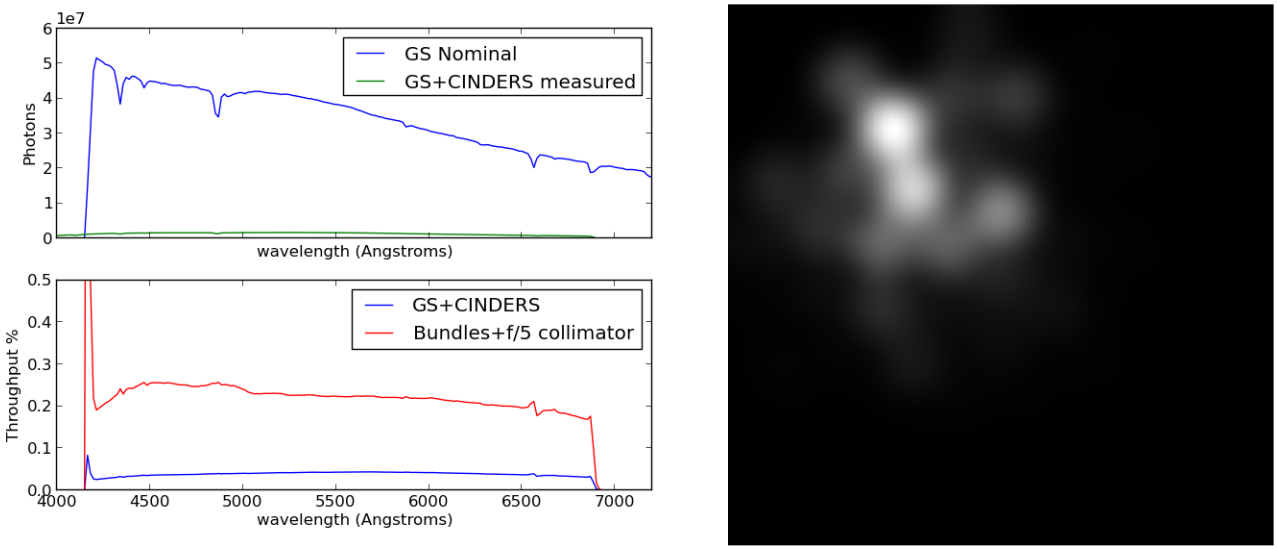

Figure 3.12: Left image: Throughtput for Bundle 3 on standard star HR3454. Right image: Reconstructed image of Bundle 3.

3.1.4: CINDERS Status

The CINDERS gantry and probes could not remain on the Goodman spectrograph indefinitely. The gantry can be lifted so the probes are out of the way of the slit mask assembly and guide probe but the height of the bundles prevented this from happening. The alignment of the probes needs to be adjusted by attaching CINDERS to an optics bench and using a system of mirrors and lasers. The unreliability of the probe positioning made the instrument impossible to use. I suggest buying more reliable y and z motion actuators. The movement of the x positioning at the limit switches needs to be accurately quantified as well. Because we cannot see through the probes, their positions must be reliably known.

3.2: MOS

Because CINDERS was unusable in the time necessary for me to complete my dissertation, I aided in the commissioning of the multi-object capabilities that were being added to the Goodman Spectrograph.

3.2.1: MOS Design and Construction

The Goodman Spectrograph is the most used instrument on SOAR. The Goodman Spectrograph utilizes volume-phase holographic gratings [153] with $0.15"/pixel$ scaling over a wavelength range of $320-850nm$.

The spectroscopic FOV of the Goodman is $3' \times 5'$ and the imagining FOV is $7.2'$ in diameter. Currently, light from the 4-meter telescope is routed through a slit mask assembly into the $f/16$ collimator where it is collimated and passed through a grating, filter wheel and finally the camera. The slit mask assembly houses numerous slit masks which can be installed the same day as observations.

Masks are designed by the observer using software developed at UNC-Chapel Hill. The observer can specify slit position and position angle of the mask. The observer must also designate three alignment stars to align the mask before taking an observation. Masks are submitted to SOAR at least one month prior to the observing run.

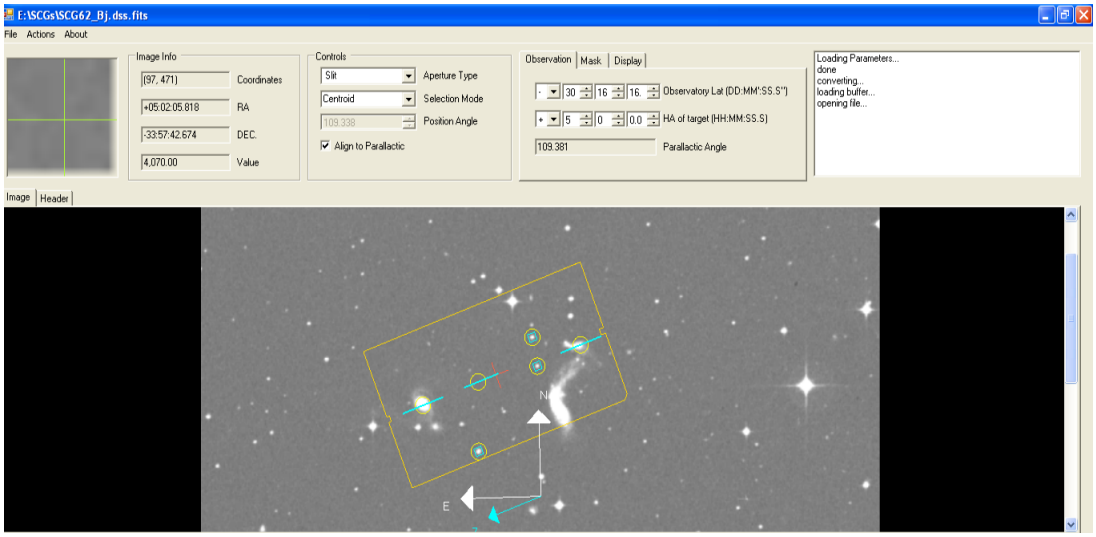

Figure 3.13: Screenshot of MOS Slit Designer tool.

The masks are installed into the slit mask assembly the day before your observations.

3.2.2: MOS Commissioning and Status

During February and March 2014, we used on sky time to test the alignment procedure of the slit masks. I chose some HCG galaxies to observe. The alignment procedure from positioning the slit mask to taking the first spectrum takes 15-30 minutes. Once the mask is in place, no further alignment is needed, even if switching between comparison lamps and the field during your observations.

The observer must first take images of the mask and the field for which the mask was designed. After opening the Multislit Alignment Tool on the Goodman LabView interface, the observer locates the alignment stars in the field image. The observer must then click on the mask tab and locate the alignment boxes on

the mask image. Once these are input, the alignment tool calculates the x, y and rotation offset necessary to align mask with field. Generally, one does this once, then a subsequent xy offset is usually necessary and can be done by hand.

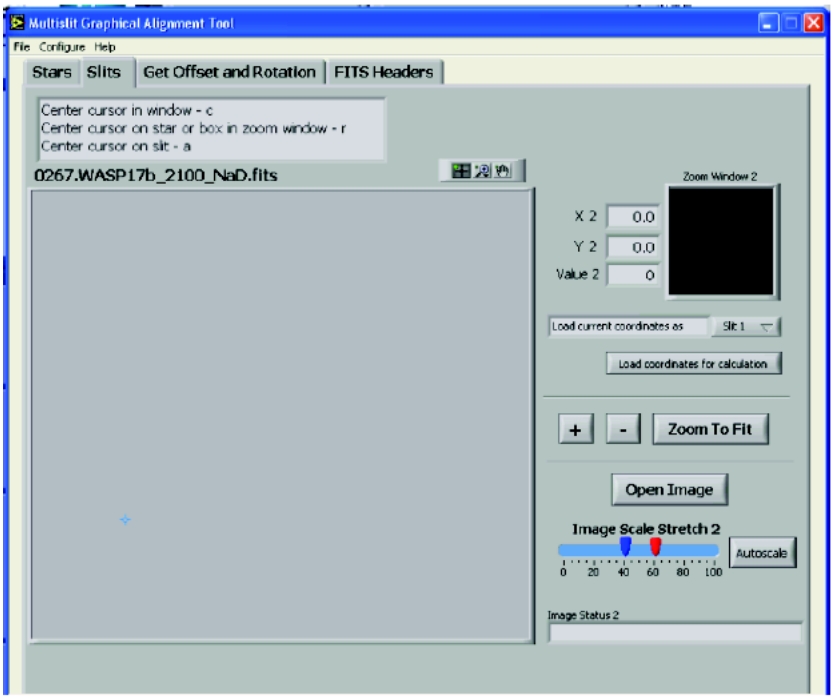

Figure 3.14: Screenshot of MOS Alignment tool.

After testing my observing strategy which involved switching between the field and comparison lamps after each 15 minute exposure, we deemed MOS commissioning a success and I proceeded to obtain data on the SCGs.

4: Data and Results

4.1: Data

I obtained data from the Goodman Spectrograph on the SOAR telescope during six nights over 2014-2015. 12 full groups and two partial groups were observed. Four groups could not be processed for this dissertation due to insufficient calibration data. In the following analysis, I focused on eight full groups and two partial groups. I used the 400 lines/mm grating, which provides spectral coverage from $3600 - 7200$Å. I binned both the spectral and spatial axes by two, which resulted in a spectral resolution of 1.98Å/pixel. Dome flats were taken for each mask with the dome lamp at 100% as well as zero second exposures (bias) with the shutter closed the afternoon before observations. I used the Atmospheric Dispersion Corrector (ADC) for all of my observations. The ADC corrects the aberrations caused by shorter wavelengths of light being refracted more than longer wavelengths by the atmosphere. Exposure times ranged from 30 minutes to 1.5 hours depending on the magnitude of the targets and the phase of the Moon.

Group	Galaxy	Magnitude (B_j)	Total exposure (s)	Date Observed
SCG07	A	14.897	1800	Aug 2014
	B	10.836	1800	Aug 2014
SCG08	A	14.107	1800	Aug 2014
	B	14.382	1800	Aug 2014
	C	10.484	1800	Aug 2014
	D	10.985	1800	Aug 2014
SCG72	A	14.219	1800	Aug 2014
	B	10.586	1800	Aug 2014
	C	10.528	1800	Aug 2014
	D	11.211	1800	Aug 2014
SCG13	A	14.729	5400	Aug 2014
	B	14.616	5400	Aug 2014
	B	14.616	1800	Aug 2014
	C	15.363	1800	Aug 2014
	D	12.821	1800	Aug 2014
SCG60	A	8.804	3600	Nov 2014*
	B	9.255	3600	Nov 2014*
	C	9.221	3600	Nov 2014*
	D	16.373	3600	Nov 2014*
SCG61	A	9.414	3600	Nov 2014*
	B	10.031	3600	Nov 2014*
	C	11.113	5400	Nov 2014*
	D	15.176	5400	Nov 2014*
SCG62	A	9.772	1800	Dec 2015
	B	11.280	5400	Dec 2015
	D	16.238	5400	Dec 2015
SCG65	A	9.645	4500	Jan 2015*
	B	9.474	5400	Jan 2015*
	C	10.267	5400	Jan 2015*
	D	11.389	4500	Jan 2015*

Group	Galaxy	Magnitude (B_j)	Total exposure (s)	Date Observed
SCG68	A	10.026	5400	Nov 2015
	B	15.530	5400	Nov 2015
	C	11.840	5400	Nov 2015
	D	15.818	5400	Nov 2015
	E	16.429	5400	Nov 2015
	F	16.458	5400	Nov 2015
SCG69	A	14.590	5400	Jan 2015*
	B	16.525	5400	Jan 2015*
	C	16.561	5400	Jan 2015*
	D	17.436	5400	Jan 2015*
SCG82	A	9.969	3600	Jul 2015
	B	15.304	3600	Jul 2015
	C	16.939	5400	Jul 2015
	D	17.048	5400	Jul 2015
SCG83	A	9.850	1800	Aug 2014
	B	10.637	2700	Aug 2014
	C	16.332	2700	Aug 2014
	C	16.332	3600	Aug 2014
	D	15.264	1800	Aug 2014
	E	16.464	3600	Aug 2014
SCG88	A	10.119	1800	Aug 2014
	B	12.252	1800	Aug 2014
	C	16.258	5400	Aug 2014
	D	16.487	5400	Aug 2014
SCG106	A	15.189	1800	Aug 2014
	B	15.923	1800	Aug 2014
	C	16.536	3600	Aug 2014
	D	16.655	3600	Aug 2014

Table 4.1: SCG observations. Observations with * were not used in this analysis.

Individual exposures were 15 minutes so that HgAr comparisons were stable. Comparison lamp spectra were taken between each 15 minute exposure. I also took spectrophotometric standards each night for flux calibration.

Standard	Date Observed
CD34241	Aug 2014
HR1996	Nov 2014,Dec 2015
LTT3218	Jan 2015
LTT9239	Jul 2015
LTT1788	Nov 2015

Table 4.2: Table of spectrophotometric standard observations.

4.2: Reduction and Processing

Data reduction and processing followed the procedure outlined below.

1. Note which regions of my images I do not want to include in the final spectrum and determine where each slit is located on my image using the IMPLOT task in Pyraf.
2. Note which slit is the sky slit, if one is present.
3. Bias subtraction using CCDPROC
4. Cosmic Ray removal using a Python version of Pieter van Dokkum's L.A.Cosmic algorithm[154].
5. Separate each slit from the image for all the science, flat and comparison files.
6. If the galaxies observed cover the entire slit so that there is no pure sky regions, process the sky slit first.
   (a) Combine dome flats using FLATCOMBINE (average)
   (b) Normalize combined dome flat using TWODSPEC.LONGSLIT.RESPONSE
   (c) Divide from sky slit images and comparison images using CCDPROC
   (d) Combine consecutive comparison files
   (e) Find wavelength solution using TWODSPEC.LONGSLIT.IDENTIFY, REIDENTIFY, FITCOORDS & TRANSFORM
   (f) Combine different sky slit images into one file using IMCOMBINE (average)
7. If there is a standard star observed, process it and determine the flux calibration.

(a) Combine dome flats using FLATCOMBINE (average)

(b) Normalize combined dome flat using TWODSPEC.LONGSLIT.RESPONSE

(c) Divide from standard images and comparison images using CCDPROC

(d) Combine consecutive comparison files

(e) Find wavelength solution using TWODSPEC.LONGSLIT.IDENTIFY, REIDENTIFY, FITCOORDS & TRANSFORM

(f) Subtract the sky from the standard spectra using TWODSPEC.LONGSLIT.BACKGROUND

(g) Extract the standard spectra TWODSPEC.APEXTRACT.APALL

(h) If there are multiple images of the standard, average them together.

(i) Calculate extinction and derive sensitivity function using ONEDSPEC.STANDARD & SENSFUNC

8. Now for each slit with a galaxy, I follow this process

(a) Combine dome flats using FLATCOMBINE (average)

(b) Normalize combined dome flat using TWODSPEC.LONGSLIT.RESPONSE

(c) Divide from galaxy images and comparison images using CCDPROC

(d) Combine consecutive comparison files

(e) Determine the FWHM of the comparison lamp lines using SPLOT and fitting Gaussians to the lines and averaging. Do this for central row in all comparison files for a single galaxy. There will most likely be one comparison file for each separate 15 minute exposure.

(f) Find wavelength solution using TWODSPEC.LONGSLIT.IDENTIFY, REIDENTIFY, FITCOORDS & TRANSFORM

(g) Perform sky subtraction:

i. If sky is present in the slit, use TWODSPEC.LONGSLIT.BACKGROUND

ii. If sky is not present in slit, I take the sky slit and divide it into two halves which I place above and below the galaxy spectrum. This allows me to use TWODSPEC.LONGSLIT.BACKGROUND to fit the background.

(h) I create a new fits file with just the galaxy spectrum, excluding any part of the slit that just has sky.

(i) Now it is time to bin up the spectra along the slit axis in 1", 3", 5" and 10" bins and add up all our observations:

   i. Determine where the brightest part of the galaxy is (center)

   ii. Create the first bin centered here

   iii. If there is room above or below create subsequent bins until we reach the edge of the galaxy on either side of the central bin

   iv. Because there is more than one observation, for each exposure the new bins are added to the previously created bins until we loop through all the exposures.

   v. Resample each bin for each image 100 times and determine the standard deviation in each pixel. Use these to determine the error in each pixel for the summed spectra.

   vi. Save the first 25 sampled spectra to feed into STARLIGHT to get errors later on.

(j) Extract the spectrum using TWODSPEC.APEXTRACT.APALL

(k) Flux calibrate each summed bin and extracted galaxy spectra:

   i. If there is a standard star observation, flux calibrate using ONEDSPEC.CALIBRATE on each bin

   ii. If there is not a standard star observation, flux calibrate using a fiducial sensitivity function derived from the Goodman Throughput, CTIO extinction curve, the energy at a given wavelength and the area of SOAR.

   iii. Do this same process on the errors.

(l) Use NED to get the A_V value for the galaxy.

(m) Deredden each summed bin using this value and ONEDSPEC.DEREDDEN. Apply to errors also.

(n) Redshift correct each summed bin and extracted spectrum by identifying the Calcium H&K lines and passing the determined redshift to ONEDSPEC.DOPCOR for each bin. Also correct errors.

(o) Resample each summed bin and extracted spectrum to 1Å for STARLIGHT using ONEDSPEC.DISPCOR. Also resample errors.

(p) Smooth each MILES template from 2.5Å to the observed resolution using Python Gaussian filters. Also smooth errors.

(q) Flag emission lines and regions where the spectrum is ≤ 0 in each summed bin so STARLIGHT ignores them.

(r) Create the text files for each summed bin and extracted spectrum to feed into STARLIGHT. If more than 1/3 of the spectrum is flagged, do not create an text file.

(s) Fit each summed bin and extracted spectrum with STARLIGHT. Then fit the Gaussian sampled files to get errors.

(t) When finished, I check the residuals of each fit and update the redshift correction if necessary using ONEDSPEC.DOPCOR.

(u) Once I have all the spectra fit, I feed each spectrum to PYSPECKIT to fit the emission lines.

i. Subtract the model spectrum from the observed spectrum to create an emission spectrum.

ii. Errors for emission spectrum are determined via propagation of error

$$\sigma_e = \sqrt{\sigma_o^2 + \sigma_m^2} \tag{4.1}$$

iii. Fit the lines listed in Table 2.4 if the flux in the region ± 10Å around the line center sums to 5 times the rms noise in the wavelength region $4730 - 4780$Å.

iv. For errors, we create 25 Gaussian sampled emission spectra and fit each of those separately. The standard deviation of the fits is the error on the final emission spectrum.

4.3: Analysis

I seek the effect that group membership has on the stellar populations and activity of galaxies in SCGs. To study the stellar populations, I took the weighted average of the ages and metallicities reported by STARLIGHT as outlined in Chapter 2.2.3. For each age and metallicity bin I also took the weighted average of the corresponding metallicities and ages. This provided the average metallicity and average age of the young, intermediate and old populations. I plotted the weighted average of the age or metallicity of the population considered versus its calculated average in metallicity or age respectively. The averages for the ages and metallicities were weighted by the fraction of light and mass contributed to the model by each template at the flux normalization wavelength described in Equations 2.6-2.9[140]. Because these are not actual light and mass fractions, contributions are not required to sum to 100%. Light weighted averages are dominated by the younger populations and mass weighted averages are dominated by the older populations. When analyzing results, I took this into consideration. For example, the metallicities of older populations were taken from the mass weighted averages in preference to the light weighted averages.

I only considered measurements made on spectra with $S/N \geq 20$ in the blue region ($\lambda \leq 5400$Å) of the observed spectrum. Other authors have used S/N ratios smaller than this ($S/N > 5$[135]), but because I am binning along the slit, the bins very quickly reach regions dominated by noise. In those cases, the summed flux is averaged, so the signal is quite low. $S/N \geq 20$ guarantees adequate STARLIGHT fits and that I am

analyzing actual signal.

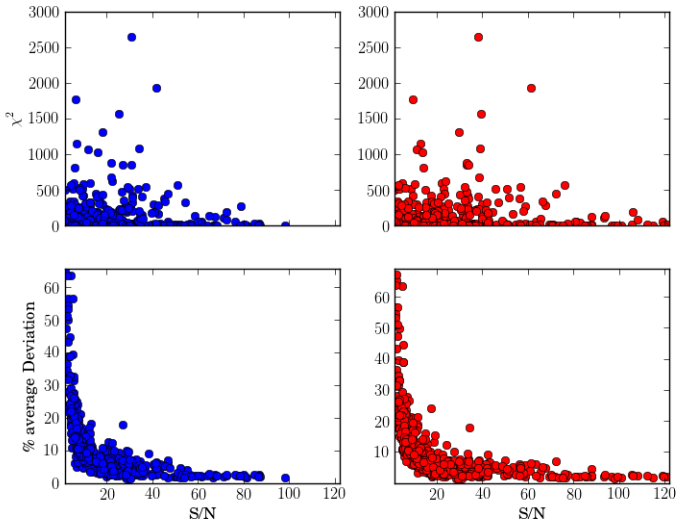

Figure 4.1: The top two plots are of the χ^2 values for our fits as a function of S/N in the blue and red regions of the observed spectrum. The bottom two plots show the percent deviation of the fitted model $\frac{|O_\lambda - M_\lambda|}{M_\lambda}$ as a function of S/N. The percent deviations are level starting at around a S/N of 15.

From the SP analysis, I can determine when the most recent episode of SF occurred and the metallicity of the gas used to create those stars. Stars with low-metallicity imply that the galaxy is fed unprocessed, cold gas from the intergalactic medium. Mid and high-metallicity stars indicate that the stars were created using preprocessed gas. Young stars mean that the last episode of SF occurred < 0.1 Gyrs ago, intermediate stars mean that the last episode occurred between $0.1 - 4$ Gyrs ago and, old stars > 4 Gyrs ago. I provide a flow chart outlining the conclusions I can draw from these plots.

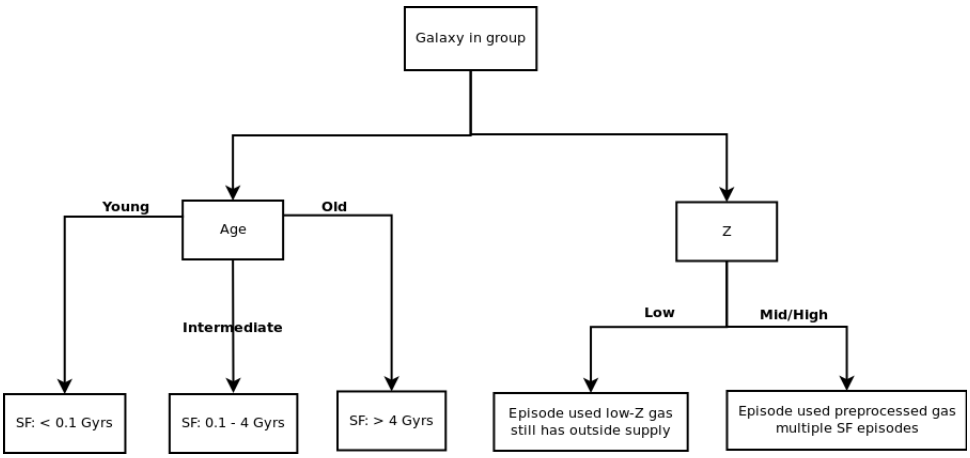

Figure 4.2: Flowchart for determining SP properties.

To study activity, I created BPT diagrams as discussed in Chapter 2.3.1. Emission lines were measured if flux in a ± 10Å window surrounding the line center summed to 5 times the rms noise in the wavelength region $4730 - 4780$Å. An example of an emission spectrum from the central 3" region of a galaxy in SCG08 is provided below.

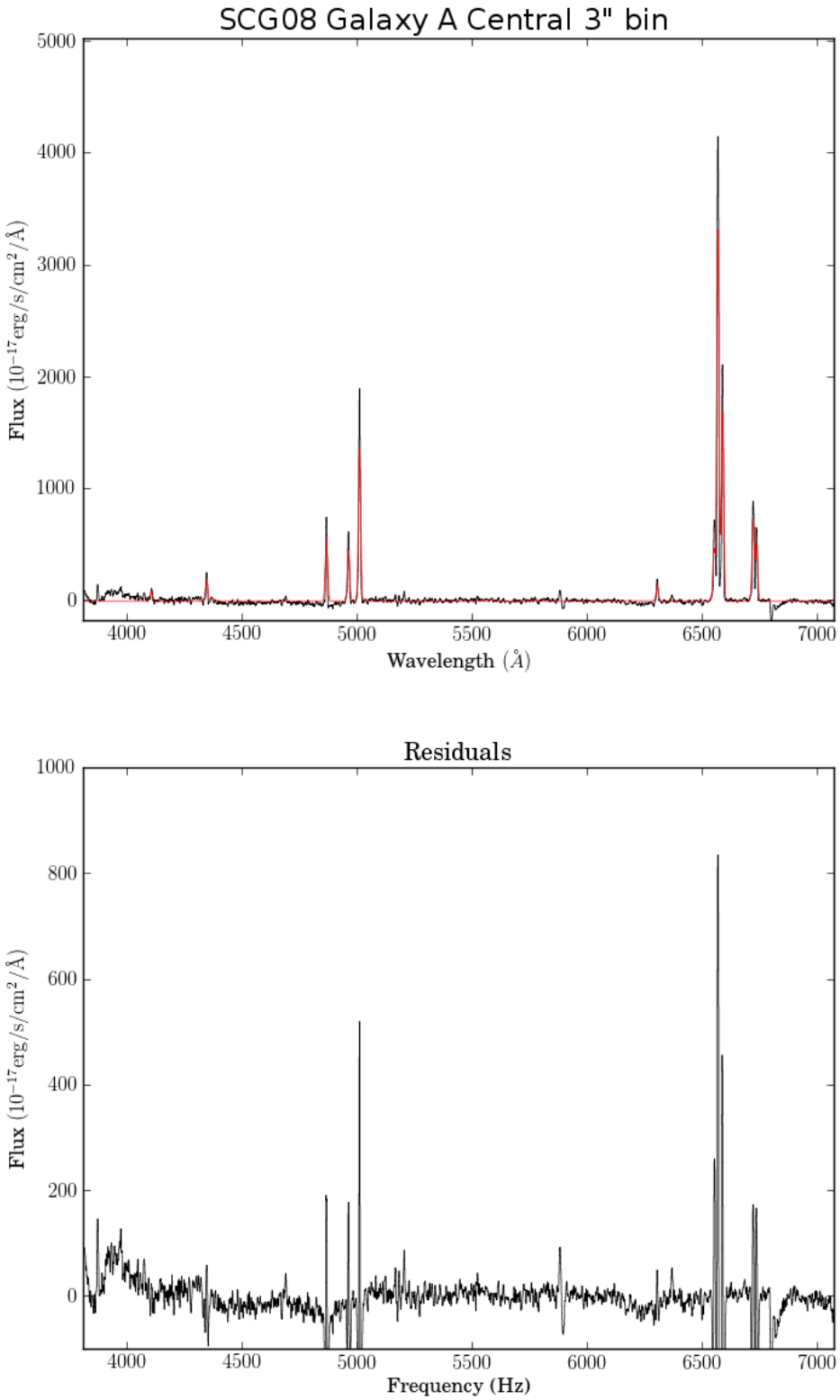

Figure 4.3: Emission spectrum and fit for SCG08 Galaxy A. The black line is the observation and the red line is the fit. The bottom plot shows the residuals of the fit, note vertical scale change.

My analysis focused on each group individually, organized by bin size, and noted the difference between galaxies that are actual members of the group, as defined by our group criteria, and those that are not. A galaxy is a member if the difference between its redshift and the redshifts of other possible members is ≤ 500 km/s. This number was chosen because it guarantees that the galaxies are close enough to have a gravitational influence on one another. On each plot, the values are represented by the group member designation (A, B, C, etc.) and are a larger font size if the galaxy is in the group. To study any radial effects on the parameters, I divided each galaxy into thirds based on the semi-major axis length and color coded each point based on the location of the spectrum along the spatial axis as shown in Figure 4.4 [23]. Errors are indicated by translucent ellipses under each member's name. To reduce clutter on plots, I ignored values with errors in age or emission greater than 1.5 dex because those errors spanned the age and emission ranges and did not provide useful information.

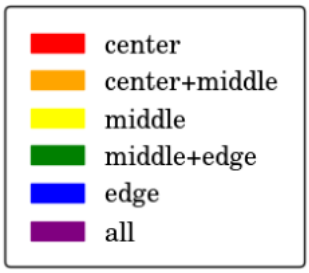

Figure 4.4: Region color coding.

In this dissertation, I include for each group my new results: a table of redshift differences between group members, an image of the group with sizes of 1", 3", 5" and 10" bins superimposed, a three dimensional plot of the galaxy distributions in space with the member designation sized as semi-major diameter measured by Iovino (2002) and converted to kiloparsecs, plots of the ages and metallicities of the stellar populations, and BPT diagrams for each bin size. I summarize the analysis of the stellar populations and activity in tables following the plots. In these tables, I abbreviate the age and metallicity designations as young (Y), intermediate (I), old (O), low (L), mid (M) and high (H), and the region designations as central (c), central+middle (cm), middle (m), middle+edge (me), edge (e) and all (a). In my analysis, only the all, central and middle regions met all requirements to be plotted.

4.3.1: Examples of Spectra

Before I discuss my results, I first show examples of the observed spectrum, the fitted STARLIGHT model, and their residuals for various bin sizes, exposure times and morphologies. In all plots, the dark gray line is the observed spectrum, the green line is the fitted model and the red line is the residual after removing the model from the observation.

Elliptical Galaxies

Below are the observed, model and residual spectra for early-type galaxies SCG88B and SCG68A. SCG88B had a 30 minute exposure and SCG68A had a 1.5 hour exposure.

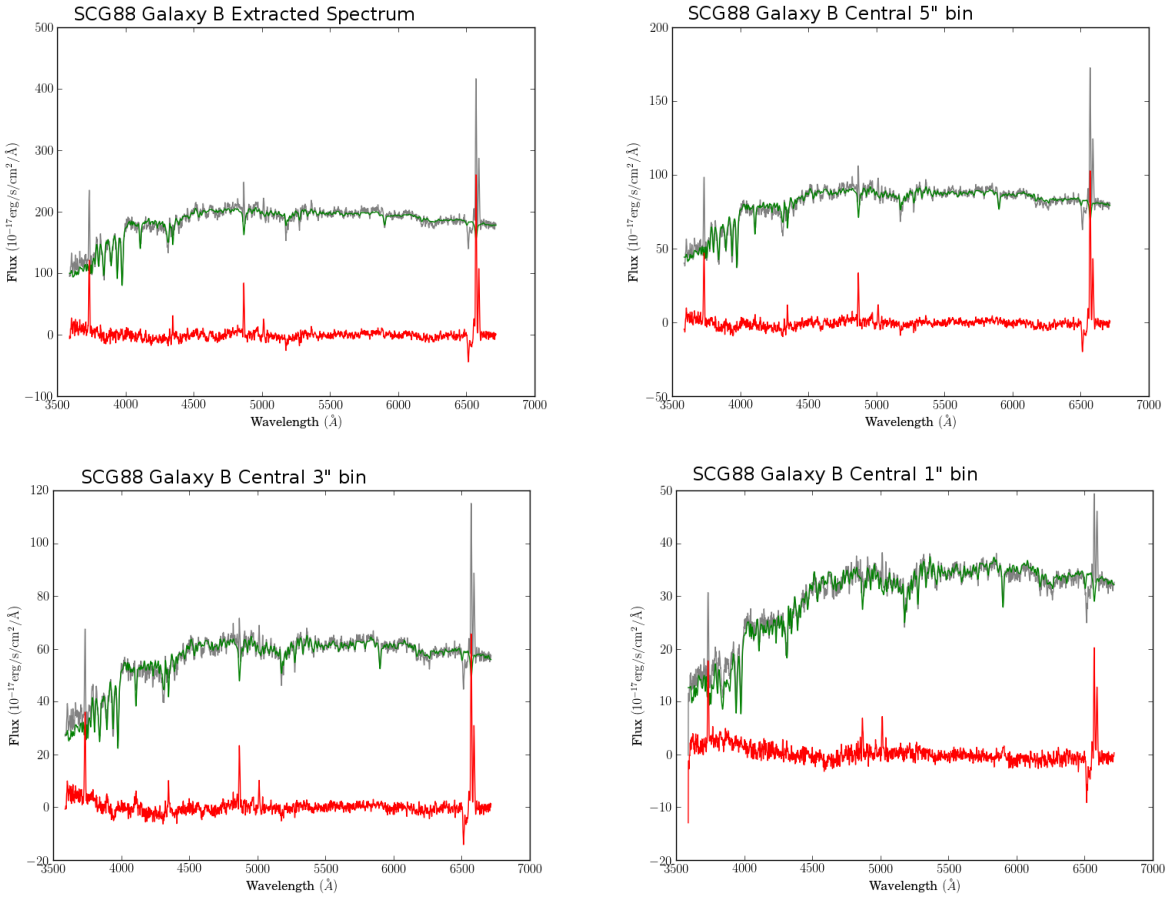

Figure 4.5: Central extractions for SCG88 B.

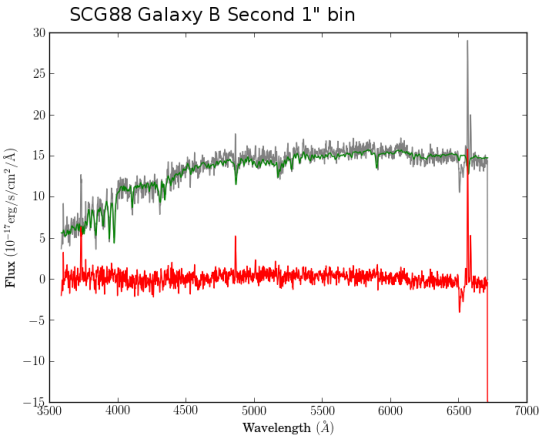

Figure 4.6: Outer extractions for SCG88 B.

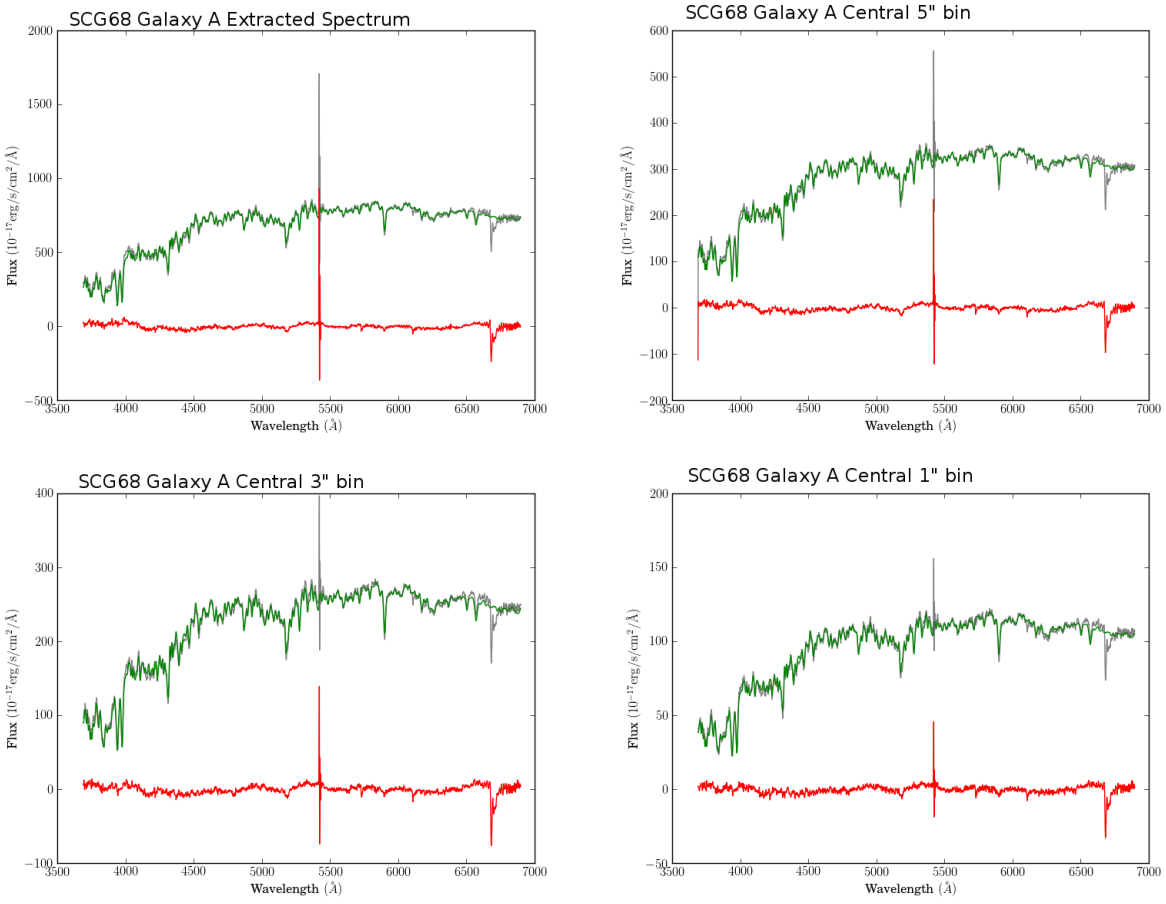

Figure 4.7: Central extractions for SCG68 A.

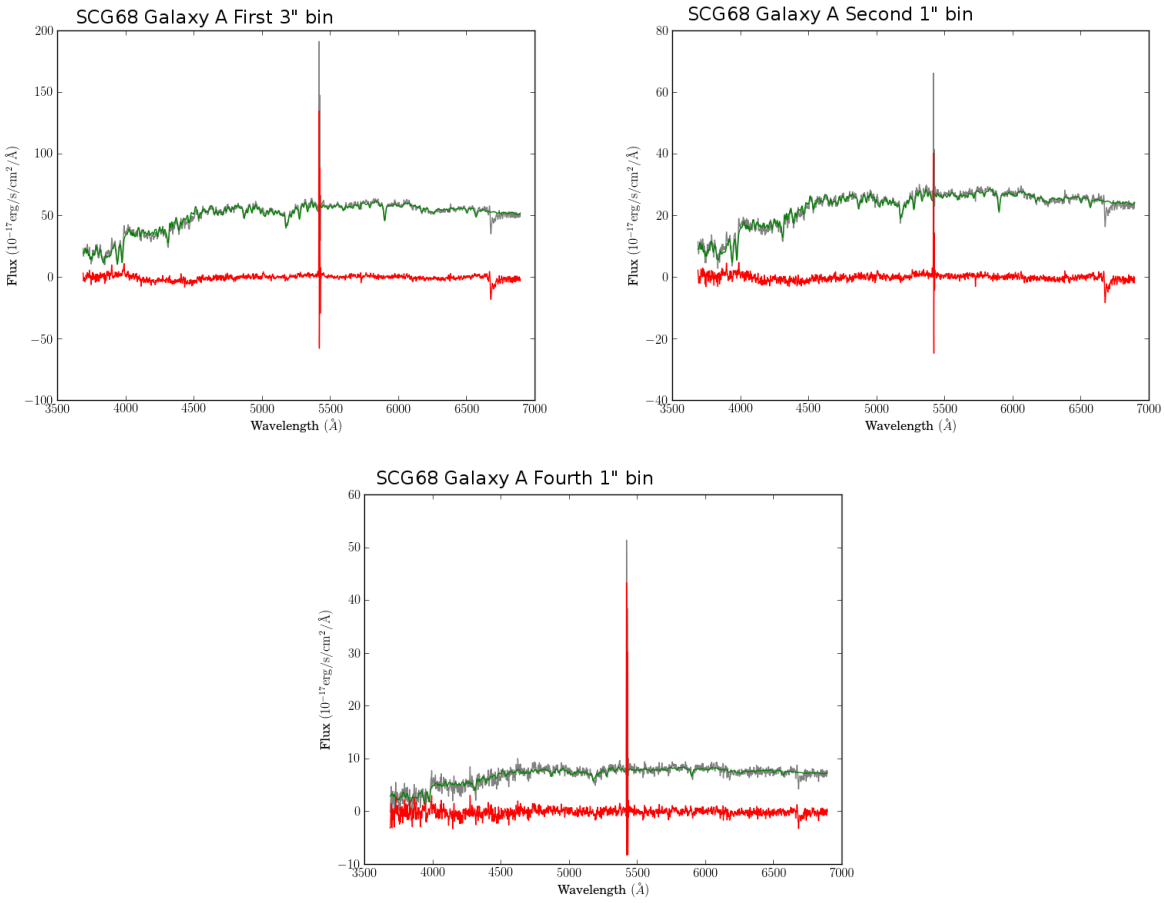

Figure 4.8: Outer extractions for SCG68 A.

Spiral Galaxies

Below are the observed, model and residual spectra for late-type galaxies SCG08A and SCG13B. SCG08A had a 30 minute exposure and SCG13B had a 1.5 hour exposure.

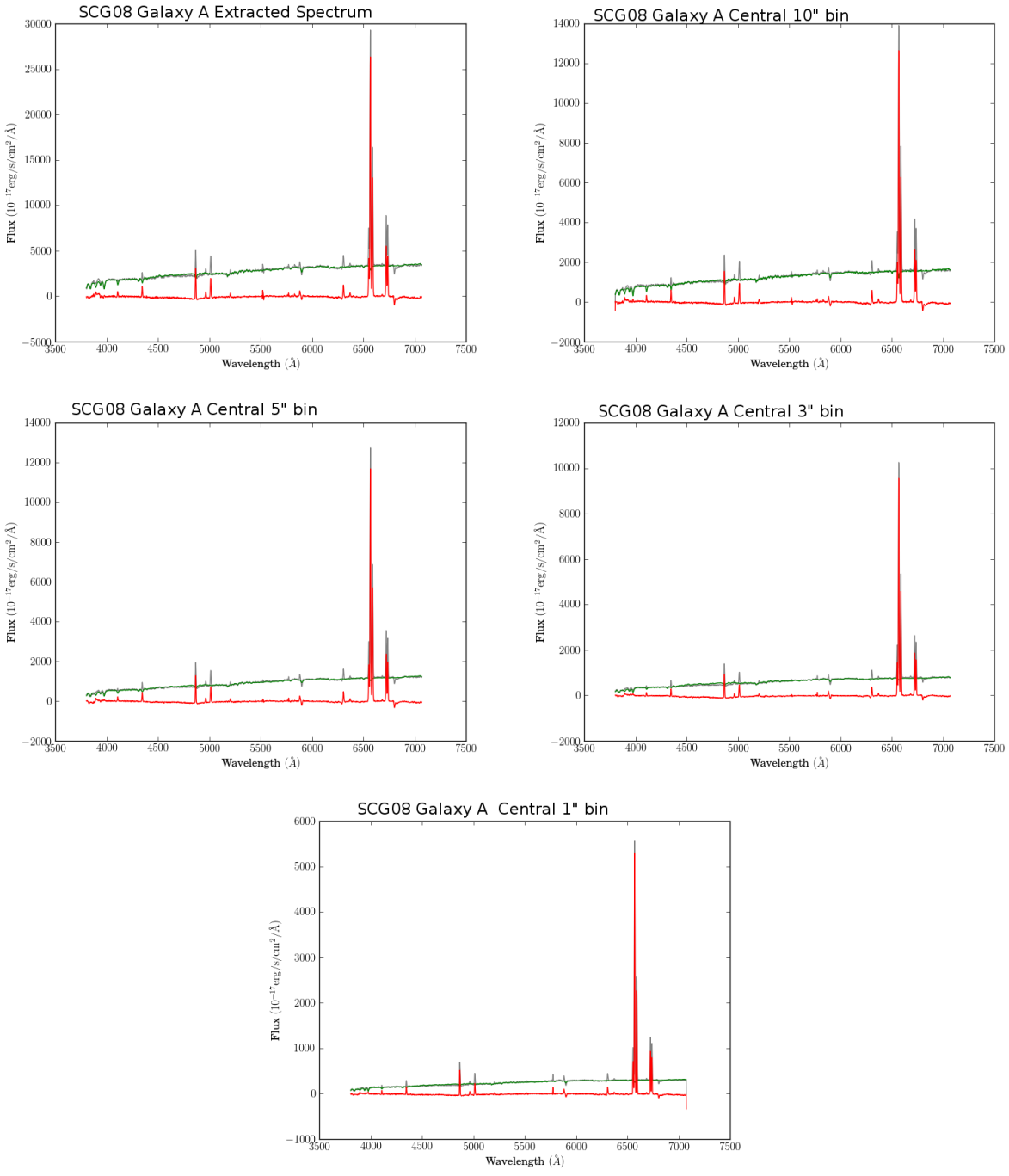

Figure 4.9: Central extractions for SCG08 A.

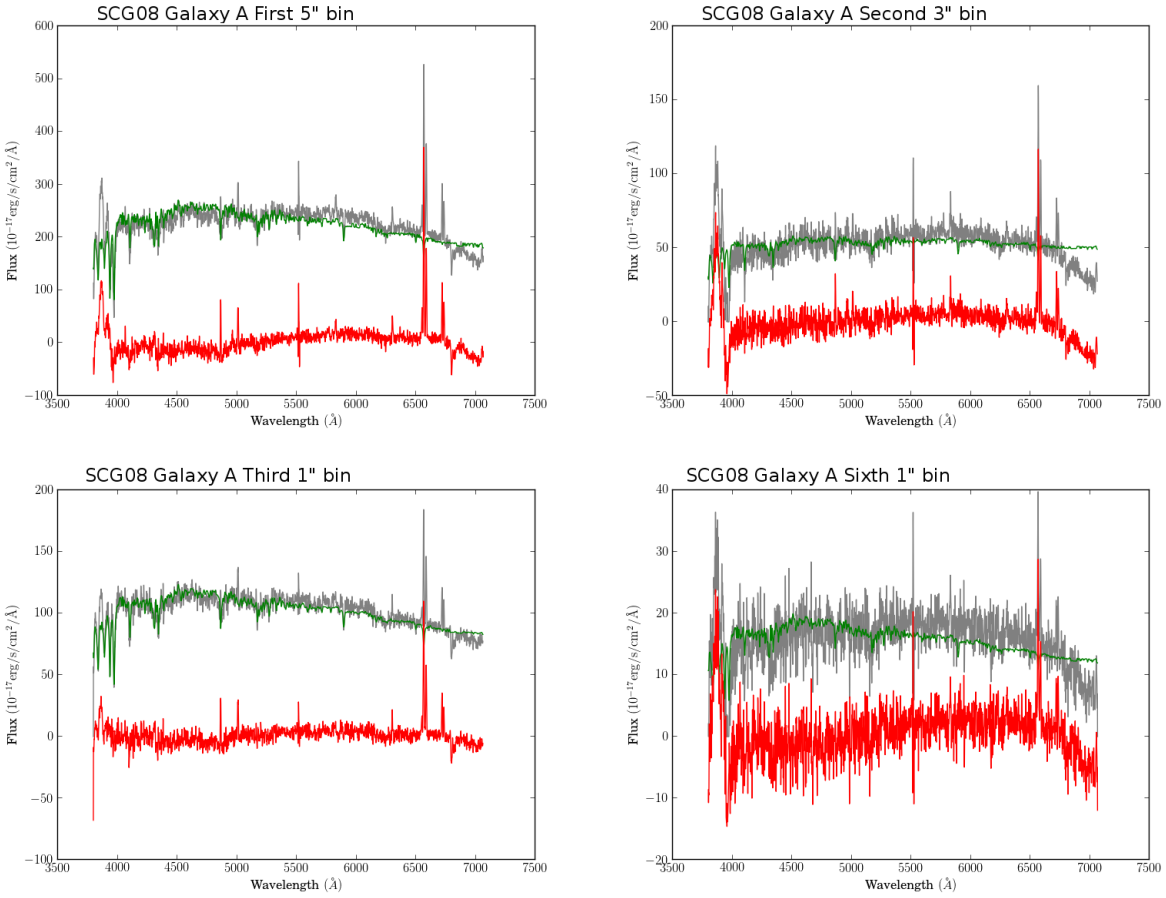

Figure 4.10: Outer extractions for SCG08 A.

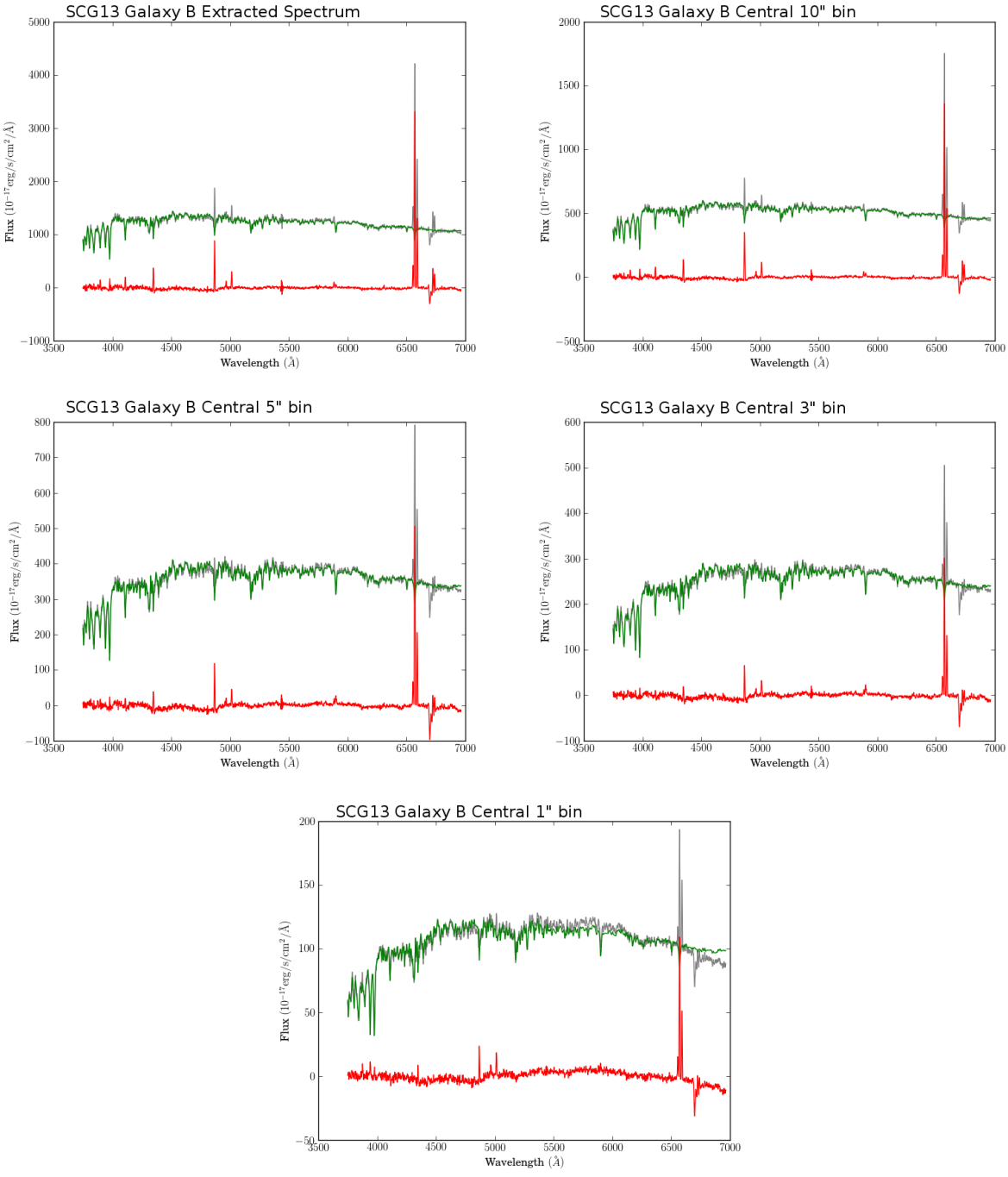

Figure 4.11: Central extractions for SCG13 B.

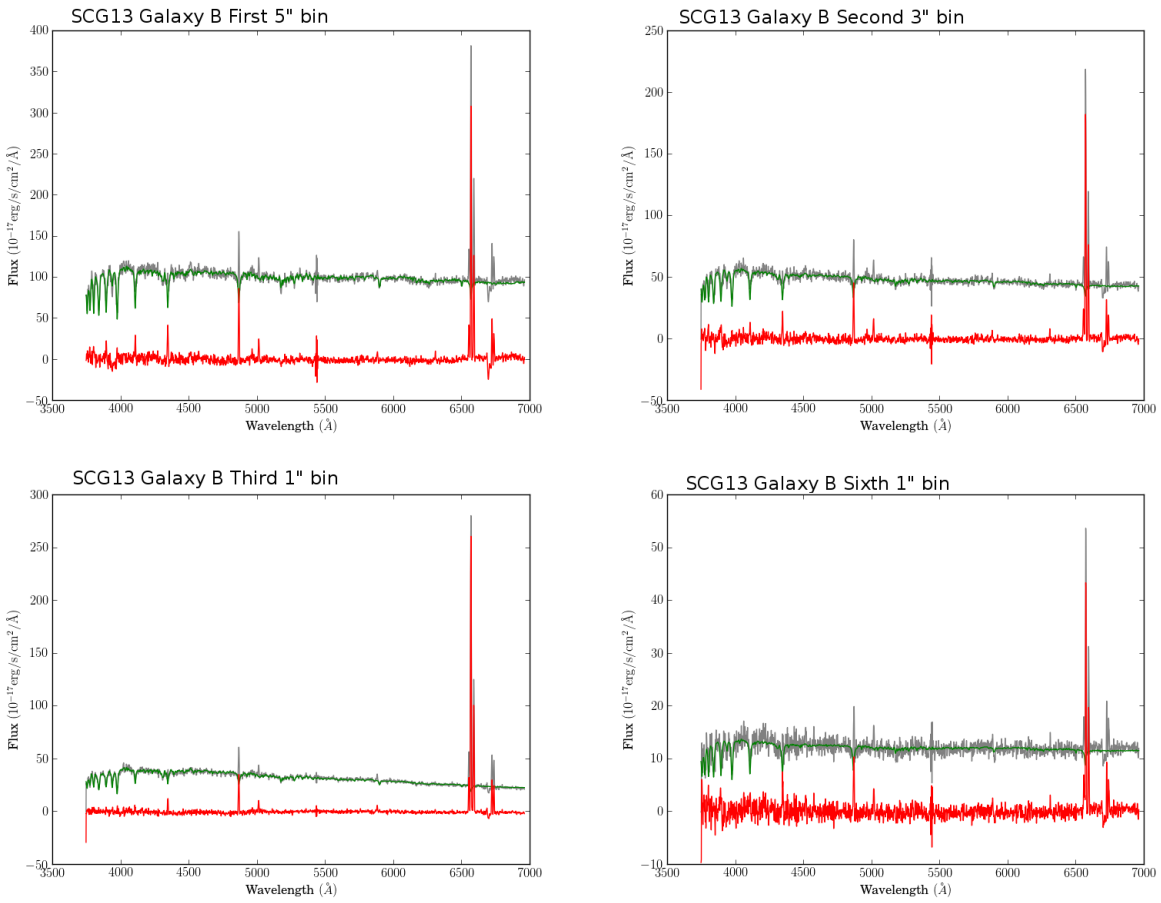

Figure 4.12: Outer extractions for SCG13 B.

Irregular Galaxies

Below are the observed, model and residual spectra for irregular galaxies SCG08C and SCG62D. SCG08C had a 30 minute exposure and SCG62D had a 1.5 hour exposure.

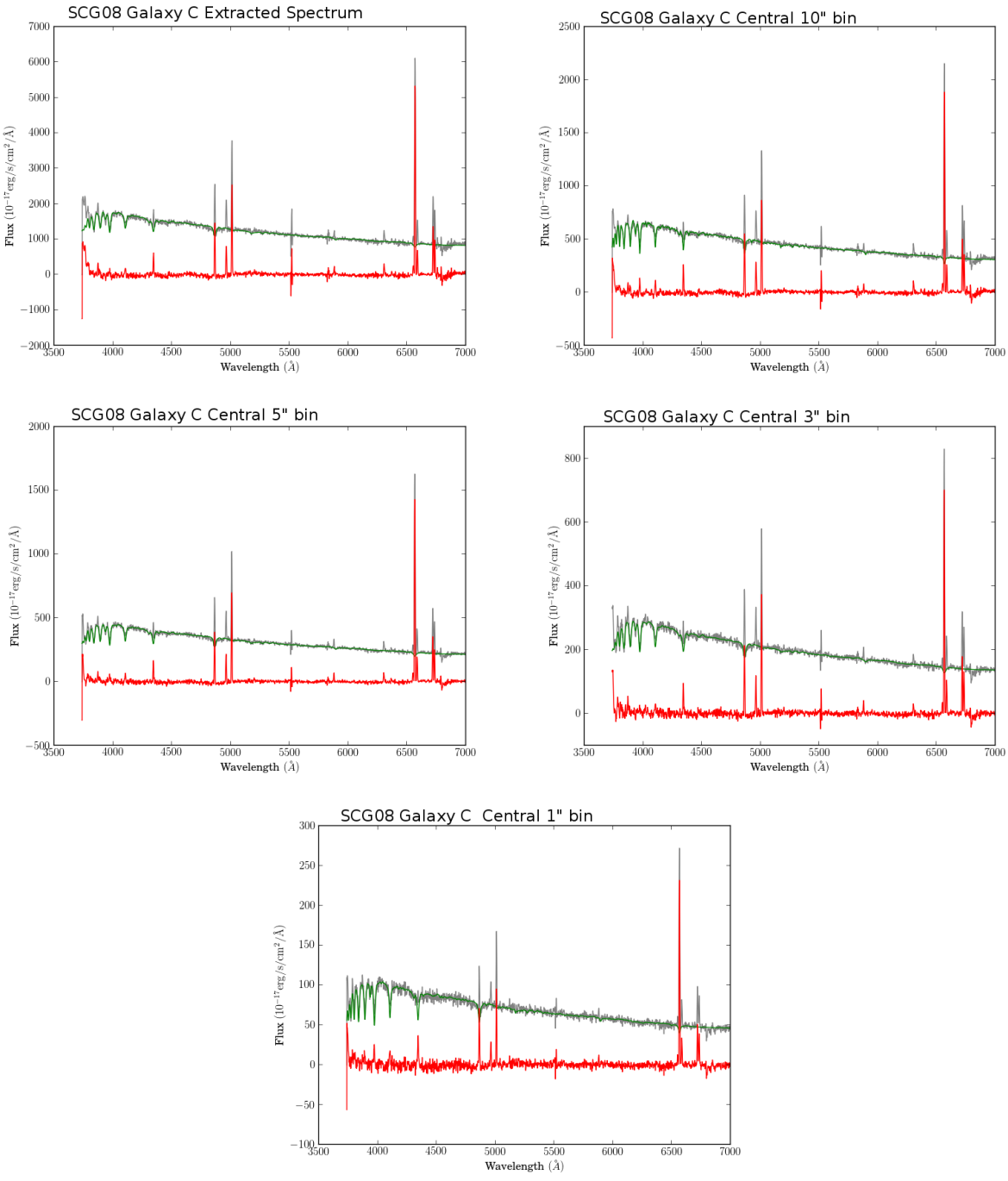

Figure 4.13: Central extractions for SCG08 C.

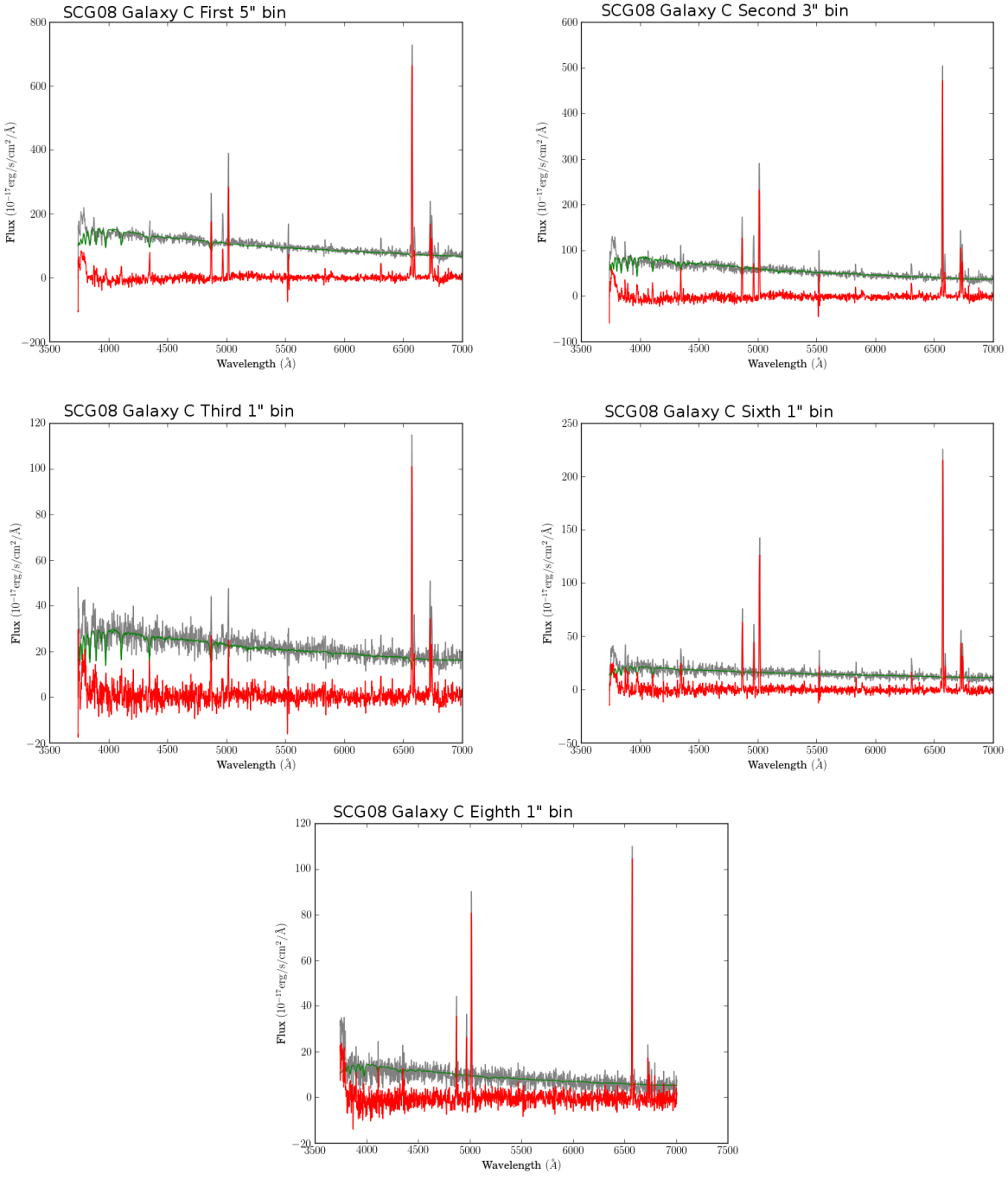

Figure 4.14: Outer extractions for SCG08 C.

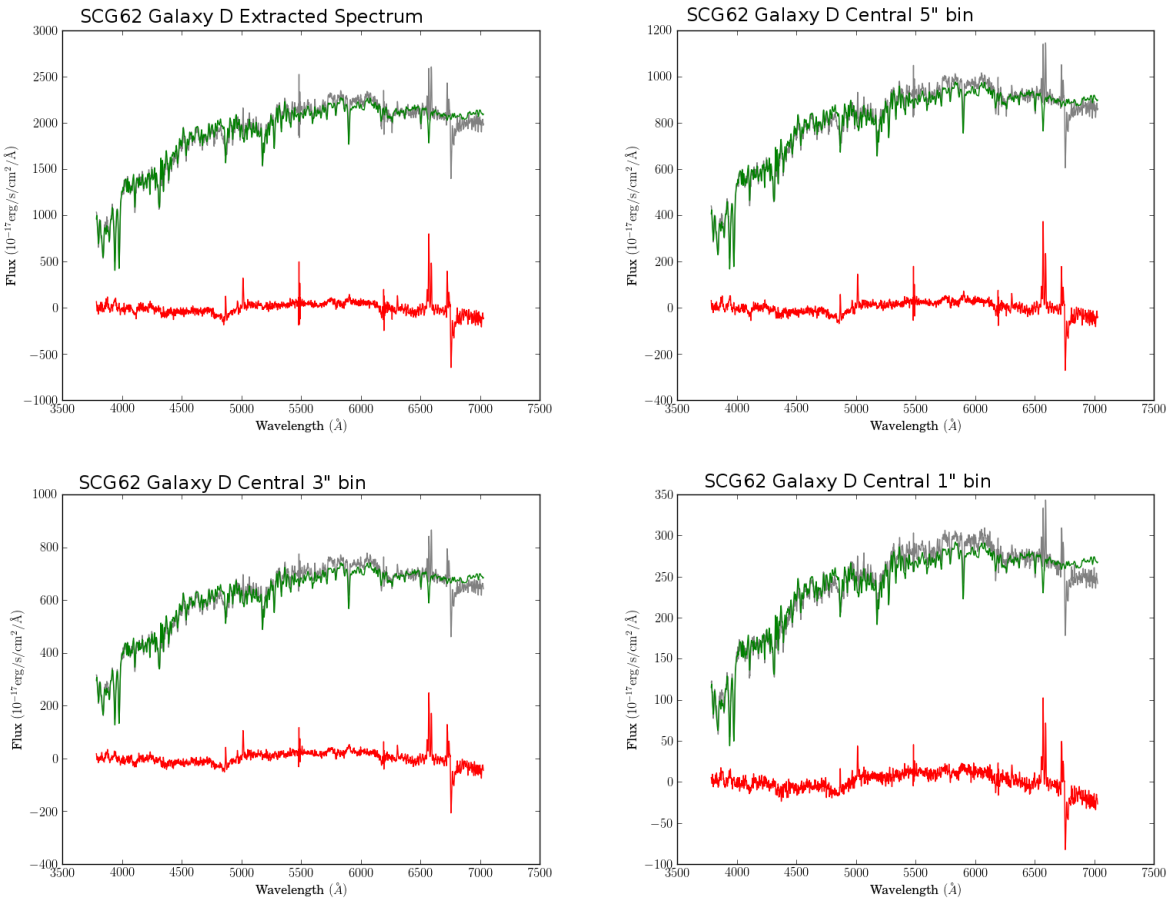

Figure 4.15: Central extractions for SCG62 D.

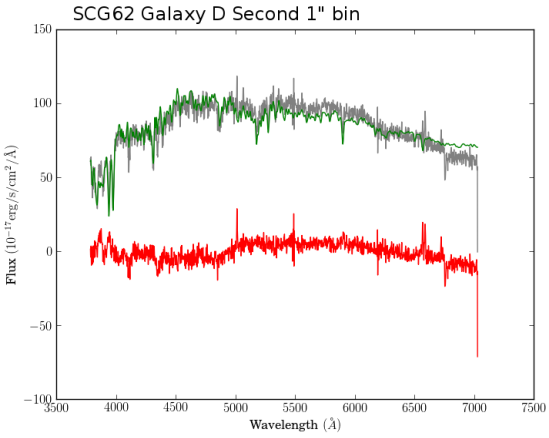

Figure 4.16: Outer extractions for SCG62 D.

4.3.2: SCG08

This group is comprised of four late-type galaxies with two members (A and C) showing signs of a recent interaction.

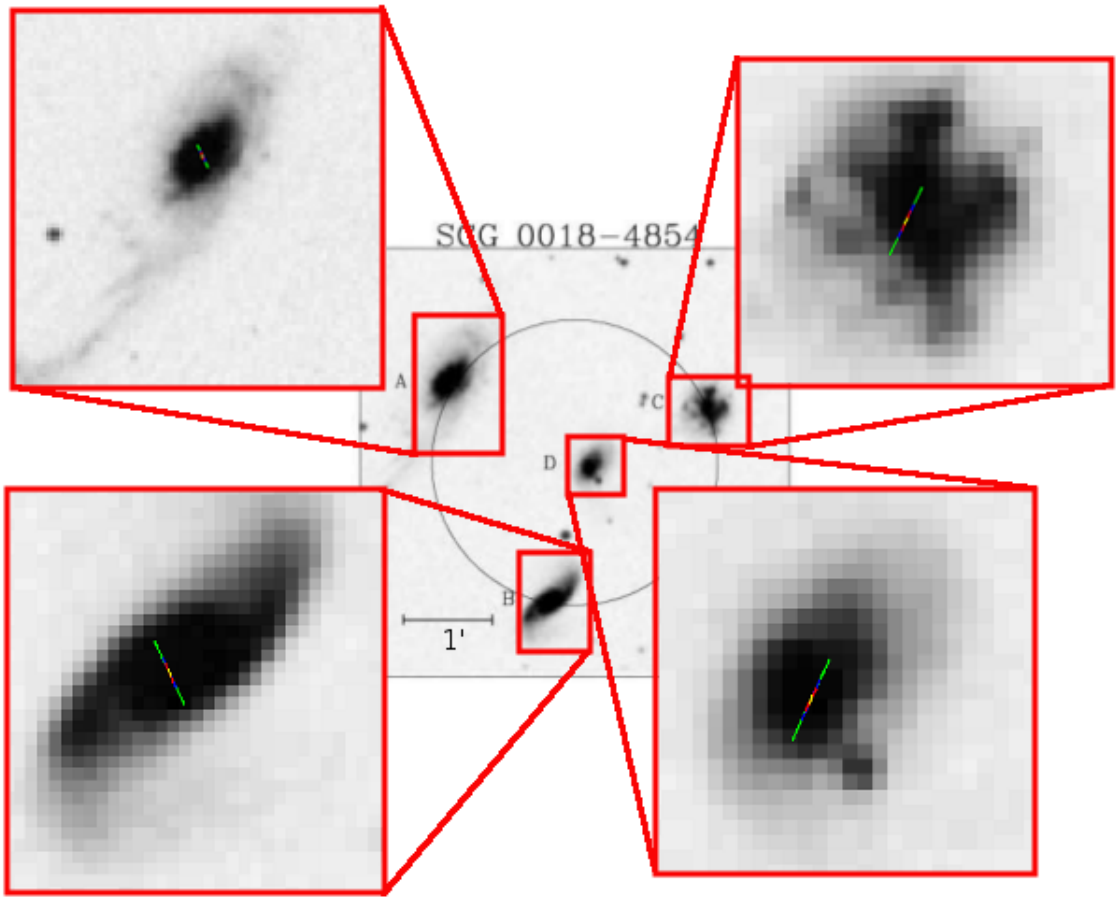

Figure 4.17: Group SCG08.

All four galaxies have velocity dispersions that include them in this group.

$\Delta z(km/s)$	B	C	D
A	−47.19	−36.9	106.74
B		10.29	153.93
C			143.64

Table 4.3: Derived redshift differences for group SCG08.

I also plot the galaxy positions in RA, DEC and redshift to get an idea of their 3d locations. From this plot, the galaxies all appear to be at the edge of the group.

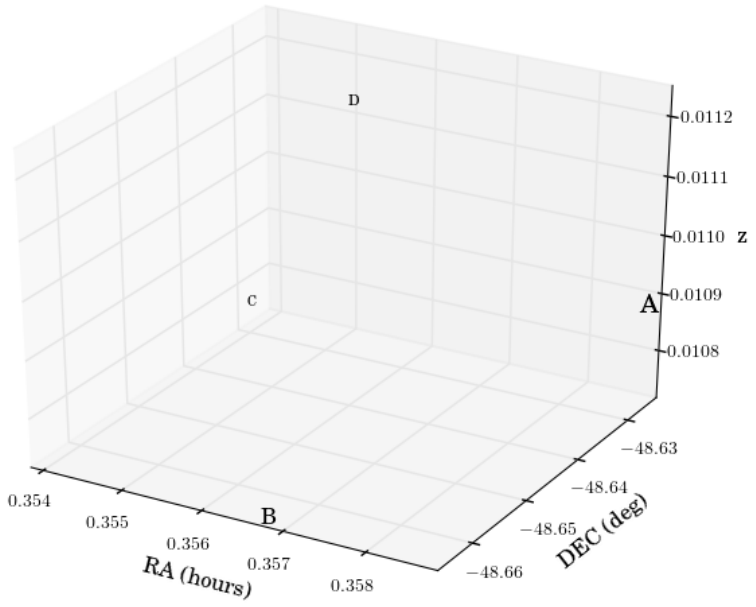

Figure 4.18: Galaxy distribution for SCG08.

In the fully extracted spectrum, only galaxies B, C and D had S/N high enough and/or errors small enough to be analyzed. For Galaxy B, I found intermediate populations with low metallicity and old populations with enhanced metallicity. The low metallicity populations are intermediate and old while the high metallicity populations are old. Galaxy C has young populations with low metallicities and old populations with mid-metallicities. The low and mid-metallicity populations are old. Galaxy D has mid-metallicity young populations and low-metallicity intermediate and old populations. The low and high metallicity SPs are dominated by intermediate populations.

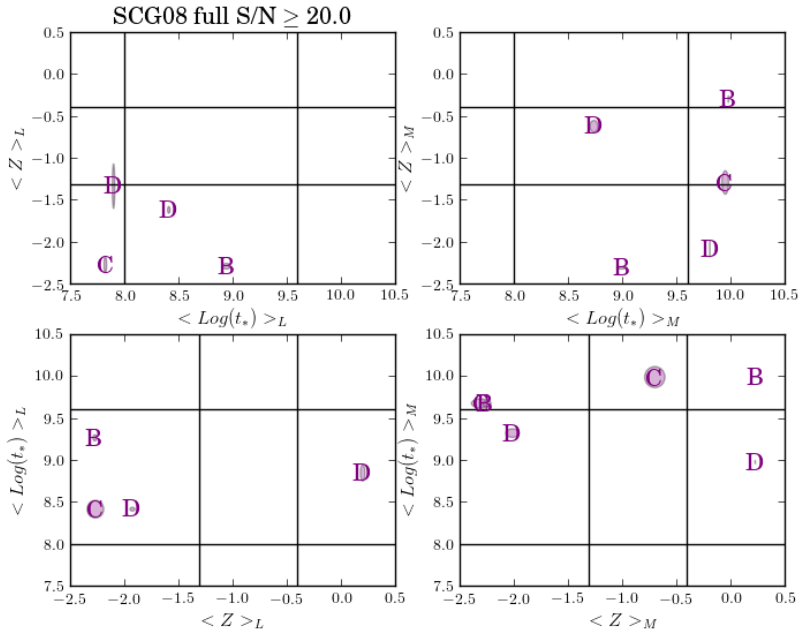

Figure 4.19: Age and metallicity plots for the extracted spectra of galaxies in SCG08.

Galaxy C was the only galaxy with a 10" spectrum. The populations showed similar features as the extracted spectrum.

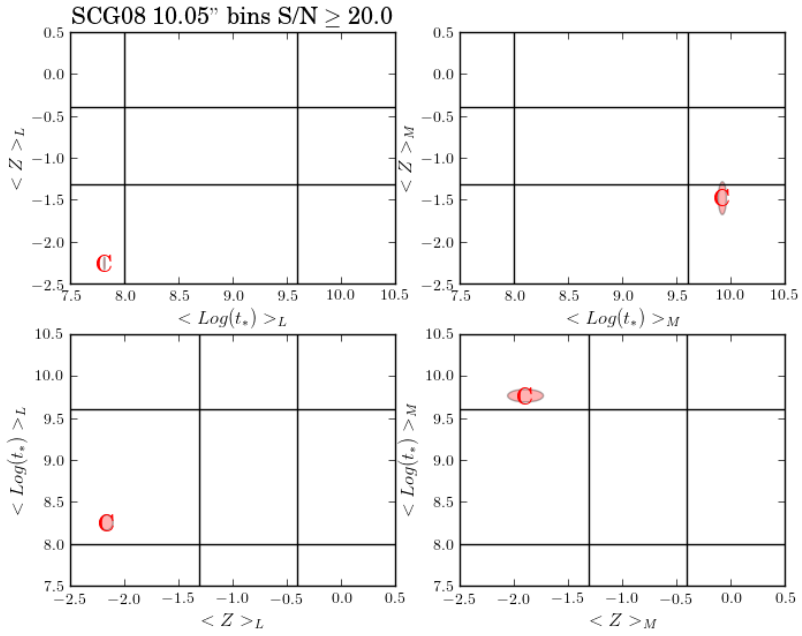

Figure 4.20: Age and metallicity plots for the 10" bin spectra of galaxies in SCG08.

Galaxies B and C had 5" bins that could be analyzed and Galaxy C had them in multiple regions. Galaxy B showed that all populations have low metallicities except the old populations which have mid-metallicity. The low and high metallicity populations are old. The central regions of Galaxy C have a low metallicity old and young population and a mid-metallicity intermediate population. The low, mid and high-metallicity populations have intermediate ages. The mid-regions of the galaxy have young populations with low metallicity and old populations with mid-metallicity, while the low metallicity population is young and the mid-metallicity population is old.

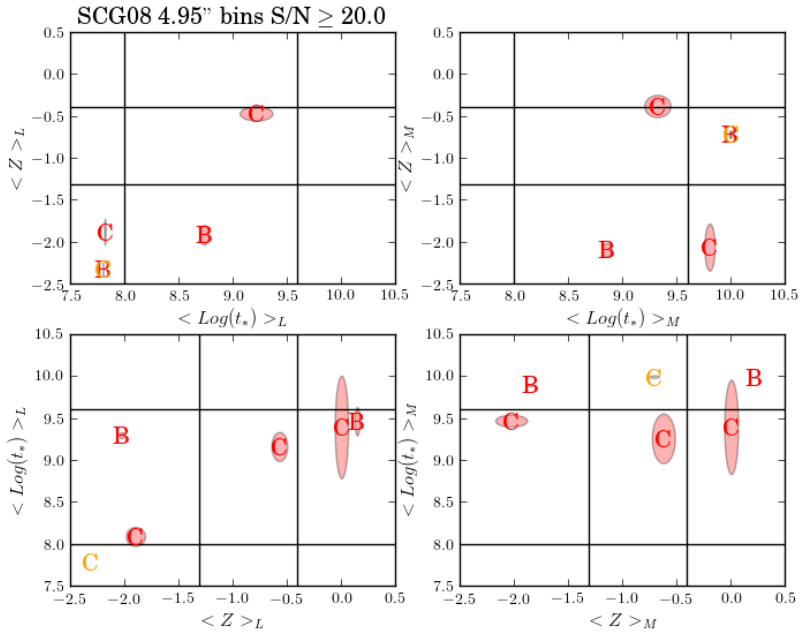

Figure 4.21: Age and metallicity plots for the 5" bin spectra of galaxies in SCG08.

In the 3" bins, the central regions of Galaxies B, C and D were analyzed. The young and old populations in Galaxy B have mid-metallicity while the intermediate populations have low-metallicity. The low and high-metallicity populations are old and the mid-metallicity population is young. In Galaxy C, the young populations have a low metallicity and the intermediate and old populations have a mid-metallicity. The low-metallicity population are young and mid-metallicity populations are intermediate and old aged. Finally, for Galaxy D, the young and old SPs have low metallicities and the intermediate SPs have mid-metallicities. The low-metallicity SPs are intermediate and old ages and the mid-metallicity SPs have intermediate ages.

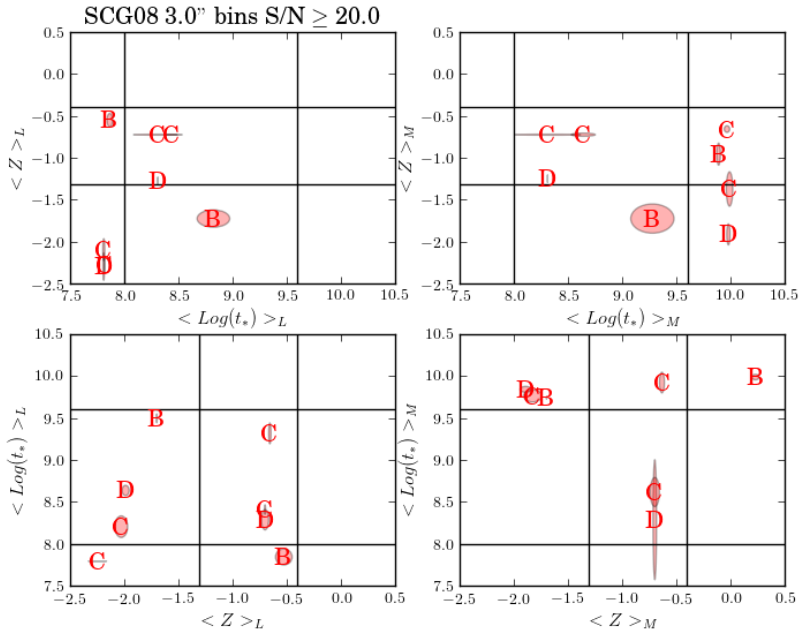

Figure 4.22: Age and metallicity plots for the 3" bin spectra of galaxies in SCG08.

The central regions of all the galaxies appear in the 1" bin analysis. Galaxy A's young population has a mid-metallicity, the intermediate population has a low metallicity and the old population has a high metallicity. The low metallicity populations has intermediate and old ages, the mid-metallicity populations are young and the high metallicity populations are old. The young population in Galaxy B has a low metallicity while the intermediate and old populations have low through high metallicities. All the metallicity bins are dominated by intermediate and old ages. Galaxy C has young populations with low metallicity, intermediate populations with low to mid-metallicity and old populations with low and high metallicity. The low metallicity population spans young and intermediate ages and the high metallicity populations are old. In Galaxy D the young and old populations have low metallicity while the intermediate population has mid-metallicity. The low and mid-metallicity populations are old.

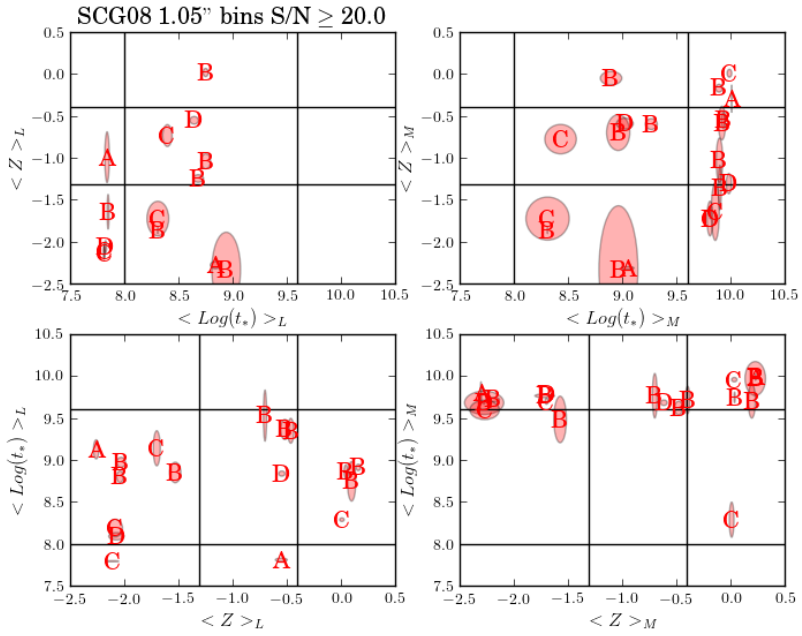

Figure 4.23: Age and metallicity plots for the 1" bin spectra of galaxies in SCG08.

The activity for the extracted spectra reveal that Galaxies A, C and D are all SF galaxies while Galaxy B is a borderline Seyfert.

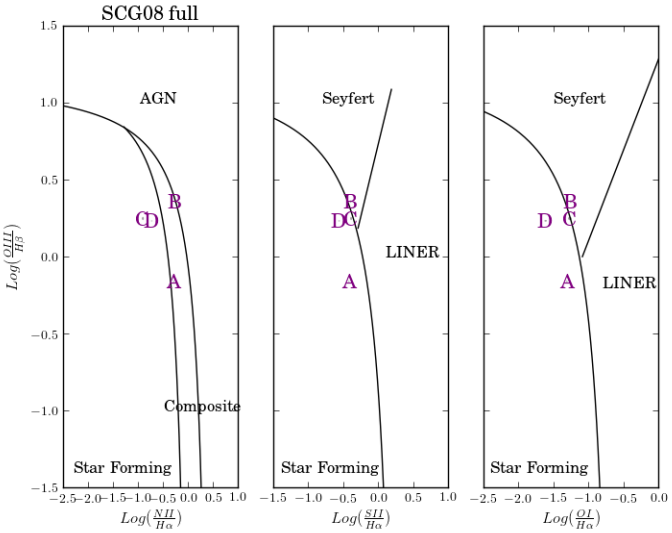

Figure 4.24: BPT diagrams for the extracted spectra of galaxies in SCG08.

Only galaxies A and C had 10” bin measurements. They are confirmed as SF.

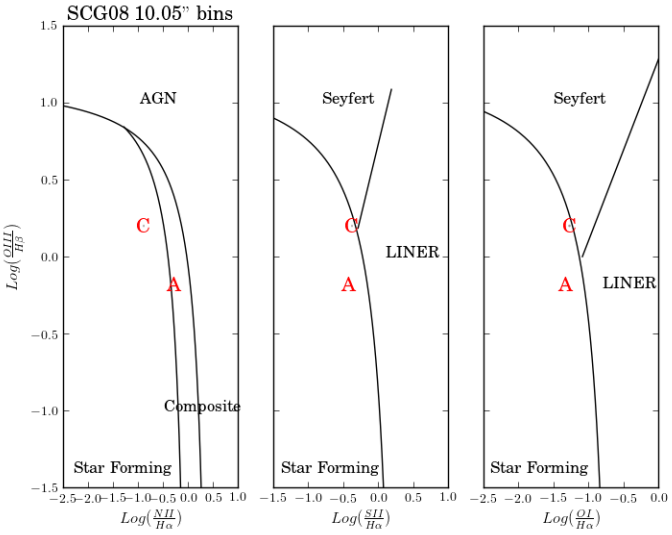

Figure 4.25: BPT diagrams for the 10” bin spectra of galaxies in SCG08.

All galaxies except D had 5” bin measurements. Galaxy A has SF. Galaxy B is a borderline Seyfert. Galaxy C has a LINER in the center with SF in its mid-regions.

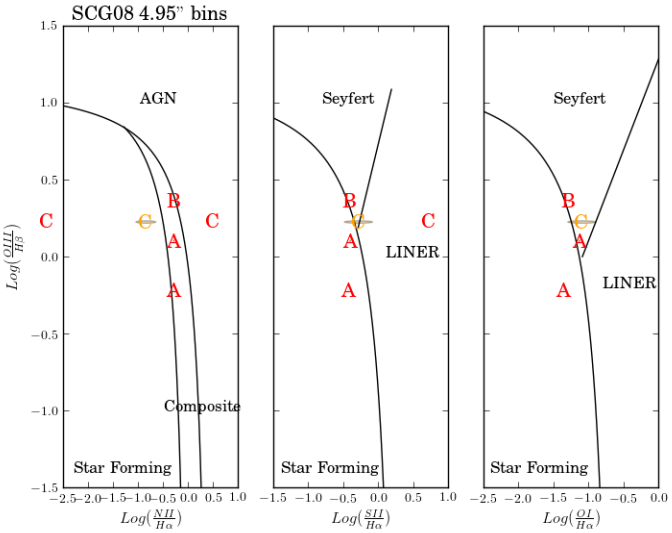

Figure 4.26: BPT diagrams for the 5” bin spectra of galaxies in SCG08.

The central regions of Galaxy A are a combination of SF and LINER according to the 3" bin measurements. Galaxy B is still a borderline Seyfert. Galaxy C has SF in the center and in it's mid-regions. Galaxy D is mostly SF in the center plus a LINER.

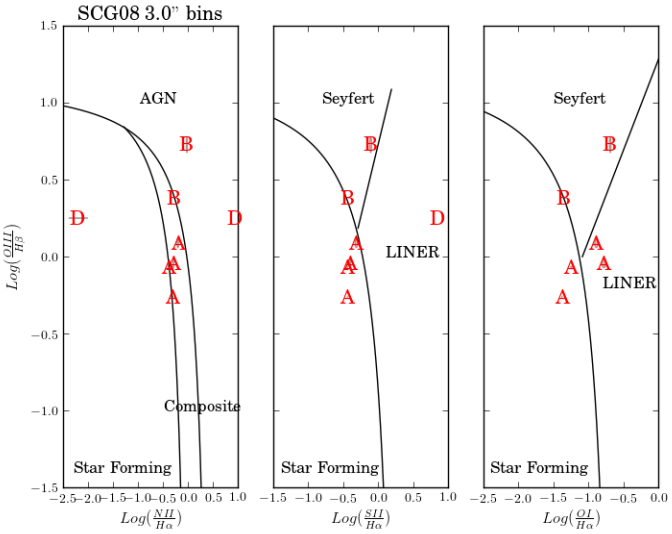

Figure 4.27: BPT diagrams for the 3" bin spectra of galaxies in SCG08.

In the 1" bins, the central regions of Galaxy A show a combination of SF and LINER. The central regions of Galaxy B show a Seyfert with some traces of SF. The center and mid-regions of Galaxy C are SF with a LINER in the center and Galaxy D is SF as well.

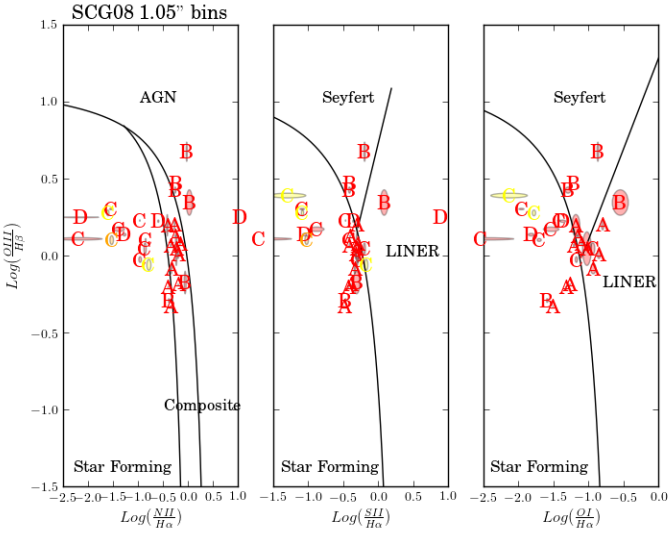

Figure 4.28: BPT diagrams for the 1" bin spectra of galaxies in SCG08.

Table 4.4 summarizes the stellar population and activity that my fits derived for each galaxy. For the SFH construction, I focus on the SP results in the 5" and 3" bins and the activity information from the 1" bins.

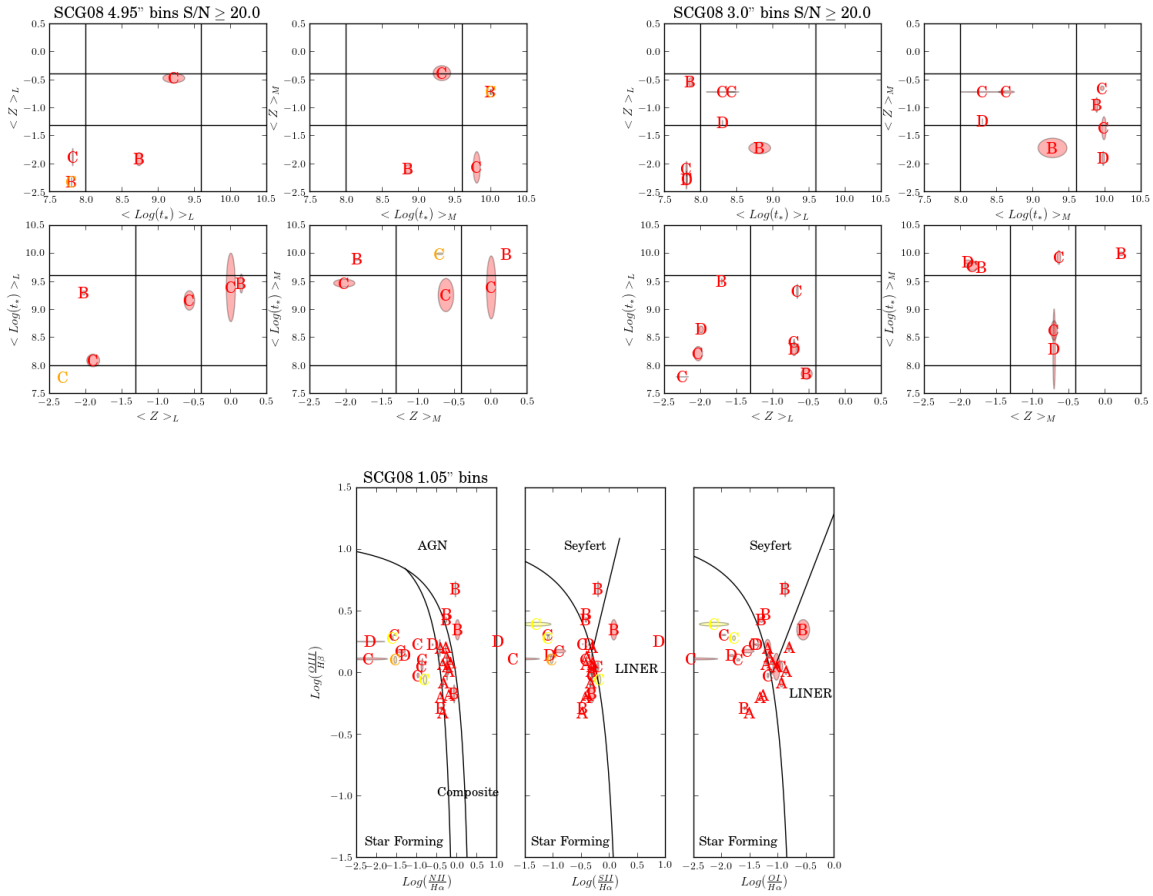

Figure 4.29: Stellar population results for the 5" and 3" bins and activity information for the 1" bins for SCG08.

Galaxy A shows composite spectral characteristics in its central regions and SP information in the 1" bins. The activity seems to be a combination of SF and LINER.

Galaxy B is a Seyfert galaxy with some SF in its central regions. There are low-metallicity young and intermediate populations suggesting that the current SF episode is using low-metallicity gas. The old SPs have mid and high metallicities suggesting multiple SF episodes which rapidly processed gas > 4 Gyrs ago. SF only shows up in the smallest bins suggesting that the current episode of SF is using up the last of the low-metallicity gas after its supply was shutoff when entering the group. Gas is being funneled towards the central black hole creating a Seyfert.

Galaxy C is a SF galaxy in its central and mid-regions. The current SF is using low-metallicity gas and there is evidence of a previous episode of SF, between $0.1 - 4$ Gyrs ago, using preprocessed gas revealed by the intermediate and old SPs with mid-metallicities. The previous episode of SF could have occurred before

Galaxy C entered the group. Once Galaxy C entered the group, it could have interacted with another galaxy which cut off the cold gas supply and funneled the remaining pristine gas towards the center, fueling the current episode of SF.

Galaxy D is further from the other members but still in the group. It may still have its cold gas supply as evidenced by the current, central SF and the low-metallicity young populations. There may have been a previous episode of SF $0.1-4$ Gyrs ago using preprocessed gas which would create the mid-metallicity intermediate populations but there is not much evidence of a mid or high-metallicity old population.

Population	full	10"	5"	3"	1"
Galaxy A					
Young					M-c
Intermediate					L-c
Old					H-c
Low					I/O-c
Mid					Y-c
High					O-c
Star Forming	X-a	X-c	X-c	X-c	X-c
Seyfert			X-c		
LINER				X-c	X-c
Galaxy B					
Young			L-c	M-c	L-c
Intermediate	L-a		L-c	L-c	L/M/H-c
Old	H-a		M-c	M-c	M/H-c
Low	I/O-a		O-c	O-c	I/O-c
Mid				Y-c	Y-c
High	O-a		O-c	O-c	I/O-c
Star Forming					X-c
Seyfert	X-a		X-c	X-c	X-c
LINER					

Population	full	10"	5"	3"	1"
Galaxy C					
Young	L-a	L-c	L-c/m	L-c	L-c
Intermediate			M-c	M-c	L/M-c
Old	M-a	L-c	L-c,M-m	L-c	L/H-c
Low	O-a	O-c	Y-m,I-c	Y-c	Y/I-c
Mid	O-a		I-c,O-m	I/O-c	
High			I-c		O-c
Star Forming	X-a	X-c	X-m	X-c/m	X-c/m
Seyfert			X-c		
LINER			X-c		
Galaxy D					
Young	M-a			L-c	L-c
Intermediate	L-a			M-c	M-c
Old	L-a			L-c	L-c
Low	I-a			I/O-c	O-c
Mid				I-c	O-c
High	I-a				
Star Forming	X-a			X-c	X-c
Seyfert					
LINER				X-c	

Table 4.4: Stellar population and activity analysis summary for SCG08. I abbreviate the age and metallicity designations as young (Y), intermediate (I), old (O), low (L), mid (M) and high (H), and the region designations as central (c), middle (m), and all (a).

4.3.3: SCG13

SCG13 has four late-type galaxies. Galaxies A and B show signs of past perturbations to their structure.

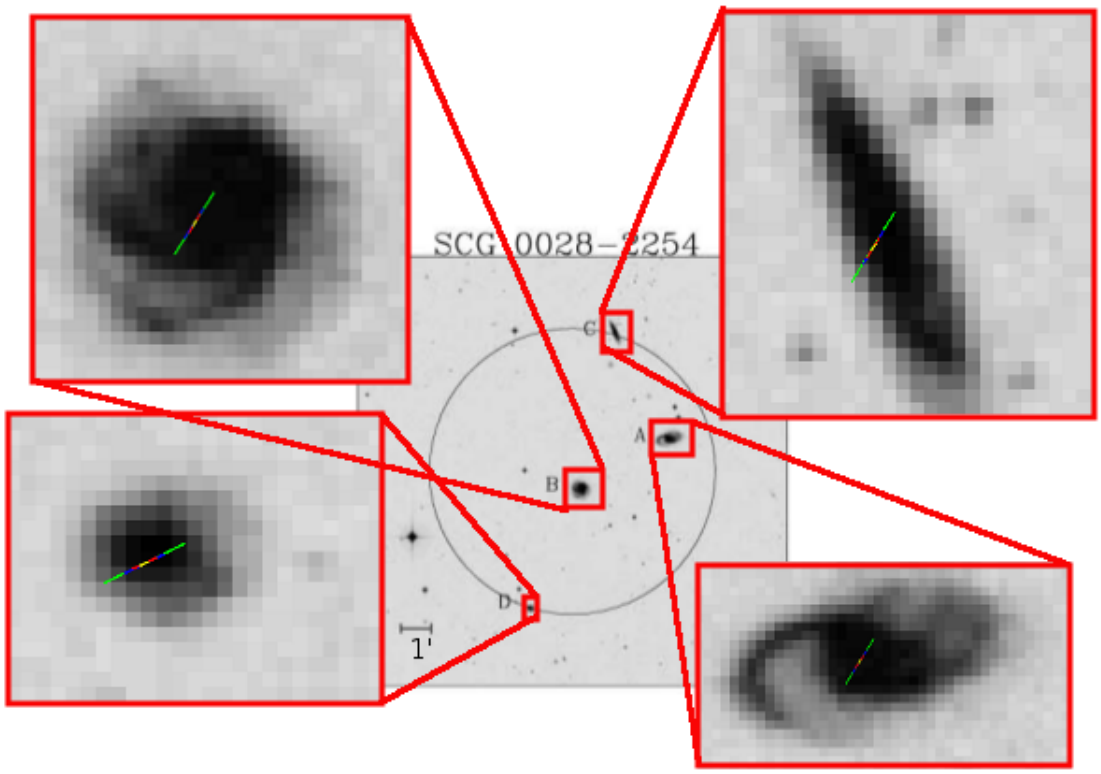

Figure 4.30: Group SCG13.

The velocity dispersions of the group members show that Galaxies A, B and C are all members of the group but D is outside the redshift difference cut off.

$\Delta z(km/s)$	B	C	D
A	189.51	108.18	2213.31
B		−81.33	2023.8
C			2105.13

Table 4.5: Derived redshift differences for group SCG13.

It is also clear from the distribution plot, that Galaxy D is not a member of this group. Galaxies A, B and C are all at similar redshifts and do not appear to have a central member.

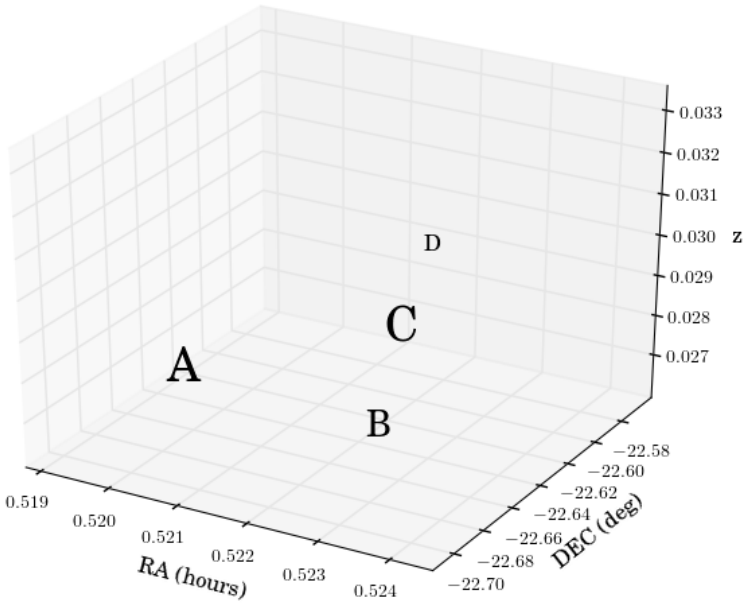

Figure 4.31: Galaxy distribution for SCG13.

The fully extracted spectrum for Galaxy A shows young and intermediate aged populations with low-metallicity and low metallicity populations with intermediate ages. Galaxy B has a young population with low-metallicity, an intermediate aged population with high-metallicity and an old population with a mid-metallicity. The low and high metallicity populations show intermediate and old ages. The young and intermediate populations of Galaxy C have mid-metallicities and the old populations have high-metallicities. All the metallicity bins are old and the low-metallicity SPs also have intermediate ages. Galaxy D did not have enough S/N to be plotted.

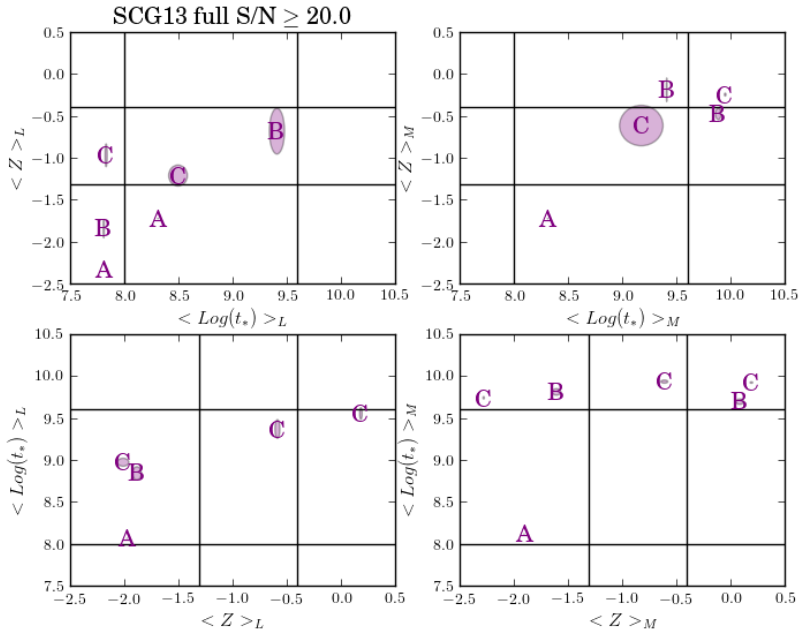

Figure 4.32: Age and metallicity plots for the extracted spectra of galaxies in SCG13.

Galaxies A and B had 10” bins. In this binning, Galaxy A has a young population with a mid-metallicity and an intermediate population with a low-metallicity. The low-metallicity population indeed has an intermediate age while the high-metallicity population is young. Galaxy B has similar metallicities and ages as in the fully extracted spectrum.

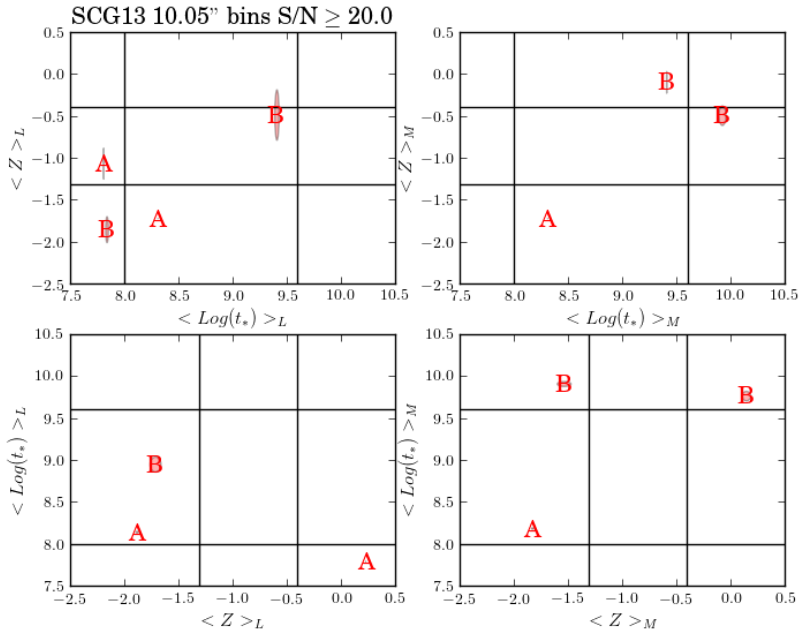

Figure 4.33: Age and metallicity plots for the 10" bin spectra of galaxies in SCG13.

In the 5" bins, the young and intermediate populations in the central and middle regions of Galaxy A have low-metallicities. This is confirmed by the low-metallicity populations in the central and middle regions showing intermediate ages. For Galaxy B, the central regions show a low-metallicity young population and a high-metallicity intermediate and a high-metallicity old population. The mid-regions of Galaxy B have mid-metallicity young and intermediate populations and a low/mid-metallicity intermediate population. The central regions of Galaxy B have a low-metallicity population with intermediate and and old, high-metallicity population. The mid-regions have mid and high-metallicity populations with intermediate ages. Galaxy C has a low-metallicity intermediate population and a mid-metallicity old population in it's central regions. The low-metallicity populations in the central regions have an intermediate age while the high-metallicity populations are old.

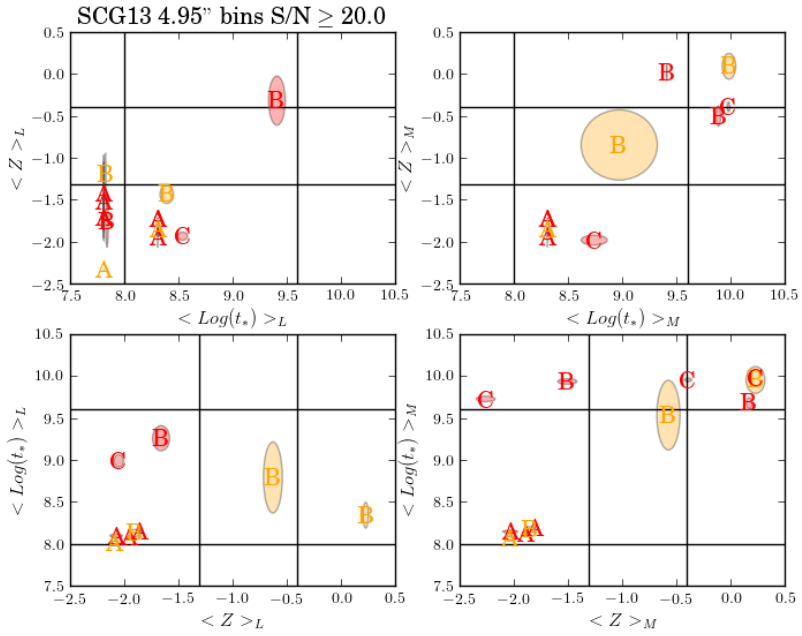

Figure 4.34: Age and metallicity plots for the 5" bin spectra of galaxies in SCG13.

The 3" bins in the central regions of Galaxy A have a young population with low and mid-metallicities and an intermediate population with low-metallicity. The mid-regions have low-metallicity, young and intermediate populations. The low-metallicity populations in the central and mid-region has an intermediate age while the high-metallicity population in the center is young. The central regions of Galaxy B house a wide range in metallicity. The young populations have a low-metallicity and the intermediate and old populations have mid and high metallicities. The mid-regions house low-metallicity, young populations. The central regions are old for all metallicity populations and the central and mid-regions house intermediate ages in the low-metallicity populations. Galaxy C shows intermediate and old populations with high-metallicity in its central regions. All the low and high-metallicity populations are old in the central regions.

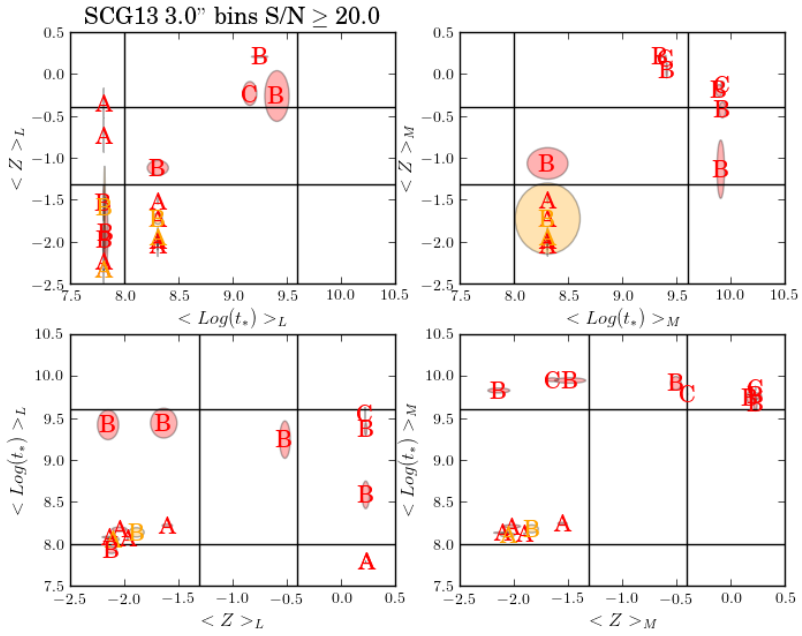

Figure 4.35: Age and metallicity plots for the 3" bin spectra of galaxies in SCG13.

Only the central regions of Galaxies A, B and D had high enough S/N for the 1" bins. Galaxy A has a young population with low to mid-metallicity and an intermediate population with low-metallicity. The low-metallicity population has intermediate ages and the high-metallicity population is young. For Galaxy B, the young population has low to mid-metallicity, the intermediate population has mid and high-metallicity and the old population has high-metallicities. The low and high-metallicity populations are intermediate and old and the mid-metallicity populations has intermediate ages. Galaxy D has an old population with a low-metallicity.

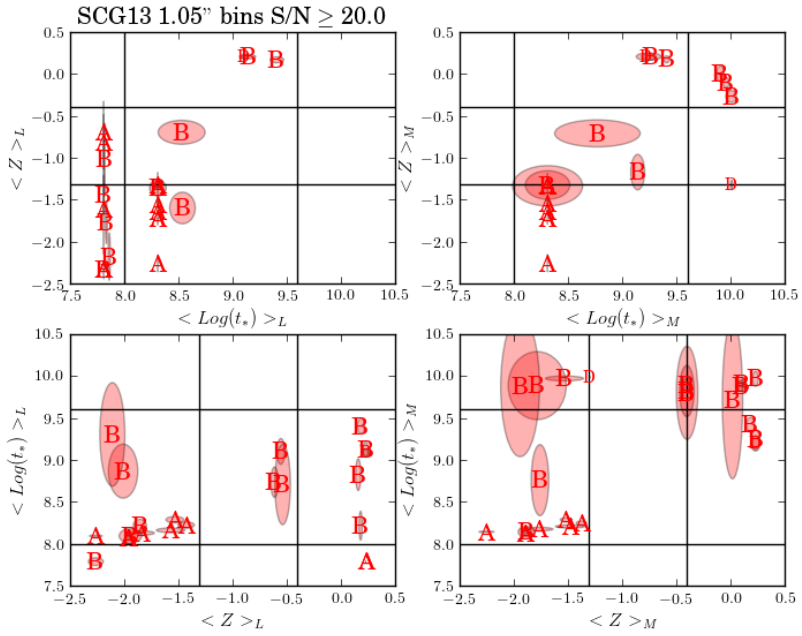

Figure 4.36: Age and metallicity plots for the 1" bin spectra of galaxies in SCG13.

The activity in the extracted spectra shows that all galaxies in the group (A, B, C and D) are star forming.

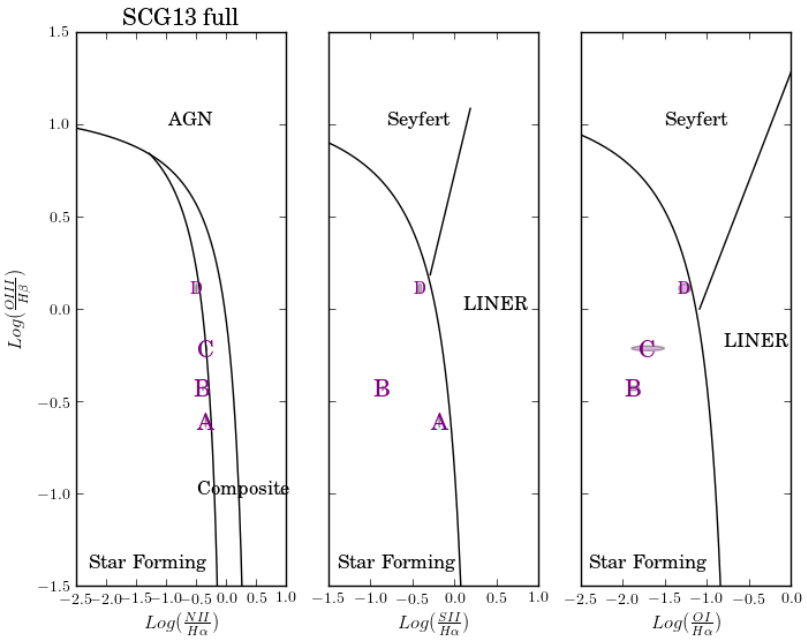

Figure 4.37: Activity plots for the extracted spectra of galaxies in SCG13.

In the 10" spectra, Galaxies A and B are star forming.

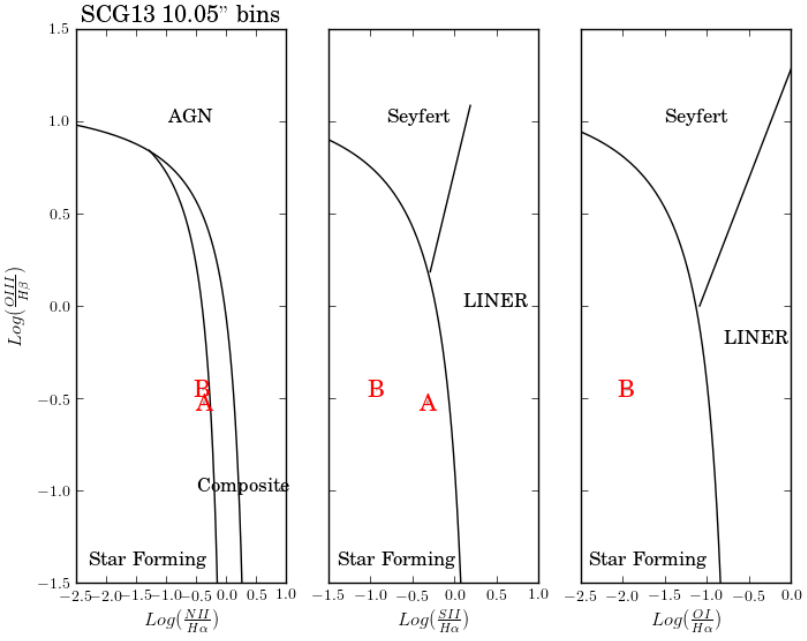

Figure 4.38: Activity plots for the 10" bin spectra of galaxies in SCG13.

All galaxies show SF in their central regions in the 5” bins, which D having some evidence for a Seyfert AGN. The mid-regions of Galaxy B show some SF as well.

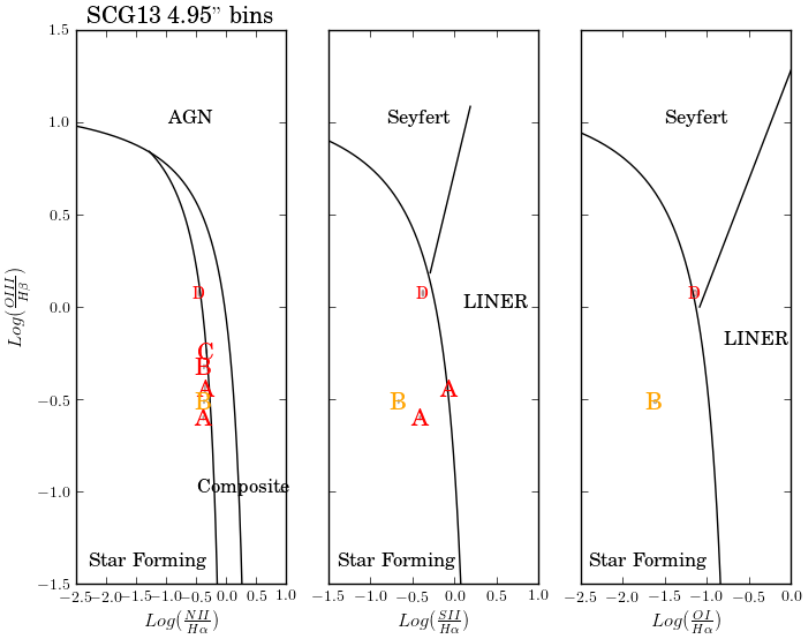

Figure 4.39: Activity plots for the 5” bin spectra of galaxies in SCG13.

Galaxy A, B and D show SF in their centers in the 3” bins. Galaxy B also shows SF in its mid-regions.

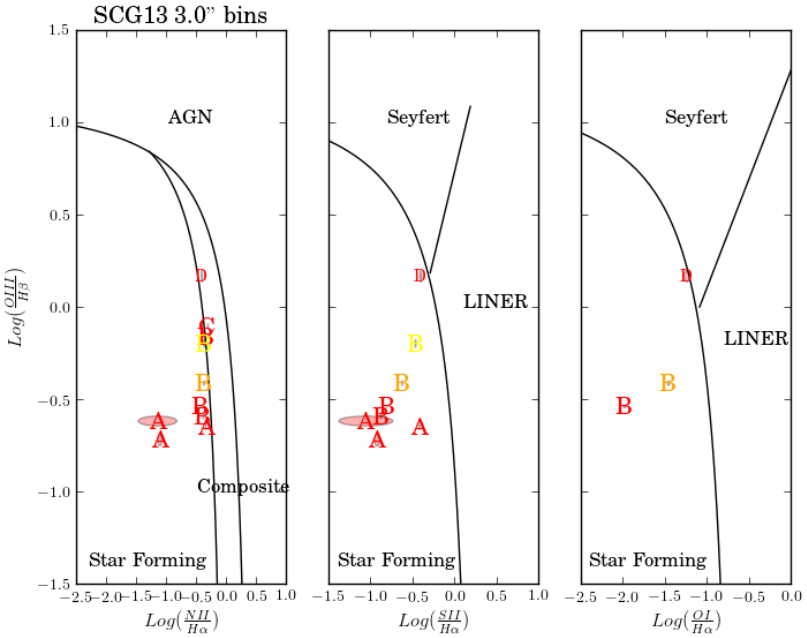

Figure 4.40: Activity plots for the 3" bin spectra of galaxies in SCG13.

In the 1" bins, All galaxies show SF in their central regions. Galaxy B has SF in its mid-region and Galaxy D has evidence of a LINER in its center.

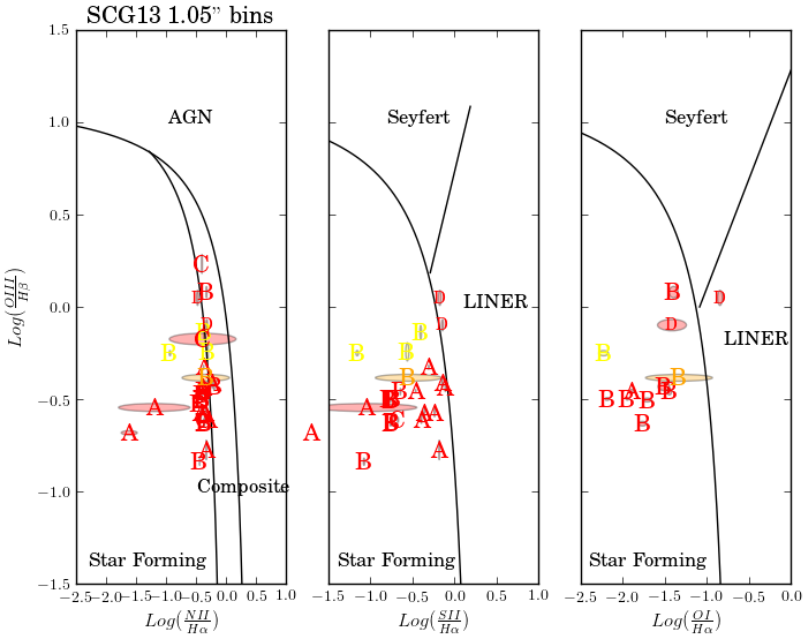

Figure 4.41: Activity plots for the 1" bin spectra of galaxies in SCG13.

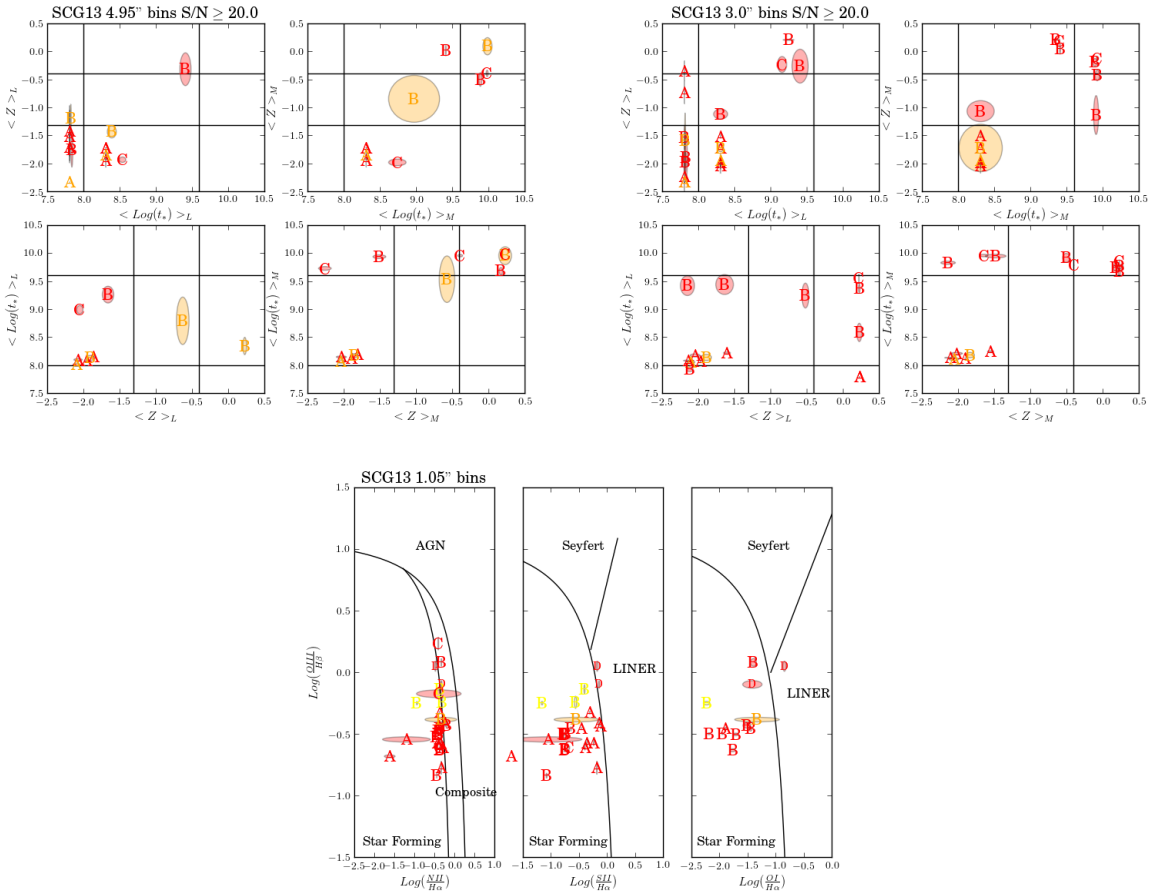

Figure 4.42: Stellar population results for the 5" and 3" bins and activity information for the 1" bins for SCG13.

Galaxy A is a SF galaxy in its central regions. This is supported by the young and intermediate aged SPs in its central and middle regions. The young SPs in the central regions have low and mid-metallicity and in the middle regions are low-metallicity. The intermediate populations in both the central and middle regions have low-metallicity. The young and intermediate populations throughout show a low-metallicity which indicates that the outside supply of gas is still present. There is evidence of the current SF episode using preprocessed gas by the mid-metallicity young populations in the center. I do not see an old population in Galaxy A which implies a very recent SF episode that is overpowering the light from the older populations.

Galaxy B is also a SF galaxy in its central and middle regions. This is supported by the young populations present in its central and middle regions. The young SPs have low and mid-metallicity in the center and middle regions and the old and intermediate SPs have mid and high-metallicity in those same regions. This implies the current SF episode is using both preprocessed and low-metallicity gas. The high-metallicity

intermediate and old stars suggest that a SF episode $0.1-4$ Gyrs ago used preprocessed gas. These SF episodes could have been initiated by an interaction because Galaxy B also has a disturbed morphology. This interaction could have funneled the remaining low-metallicity gas towards the center.

Galaxy C has a composite spectrum which is mostly dominated by SF but its young SPs only show up in the extracted spectrum and have mid-metallicity. The intermediate and old populations have enhanced metallicities and any low-metallicity populations show intermediate ages. This implies that Galaxy C lost its cold gas supply between $0.1-4.0$ Gyrs ago.

Galaxy D has a composite spectrum with evidence of a LINER. But redshift shows that it is not part of this group and its SP information is only recorded in the 1" bins.

Population	full	10"	5"	3"	1"	Population	full	10"	5"	3"	1"
Galaxy A						Galaxy C					
Young	L-a	M-c	L-c/m	L/M-c,L-m	L/M-c	Young	M-a				
Intermediate	L-a	L-c	L-c/m	L-c/m	L-c	Intermediate	M-a		L-c	H-c	
Old						Old	H-a		M-c	H-c	
Low	I-a	I-c	I-c/m	I-c/m	I-c	Low	I/O-a		I-c	O-c	
Mid						Mid	O-a			O-c	
High		Y-c		Y-c	Y-c	High	O-a		O-c	O-c	
Star Forming	X-a	X-c	X-c	X-c	X-c	Star Forming	X-a		X-c		X-c
Seyfert						Seyfert					
LINER						LINER					
Galaxy B						Galaxy D					
Young	L-a	L-c	L-c,M-m	L-c/m	L/M-c	Young					
Intermediate	H-a	H-c	H-c,L/M-m	M/H-c	M/H-c	Intermediate					
Old	M-a	M-c	M-c,H-m	M/H-c	H-c	Old					L-c
Low	I/O-a	I/O-c	I/O-c, I-m	I-c/m, O-c	I/O-c	Low					O-c
Mid			I-m	O-c	I-c	Mid					
High	O-a	O-c	O-c,I-m	O-c	I/O-c	High					
Star Forming	X-a	X-c	X-c/m	X-c/m	X-c/m	Star Forming	X-a			X-c	X-c
Seyfert						Seyfert			X-c		
LINER						LINER					X-c

Table 4.6: Stellar population and activity analysis summary for SCG13. Same codes as in Table 4.4

4.3.4: SCG68

SCG68 is comprised of six galaxies with early-type morphologies.

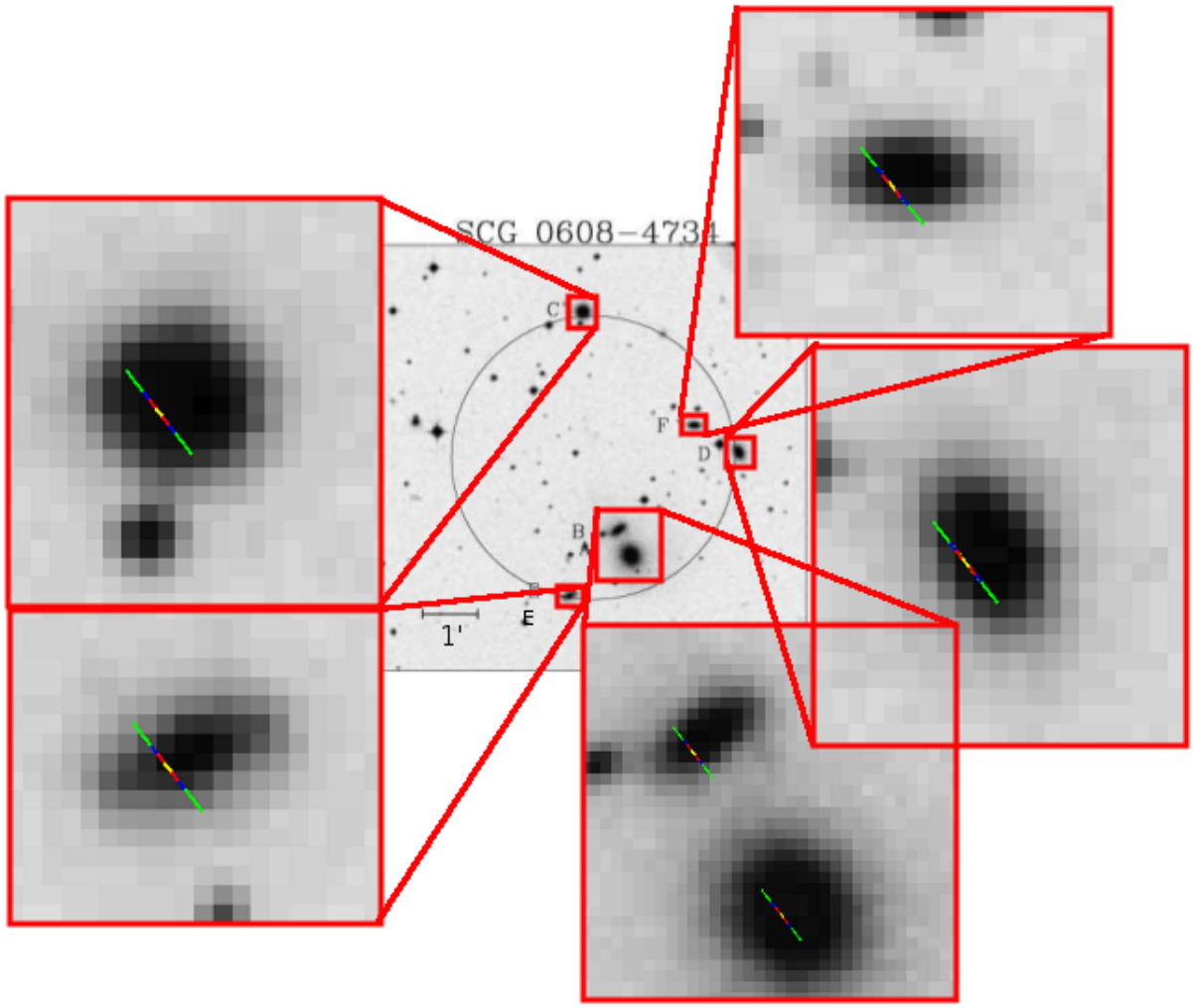

Figure 4.43: Group SCG68.

All the galaxies are within the velocity dispersion cutoff with Galaxy A. Galaxy D is only within the cutoff with Galaxy A, it does not meet the crieria when compared with the other galaxies in the group.

$\Delta z(km/s)$	B	C	D	E	F
A	207.57	142.71	−402.21	319.95	213.51
B		−64.86	−609.78	112.38	5.94
C			−544.92	177.24	70.8
D				722.16	615.72
E					−106.44

Table 4.7: Derived redshift differences for group SCG68.

The distribution plot allows us to see how these galaxies are distributed in redshift space and that Galaxy B could be central to the group.

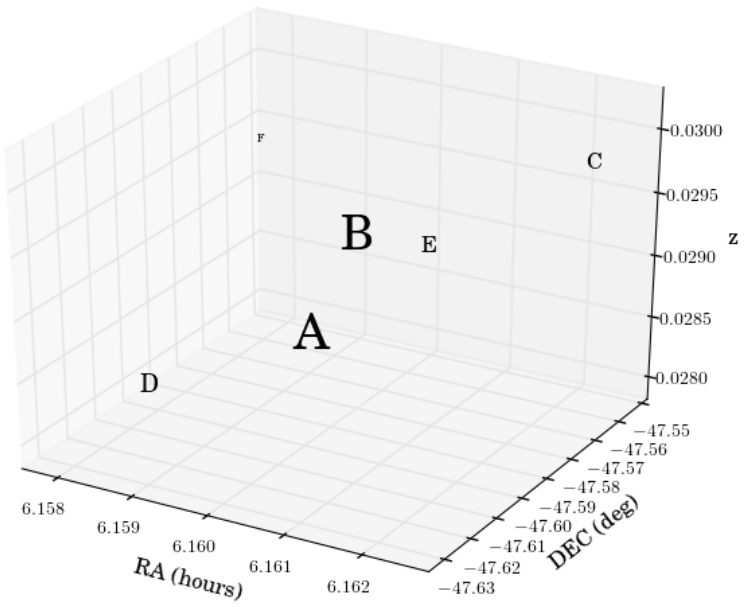

Figure 4.44: Galaxy distribution for SCG68.

Galaxies A and B have high-metallicity old populations from their extracted spectrum. Galaxies C, E and F show high-metallicity intermediate and old SPs and old high-metallicity populations. Galaxy D has

low-metallicity young SPs and high-metallicity old SPs.

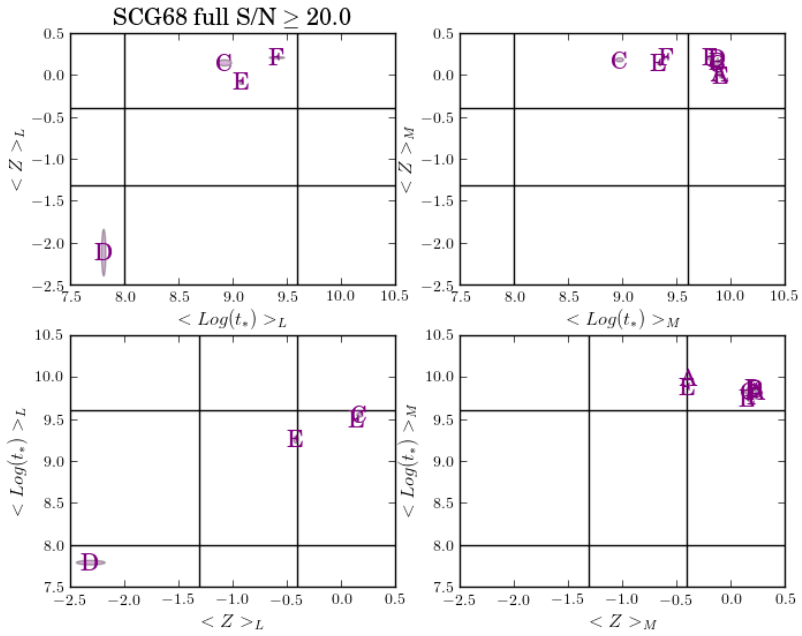

Figure 4.45: Age and metallicity plots for the extracted spectra of galaxies in SCG68.

In the 5" bins, Galaxies A and B have high-metallicity old SPs. Galaxy C has high-metallicity intermediate and old SPs. Galaxy D shows a low-metallicity young population and a high-metallicity old population.

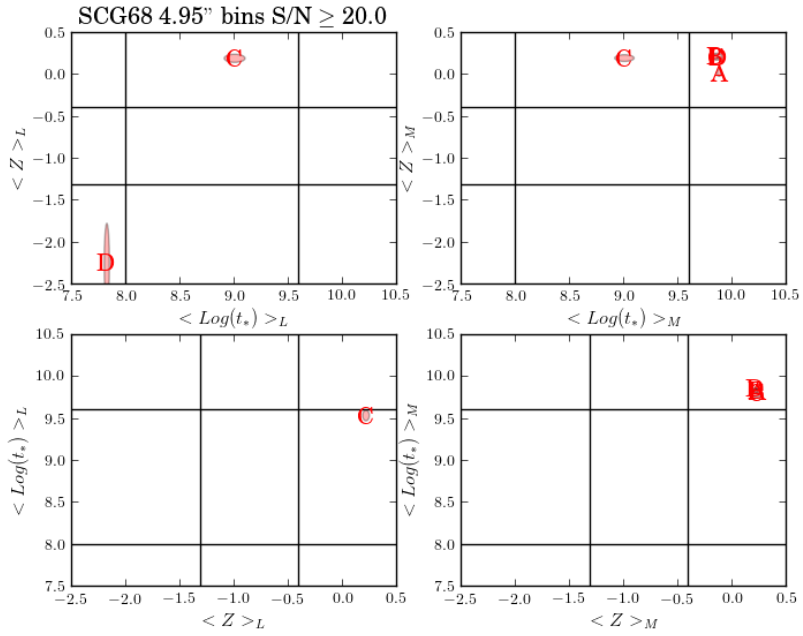

Figure 4.46: Age and metallicity plots for the 5" bin spectra of galaxies in SCG68.

Similar results are seen for the 3" bins as with the 5" bins with Galaxy E adding an intermediate aged mid-metallicity population. All measurements are from the central regions of the galaxies.

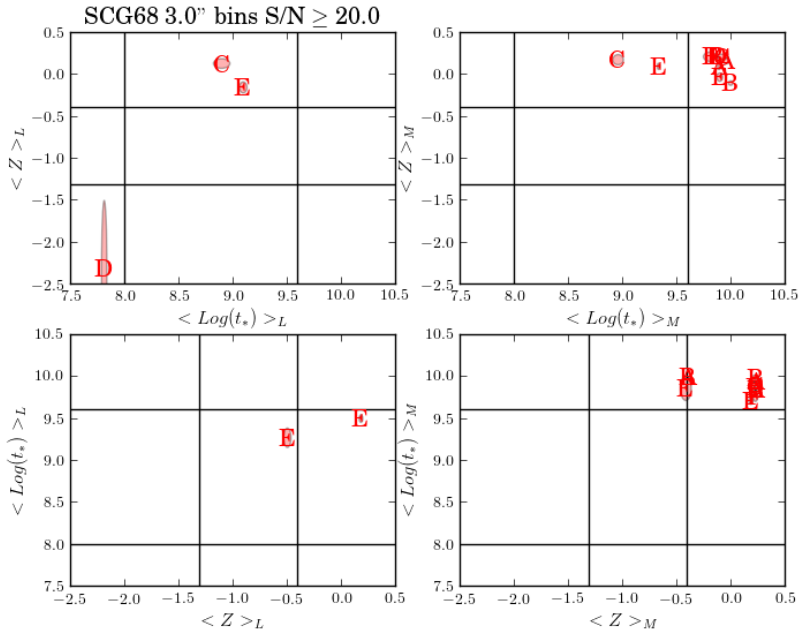

Figure 4.47: Age and metallicity plots for the 3" bin spectra of galaxies in SCG68.

In the 1" bins there is further detail revealed about the central regions. Galaxy A has evidence of a young population with low-metallicity along with high-metallicity old populations. Galaxy B has high-metallicity intermediate and old SPs for its high-metallicity populations. Galaxy C still shows high-metallicity old populations with a high-metallicity intermediate aged SP. Galaxy D continues to show a low-metallicity young SP in its center with old and intermediate SPs with high-metallicities. Galaxy E shows high-metallicity intermediate and old SPs with intermediate and old mid and high-metallicity populations respectively. Galaxy F has high-metallicity intermediate and old SPs with old high-metallicity populations.

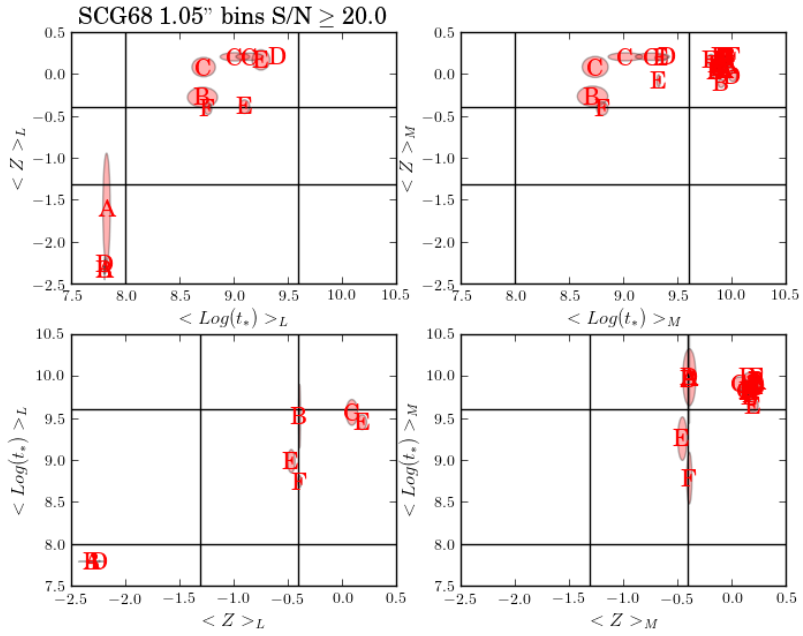

Figure 4.48: Age and metallicity plots for the 1" bin spectra of galaxies in SCG68.

The activity for the fully extracted spectra show AGN activity for all galaxies with Galaxy C and E being classified as a Seyfert.

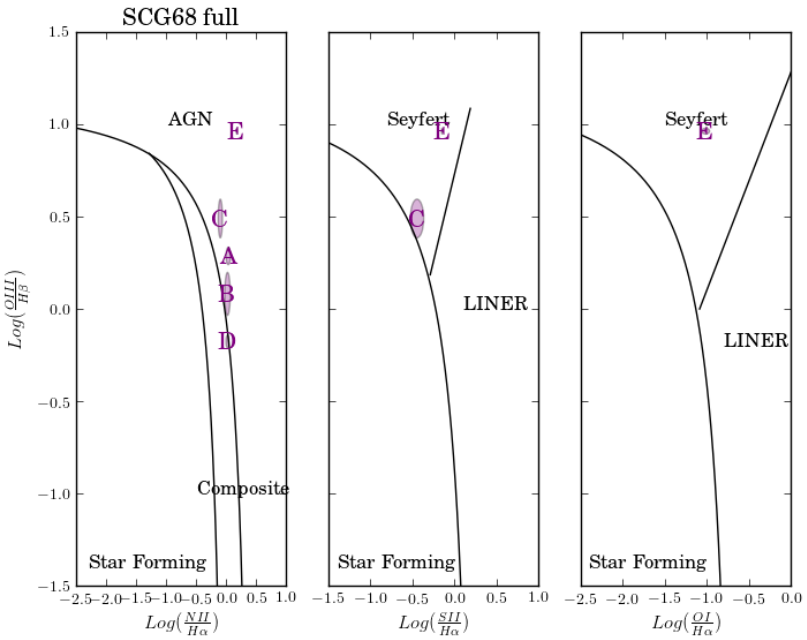

Figure 4.49: Activity plots for the extracted spectra of galaxies in SCG68.

Galaxies A, B, C and D all show AGN in their 5" bin spectra with Galaxy C again being classified as a Seyfert.

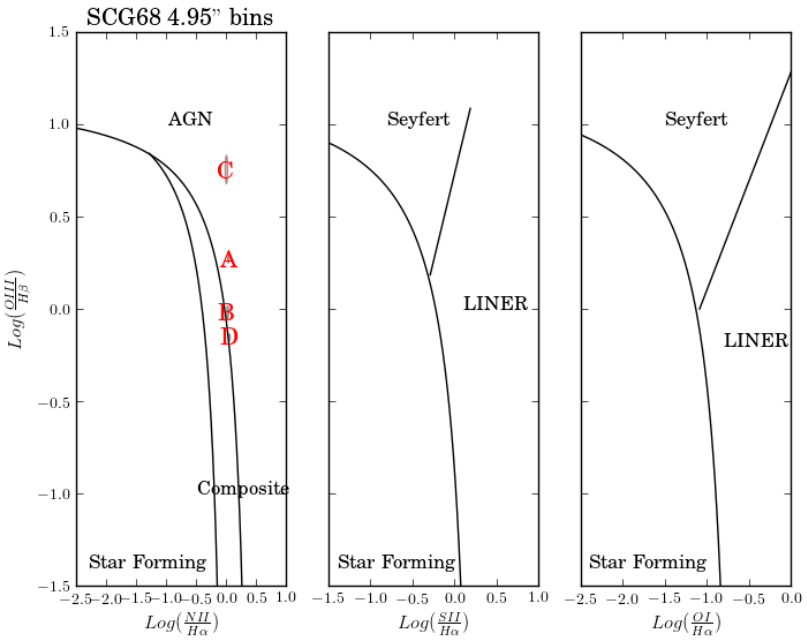

Figure 4.50: Activity plots for the 5" bin spectra of galaxies in SCG68.

All galaxies show AGN in their 3" spectra of the central regions with Galaxies C and E again being classified as Seyfert. Galaxy D shows signs of being a composite galaxy.

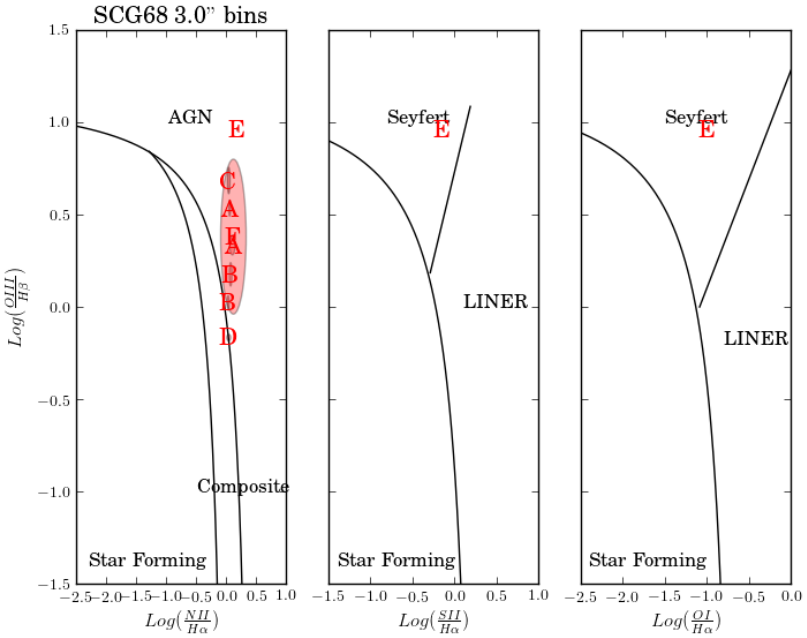

Figure 4.51: Activity plots for the 3" bin spectra of galaxies in SCG68.

In the 1" bin spectra, all galaxies again show AGN in their central regions with C and E being Seyferts. Galaxy D is a composite while Galaxy F shows evidence for LINER characteristics.

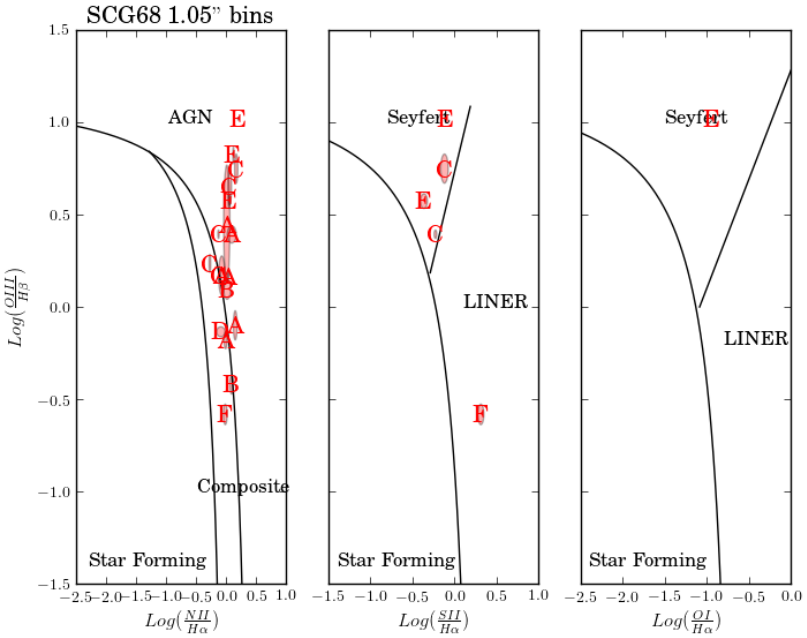

Figure 4.52: Activity plots for the 1" bin spectra of galaxies in SCG68.

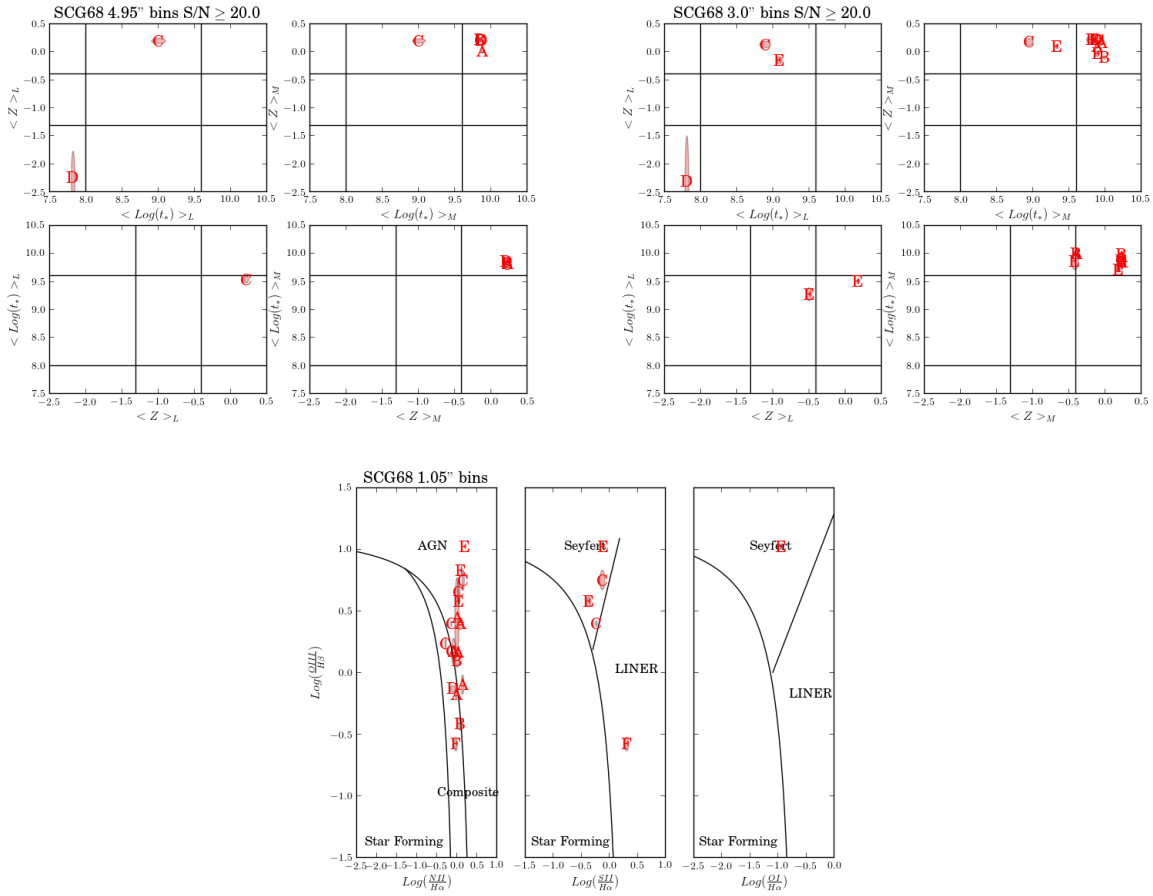

Figure 4.53: Stellar population results for the 5" and 3" bins and activity information for the 1" bins for SCG68.

The galaxies in SCG68 show many of the classic signs of early-type spectra, old aged populations. Galaxies A, B, C, E and F are all AGN and Galaxy D is a composite. This is supported by the old ages and high metallicities of the galaxies and Galaxy D's detection of a young low-metallicity population. This also provides evidence that Galaxy D may still have its cold gas supply along with the galaxy being at the outermost edges of the group. All of the other galaxies show high-metallicity old populations which suggests multiple episodes of SF > 4 Gyrs ago and the removal of the cold gas supply early in their lives. These galaxies may have been part of this group for a long time.

Population	full	10”	5”	3”	1”
Galaxy A					
Young					L-c
Intermediate					
Old	H-a		H-c	H-c	H-c
Low					Y-c
Mid	O-a				
High	O-a		O-c	O-c	O-c
Star Forming					
Seyfert					
LINER					
AGN	X-a		X-c	X-c	X-c
Comp					
Galaxy B					
Young					
Intermediate					H-c
Old	H-a		H-c	H-c	H-c
Low					Y-c
Mid					
High	O-a		O-c	O-c	O-c
Star Forming					
Seyfert					
LINER					
AGN	X-a		X-c	X-c	X-c
Comp					
Galaxy C					
Young					
Intermediate	H-a		H-c	H-c	H-c
Old			H-c	H-c	H-c
Low					
Mid					
High	O-a		O-c	O-c	O-c
Star Forming					
Seyfert	X-a		X-c	X-c	X-c
LINER					
AGN					
Comp					

Population	full	10”	5”	3”	1”
Galaxy D					
Young	L-a		L-c	L-c	L-c
Intermediate					H-c
Old	H-a		H-c	H-c	H-c
Low	Y-a				Y-c
Mid					
High	O-a		O-c	O-c	O-c
Star Forming					
Seyfert					
LINER					
AGN	X-a		X-c		
Comp				X-c	X-c
Galaxy E					
Young					
Intermediate	H-a			H-c	H-c
Old	H-a			H-c	H-c
Low					Y-c
Mid				I-c	I-c
High	O-a			O-c	O-c
Star Forming					
Seyfert	X-a			X-c	X-c
LINER					
AGN					
Comp					
Galaxy F					
Young					
Intermediate	H-a				H-c
Old	H-a				H-c
Low					
Mid					
High	O-a				O-c
Star Forming					
Seyfert					
LINER					X-c
AGN	X-a			X-c	
Comp					X-c

Table 4.8: Stellar population and activity analysis summary for SCG68. Same codes as in Table 4.4

4.3.5: SCG72

SCG72 is comprised of four galaxies. Three have late-type morphologies and one has early-type. Two may show evidence of disturbed morphology.

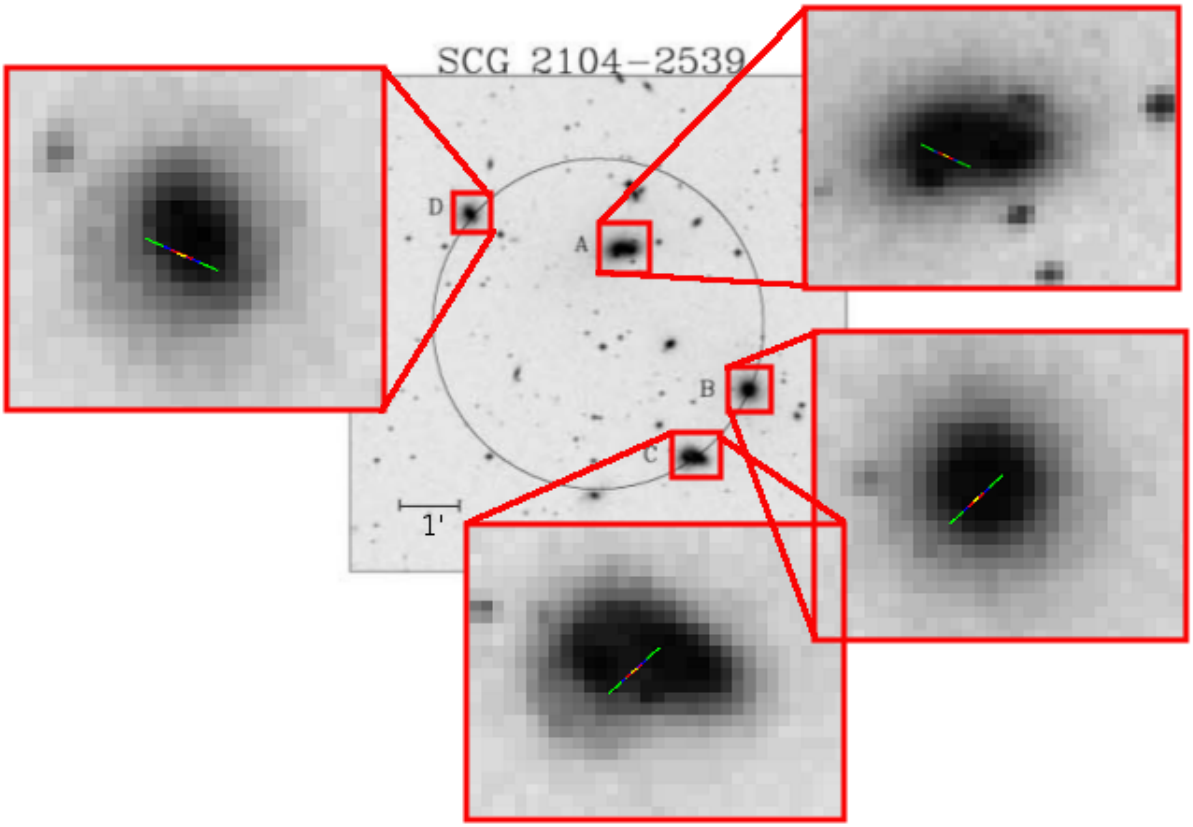

Figure 4.54: Group SCG72.

According to the velocity dispersion analysis, Galaxy C is not part of this group gravitationally. Galaxies A, B and D, however, are most likely gravitationally bound.

$\Delta z(km/s)$	B	C	D
A	−518.4	−1270.5	−180.3
B		−752.1	338.1
C			1090.2

Table 4.9: Derived redshift differences for group SCG72.

This is also clear from the distribution plot. Galaxy B is barely outside of the redshift cutoff with Galaxy A but both are included with Galaxy D. Galaxy D could be the most central member of this group.

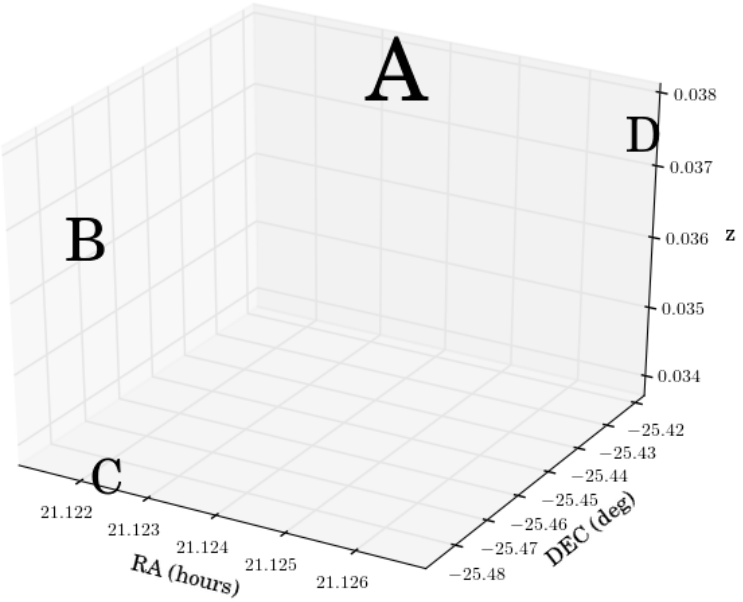

Figure 4.55: Galaxy distribution for SCG72.

The SP analysis of the fully extracted spectrum has been plotted for Galaxies A, B and D. Galaxies A, B and D show a high-metallicity for its old SPs and old ages for all the metallicity populations. Galaxy A has old low-metallicity populations.

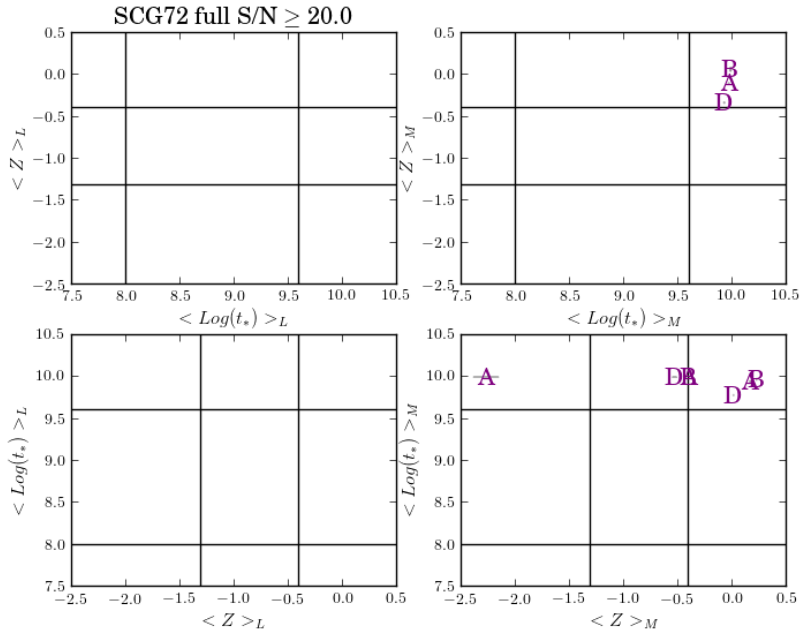

Figure 4.56: Age and metallicity plots for the extracted spectra of galaxies in SCG72.

In the 10” bin spectra, Galaxies B and D had spectra that fit within our noise and size limits. Here, Galaxy B has a low-metallicity young SP plus old, high-metallicity populations. Galaxy D shows intermediate aged, high-metallicity populations and a low-metallicity old population.

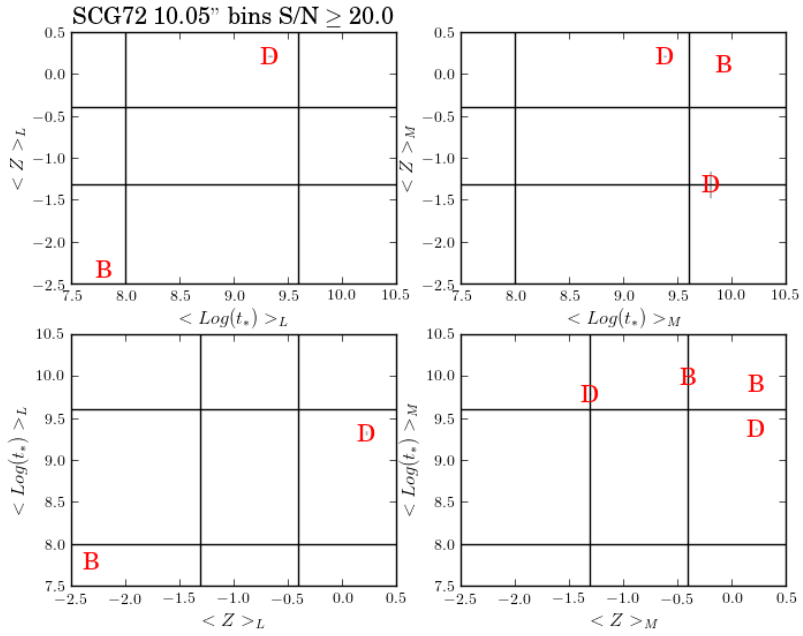

Figure 4.57: Age and metallicity plots for the 10" bin spectra of galaxies in SCG72.

Galaxy A shows a low-metallicity young SP in its central regions with high-metallicity intermediate populations and mid and high-metallicity old populations. Galaxies B and D have a high-metallicity old SP and old ages of all metallicities in their central regions. Galaxy C has similar SPs to Galaxies B and D except the low-metallicity population has intemediate ages instead of old.

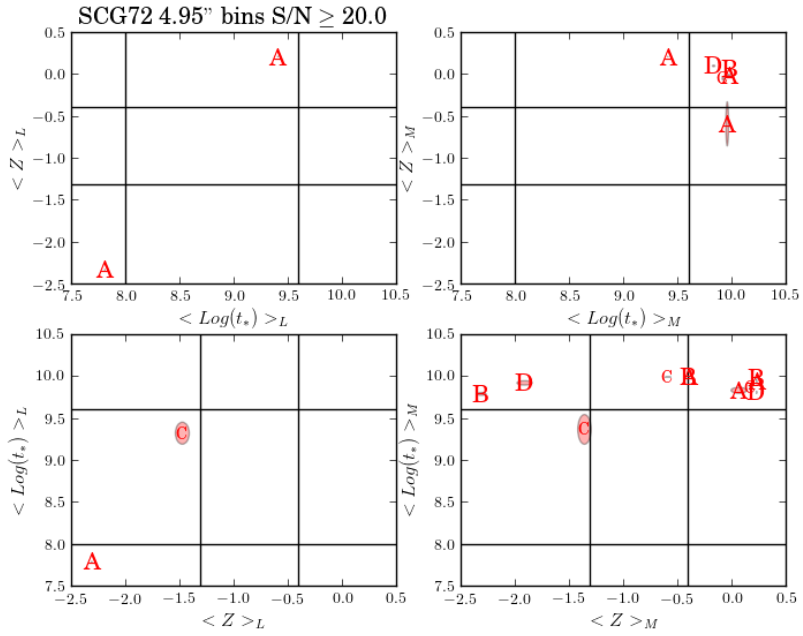

Figure 4.58: Age and metallicity plots for the 5" bin spectra of galaxies in SCG72.

In the 3" bins, Galaxy A shows a low-metallicity young populations and high-metallicity old populations. Galaxy B shows a high-metallicity young population but its low-metallicity population is young. The old populations have high-metallicities. Galaxy C has a high-metallicity old population. Galaxy D shows high-metallicities for its intermediate and old SPs.

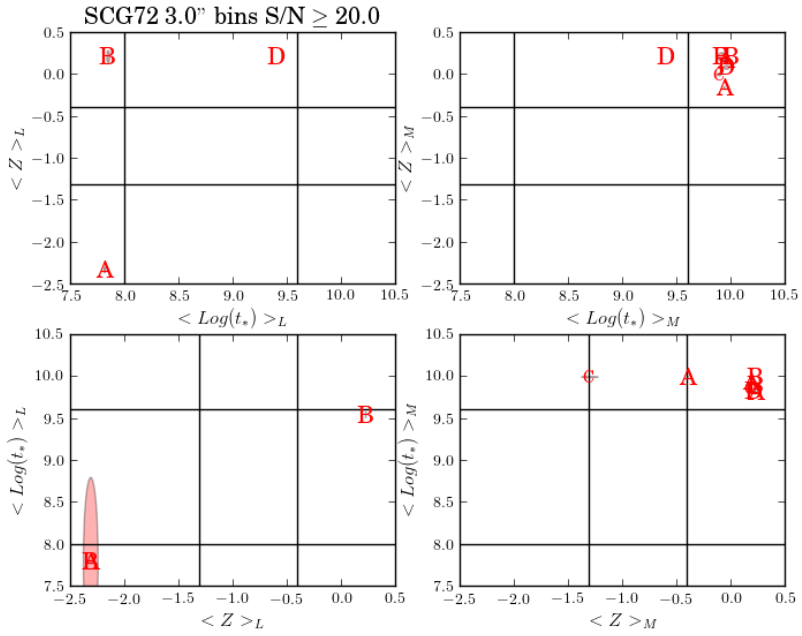

Figure 4.59: Age and metallicity plots for the 3" bin spectra of galaxies in SCG72.

Galaxy A's 1" bin spectra of its central regions shows a young, low-metallicity SP and high-metallicity intermediate and old SPs. The mid and high-metallicity populations are old. Galaxy B has a low-metallicity young SP and high-metallicity old SPs. The intermediate and old populations have high-metallicity for Galaxy C. The high-metallicity populations are old. Galaxy D has young populations with mid-metallicity, intermediate populations with low and high-metallicities and old populations with high-metallicities in its central regions. The low and high metallicity populations are old.

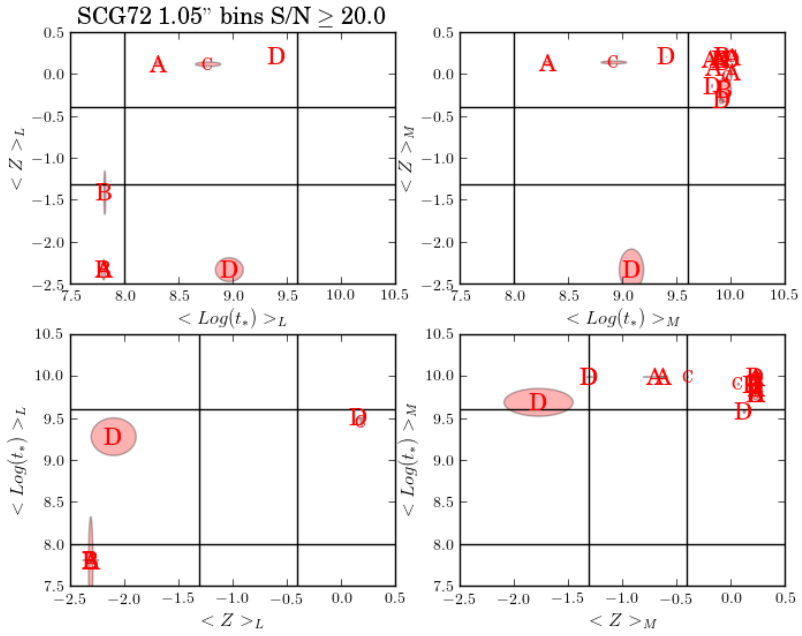

Figure 4.60: Age and metallicity plots for the 1" bin spectra of galaxies in SCG72.

In the fully extracted spectra, Galaxy A is SF, Galaxies B and C are composites and Galaxy D is either a Seyfert or a LINER.

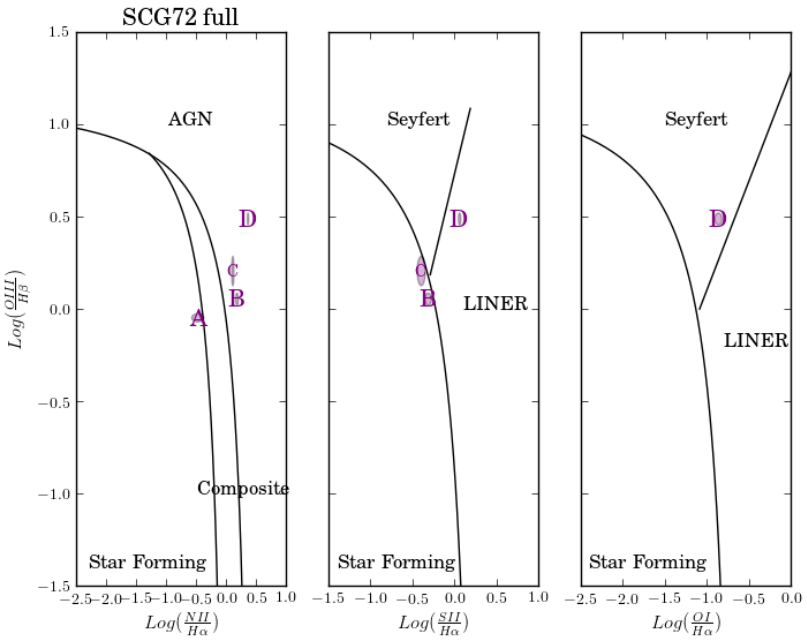

Figure 4.61: Activity plots for the extracted spectra of galaxies in SCG72.

In the 10" spectra, Galaxies B and D are LINER galaxies.

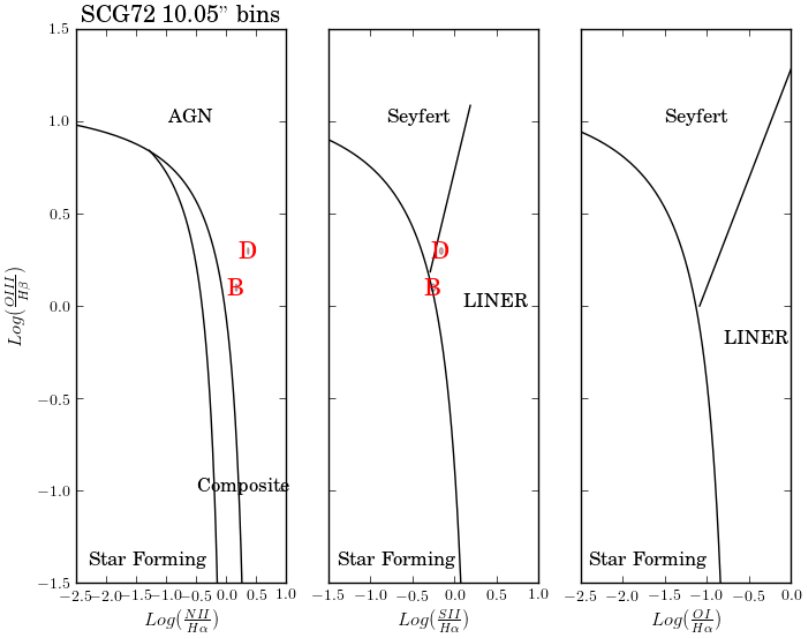

Figure 4.62: Activity plots for the 10" bin spectra of galaxies in SCG72.

Galaxy A is SF, Galaxies B and C are composites and Galaxy D is a LINER in the 5” bins.

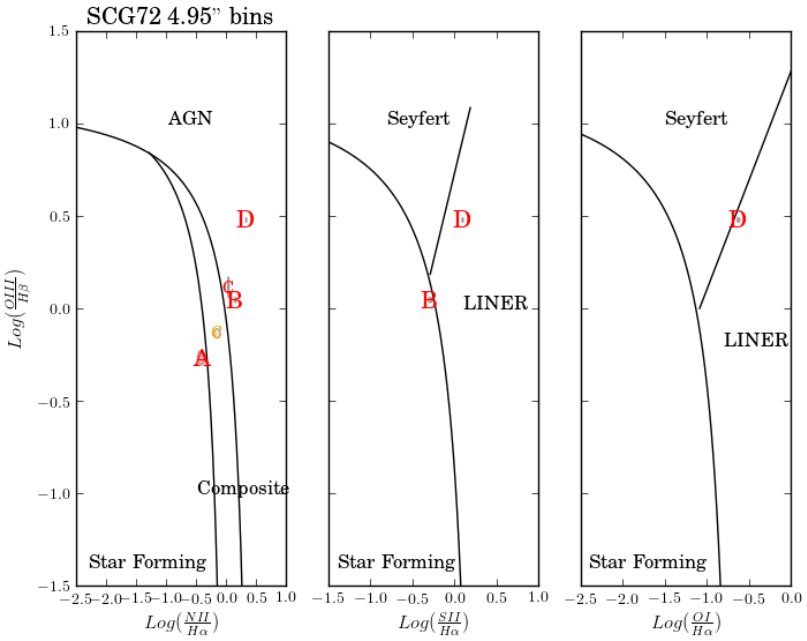

Figure 4.63: Activity plots for the 5” bin spectra of galaxies in SCG72.

In the 3” bins, Galaxies B and C are still composite galaxies with Galaxy B possibly being a LINER. Galaxy D is some kind of AGN.

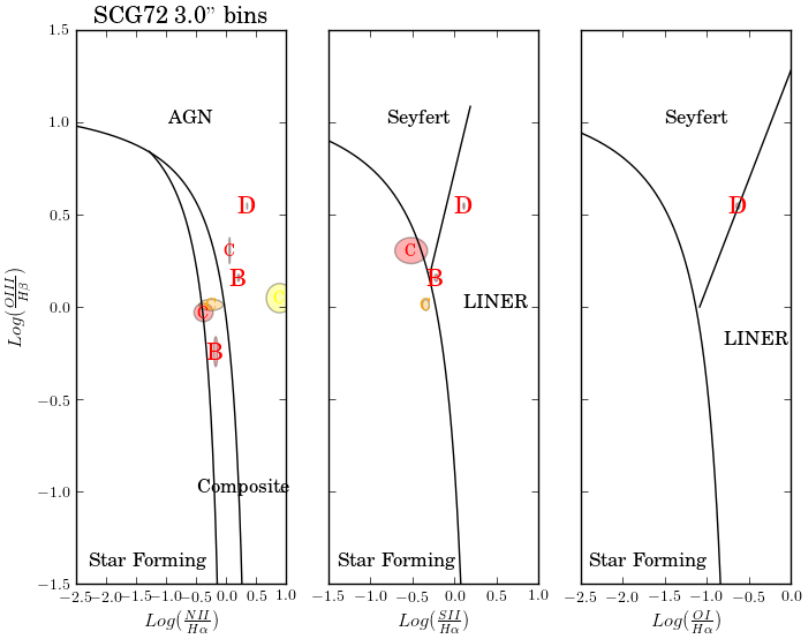

Figure 4.64: Activity plots for the 3" bin spectra of galaxies in SCG72.

All of the galaxies appear to show composite spectra in the 1" bins with C showing LINER characteristics and B and D showing both Seyfert and LINER characteristics.

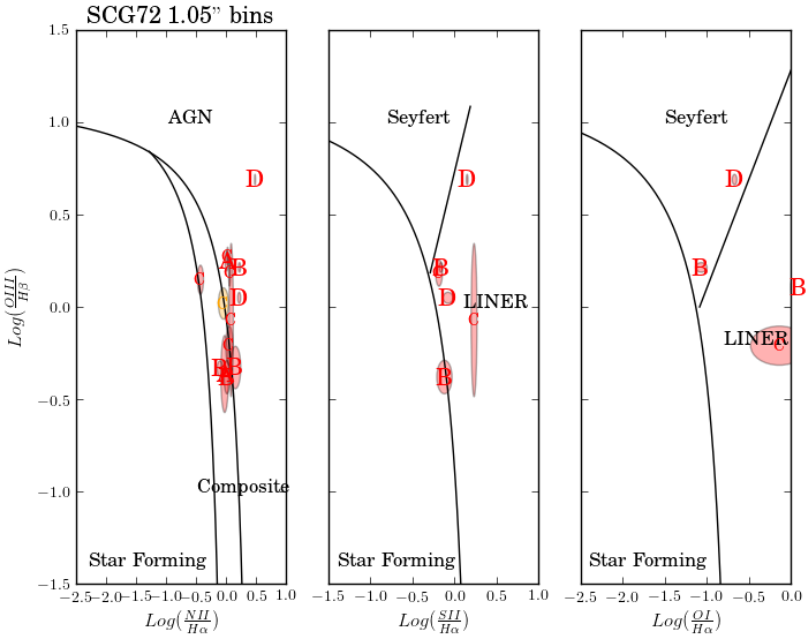

Figure 4.65: Activity plots for the 1" bin spectra of galaxies in SCG72.

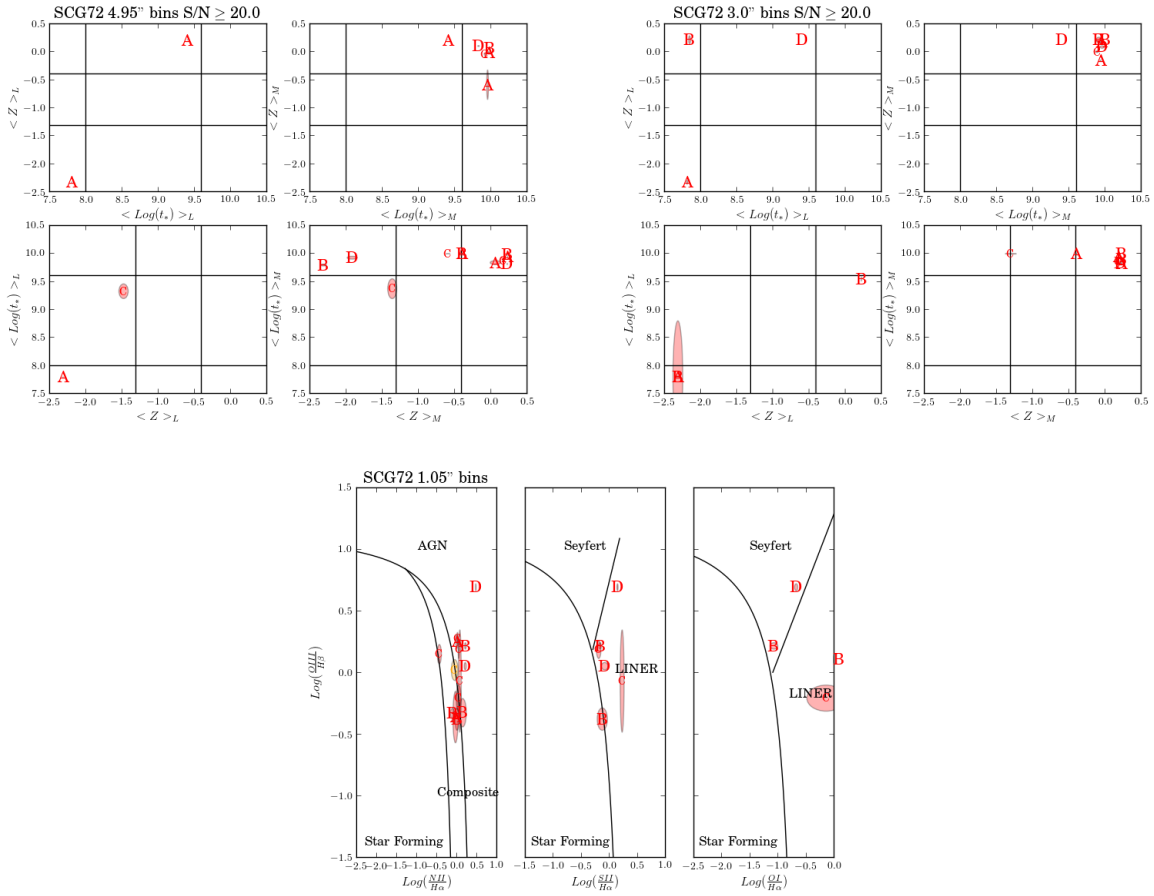

Figure 4.66: Stellar population results for the 5" and 3" bins and activity information for the 1" bins for SCG72.

In my summary of the SPs, Galaxy C, which is not a member of this group, shows signs of having lost its cold gas supply between > 4 Gyrs ago. This is indicated by the high-metallicity old populations. This also indicates multiple episodes of SF. Galaxy A has a composite spectrum which is supported by its low-metallicity young populations. This implies that Galaxy A still has its cold gas supply. The old and intermediate populations show high-metallicities which indicates multiple SF episodes between $0.1 - 4$ Gyrs ago which rapidly processed gas. Galaxy B has young and old populations with both high and low metallicities, suggesting that it too still has access to a cold gas supply. Both galaxies A and B appear to be at the edges of the group from the 3d plots. Galaxy D has high-metallicity old populations, so its cold gas supply was most likely cut off > 4 Gyrs ago, after which, it underwent multiple episodes of SF rapidly processing its gas.

Population	full	10”	5”	3”	1”
Galaxy A					
Young			L-c	L-c	L-c
Intermediate			H-c		H-c
Old	H-a		M/H-c	H-c	H-c
Low	O-a		Y-c	Y-c	Y-c
Mid			O-c		O-c
High	O-a		O-c	O-c	O-c
Star Forming	X-a		X-c		
Seyfert					
LINER					
AGN			X-c		X-c
Comp					X-c
Galaxy B					
Young		L-c		H-c	L-c
Intermediate					
Old	H-a	H-c	H-c	H-c	H-c
Low		Y-c	O-c	Y-c	Y-c
Mid			O-c		
High	O-a	O-c	O-c	O-c	O-c
Star Forming	X-a		X-c	X-c	
Seyfert					X-c
LINER		X-c		X-c	X-c
AGN	X-a		X-c	X-c	X-c
Comp				X-c	X-c

Population	full	10”	5”	3”	1”
Galaxy C					
Young					H-c
Intermediate					
Old			H-c	H-c	H-c
Low			I-c		
Mid			O-c		
High			O-c	O-c	O-c
Star Forming	X-a			X-c/m	
Seyfert					
LINER					X-c/m
AGN	X-a		X-c	X-c/m	X-c
Comp			X-m	X-c/m	X-c/m
Galaxy D					
Young					M-c
Intermediate		H-c		H-c	L/H-c
Old	H-a	L-c	H-c	H-c	H-c
Low		O-c	O-c		O-c
Mid					
High	O-a	I-c	O-c	O-c	O-c
Star Forming					
Seyfert	X-a			X-c	X-c
LINER	X-a	X-c	X-c	X-c	X-c
AGN					X-c
Comp					X-c

Table 4.10: Stellar population and activity analysis summary for SCG72. Same codes as in Table 4.4

4.3.6: SCG82

SCG82 is comprised of four galaxies with one showing late-type morphology and the other three appearing more early-type.

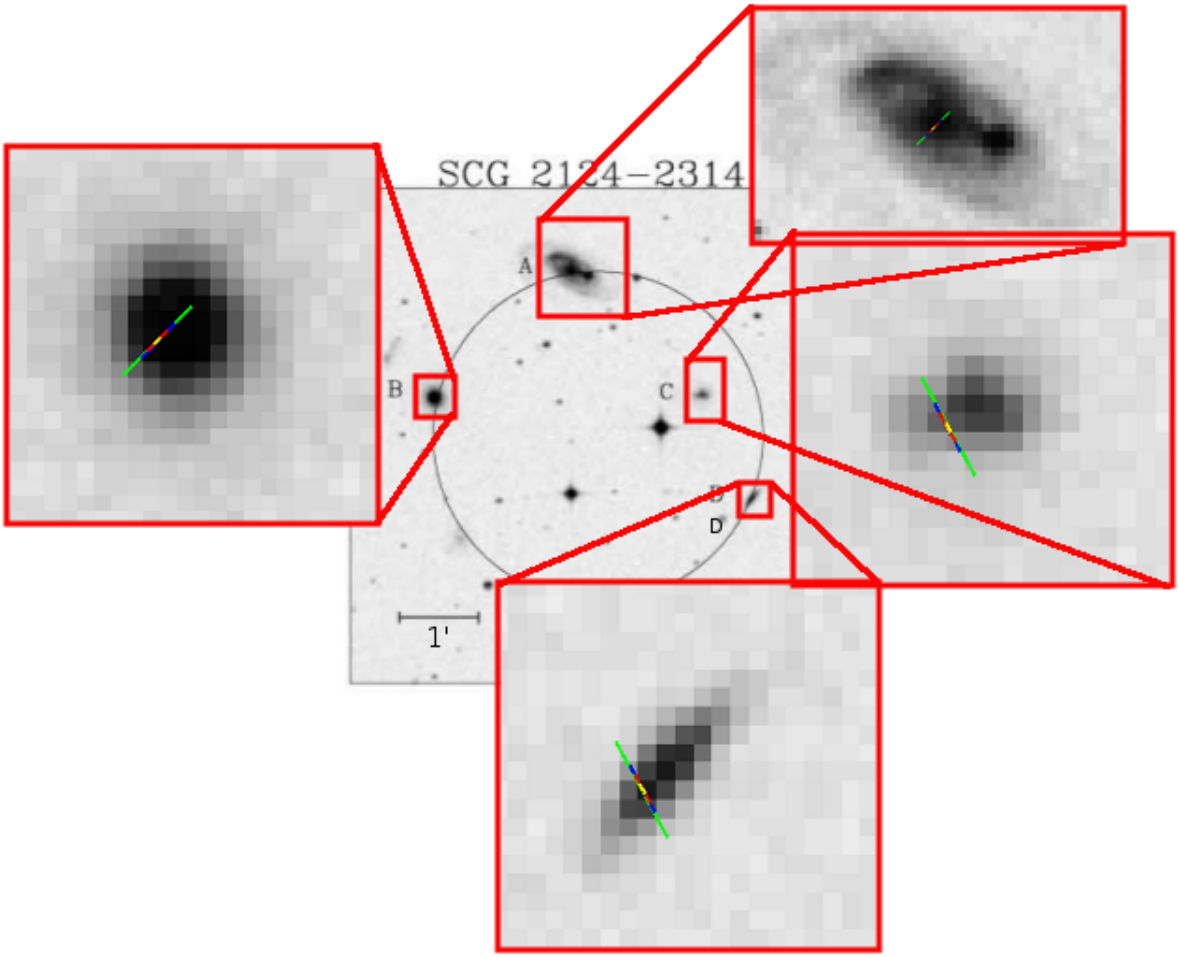

Figure 4.67: Group SCG82.

The redshift analysis reveals that all galaxies are members of this group with all galaxies showing very low velocity dispersions.

$\Delta z(km/s)$	B	C	D
A	−114.72	−128.28	−27.15
B		−13.56	87.57
C			101.13

Table 4.11: Derived redshift differences for group SCG82.

We get an idea of how the galaxies are distributed with respect to each other in the following figure. There doesn't appear to be a central member for this group.

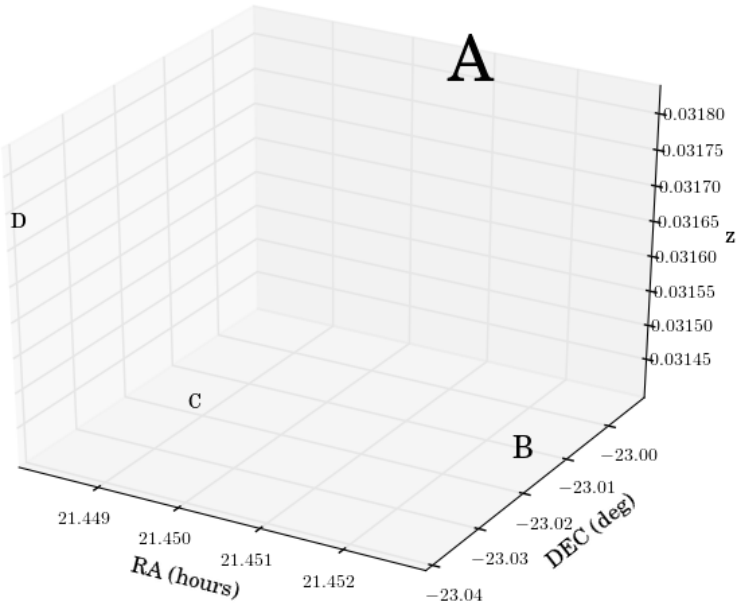

Figure 4.68: Galaxy distribution for SCG82.

The SP analysis could only be completed on Galaxies B, C and D for this group. In the fully extracted spectra, the intermediate and old populations for Galaxy B have high-metallicities while the high-metallicity populations are old. Galaxy C has low metallicities for all ages but its low-metallicity population is dominated by intermediate and old ages. The young population for Galaxy D has low-metallicity, the intermediate population has low and high-metallicity and the old populations have mid-metallicity. The low metallicity population has intermediate and old ages and the high-metallicity population is old.

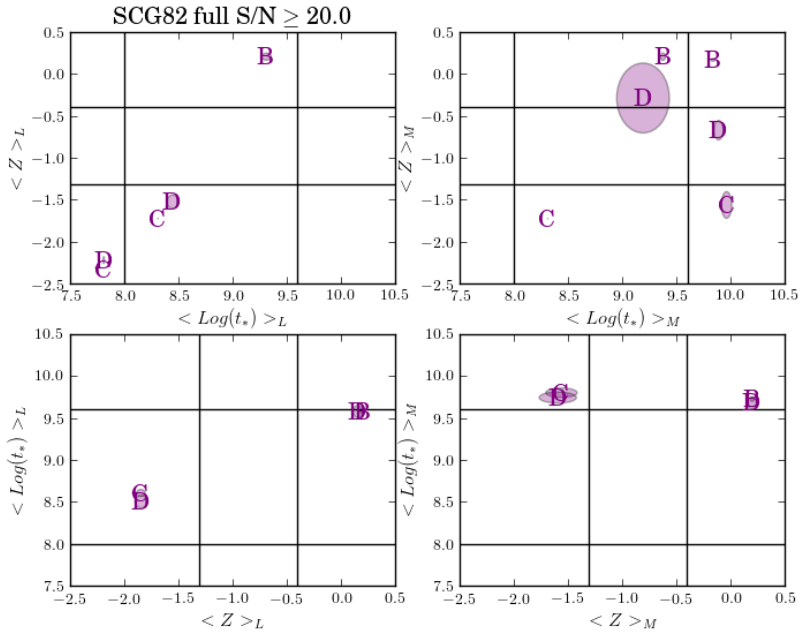

Figure 4.69: Age and metallicity plots for the extracted spectra of galaxies in SCG82.

Only Galaxy B could be analyzed in the 5” bins and its SPs reflect the extracted spectra.

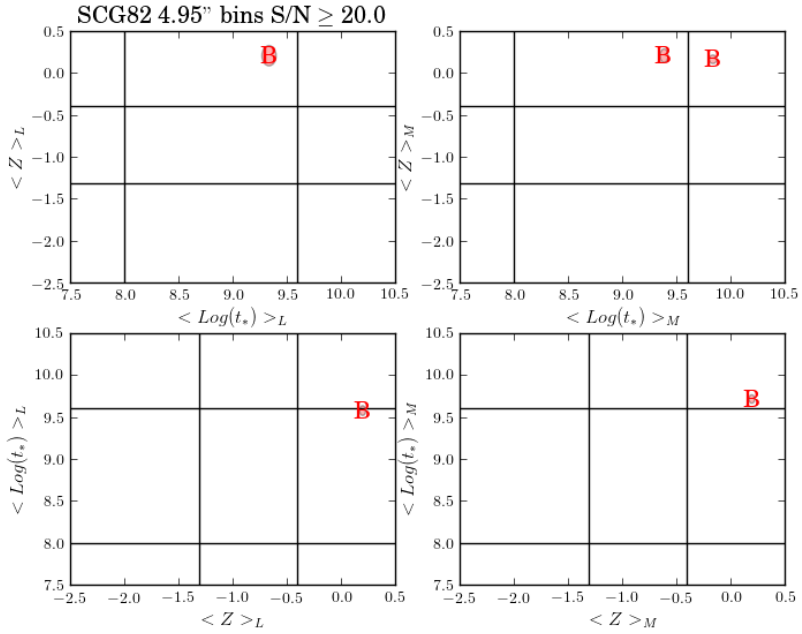

Figure 4.70: Age and metallicity plots for the 5” bin spectra of galaxies in SCG82.

In the 3” bins, Galaxy B still has the same SPs as in the previous two analyses. Galaxy C has low-metallicity intermediate and old populations. Galaxy D has similar SP characteristics as in the extracted spectrum except its intermediate aged population is described by low and mid metallicities.

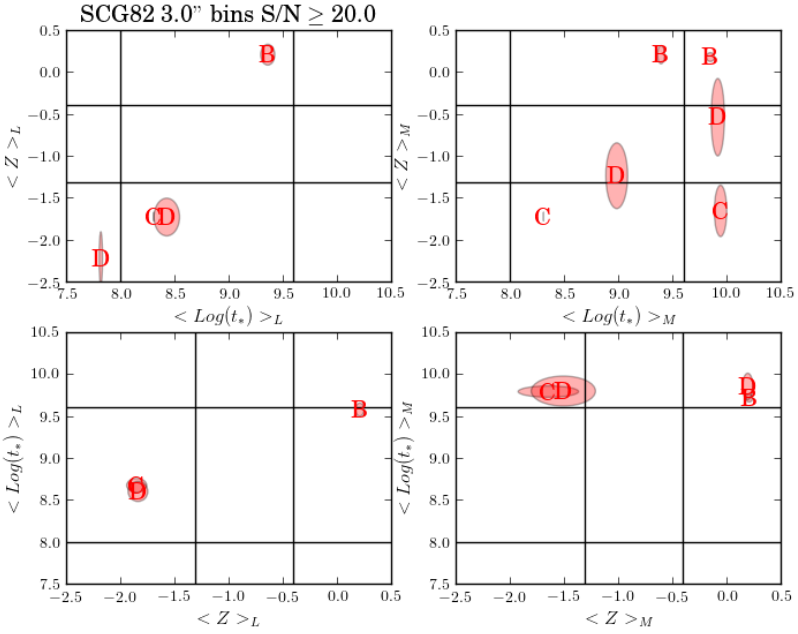

Figure 4.71: Age and metallicity plots for the 3” bin spectra of galaxies in SCG82.

Galaxies B and D had S/N high enough in their 1” spectra to be analyzed. Galaxy B still shows the same SP characteristics except now I see evidence of a young, low-metallicity population in its central region. Galaxy D continues to have the same SPs as in its 3” spectra except its old SPs have a high-metallicity.

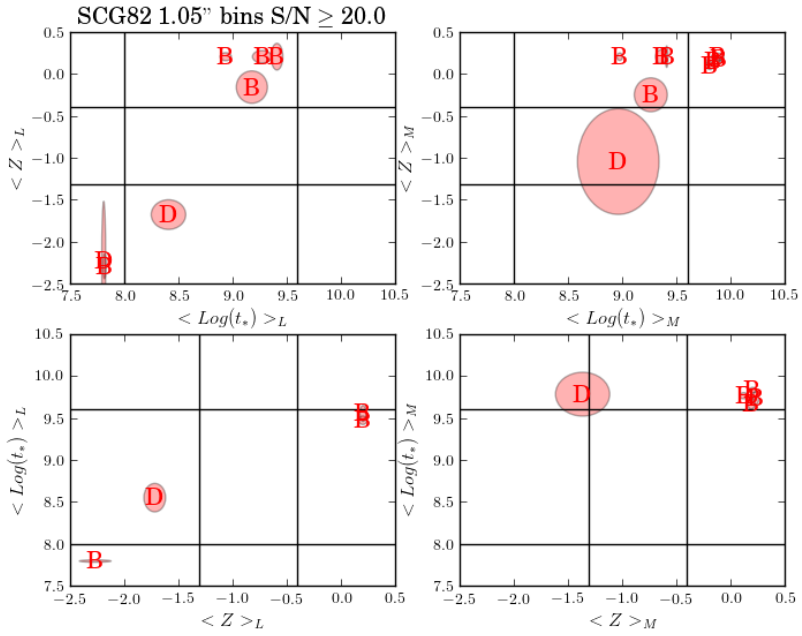

Figure 4.72: Age and metallicity plots for the 1" bin spectra of galaxies in SCG82.

In the activity plots for the fully extracted spectra, Galaxy A is a Seyfert AGN, Galaxy B is a LINER and Galaxies C and D are SF.

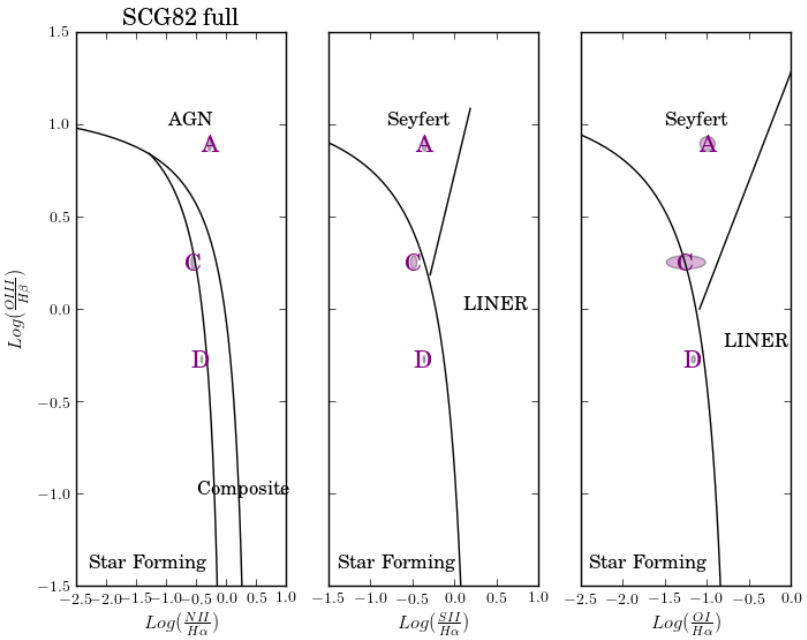

Figure 4.73: Activity plots for the extracted spectra of galaxies in SCG82.

In the 10" and 5" spectra, Galaxy A is still a Seyfert AGN.

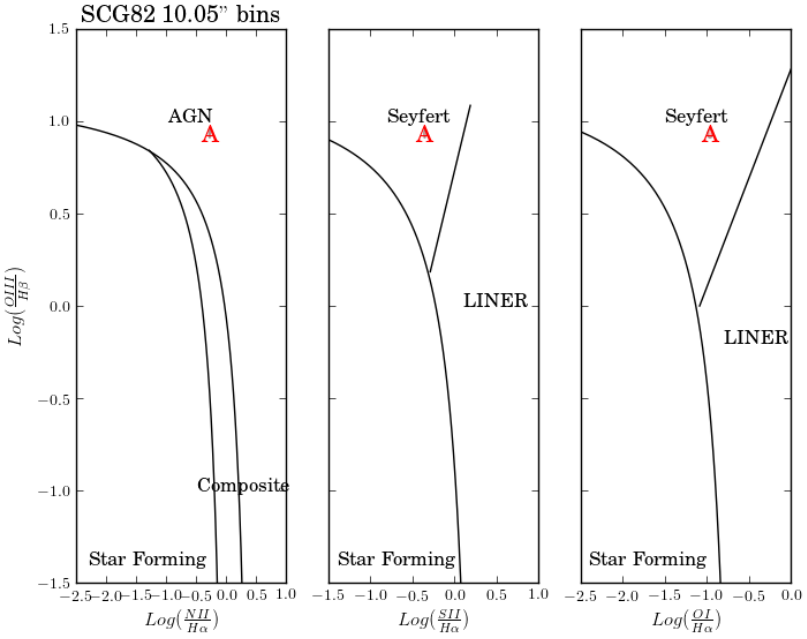

Figure 4.74: Activity plots for the 10" bin spectra of galaxies in SCG82.

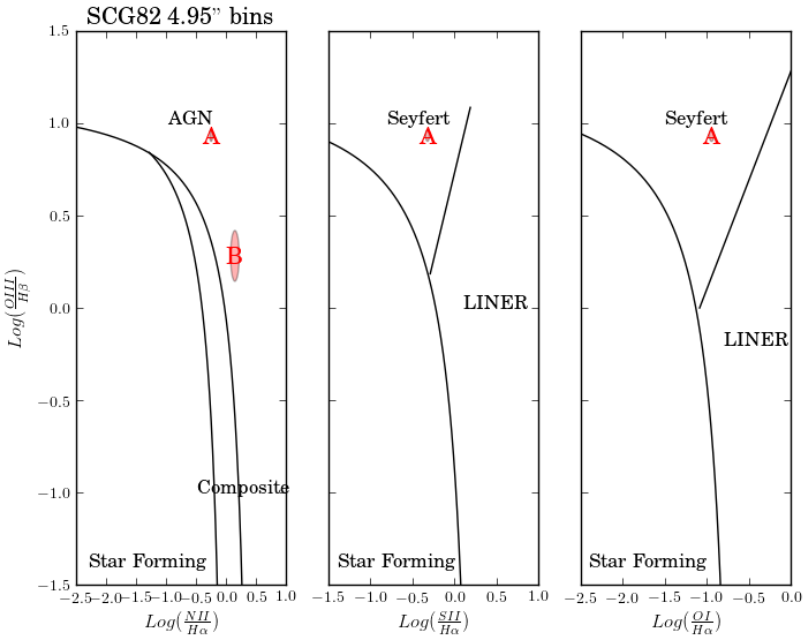

Figure 4.75: Activity plots for the 5" bin spectra of galaxies in SCG82.

In the 3" spectra, the activity analysis is the same as in the extracted spectra only Galaxy B now shows a LINER in its mid-regions and some AGN activity in its central regions.

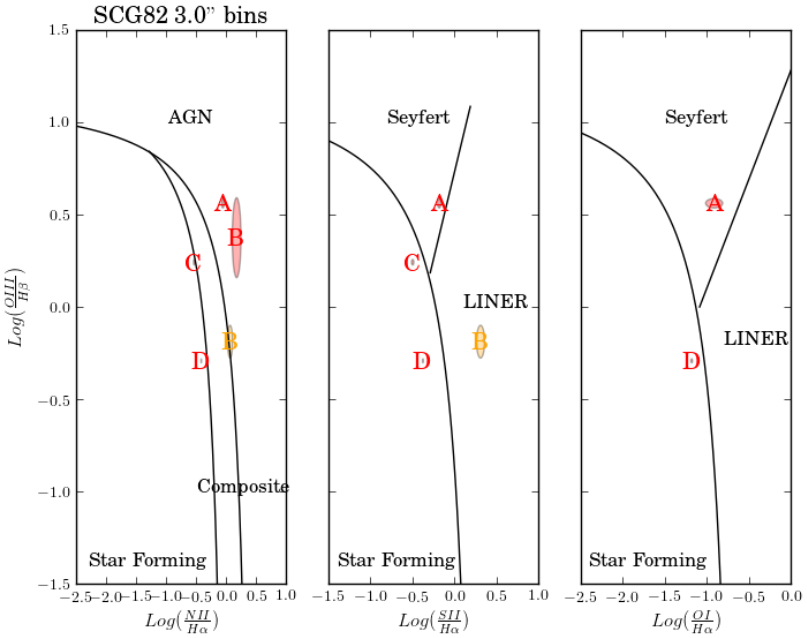

Figure 4.76: Activity plots for the 3" bin spectra of galaxies in SCG82.

At the smallest bin size, Galaxy A remains a Seyfert and Galaxy B remains a LINER in both its central and mid-regions but Galaxy C becomes a composite/SF galaxy and D becomes a LINER/SF galaxy.

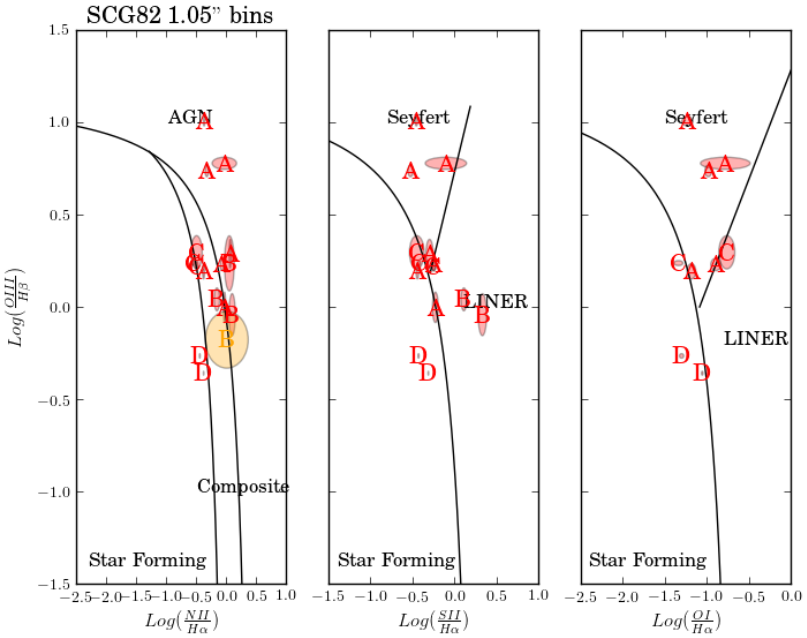

Figure 4.77: Activity plots for the 1" bin spectra of galaxies in SCG82.

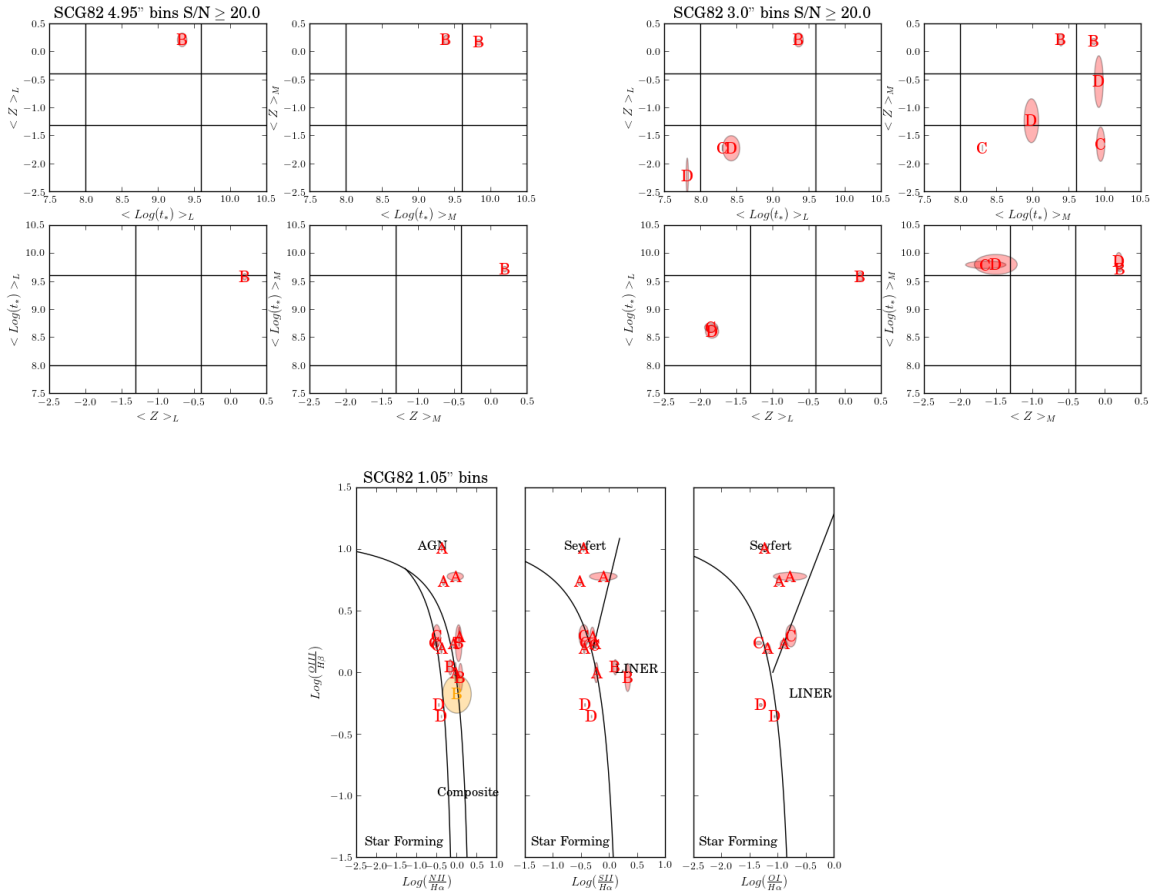

Figure 4.78: Stellar population results for the 5" and 3" bins and activity information for the 1" bins for SCG82.

Spiral galaxy A did not have any SP information that could be analyzed and registers as a Seyfert and SF on its BPT diagrams. Galaxy B has high-metallicity intermediate and old populations which implies that it underwent multiple SF episodes > 4 Gyrs ago that processed its gas. Galaxy C has an irregular morphology and is a composite with low metallicities in its intermediate and old populations. This implies that it still had low-metallicity cold gas between $0.1 - 4$ Gyrs ago. Galaxy D is SF with low-metallicity young and intermediate populations. It also shows mid and high-metallicity intermediate and old populations which suggests that a SF episode occurred a $0.1 - 4$ Gyrs ago using preprocessed gas but the current episode of SF is using low-metallicity gas.

Population	full	10”	5”	3”	1”
Galaxy A					
Young					
Intermediate					
Old					
Low					
Mid					
High					
Star Forming					
Seyfert	X-a	X-c	X-c	X-c	X-c
LINER					
AGN					
Comp					
Galaxy B					
Young					L-c
Intermediate	H-a		H-c	H-c	H-c
Old	H-a		H-c	H-c	H-c
Low					Y-c
Mid					
High	O-a		O-c	O-c	O-c
Star Forming					
Seyfert					
LINER	X-a			X-m	X-c/m
AGN			X-c	X-c	
Comp					

Population	full	10”	5”	3”	1”
Galaxy C					
Young	L-a				
Intermediate	L-a			L-c	
Old	L-a			L-c	
Low	I/O-a			I/O-c	
Mid					
High					
Star Forming	X-a			X-c	X-c
Seyfert					
LINER					
AGN				X-c	
Comp					X-c
Galaxy D					
Young	L-a			L-c	L-c
Intermediate	L/H-a			L/M-c	L/M-c
Old	M-a			M-c	H-c
Low	I/O-a			I/O-c	I/O-c
Mid					
High	O-a			O-c	O-c
Star Forming	X-a			X-c	X-c
Seyfert					
LINER					X-c
AGN					
Comp					

Table 4.12: Stellar population and activity analysis summary for SCG82. Same codes as in Table 4.4

4.3.7: SCG83

SCG83 is made up of five galaxies with two showing early-type morphologies and three having late-type. Galaxies A and C show signs of tidal streams from a previous interaction.

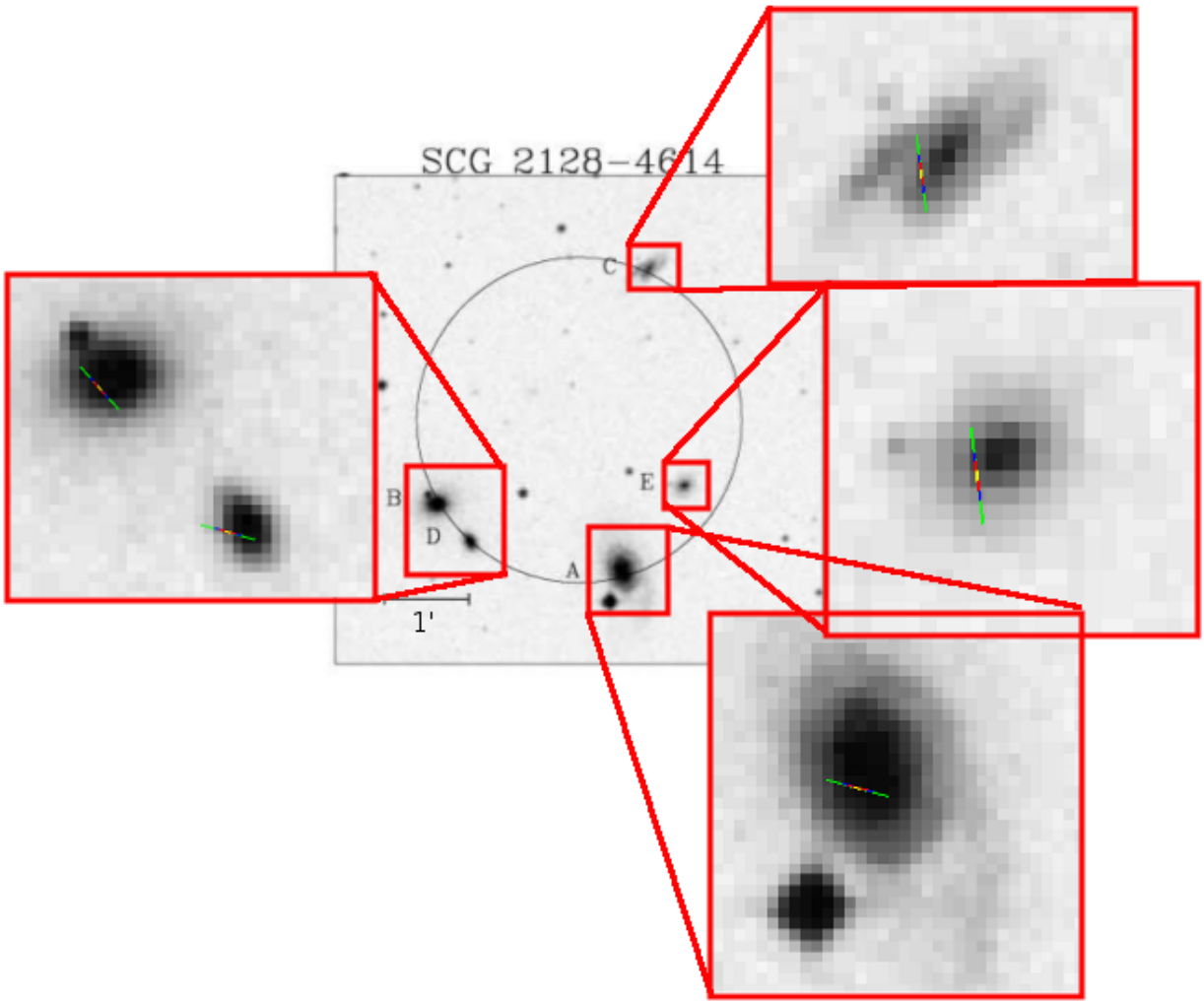

Figure 4.79: Group SCG83.

All galaxies are members of this group according to our velocity dispersion analysis.

$\Delta z(km/s)$	B	C	D	E
A	153.69	−9.24	283.95	111.63
B		−162.93	130.26	−42.06
C			293.19	120.87
D				−172.32

Table 4.13: Derived redshift differences for group SCG83.

The distribution of galaxies in redshift space is plotted below. Galaxies A, C and E appear to be near the edges of the group and Galaxy B may be the most central member.

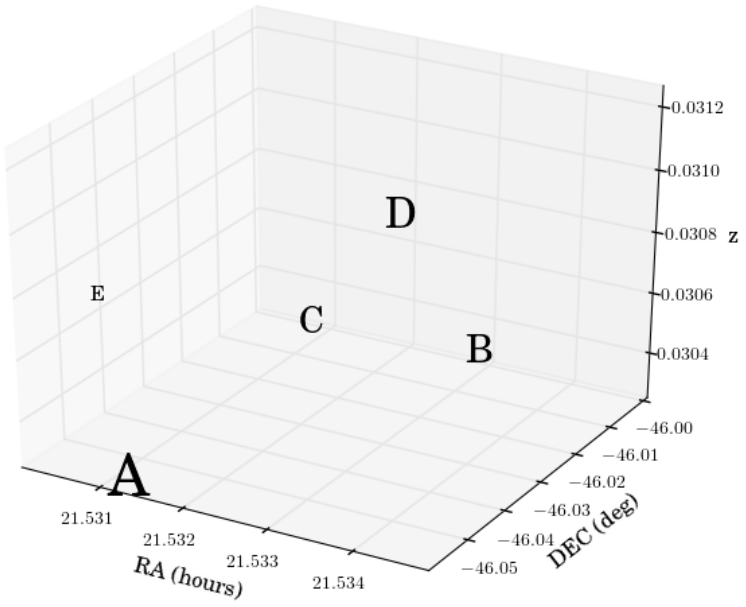

Figure 4.80: Galaxy distribution for SCG83.

Galaxy C could not be plotted in this analysis. The SPs of the extracted spectra reveal that Galaxy A has a low-metallicity young population and high-metallicity intermediate and old populations. The low metallicity populations have intermediate ages while the mid and high-metallicity populations are old. Galaxy B has old populations with high-metallicity. Galaxy D has mid-metallicity young SPs, low-metallicity intermediate SPs and high-metallicity old SPs. The mid and high-metallicity populations are old and the low-metallicity populations are intermediate. Galaxy E has low-metallicity young SPs and mid-metallicity old SPs. The low-metallicity populations are intermediate and the mid and high-metallicity populations are old.

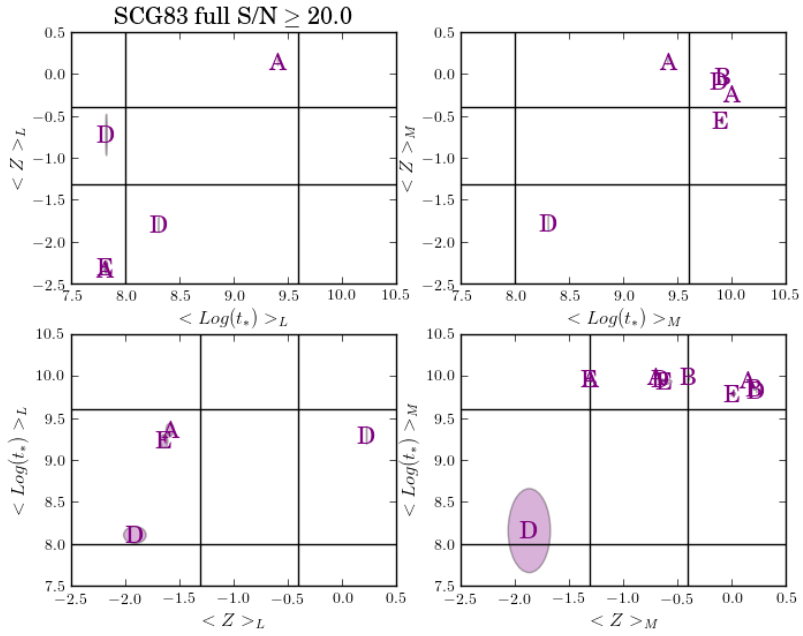

Figure 4.81: Age and metallicity plots for the extracted spectra of galaxies in SCG83.

Only Galaxy A has a 10” spectrum which shows low-metallicity young SPs and high-metallicity intermediate and old SPs.

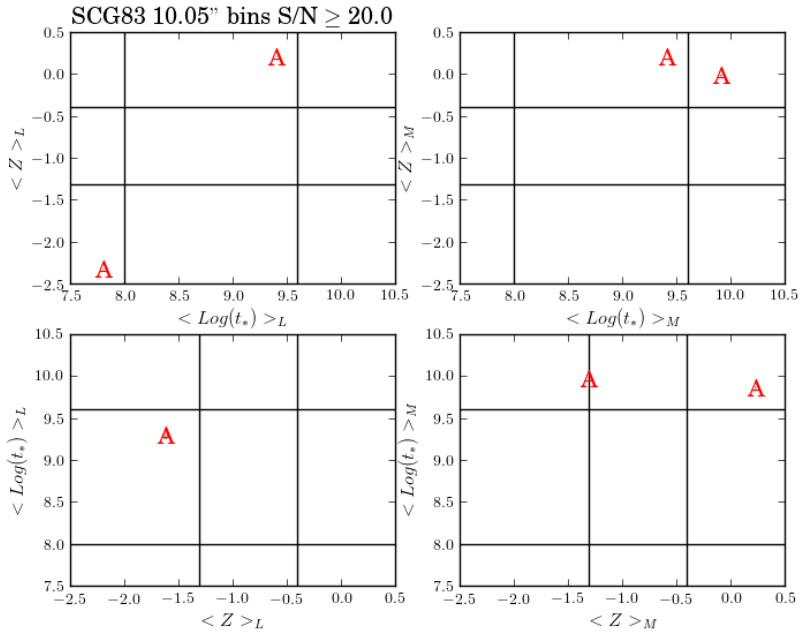

Figure 4.82: Age and metallicity plots for the 10" bin spectra of galaxies in SCG83.

In the 5" spectra, Galaxy A has young, low-metallicity SPs and old, mid and high-metallicity populations. Galaxy B shows the same SPs as in its extracted spectrum with an added old mid-metallicity population. Galaxy E has a low-metallicity young SP, a high-metallicity intermediate SP and a mid-metallicity old SP. The low, mid and high-metallicity SPs are old.

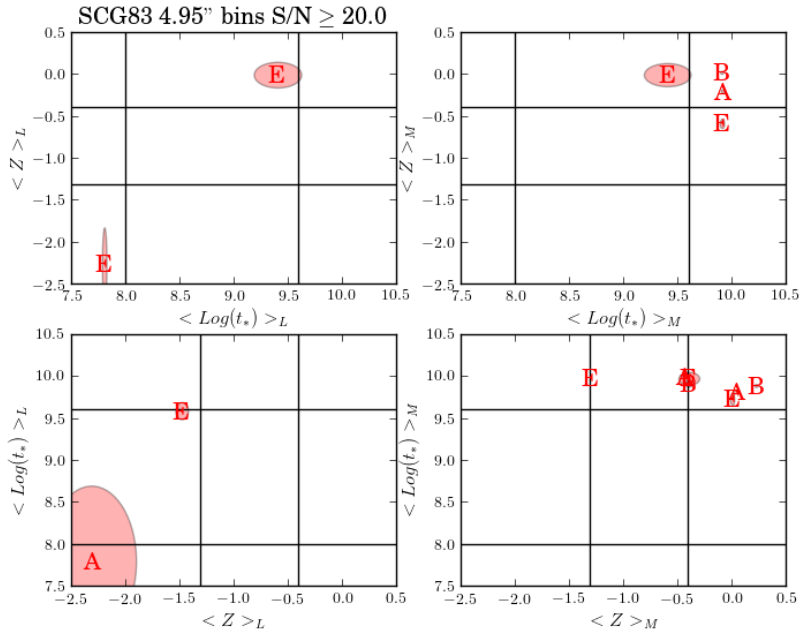

Figure 4.83: Age and metallicity plots for the 5" bin spectra of galaxies in SCG83.

Galaxy A has low-metallicity young SPs and high-metallicity old SPs in its 3" bins. All the metallicity populations are old. Galaxy B has the same SP properties as the 5" bins. Galaxy D has low-metallicity young SP and high-metallicity old SPs. The low and high-metallicity SPs are old. Galaxy E has high-metallicity intermediate populations and mid-metallicity old populations. The low and high-metallicity populations are old.

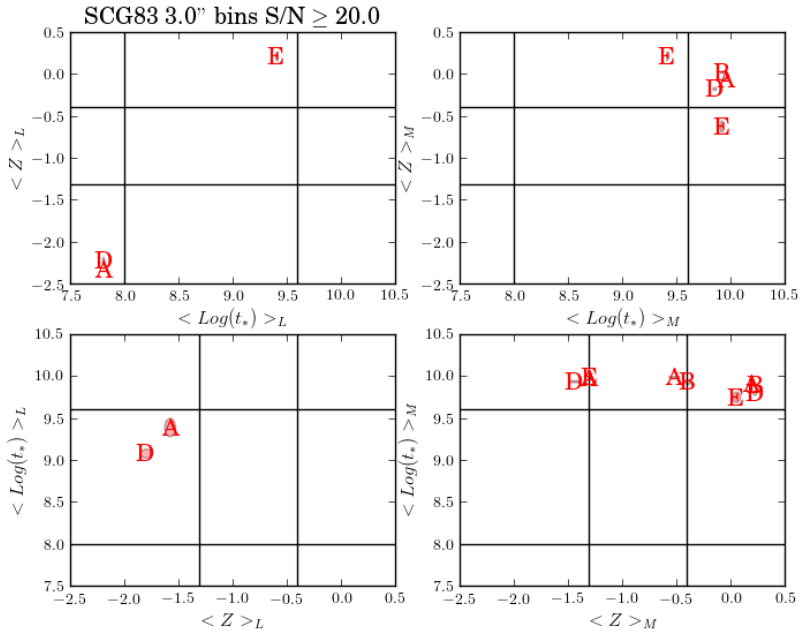

Figure 4.84: Age and metallicity plots for the 3" bin spectra of galaxies in SCG83.

In the 1" bins, Galaxy A has high-metallicity intermediate and old SPs. The low and high-metallicity SPs are old. Galaxy B continues to have the same SPs as discussed above. Galaxy D has the same SPs as the 3" bins with an added mid-metallicity population with old ages and low-metallicity SP with intermediate ages. Galaxy E has high metallicity intermediate SPs and mid old SPs. The low and mid-metallicity SPs are old and the high-metallicity SPs are intermediate and old.

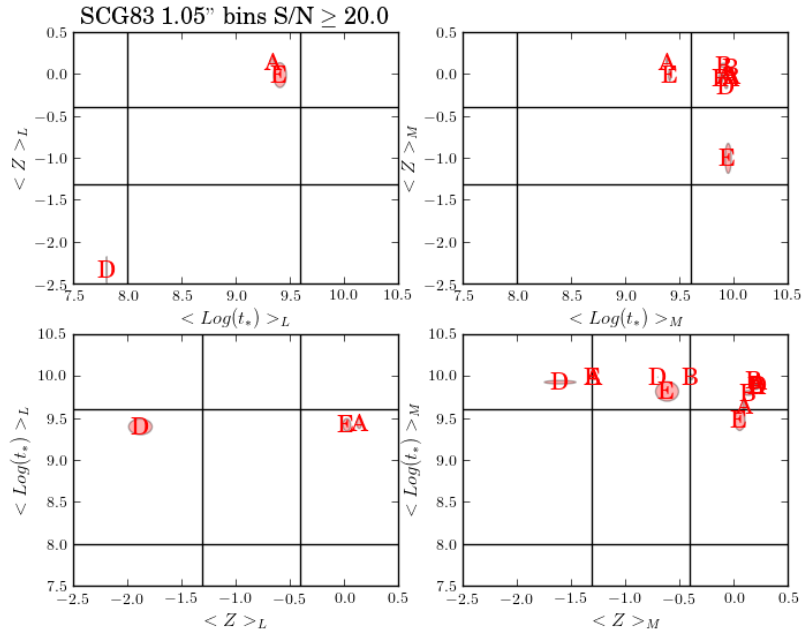

Figure 4.85: Age and metallicity plots for the 1" bin spectra of galaxies in SCG83.

Galaxies A and B show AGN activity in their fully extracted spectra. Galaxies C and D are SF.

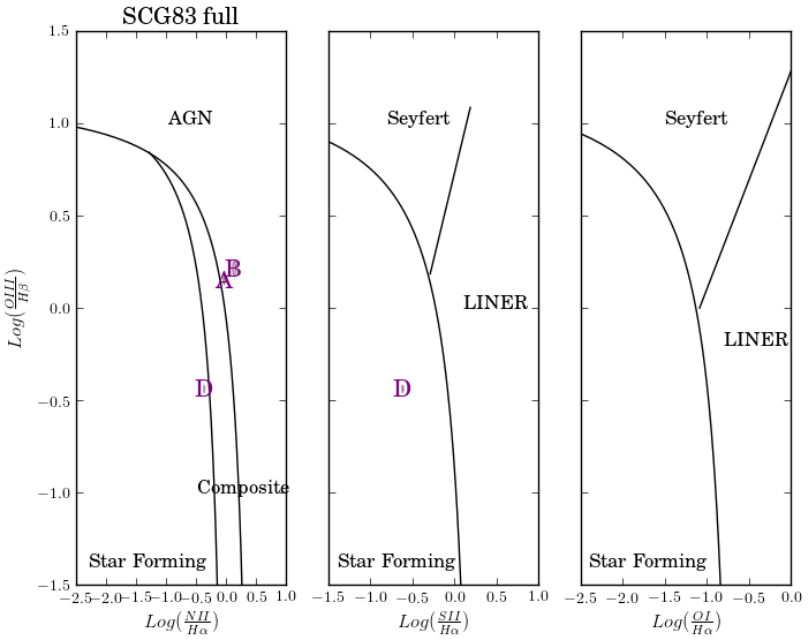

Figure 4.86: Activity plots for the extracted spectra of galaxies in SCG83.

Galaxy A shows AGN activity in its 10” spectrum.

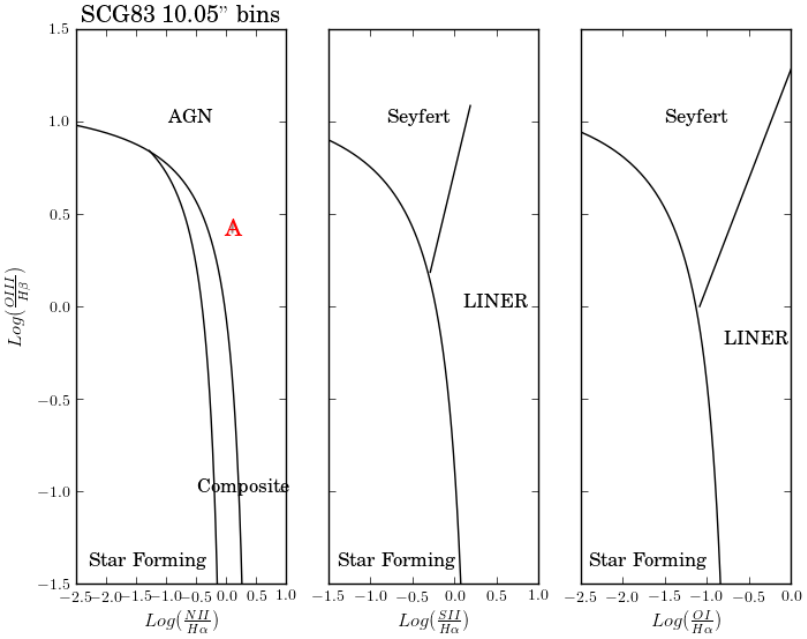

Figure 4.87: Activity plots for the 10” bin spectra of galaxies in SCG83.

In the 5” spectra, Galaxy A shows a SF and composite spectrum, Galaxy B shows a composite spectrum and Galaxy C is SF.

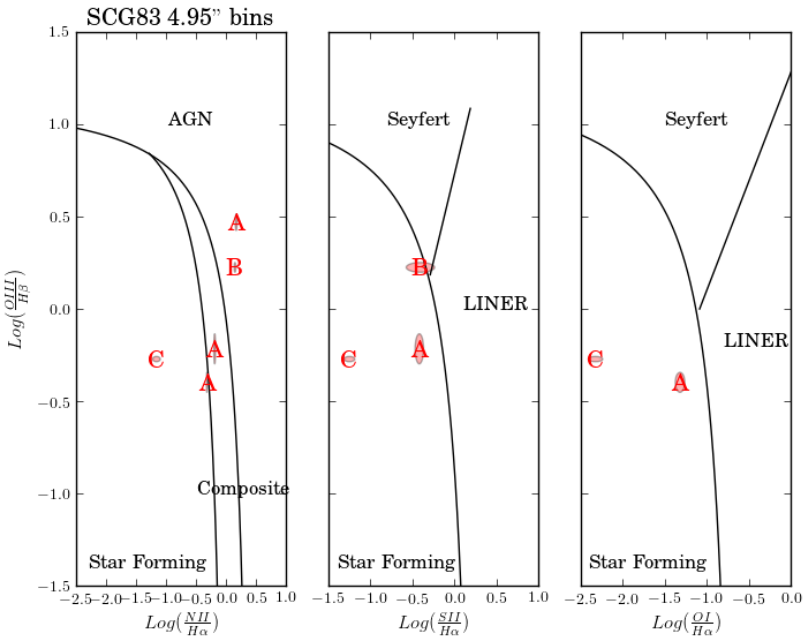

Figure 4.88: Activity plots for the 5" bin spectra of galaxies in SCG83.

In the 3" spectra, Galaxy A is a composite galaxy, Galaxy B is a Seyfert, Galaxy C is a LINER, Galaxy D is SF and Galaxy E is SF in its central and mid-regions.

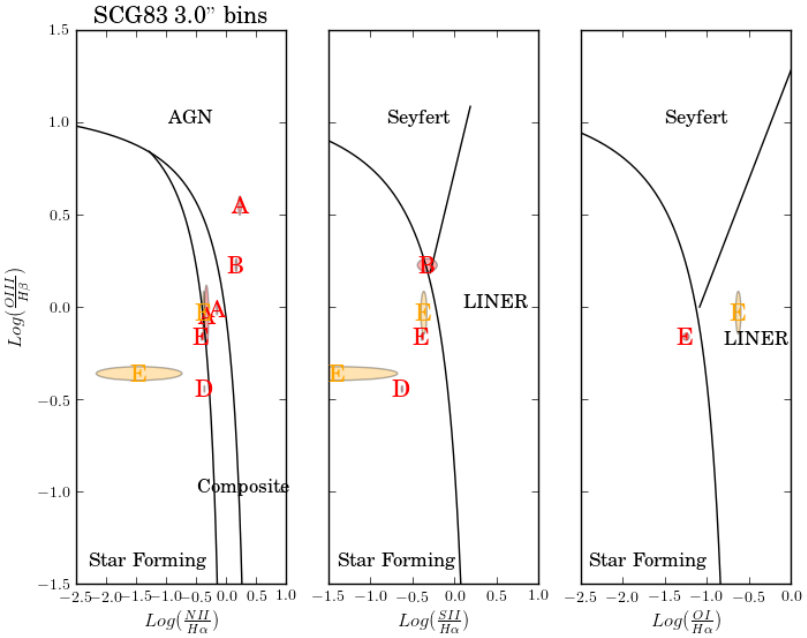

Figure 4.89: Activity plots for the 3" bin spectra of galaxies in SCG83.

Finally in the 1" spectra, Galaxy A is SF and AGN, Galaxy B is a LINER, Galaxy C is SF and LINER and Galaxies D and E are SF.

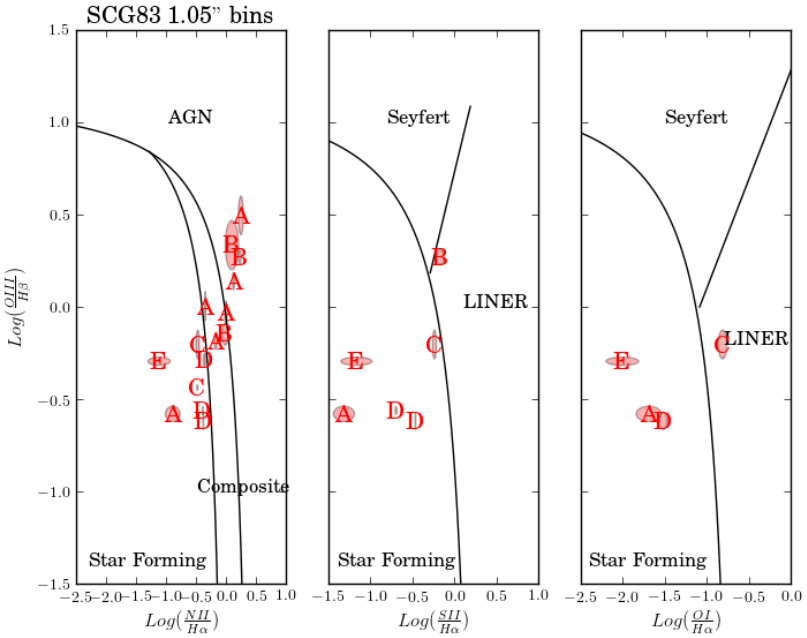

Figure 4.90: Activity plots for the 1" bin spectra of galaxies in SCG83.

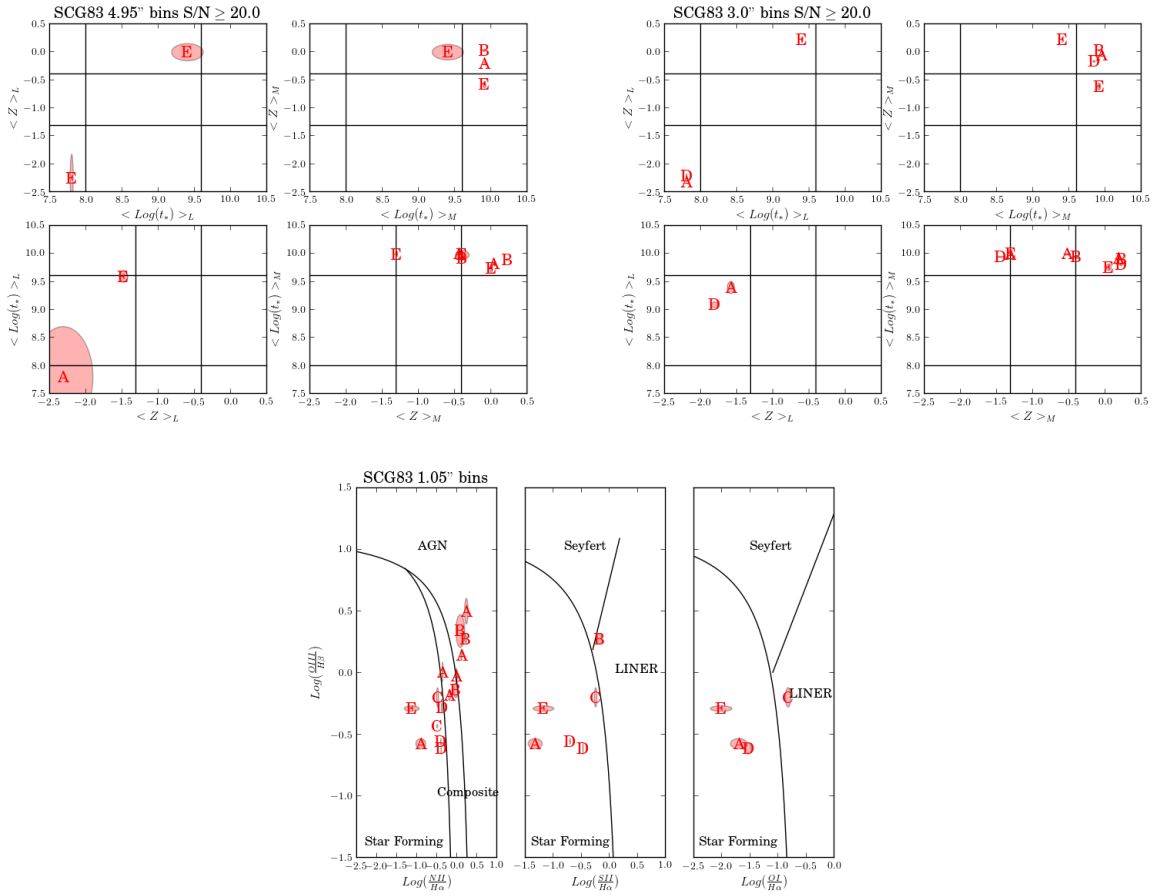

Figure 4.91: Stellar population results for the 5" and 3" bins and activity information for the 1" bins for SCG83.

According to the SP analysis, Galaxies A, D and E may still have their cold gas supplies as evidenced by their low-metallicity young SPs. Galaxy A has an active nucleus with recent SF in its central regions. It also has evidence of a SF episode between > 4 Gyrs ago using preprocessed gas. The old populations with high-metallicity support this. An interaction may have also funneled low-metallicity cold gas into the center, which is fueling the current episode of SF. Galaxy B appears to have lost its cold gas supply > 4 Gyrs ago, most likely cut off via strangulation and used up during multiple episodes of SF. Galaxy C has a disturbed morphology and is a SF galaxy but does not have SP information. It is at the same redshift as Galaxy A so is a good interaction candidate for Galaxy A. Galaxies D and E appear to still have their cold gas supplies because they are both SF at their centers and have low-metallicity young SPs. They both also have high-metallicity older populations suggesting multiple, rapid episodes of SF quickly processed the gas between > 4 Gyrs ago.

Population	full	10”	5”	3”	1”
Galaxy A					
Young	L-a	L-c		L-c	
Intermediate	H-a	H-c			H-c
Old	H-a	H-c	H-c	H-c	H-c
Low	I-a	Y-c	Y-c	O-c	O-c
Mid	O-a		O-c	O-c	
High	O-a	O-c	O-c	O-c	O-c
Star Forming					X-c
Seyfert					
LINER					
AGN	X-a	X-c			X-c
Comp			X-c	X-c	
Galaxy B					
Young					
Intermediate					
Old	H-a		H-c	H-c	H-c
Low					
Mid			O-c	O-c	O-c
High	O-a		O-c	O-c	O-c
Star Forming					
Seyfert				X-c	
LINER					X-c
AGN	X-a				
Comp			X-c		
Galaxy C					
Young					
Intermediate					
Old					
Low					
Mid					
High					
Star Forming	X-a		X-c		X-c
Seyfert					
LINER				X-c	X-c
AGN					
Comp					

Population	full	10”	5”	3”	1”
Galaxy D					
Young	M-a			L-c	L-c
Intermediate	L-a				
Old	H-a			H-c	H-c
Low	I-a			O-c	I/O-c
Mid	O-a				O-c
High	O-a			O-c	O-c
Star Forming	X-a			X-c	X-c
Seyfert					
LINER					
AGN					
Comp					
Galaxy E					
Young	L-a		L-c		
Intermediate			H-c	H-c	H-c
Old	M-a		M-c	M-c	M-c
Low	I-a		O-c	O-c	O-c
Mid	O-a		O-c		O-c
High	O-a		O-c	O-c	I/O-c
Star Forming				X-c/m	X-c
Seyfert					
LINER					
AGN					
Comp					

Table 4.14: Stellar population and activity analysis summary for SCG83. Same codes as in Table 4.4

4.3.8: SCG88

SCG88 is comprised of four galaxies. Two are early-type galaxies and two are late-type galaxies. Galaxy A appears to have had an encounter in its past.

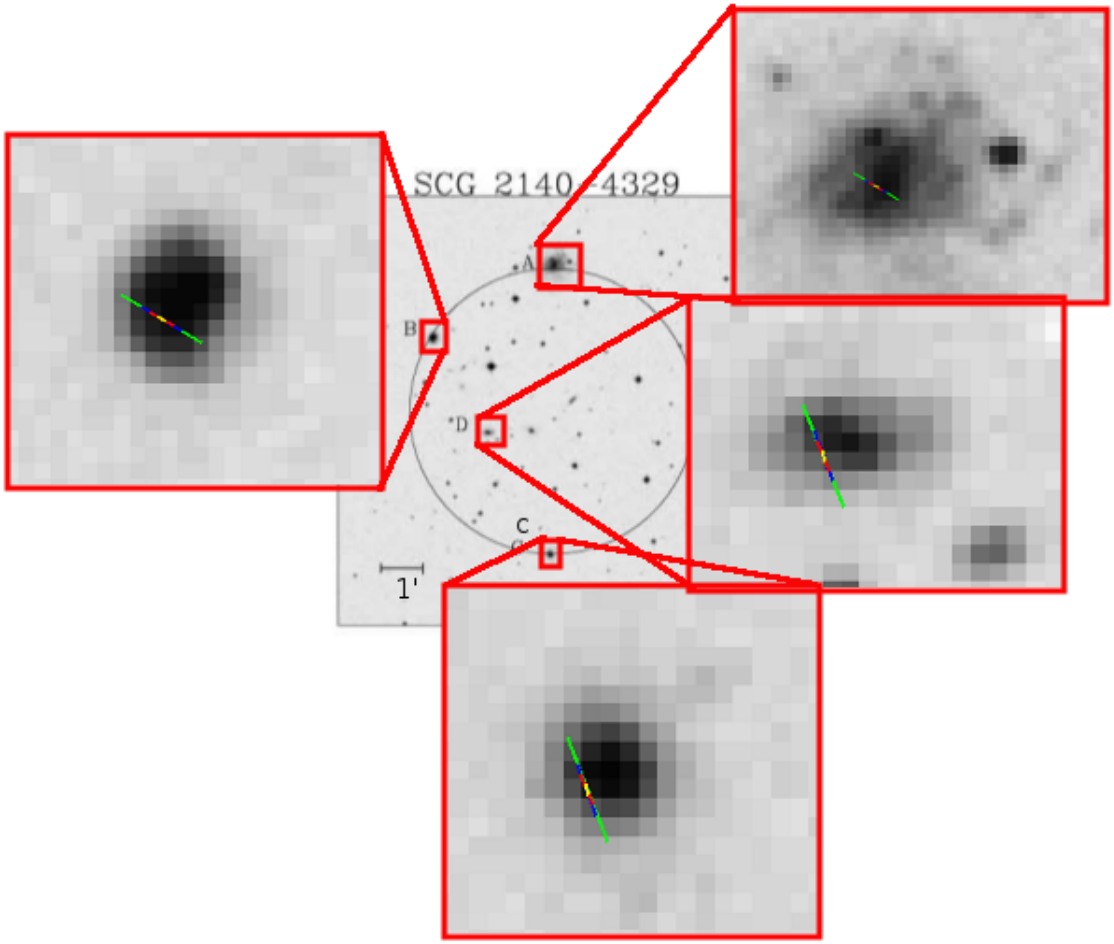

Figure 4.92: Group SCG88.

Galaxy A is not a part of this group. The other three galaxies are within the velocity dispersion limits I set.

$\Delta z(km/s)$	B	C	D
A	14032.77	13730.67	14015.67
B		−302.1	−17.1
C			285.0

Table 4.15: Derived redshift differences for group SCG88.

This is also clear from the distribution plot. Galaxies B, C and D do not have a clear central member.

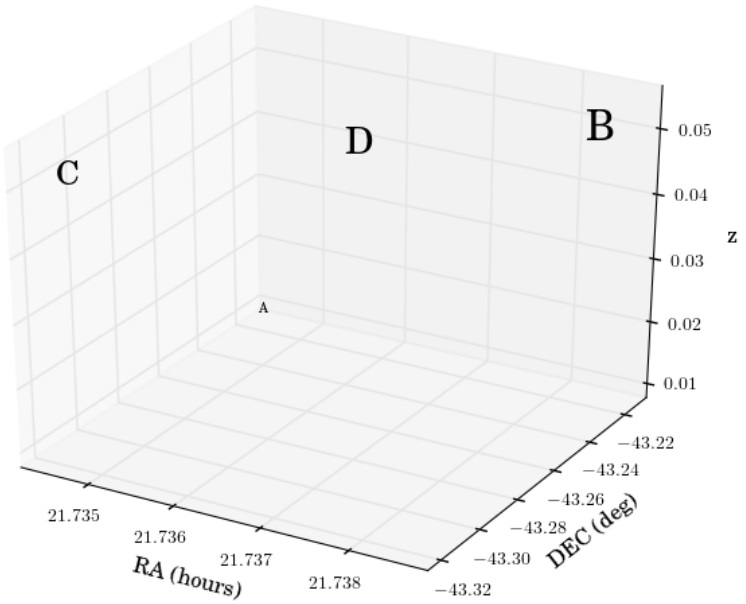

Figure 4.93: Galaxy distribution for SCG88.

In the extracted spectra, Galaxies B and D both have low-metallicity old populations and their low and mid-metallicity populations are old. Galaxy D has intermediate ages for its high-metallicity SPs.

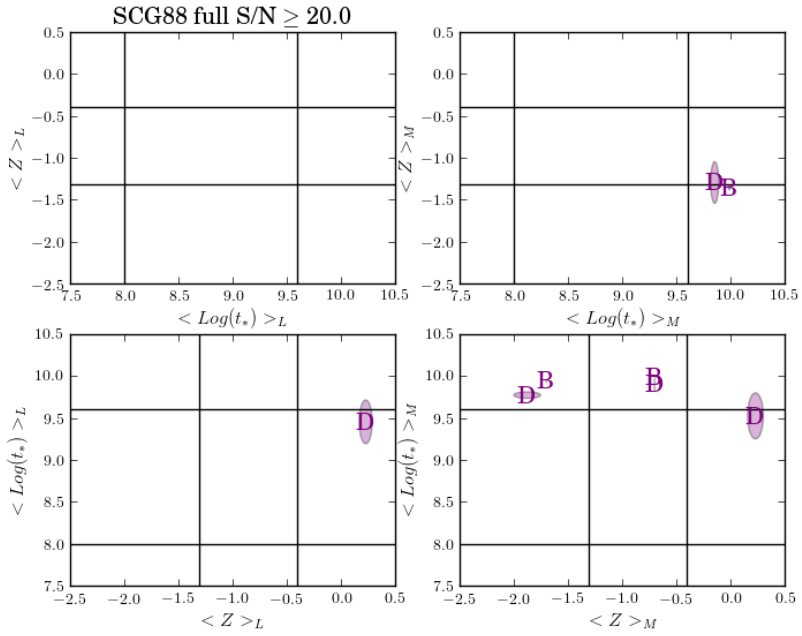

Figure 4.94: Age and metallicity plots for the extracted spectra of galaxies in SCG88.

In the 5” spectra, Galaxies A and B show mid-metallicity old SPs and old low and high-metallicity SPs.

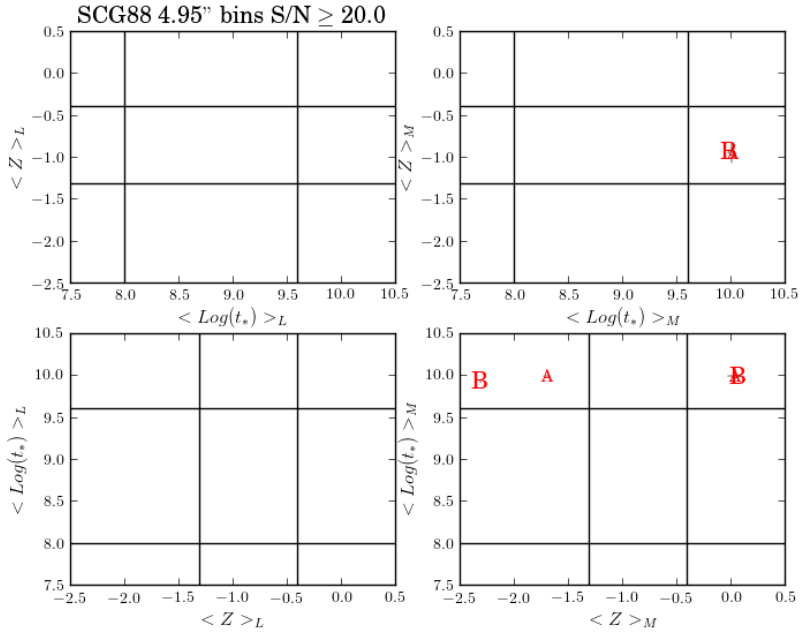

Figure 4.95: Age and metallicity plots for the 5” bin spectra of galaxies in SCG88.

Galaxy B has low-metallicity intermediate SPs and high-metallicity old SPs. The low and high-metallicity SPs are old and the mid-metallicity SPs have intermediate ages. Galaxy D has mid-metallicity old SPs and old, low and mid-metallicity populations. All measurements are for the central regions.

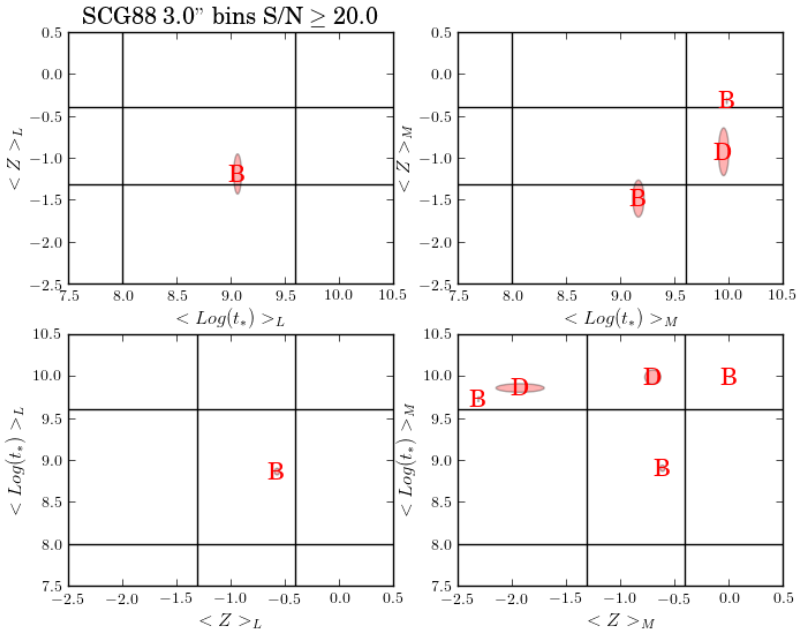

Figure 4.96: Age and metallicity plots for the 3" bin spectra of galaxies in SCG88.

The central regions in the 1" bins for Galaxy B has low, mid and high-metallicity intermediate SPs and high-metallicity old SPs. The low-metallicity populations have intermediate ages and the mid and high-metallicity populations have intermediate and old ages. For Galaxy D, the intermediate SPs have high metallicities and the old populations have mid-metallicity. The low and mid-metallicity SPs are old while the high-metallicity populations have intermediate and old ages.

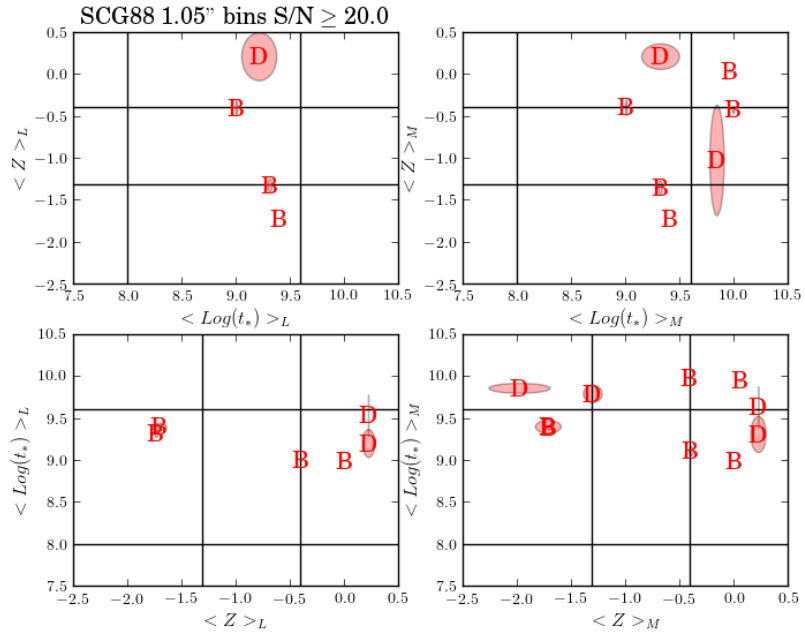

Figure 4.97: Age and metallicity plots for the 1" bin spectra of galaxies in SCG88.

The activity in the fully extracted spectra shows that Galaxies B and D are SF galaxies.

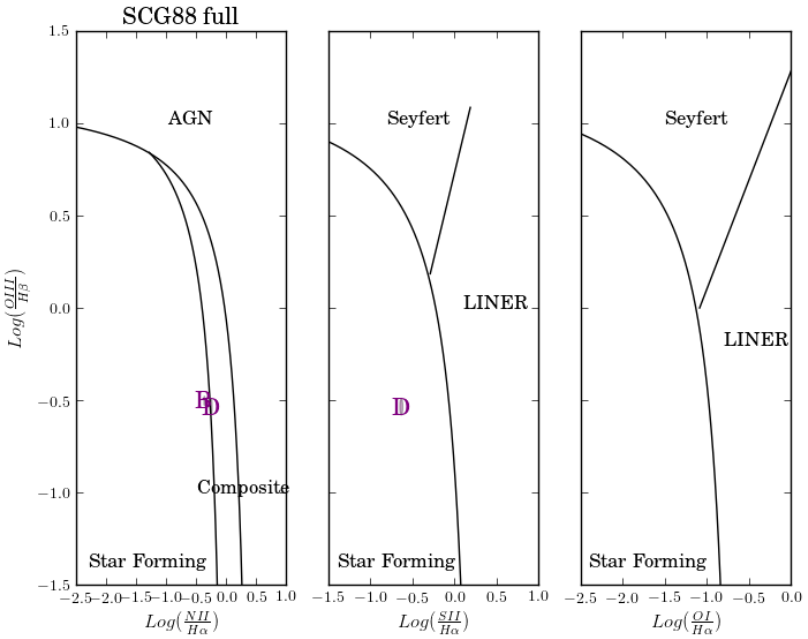

Figure 4.98: Activity plots for the extracted spectra of galaxies in SCG88.

In the 10” bin plot, Galaxy A is SF.

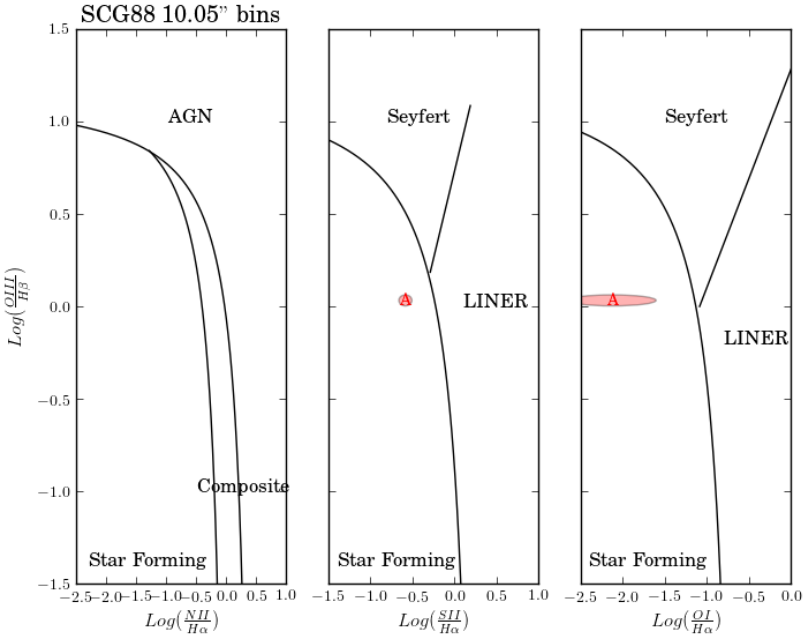

Figure 4.99: Activity plots for the 10” bin spectra of galaxies in SCG88.

Galaxies A and B are both SF in the 5” spectra.

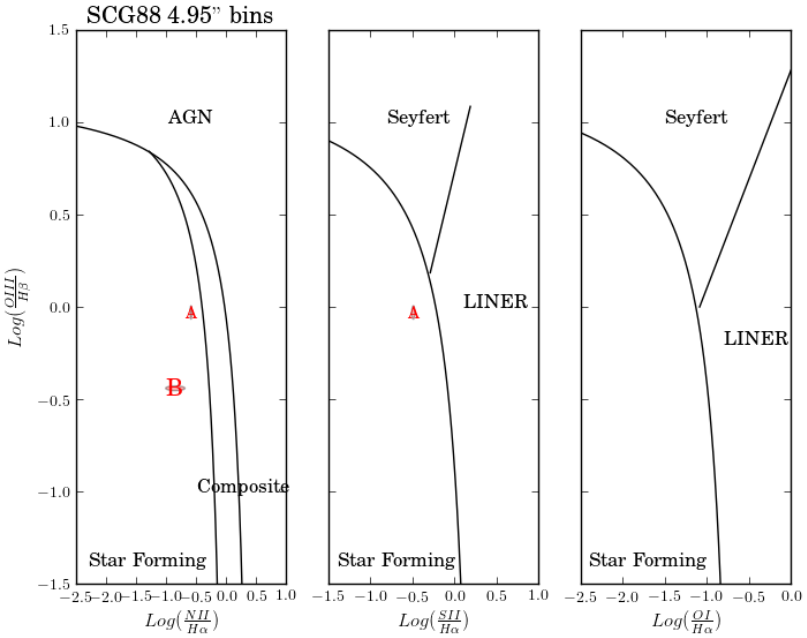

Figure 4.100: Activity plots for the 5" bin spectra of galaxies in SCG88.

Galaxies A, B and D are all SF in the 3" spectra.

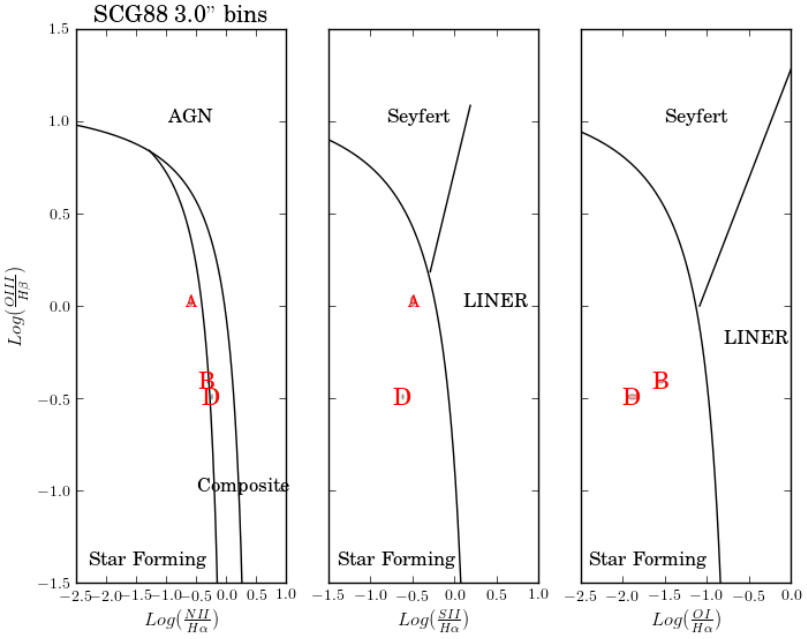

Figure 4.101: Activity plots for the 3" bin spectra of galaxies in SCG88.

In the 1” spectra, Galaxies A, B and D are all SF in their centers. Galaxy A shows evidence of a LINER in its center and SF in it’s mid-regions. Galaxies C and D have composite spectra in their central regions.

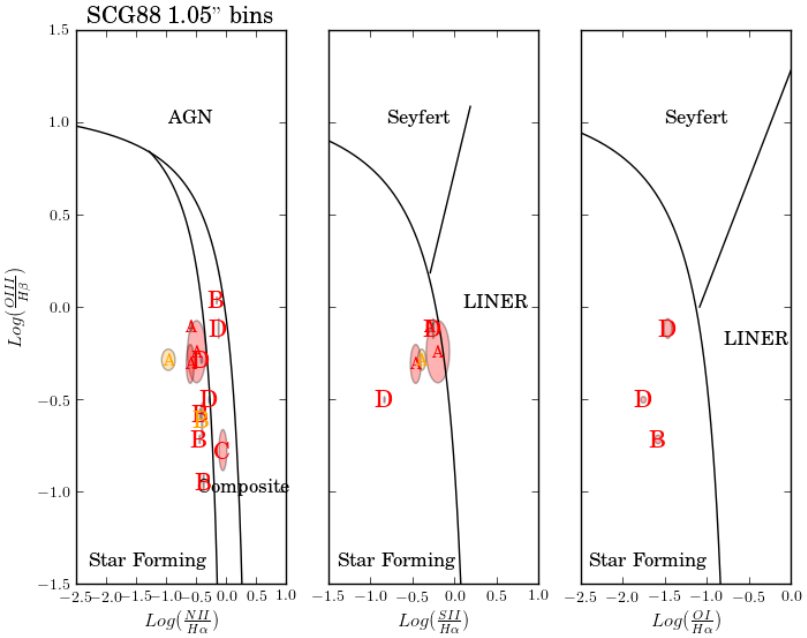

Figure 4.102: Activity plots for the 1” bin spectra of galaxies in SCG88.

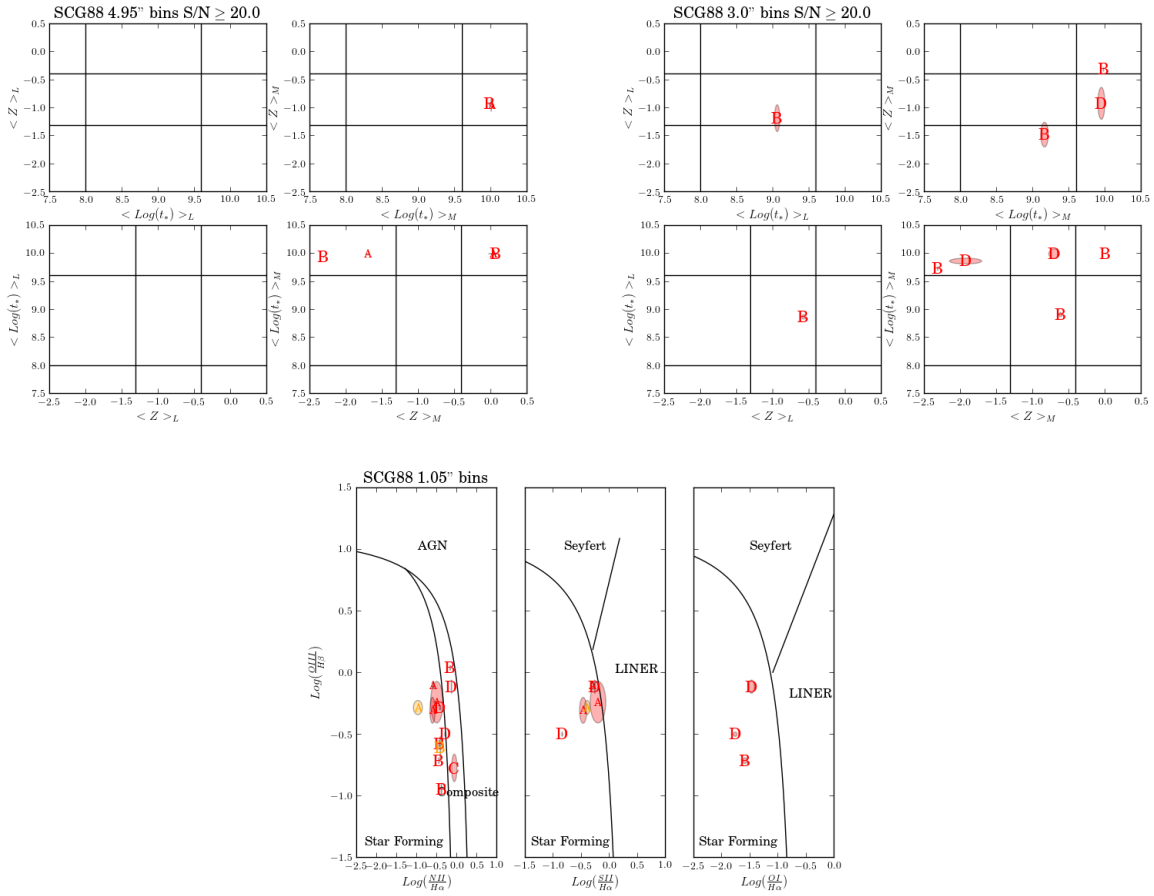

Figure 4.103: Stellar population results for the 5" and 3" bins and activity information for the 1" bins for SCG88.

All galaxies except C show evidence of being SF galaxies in their BPT diagrams but do not have any young SPs in their central regions. Galaxy A is not in the group and has an irregular morphology. Its SPs are dominated by older stars of low and mid-metallicities. Galaxy B has old and intermediate aged populations with low and mid-metallicities so could still have its cold gas supply or it was shut off between $0.1-4$ Gyrs ago when this SF episode began. Galaxy D is made up of mostly low and mid-metallicity old populations with some low-metallicity old populations as well. This could indicate a rapid processing of gas through multiple episodes of SF between $0.1-4$ Gyrs ago. Galaxy C has no SP analysis and shows a composite spectrum. Ultimately, this group needs longer exposures. The SF could be happening in the outer regions of the galaxies so my SP analysis is missing those regions because the S/N is too low.

Population	full	10”	5”	3”	1”
Galaxy A					
Young					
Intermediate					
Old			M-c		
Low			O-c		
Mid					
High			O-c		
Star Forming		X-c	X-c	X-c	X-c/m
Seyfert					
LINER					X-c
AGN					
Comp					
Galaxy B					
Young					
Intermediate				L-c	L/M/H-c
Old	L-a		M-c	H-c	H-c
Low	O-a		O-c	O-c	I-c
Mid	O-a			I-c	I/O-c
High			O-c	O-c	I/O-c
Star Forming	X-a		X-c	X-c	X-c
Seyfert					
LINER					
AGN					
Comp					

Population	full	10”	5”	3”	1”
Galaxy C					
Young					
Intermediate					
Old					
Low					
Mid					
High					
Star Forming					
Seyfert					
LINER					
AGN					
Comp					X-c
Galaxy D					
Young					
Intermediate					H-c
Old	L-a			M-c	M-c
Low	O-a			O-c	O-c
Mid	O-a			O-c	O-c
High	I-a				I/O-c
Star Forming	X-a			X-c	X-c
Seyfert					
LINER					
AGN					
Comp					X-c

Table 4.16: Stellar population and activity analysis summary for SCG88. Same codes as in Table 4.4

4.3.9: SCG106

The four galaxies that make up SCG106 appear to all be early-type galaxies.

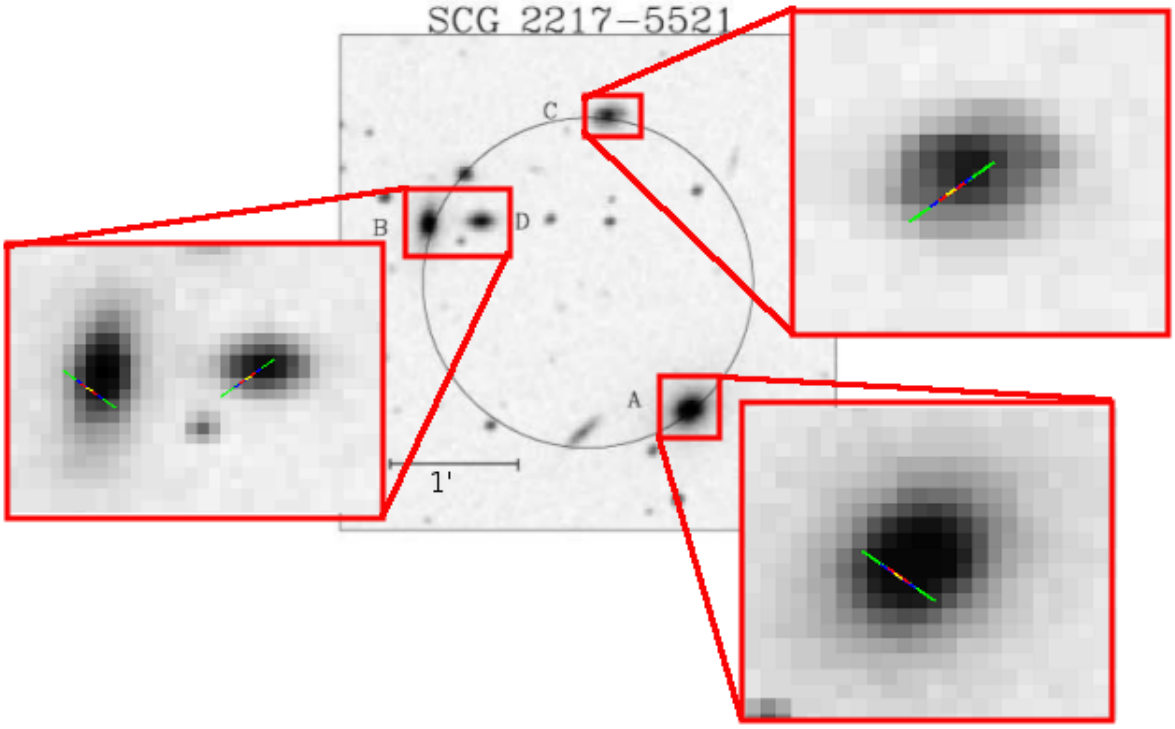

Figure 4.104: Group SCG106.

My redshift analysis reveals that Galaxy D is not a part of this group. The other members have very low velocity dispersions.

$\Delta z(km/s)$	B	C	D
A	89.7	127.8	624.0
B		38.1	534.3
C			496.2

Table 4.17: Derived redshift differences for group SCG106.

The distribution of galaxies in redshift space is plotted below. Galaxies A, B and C do not have a clear center but C is at a higher redshift than A and B so may be at the edge of the group.

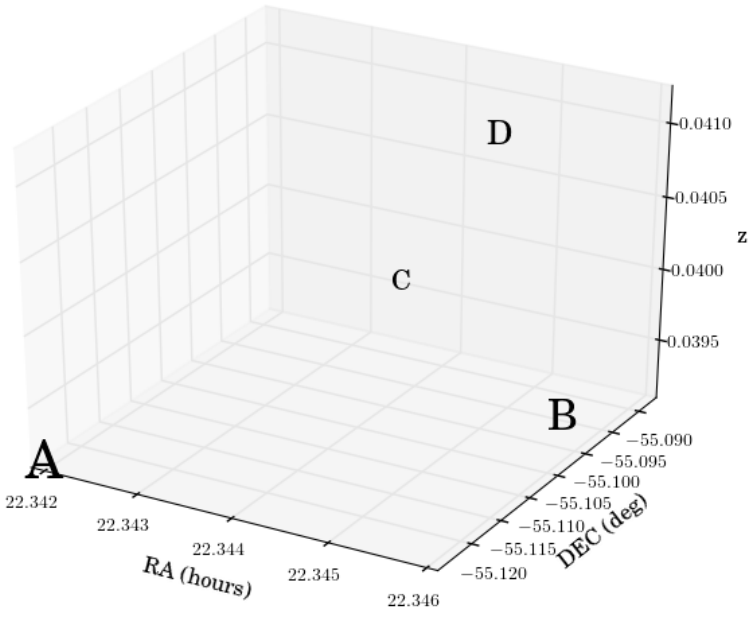

Figure 4.105: Galaxy distribution for SCG106.

Galaxy A has low-metallicity intermediate SPs and high-metallicity old SPs in its extracted spectrum. Galaxy B has high-metallicity old SPs. Galaxy C has mid-metallicity old SPs and its low and high-metallicity SPs are old. Galaxy D has mid-metallicity intermediate and old populations. Its low and high-metallicity populations are old.

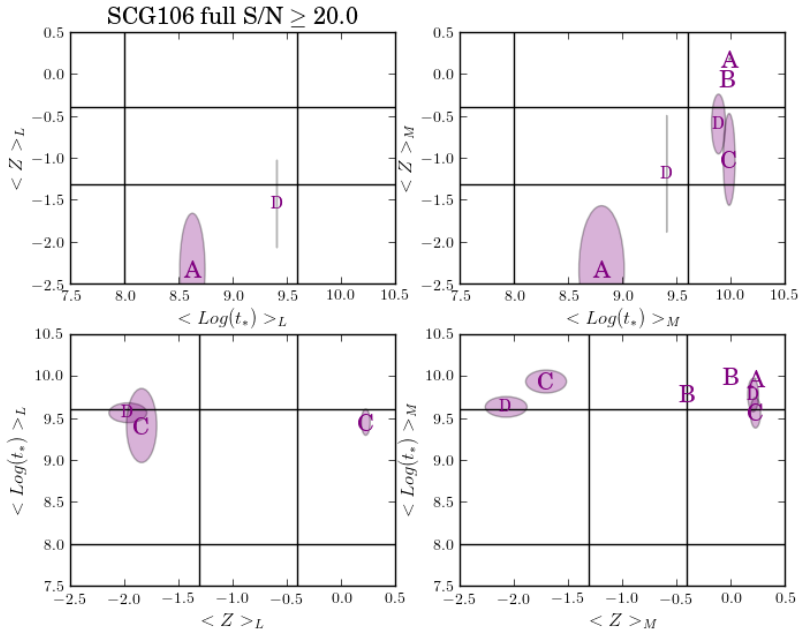

Figure 4.106: Age and metallicity plots for the extracted spectra of galaxies in SCG106.

In the 5" bins, Galaxy A has high-metallicity intermediate and old SPs. The high-metallicity SPs are old. Galaxy B has the same SP properties as its extracted spectrum. Galaxy C has mid-metallicity intermediate and old SPs. The low-metallicity population are old. Galaxy D has mid-metallicity old populations and its low-metallicity populations are old.

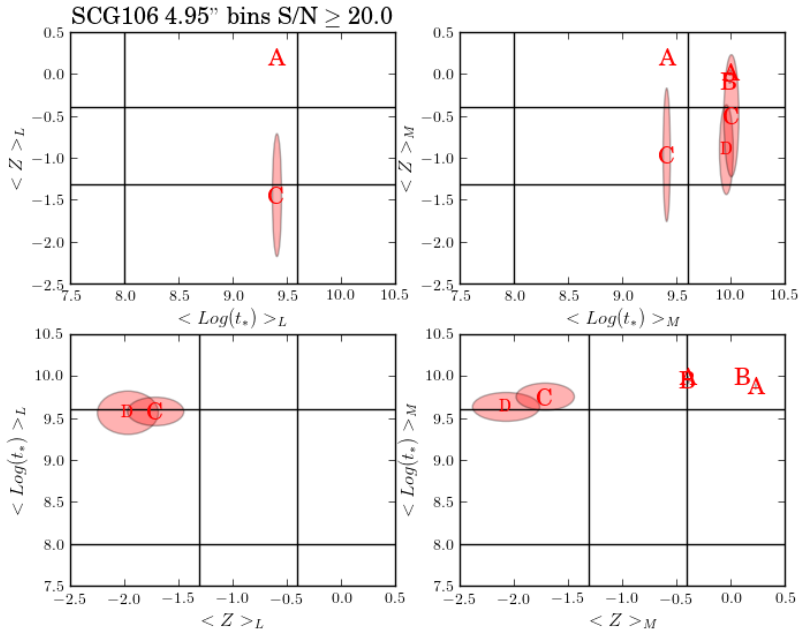

Figure 4.107: Age and metallicity plots for the 5" bin spectra of galaxies in SCG106.

Galaxy A shows high-metallicity old populations in its 3" spectra. Galaxy B has high-metallicity intermediate and old populations. Galaxy C has mid-metallicity intermediate populations and low and high-metallicity old populations. Galaxy D has low and mid-metallicity old populations.

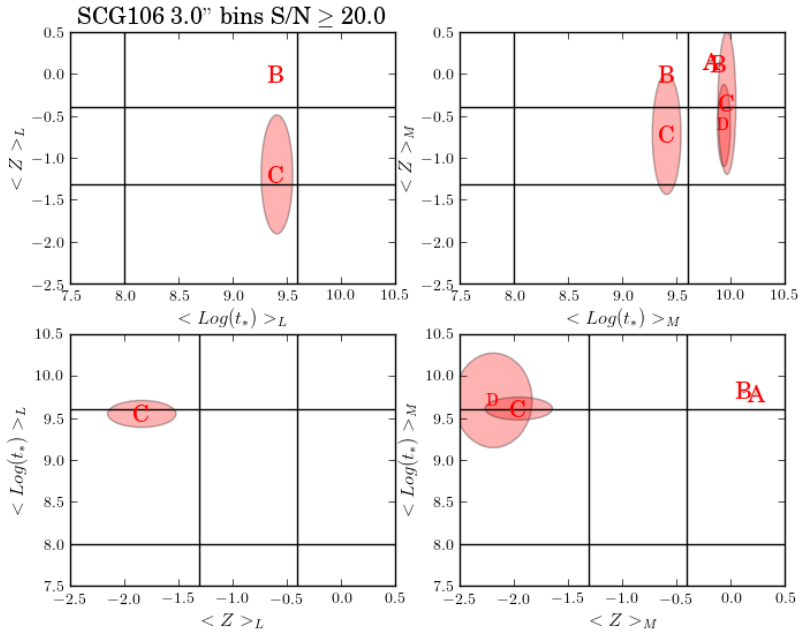

Figure 4.108: Age and metallicity plots for the 3" bin spectra of galaxies in SCG106.

In the 1" spectra, Galaxy A has high-metallicity intermediate and old ages. Its low-metallicity populations are young and its mid and high-metallicity populations are old. Galaxy B still has high-metallicity old SPs and old ages for its mid and high-metallicity populations. Galaxy D has mid-metallicity old SPs and old ages for its low and high-metallicity SPs.

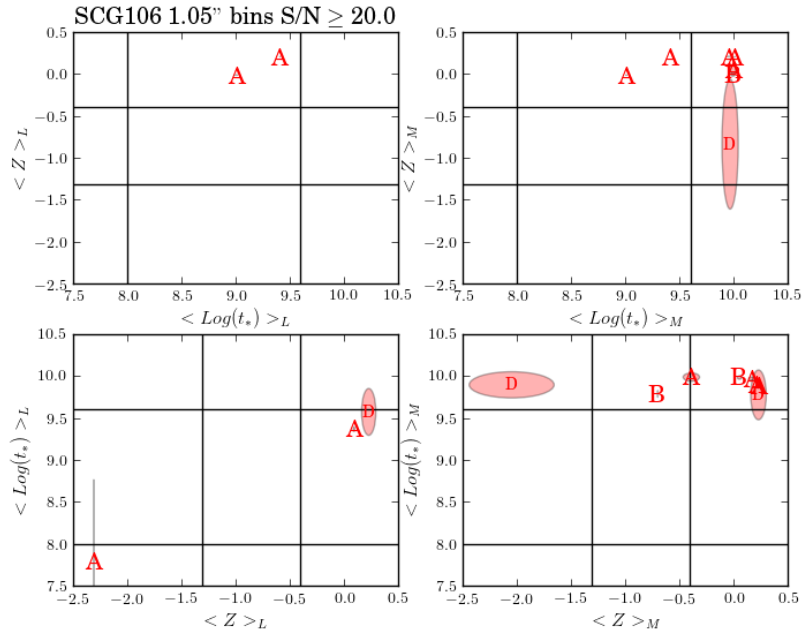

Figure 4.109: Age and metallicity plots for the 1" bin spectra of galaxies in SCG106.

In the fully extracted spectra, Galaxy B shows AGN activity and Galaxies C and D are star forming.

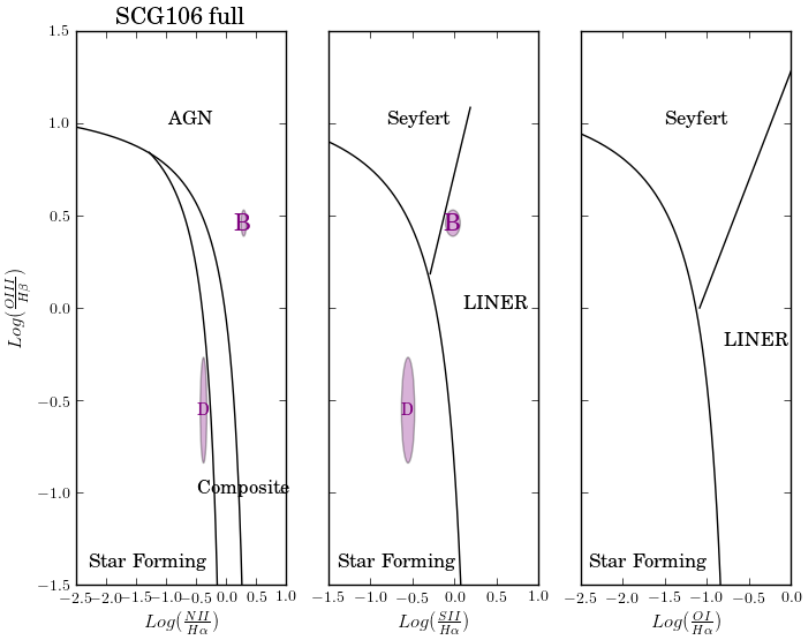

Figure 4.110: Activity plots for the extracted spectra of galaxies in SCG106.

Galaxies A and D are a SF galaxies and Galaxy B is a Seyfert type in the 5” spectra.

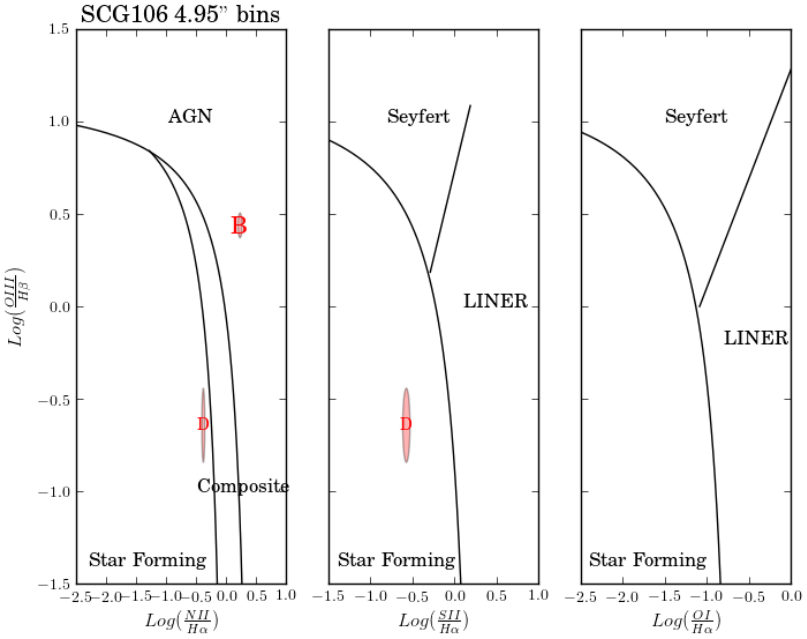

Figure 4.111: Activity plots for the 5” bin spectra of galaxies in SCG106.

The 3” spectra reveal that Galaxy A is a composite galaxy, Galaxy B shows characteristics of both a LINER and Seyfert, Galaxy C has SF and composite properties and Galaxy D is SF.

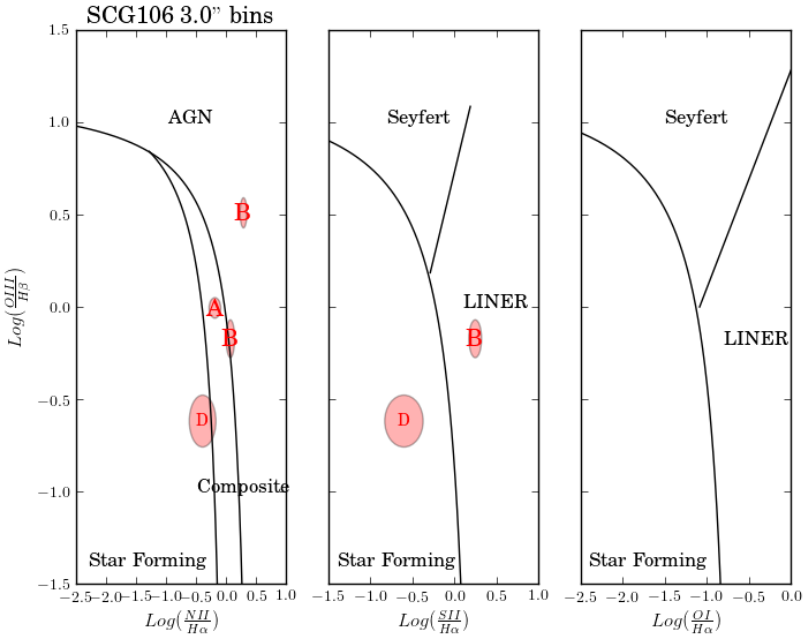

Figure 4.112: Activity plots for the 3" bin spectra of galaxies in SCG106.

In the 1" spectra, Galaxy B is a LINER, Galaxy C has a LINER and SF in its central regions and SF in its mid-regions and Galaxy D is SF.

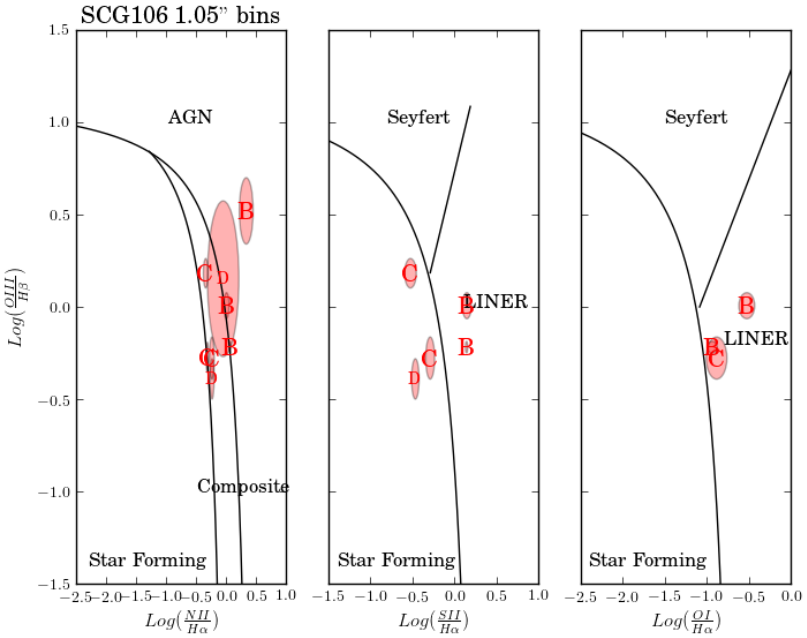

Figure 4.113: Activity plots for the 1" bin spectra of galaxies in SCG106.

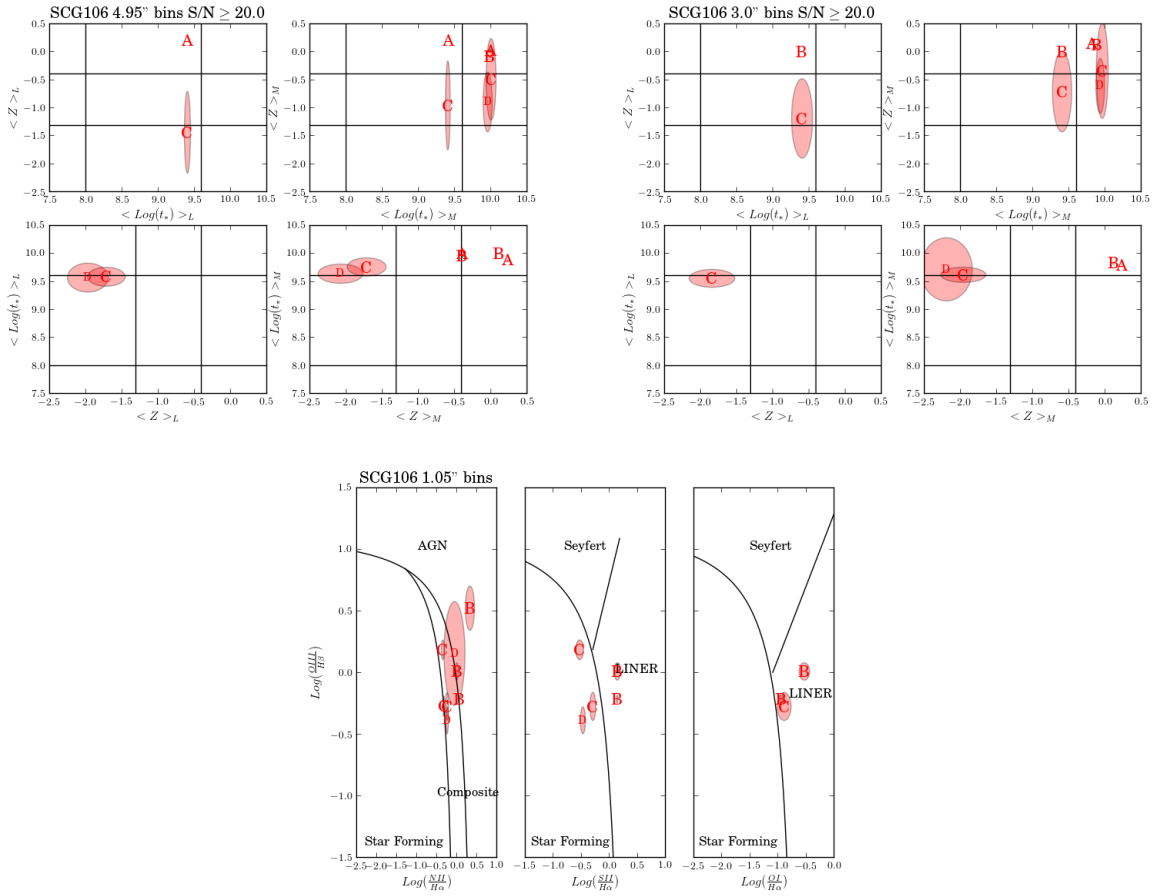

Figure 4.114: Stellar population results for the 5" and 3" bins and activity information for the 1" bins for SCG106.

Galaxies A, B and C all have evidence for rapid processing of gas via SF and not having a cold gas supply. Galaxy A has SPs with mostly high-metallicity intermediate and old SPs indicating it lost its outside gas supply before the SF episode that occurred $0.1-4$ Grys ago. Galaxy B is a LINER and is mostly comprised of high-metallicity old SPs suggesting its low-metallicity gas was used up >4 Gyrs ago. Galaxy C is a composite galaxy with evidence of a LINER and old populations of all metallicities and low and mid-metallicity intermediate populations. This implies the outside gas supply was shut off $0.1-4$ Gyrs ago. Galaxy D is not in the group and has more evidence for SF than the others. It has old populations with low and mid-metallicities. This could indicate that the processing of gas is proceeding more slowly than in the group environment, but we need environment information for Galaxy D to be sure.

Population	full	10”	5”	3”	1”
Galaxy A					
Young					
Intermediate	L-a		H-c		H-c
Old	H-a		H-c	H-c	H-c
Low			O-c		Y-c
Mid					O-c
High	O-a		O-c	O-c	O-c
Star Forming			X-c		
Seyfert					
LINER					
AGN					
Comp				X-c	
Galaxy B					
Young					
Intermediate				H-c	
Old	H-a		H-c	H-c	H-c
Low					
Mid					O-c
High	O-a		O-c	O-c	O-c
Star Forming					
Seyfert			X-c	X-c	
LINER				X-c	X-c
AGN	X-a				
Comp					

Population	full	10”	5”	3”	1”
Galaxy C					
Young					
Intermediate			M-c	M-c	
Old	M-a		M-c	H-c	
Low	O-a		O-c	O-c	
Mid					
High	O-a				
Star Forming	X-a			X-c	X-c/m
Seyfert					
LINER					X-c
AGN					
Comp				X-c	X-c
Galaxy D					
Young					
Intermediate	M-a				
Old	M-a		M-c	M-c	M-c
Low	O-a		O-c	O-c	O-c
Mid					
High	O-a				O-c
Star Forming	X-a		X-c	X-c	X-c
Seyfert					
LINER					
AGN					
Comp					

Table 4.18: Stellar population and activity analysis summary for SCG106. Same codes as in Table 4.4

4.3.10: SCG62

I only observed three of the members of SCG62 due to time constraints. I picked the three galaxies that were closest together on the sky. All galaxies have a late-type morphology.

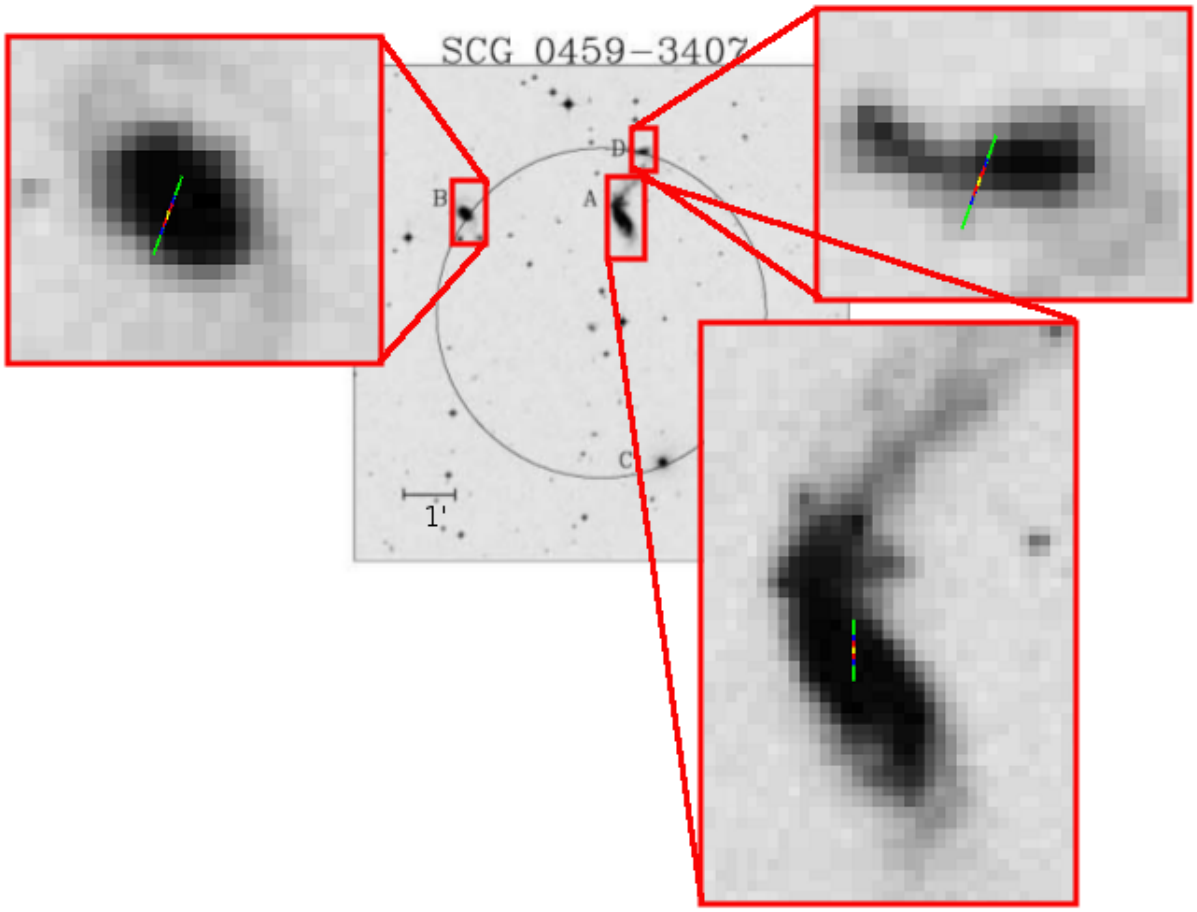

Figure 4.115: Group SCG62.

All three galaxies are members of this group.

$\Delta z(km/s)$	B	D
A	−264.36	−58.11
B		206.25

Table 4.19: Derived redshift differences for group SCG62.

Below is the redshift distribution of the galaxies.

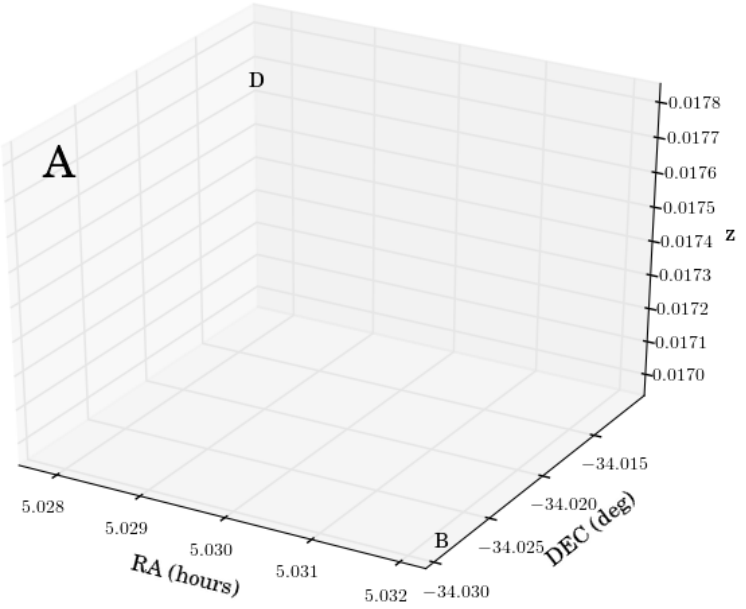

Figure 4.116: Group SCG62.

The extracted spectrum for Galaxy B indicates that the old populations have low-metallicity. For Galaxy D, the intermediate SPs have high-metallicity and the old SPs have mid-metallicity. The low and high-metallicity populations are both old.

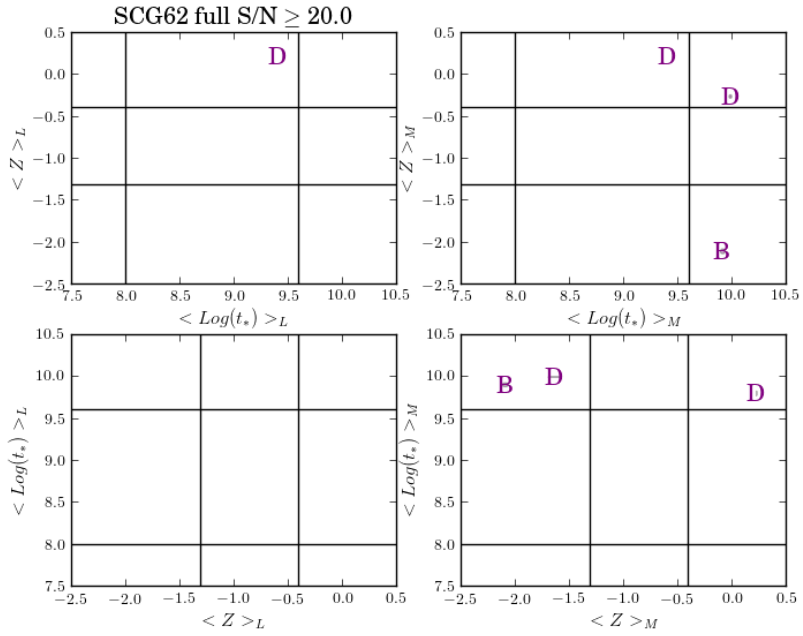

Figure 4.117: Age and metallicity plots for the extracted spectra of galaxies in SCG62.

In the 10" spectra, Galaxy A shows a mid-metallicity intermediate population and Galaxy B shows old populations with low-metallicity.

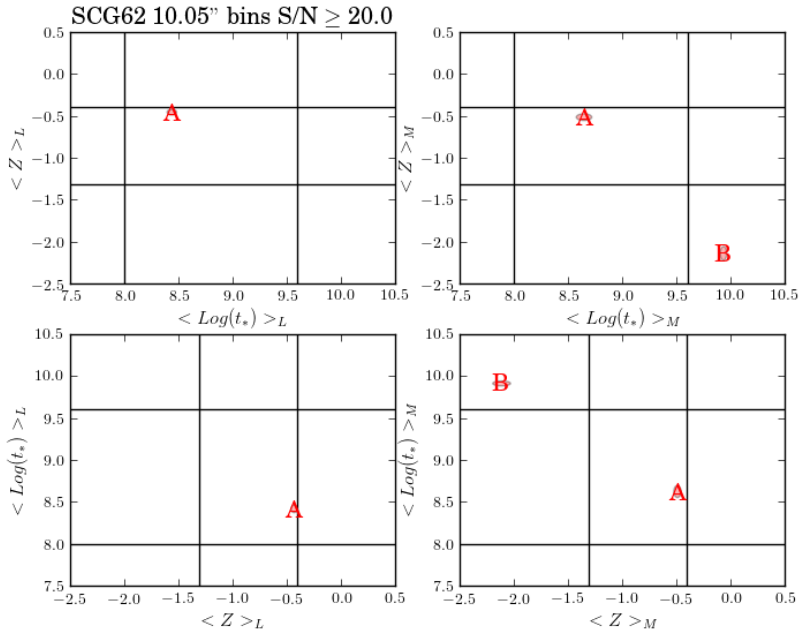

Figure 4.118: Age and metallicity plots for the 10" bin spectra of galaxies in SCG62.

Galaxy A has mid-metallicity intermediate SPs and low-metallicity old SPs in its 5" spectra. The low and high-metallicity populations show old ages. Galaxy B continues to show low-metallicity old populations. Galaxy D shows similar SPs as in its extracted spectrum.

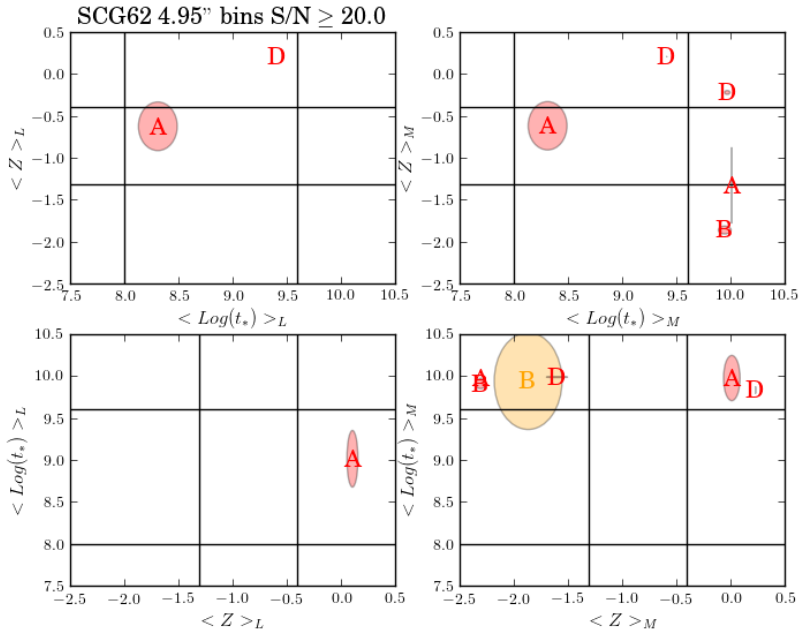

Figure 4.119: Age and metallicity plots for the 5" bin spectra of galaxies in SCG62.

In the 3" spectra, the young SPs for Galaxy A have low and mid-metallicities, the intermediate populations have mid-metallicities and the old populations have low metallicities. There are low-metallicity populations with young and old ages and mid and high-metallicity populations with intermediate ages. Galaxy B has low-metallicity young SPs and high-metallicity intermediate SPs. The old populations again show a low-metallicity. Galaxy D has old SPs of both high and low metallicity.

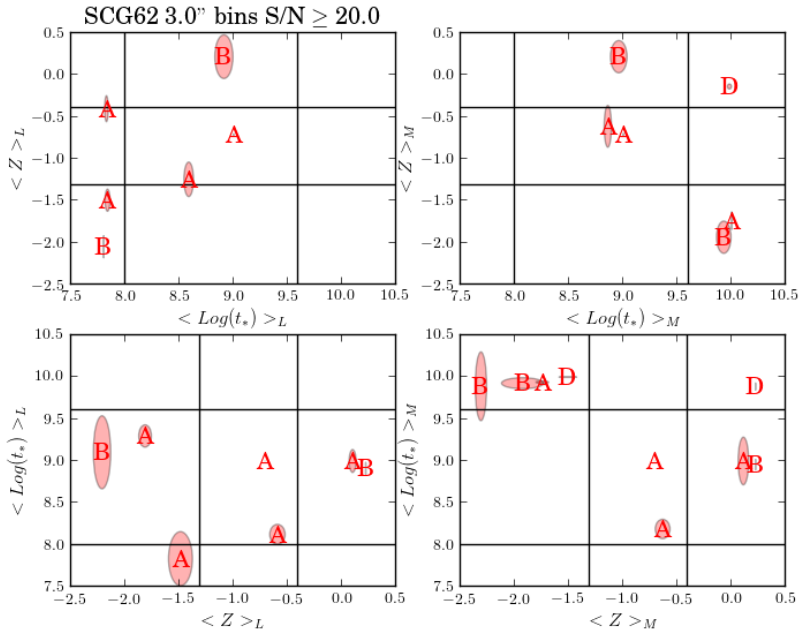

Figure 4.120: Age and metallicity plots for the 3" bin spectra of galaxies in SCG62.

Galaxy B has high-metallicity intermediate SPs and low-metallicity old SPs in its 1" spectra. Galaxy D has low and mid-metallicity young SPs and mid and high-metallicity intermediate and old SPs. The low-metallicity populations are intermediate and old ages and the mid and high-metallicity populations are old.

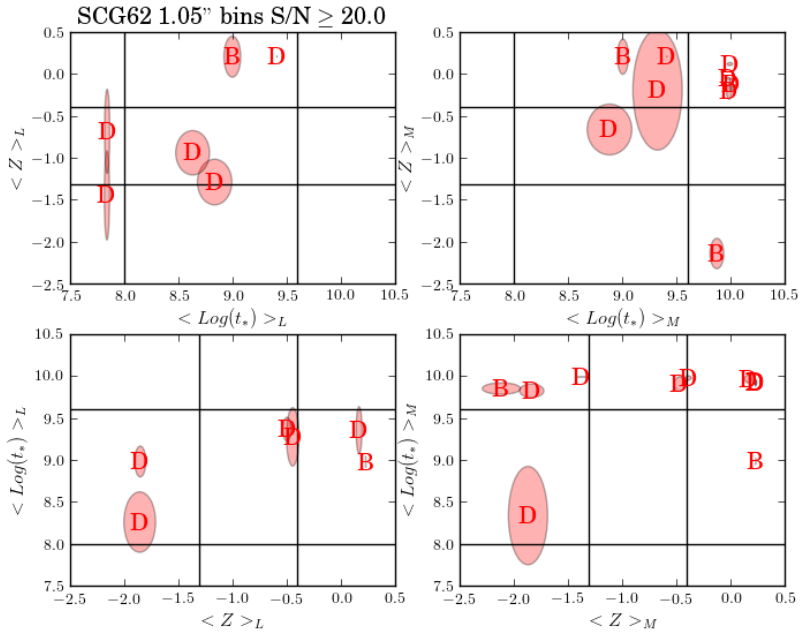

Figure 4.121: Age and metallicity plots for the 1" bin spectra of galaxies in SCG62.

In the 10" spectra, Galaxy A has SF in its central and mid-regions. Galaxy B shows both LINER and SF characteristics in its central regions.

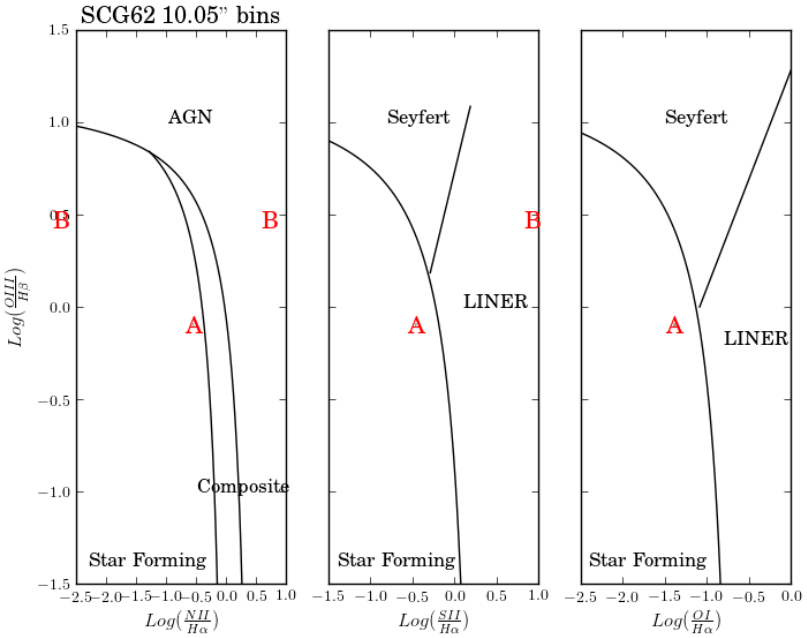

Figure 4.122: Activity plots for the 10" bin spectra of galaxies in SCG62.

Galaxy A again has SF in its central and mid-regions in the 5" spectra but it also has evidence of a LINER in its central regions. Galaxy B has SF and Seyfert activity in its mid-regions.

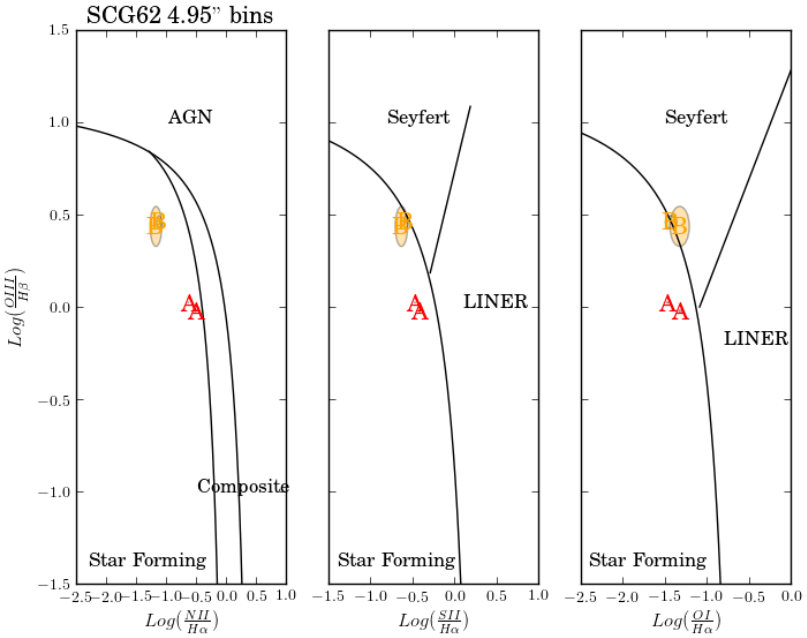

Figure 4.123: Activity plots for the 5" bin spectra of galaxies in SCG62.

In the 3" spectra, Galaxy A shows SF in its central regions and Galaxy B shows SF in its central and mid-regions.

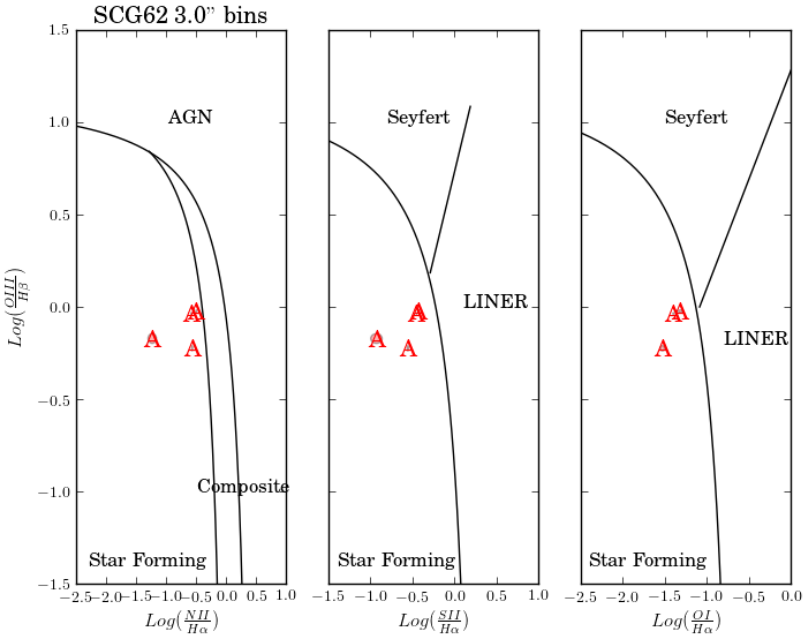

Figure 4.124: Activity plots for the 3" bin spectra of galaxies in SCG62.

Galaxy A shows signatures of SF, Seyfert and LINER activity in its central regions of the 1" spectra. Galaxy B has SF in its central and mid-regions as well as Seyfert activity in its central regions. Galaxy D shows evidence of a LINER in its central regions.

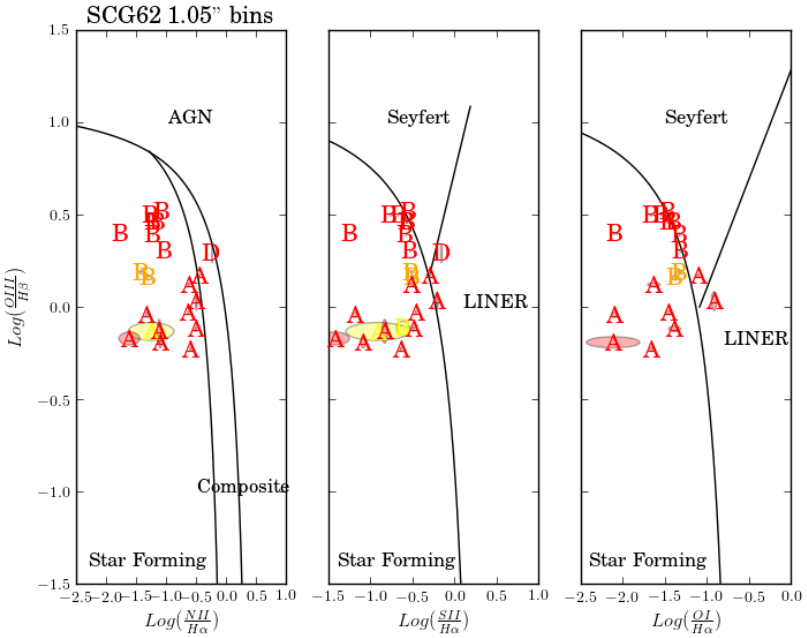

Figure 4.125: Activity plots for the 1" bin spectra of galaxies in SCG62.

Galaxies A and D appear to be interacting. Galaxy A is a SF galaxy in its central and mid-regions. The SPs of all ages span the metallicity bins which implies rapid processing of gas via multiple SF episodes and that the outside gas supply was shut off very recently, < 0.1 Gyr ago. This could be due to interactions with Galaxy D. Galaxy D is a LINER with high metallicity intermediate and old aged populations. This implies a SF episode between $0.1 - 4$ Gyrs ago ago using preprocessed gas. Both galaxies show signs of having lost their cold gas supply before these multiple episodes of SF began. Galaxy B is a SF galaxy with a Seyfert nucleus, which is common. It has low-metallicity old SPs and high-metallicity intermediate populations. This implies a SF episode between $0.1 - 4$ Gyrs ago with preprocessed gas. The cold gas supply was likely shut off before this SF episode began. All three galaxies have at least one measurement of low-metallicity young populations, implying that the low-metallicity gas is currently being consumed in on-going SF episodes.

Population	full	10”	5”	3”	1”
Galaxy A					
Young				L/M-c	
Intermediate		M-c	M-c	M-c	
Old			L-c	L-c	
Low			O-c	Y/O-c	
Mid		I-c		I-c	
High			O-c	I-c	
Star Forming		X-c/m	X-c/m	X-c	X-c/m
Seyfert					X-c
LINER			X-c/m		X-c
AGN					
Comp					
Galaxy B					
Young				L-c	
Intermediate				H-c	H-c
Old	L-a	L-c	L-c	L-c	L-c
Low	O-a	O-c	O-c/m	O-c	O-c
Mid					
High				I-c	I-c
Star Forming		X-c	X-m	X-c/m	X-c/m
Seyfert			X-m		X-c
LINER					
AGN					
Comp					

Population	full	10”	5”	3”	1”
Galaxy D					
Young					L/M-c
Intermediate	H-a		H-c		M/H-c
Old	H-a		H-c	H-c	H-c
Low	O-a		O-c	O-c	I/O-c
Mid					O-c
High	O-a		O-c	O-c	O-c
Star Forming					
Seyfert					
LINER					X-c
AGN					
Comp					

Table 4.20: Stellar population and activity analysis summary for SCG62. Same codes as in Table 4.4

4.3.11: SCG07

I only observed Galaxies A and B in SCG07 due to time constraints. Both galaxies have a late-type morphology.

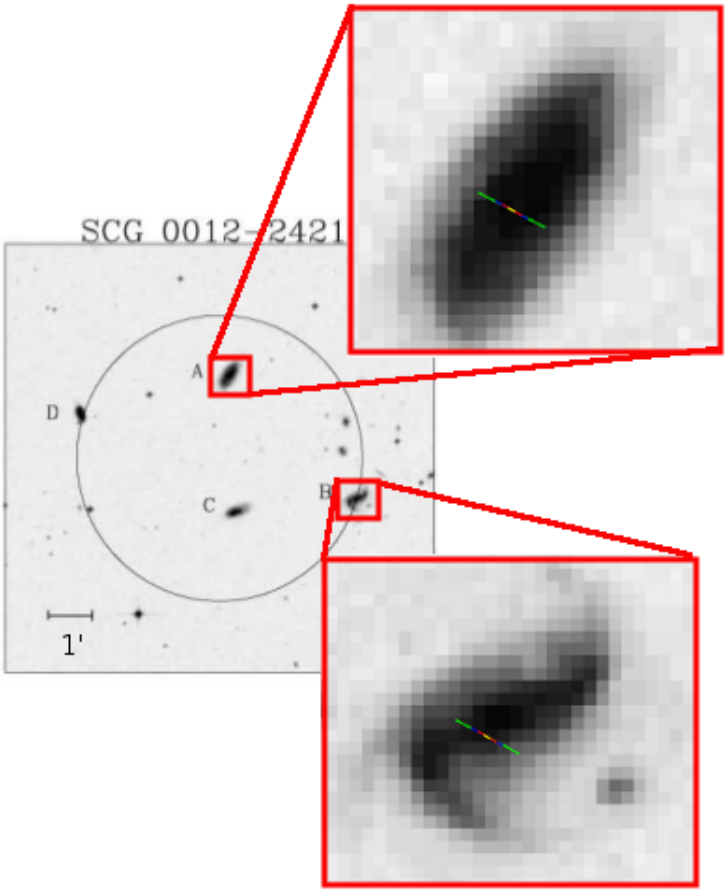

Figure 4.126: Group SCG07.

These galaxies are gravitationally bound according to my velocity dispersion analysis.

$\Delta z(km/s)$	B
A	−110.58

Table 4.21: Derived redshift differences for group SCG07.

Below is the redshift distribution of the galaxies.

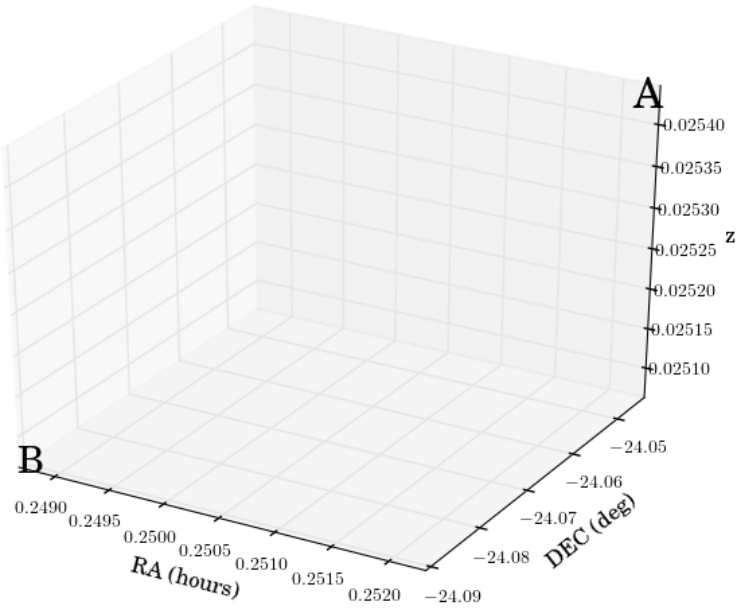

Figure 4.127: Group SCG07.

In the extracted spectra for Galaxy A, there are low-metallicity young SPs and high-metallicity old SPs. The mid and high-metallicity populations are old. For Galaxy B, the young and old SPs have mid-metallicity and the intermediate SPs have high-metallicity. The low-metallicity populations have intermediate and old ages and the high-metallicity populations have intermediate ages.

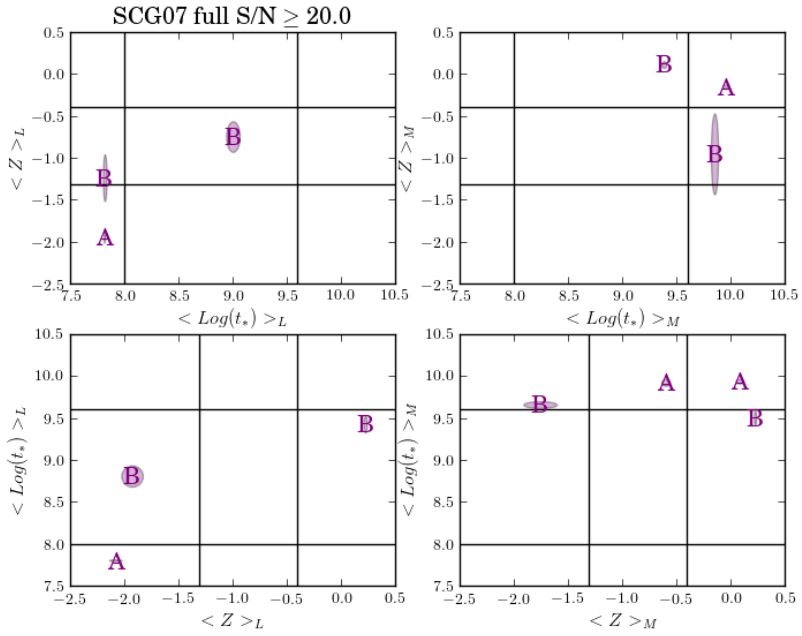

Figure 4.128: Age and metallicity plots for the extracted spectra of galaxies in SCG07.

The SPs in Galaxy A for the 10” bins are similar to the extracted spectrum. For Galaxy B, the young SPs have low-metallicity, the intermediate SPs have high-metallicity and the old SPs have mid-metallicity. The low-metallicity SPs have intermediate and old ages, the mid-metallicity SPs are young and the high-metallicity SPs are old.

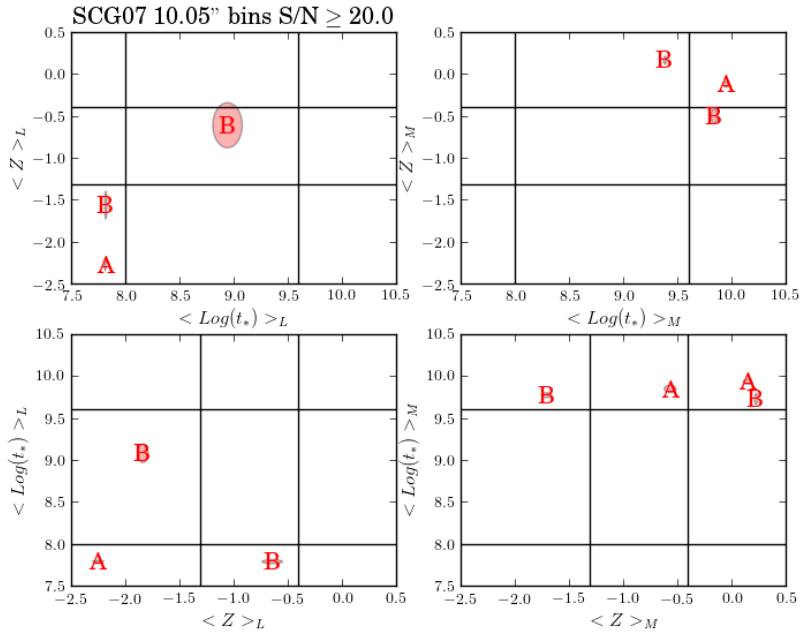

Figure 4.129: Age and metallicity plots for the 10" bin spectra of galaxies in SCG07.

In the 5" bins, Galaxy A has similar SP characteristics as above. Galaxy B has young SPs with low-metallicity and intermediate and old SPs with high-metallicity. The low and high-metallicity SPs have intermediate ages.

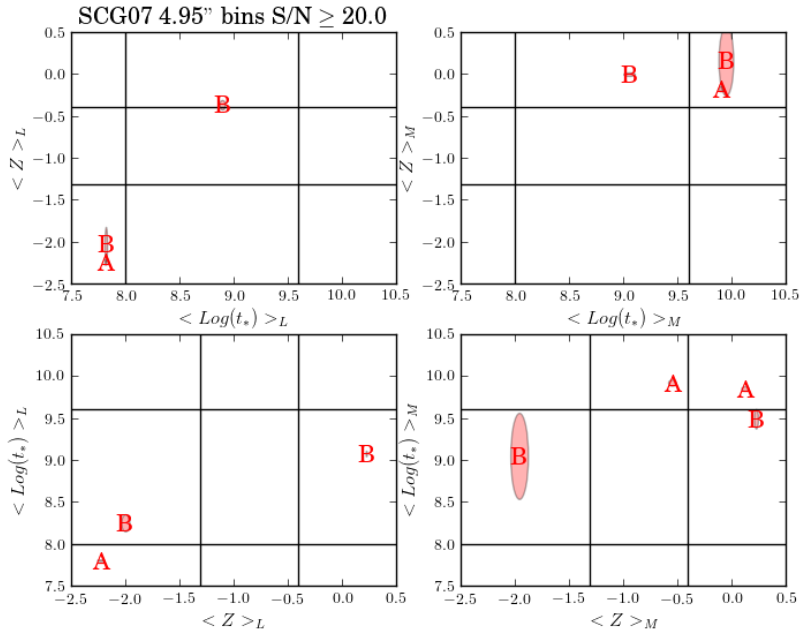

Figure 4.130: Age and metallicity plots for the 5" bin spectra of galaxies in SCG07.

Galaxy A again has similar SP properties in its 3" bins. Galaxy B, however, has intermediate SPs with high-metallicity and old SPs with low-metallicity. The low-metallicity SPs are old and the high-metallicity SPs have intermediate ages.

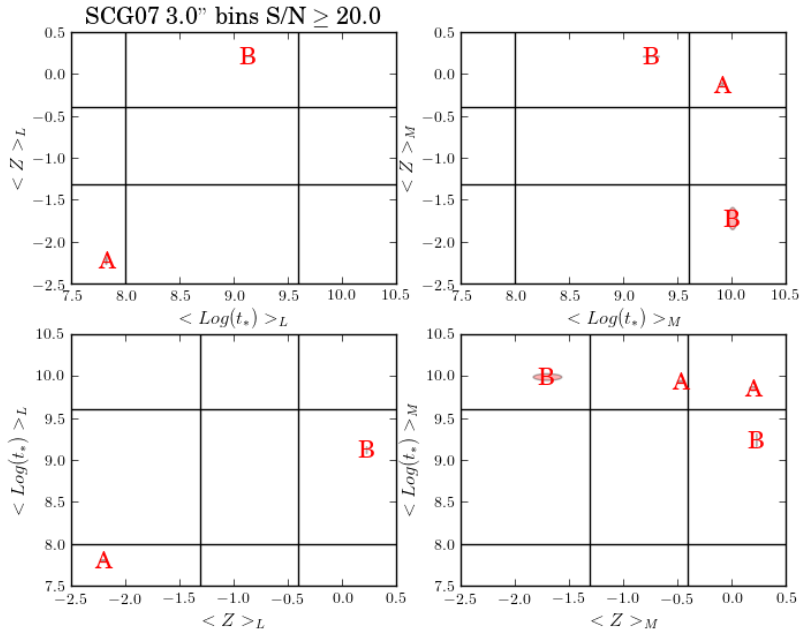

Figure 4.131: Age and metallicity plots for the 3" bin spectra of galaxies in SCG07.

Only Galaxy A had measurements in the 1" bin and they are similar to the properties in the other bins.

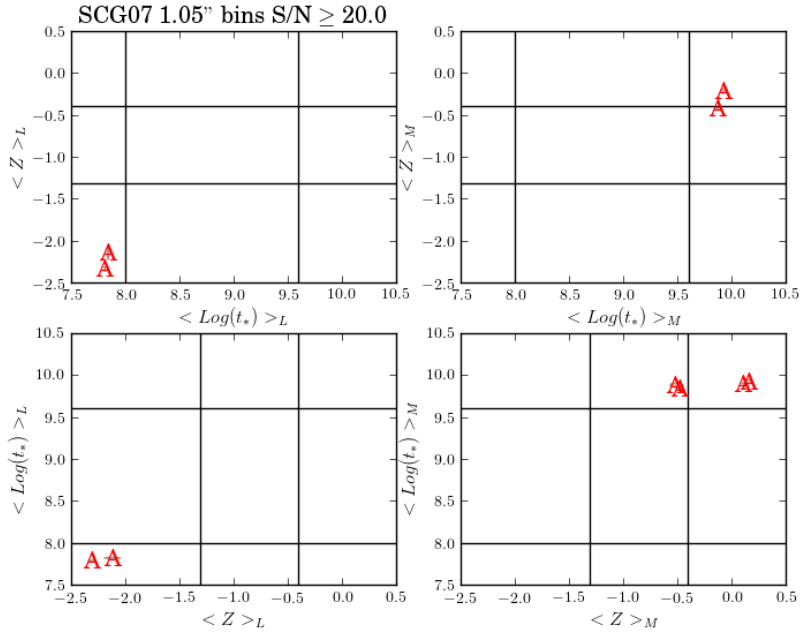

Figure 4.132: Age and metallicity plots for the 1" bin spectra of galaxies in SCG07.

In the extracted, 10”, 5” and 3” bins, both Galaxies A and B are SF galaxies.

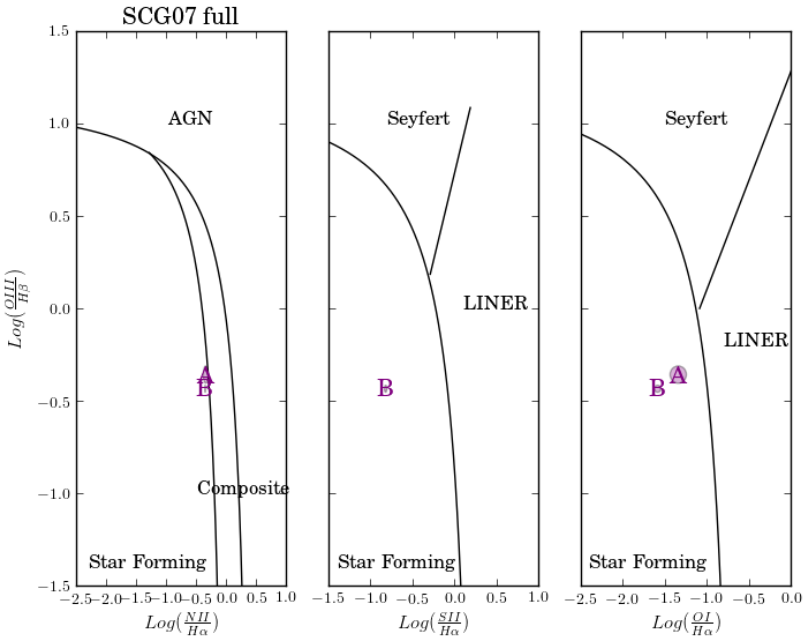

Figure 4.133: Activity plots for the extracted spectra of galaxies in SCG07.

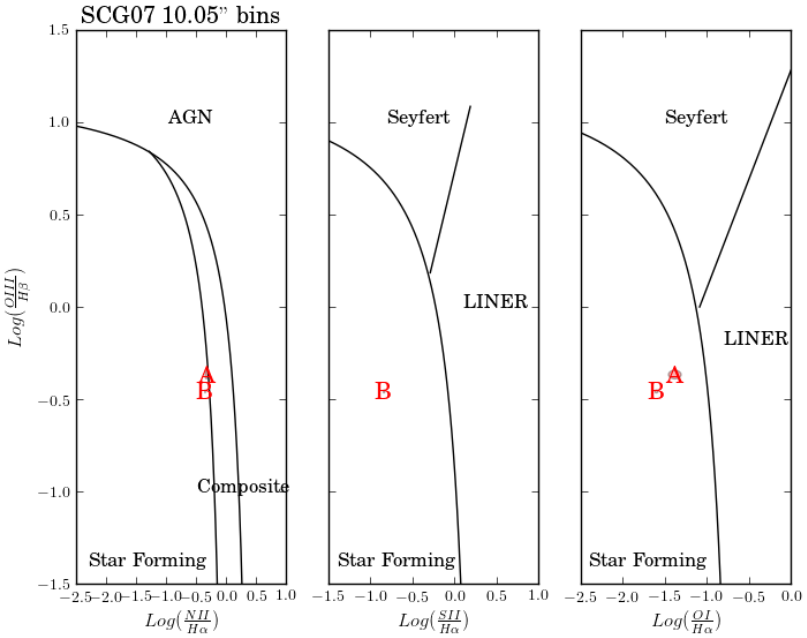

Figure 4.134: Activity plots for the 10" bin spectra of galaxies in SCG07.

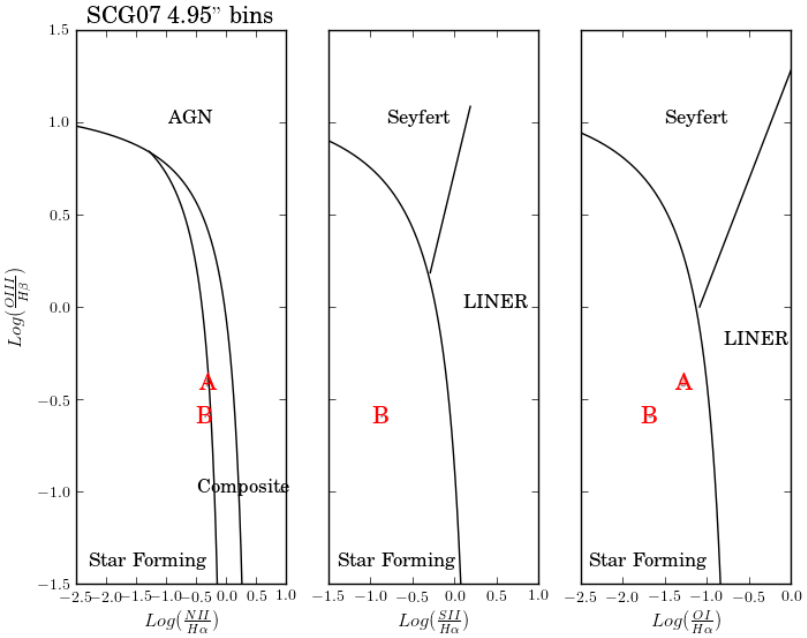

Figure 4.135: Activity plots for the 5" bin spectra of galaxies in SCG07.

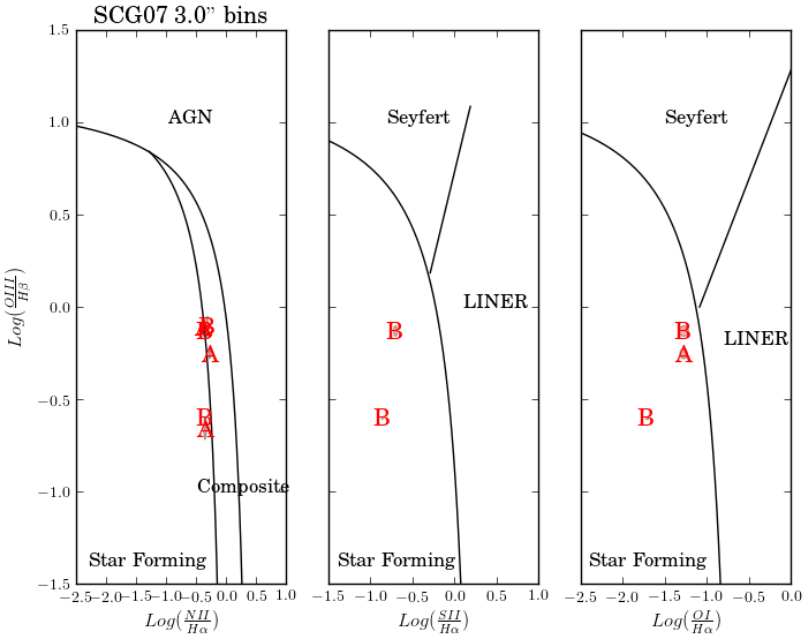

Figure 4.136: Activity plots for the 3" bin spectra of galaxies in SCG07.

In the 1" spectra, Galaxy A shows evidence of a composite spectrum with LINER activity and Galaxy B show evidence of both SF and LINER activity.

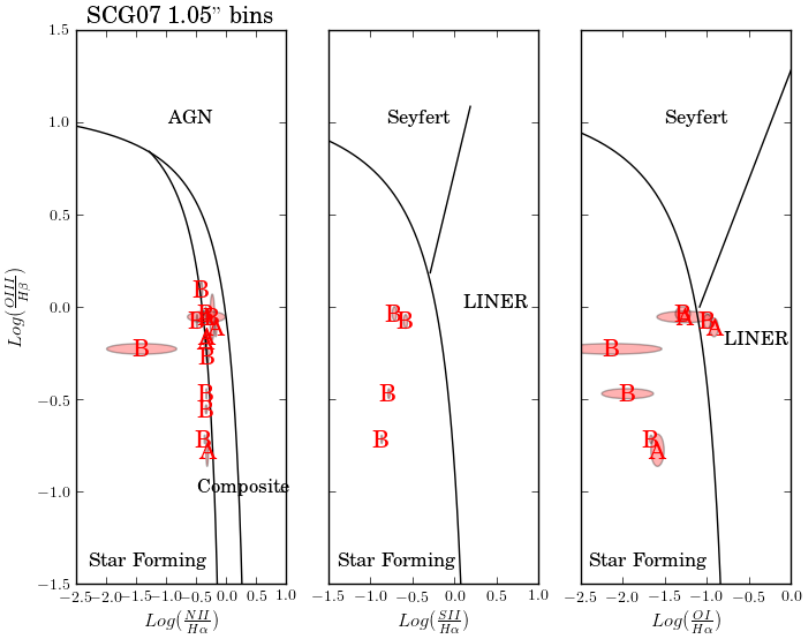

Figure 4.137: Activity plots for the 1" bin spectra of galaxies in SCG07.

Galaxy A is a SF galaxy with low-metallicity young populations and mid and high-metallicity old populations. This implies that the current episode of SF is using low-metallicity gas but the galaxy has undergone rapid processing of gas via SF >4 Gyrs ago. Galaxy B is also a SF galaxy with low-metallicity populations of all ages implying that it too still has its cold gas supply. There is also evidence of mid-metallicity young and old populations and high-metallicity intermediate populations which points to multiple episodes of SF using preprocessed gas. Galaxy B has a disturbed morphology.

Population	full	10"	5"	3"	1"
Galaxy A					
Young	L-a	L-c	L-c	L-c	L-c
Intermediate					
Old	H-a	H-c	H-c	H-c	H-c
Low	Y-a	Y-c	Y-c	Y-c	Y-c
Mid	O-a	O-c	O-c	O-c	O-c
High	O-a	O-c	O-c	O-c	O-c
Star Forming	X-a	X-c	X-c	X-c	X-c
Seyfert					
LINER					X-c
AGN					
Comp					X-c

Population	full	10"	5"	3"	1"
Galaxy B					
Young	M-a	L-c	L-c		
Intermediate	H-a	H-c	H-c	H-c	
Old	M-a	M-c	H-c	L-c	
Low	I/O-a	I/O-c	I-c	O-c	
Mid		Y-c			
High	I-a	O-c	I-c	I-c	
Star Forming	X-a	X-c	X-c	X-c	X-c
Seyfert					
LINER					X-c
AGN					
Comp					

Table 4.22: Stellar population and activity analysis summary for SCG07. Same codes as in Table 4.4

4.3.12: All Galaxies

The intermediate density configurations of compact groups appear to be a common phase in galaxy evolution so it is important to look at how this stage affects all the galaxies in compact groups. It has been noted in previous studies in Chapter 1 that groups with higher velocity dispersions tend to have more early-type galaxies. This trend is also present in my data set. In Table , I provide the average velocity dispersion and the morphological make-up of each group. Studies also show that late-type galaxies tend to reside at the edges of groups. Groups SCG08, SCG13, SCG82, SCG83, SCG88 and SCG106 all have late-type member galaxies. Many of these groups (SCG08, SCG13, SCG82 and SCG88) do not show a clear central galaxy, implying they have recently approached this configuration. The groups with a mix of morphologies (SCG83 and SCG106) generally show evidence that the early-type members reside closer to the center of the group and the late-type members are at the edges.

Figure 4.138 plots the SP properties for all galaxies that are members of a compact group separated by bin size. Many of the galaxies show high metallicity intermediate and old populations, which implies multiple SF episodes processing the gas. There are more young populations with low-metallicity than with mid-metallicity, which indicates that many of the galaxies undergoing SF are using low-metallicity gas. This could indicate that the cold gas supply was recently shutoff or is still present in many of these galaxies, suggesting that these are recently formed groups.

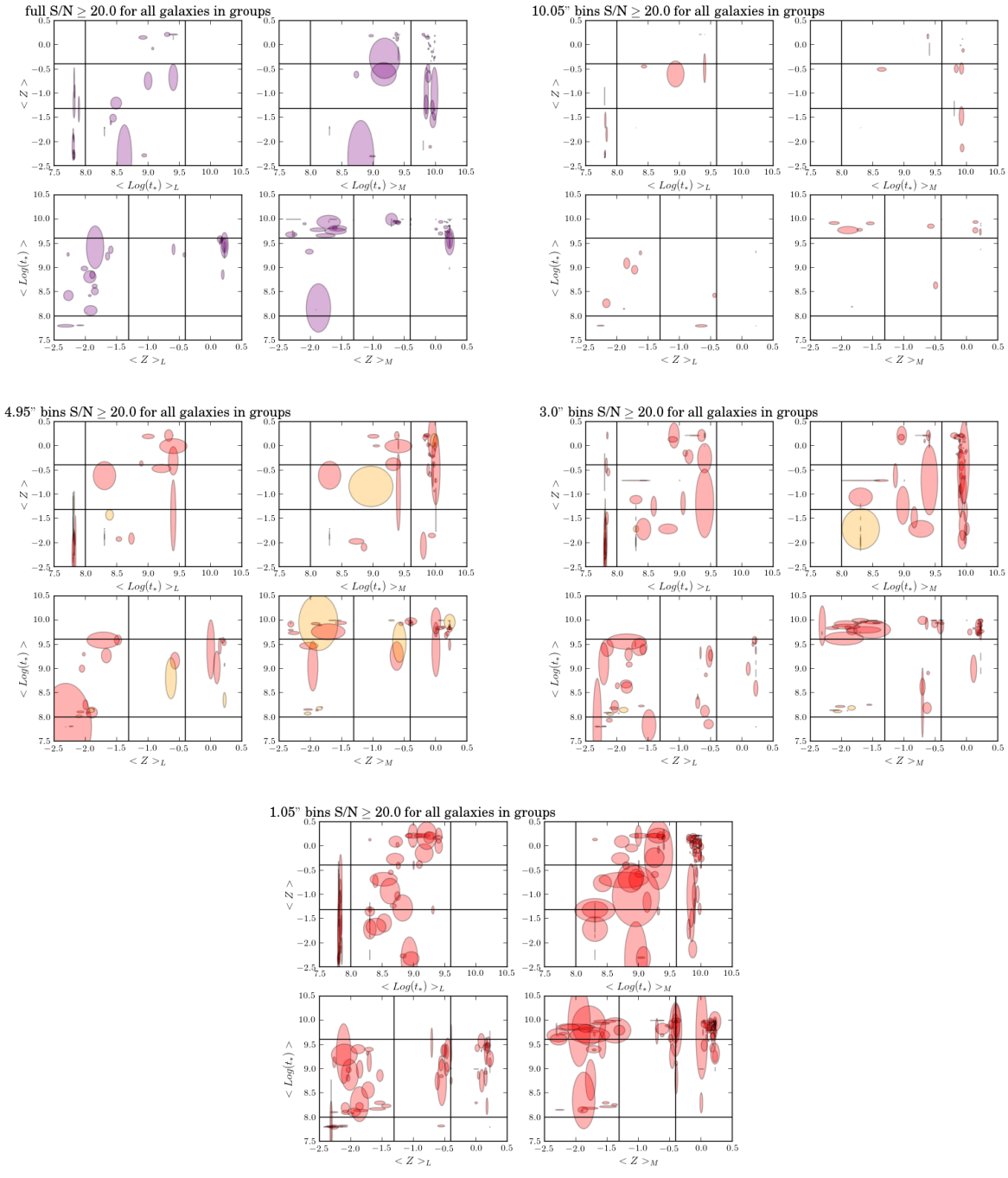

Figure 4.138: Age and metallicity plots for all galaxies in a group.

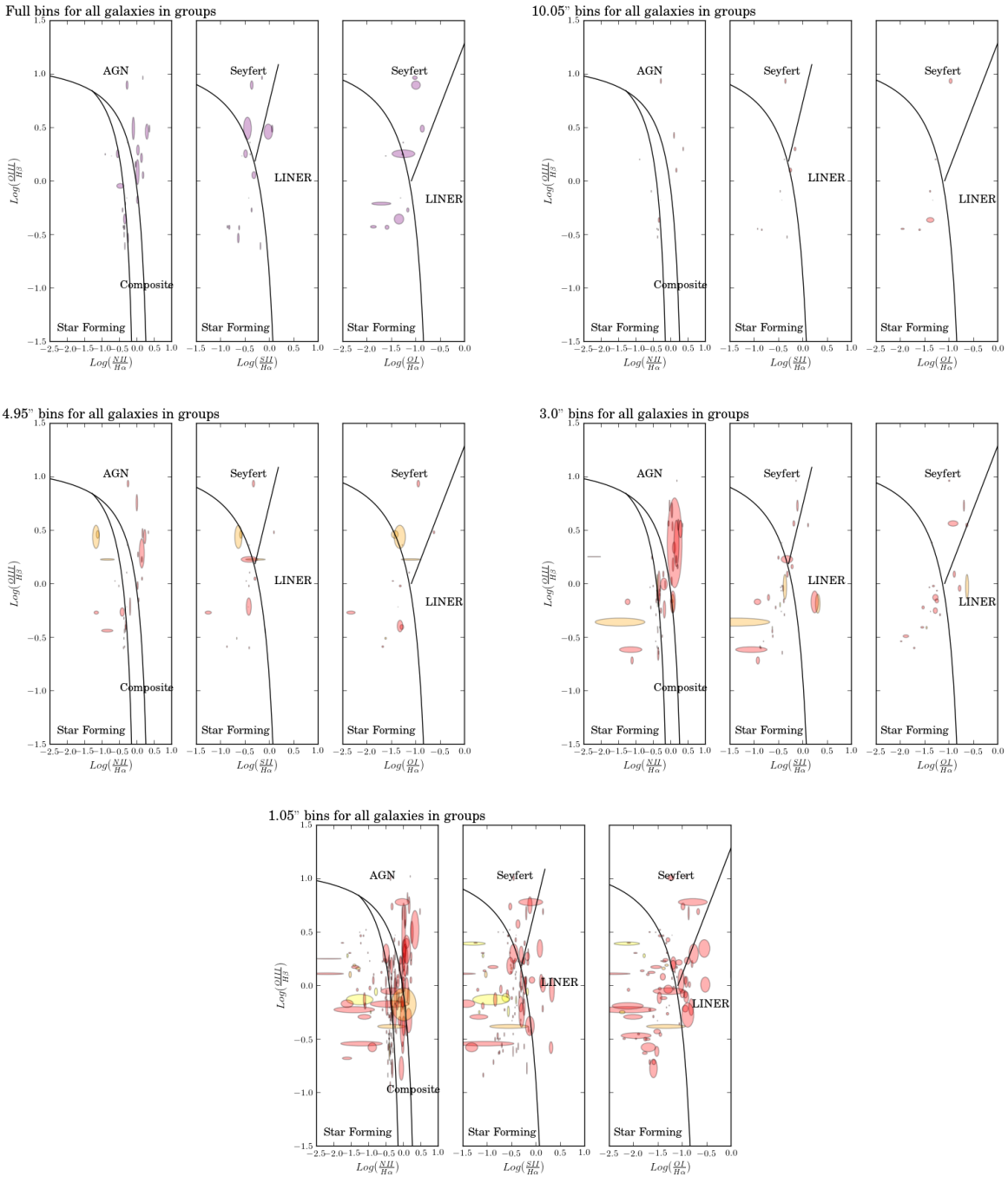

Figure 4.139: BPT diagrams for all galaxies in a group.

Figure 4.140 plots the SP properties for the 5" and 3" bins for all SF galaxies in a group. There is a noticeable trend in age and metallicity. As age increases, so does metallicity. The old populations span the entire metallicity range, which is expected if these galaxies are going through multiple SF episodes in their

lifetimes, but are more concentrated in the high metallicity bin.

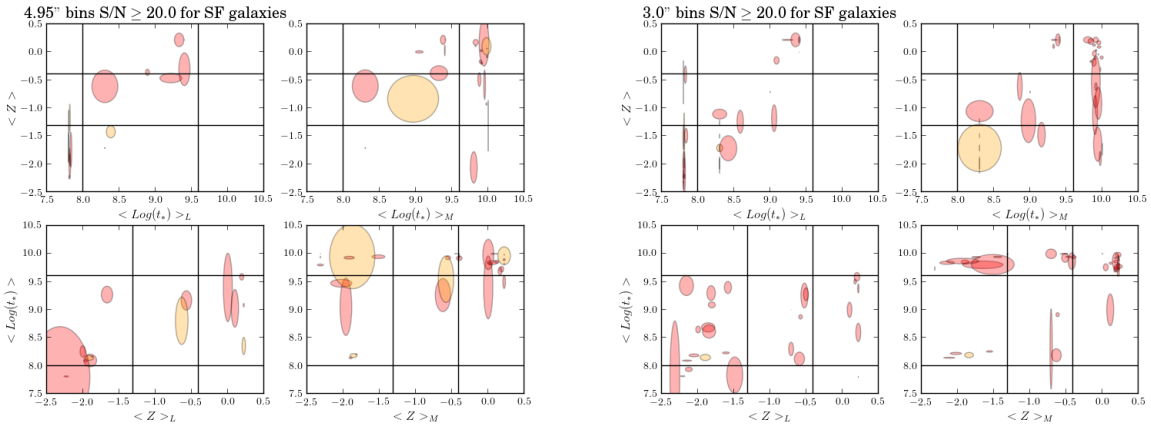

Figure 4.140: SP properties for all SF galaxies in a group.

Finally, Figure 4.141 plots the SP properties in the 1" bins for all galaxies that show activity other than SF. In the Composite galaxies I see a similar trend as the SF galaxies, which makes sense because they are a combination of SF and AGN. The galaxies that are classified as AGN, LINER, or Seyfert have intermediate and old stars that span the metallicity range but the young stars are only found in low-metallicity bins. Young and intermediate stars are found in both SF and AGN galaxies.

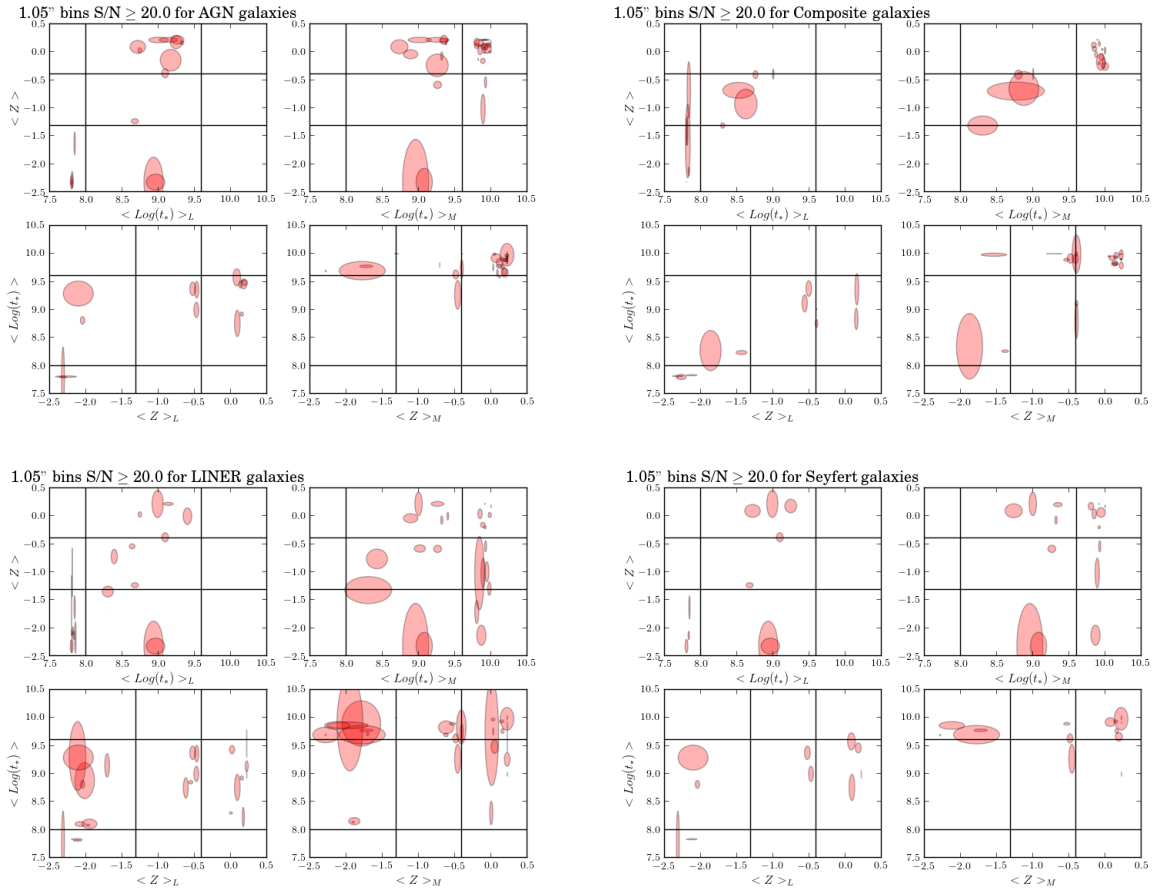

Figure 4.141: SP properties for all active galaxies other than SF in a group.

To determine the likelihood of a galaxy having been through an interaction that triggered SF, I assign a score based on characteristics that are expected in those systems. Points were given to galaxies that are in a group (+1), have a disturbed morphology (DM, +1), have a neighbor < 150 km/s (M_c, +1 for each galaxy), have a neighbor within $150 - 300$ km/s (M_n, +0.5 for each galaxy), have measured SF activity (+1), have detected young populations in their 3" bins (SP_y, +1), have similar young, intermediate or old populations as the other neighbors indicating similar SF epochs (SP_c, SP_n, +1 for each galaxy). I can populate this table as more data is acquired. Deep photometry and kinematic analysis will help populate the disturbed morphology column.

Group	Mem	In Grp	DM	M_c	M_n	SF	SP_y	SP_c	SP_n	Total
SCG07	A	1	0	1	0.0	1	1	1	0	5.0
SCG07	B	1	1	1	0.0	1	0	1	0	5.0
SCG08	B	1	1	2	0.5	1	1	3	3	12.5
SCG08	A	1	1	3	0.0	1	0	0	0	6.0
SCG08	D	1	0	2	0.5	1	1	3	3	11.5
SCG08	C	1	1	3	0.0	1	1	6	0	13.0
SCG13	A	1	1	1	0.5	1	1	1	2	8.5
SCG13	B	1	0	1	0.5	1	1	2	2	8.5
SCG13	D	0	0	0	0.0	0	0	0	0	0.0
SCG13	C	1	0	2	0.0	1	0	3	0	7.0
SCG62	B	1	1	1	0.5	1	1	1	3	9.5
SCG62	D	1	1	0	1.0	0	0	0	2	5.0
SCG62	A	1	1	1	0.5	1	1	3	3	11.5
SCG68	A	1	0	1	1.0	1	0	1	2	7.0
SCG68	D	1	0	0	0.0	0	1	0	0	2.0
SCG68	E	1	0	2	0.5	1	0	2	2	8.5
SCG68	B	1	0	3	0.5	1	0	3	1	9.5
SCG68	F	1	0	3	0.5	0	0	3	1	8.5
SCG68	C	1	0	3	0.5	1	0	3	2	10.5
SCG72	D	1	0	0	0.5	1	0	0	1	3.5
SCG72	A	1	0	0	0.5	0	1	0	1	3.5
SCG72	B	1	0	0	0.0	1	1	0	0	3.0
SCG72	C	0	0	0	0.0	0	0	0	0	0.0

Group	Mem	In Grp	DM	M_c	M_n	SF	SP_y	SP_c	SP_n	Total
SCG82	A	1	1	3	0.0	1	0	0	0	6.0
SCG82	B	1	0	3	0.0	1	0	4	0	9.0
SCG82	C	1	0	3	0.0	1	0	4	0	9.0
SCG82	D	1	0	3	0.0	1	1	4	0	10.0
SCG83	A	1	1	2	1.0	1	1	1	3	11.0
SCG83	D	1	0	1	1.5	1	1	1	3	9.5
SCG83	B	1	0	2	1.0	1	0	2	1	8.0
SCG83	E	1	0	3	0.5	1	0	2	1	8.5
SCG83	C	1	1	2	1.0	1	0	0	0	6.0
SCG88	B	1	0	1	0.0	1	0	1	0	4.0
SCG88	A	0	0	0	0.0	0	0	0	0	0.0
SCG88	C	1	0	0	0.5	0	0	0	0	1.5
SCG88	D	1	0	1	0.5	1	0	1	0	4.5
SCG106	A	1	0	2	0.0	0	0	2	0	5.0
SCG106	B	1	0	2	0.0	1	0	3	0	7.0
SCG106	D	0	0	0	0.0	0	0	0	0	0.0
SCG106	C	1	0	2	0.0	1	0	3	0	7.0
Total		36.0	11.0	60.0	14.0	30.0	14.0			

Table 4.23: Interaction code for each galaxy.

The average score for members with DM is 8. I use this value as the dividing line between galaxies that have interaction induced SF and those that do not. Members with scores above this value that do not show a DM are good candidates for follow-up broad-band photometry. Members with low scores and a DM warrant narrow-band photometry to verify the SPs.

SCG08 and SCG13 both had SFH summaries that suggested past interactions inducing SF. SCG08 has three members with high interaction scores. SCG13 only had two members (A and B) with scores at the cut-off, suggesting that Galaxy C is not the harasser that induced their SF. SCG68 is a group comprised of early-type galaxies yet four of its members have interactions scores at or above the cut-off. Galaxies A and D in SCG62 appear in Figure 4.115 to be in the process of interacting but only Galaxy A's interaction score is high. These four groups warrant further study with deep broad-band photometry to look for interaction effects on the stars, narrow-band photometry to confirm the SPs and deeper spectroscopy to study the radial distribution of the SPs and SF activity.

5: Summary and Future Work

In Chapter 1.1, I summarized my motivations. The most notable observed property of galaxies is the dependence of morphology on environment. Morphology is defined by the SFH of a galaxy which also depends on environment. Compact groups of galaxies probe the intermediate density environment to uncover the mechanisms that remove cold gas from galaxies as they transition from low-density to high-density environments. Proximity on sky and low velocity dispersions are what sets them apart from other groupings of galaxies. In this dissertation, I focus on the Southern Compact Groups (SCG) of galaxies discovered by Iovino, 2002 because they show an interesting distribution of morphology and fit in the FOV of the Goodman Spectrograph.

In Chapters 2 and 3 I described the two set-ups for my project and the instrumentation results. The first set-up used the deployable IFU module, CINDERS, with the Goodman Spectrograph on the SOAR telescope. Because CINDERS was a new instrument, I created a back-up observing strategy using the MOS capabilities recently added to the Goodman Spectrograph. I would bin along the slit axis in 1", 3", 5" and 10" bins to recover some spatial information.

The CINDERS gantry and probes could not remain on the Goodman spectrograph indefinitely. The unreliability of the probe positioning on sky made the instrument impossible to use and the movement of the x axis probe at the limit switches must be accurately quantified. Because we cannot see through the probes, their positions must be reliably known.

To obtain SP information in the MOS spectra, I used the simple stellar population (SSP) fitting routine STARLIGHT[130]. STARLIGHT fits a spectrum synthesized from many observed template stars to an observed spectrum, to constrain properties of the SP. I used 56 MILES SSP template spectra that spanned their expected age and metallicity ranges of my data as my base[123]. The activity information (SF or AGN) is measured from the emission lines after the STARLIGHT model is subtracted from the observed spectrum. I fit emission lines using PYSPECKIT[151].

In Chapter 4, I described how I used the MOS on the Goodman Spectrograph to obtain slit spectra on 40 galaxies in 10 SCGs. I complete SP analysis on spectra with S/N in the blue region ≥ 20. To study the SPs, I binned my results into a 3×3 grid of ages and metallicities[130]. Young populations have ages ≤ 0.1 Gyrs, intermediate populations have ages $0.1 < t < 4$ Gyrs and old populations have ages ≥ 4 Gyrs. Low metallicity populations have metallicities ≤ -1.31 [M/H], mid-metallicity populations have metallicities

$-0.7 \leq Z \leq -0.4$ [M/H] and high metallicity populations have metallicities ≥ 0.0 [M/H]. I plotted the light and mass weighted averages of the ages versus the light and mass weighted averages of their metallicities. I also plotted the light and mass weighted metallicities versus the light and mass weighted averages of their ages. Light weighted averages focus on the younger populations and mass weighted averages focus on the older populations. Activity properties were determined using BPT diagrams with the emission lines $H\alpha$, $H\beta$, [NII], [OIII], [SII] and [OI]. The plots were divided into regions where we expect to find SF, AGN, Seyfert and LINER type galaxies[141]. If a galaxy had a velocity dispersion > 500 km/s from the rest of the group members, it was considered out of the group.

From the SP and activity analysis, I constructed a crude SFH for all the groups. I provide snapshots of the groups that had all members observed. In the snapshots, is a summary of the SP properties from the 5" or 3" bins and the AGN properties for the 1" bins for group members.

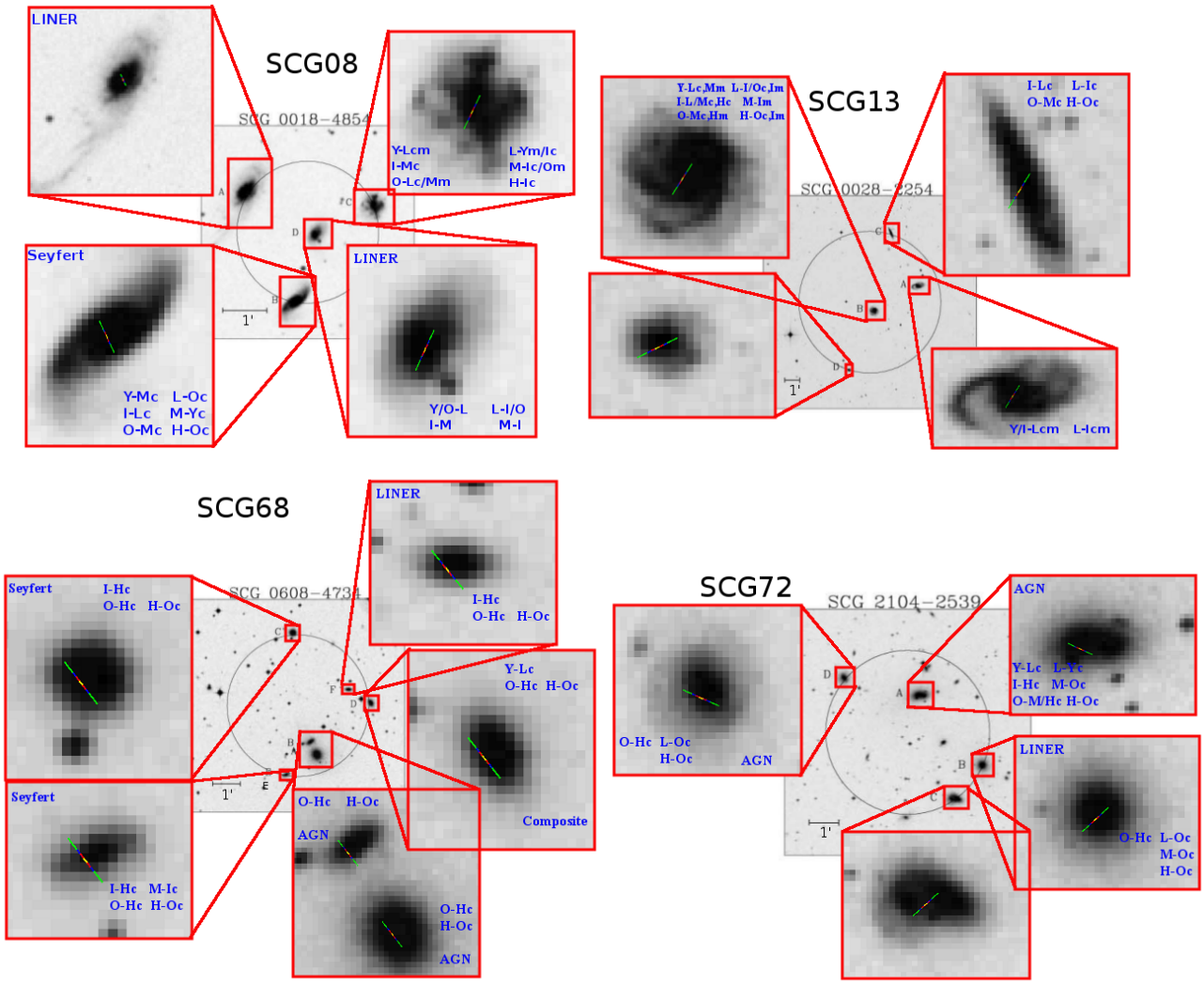

Figure 5.1: Summaries for group members. I abbreviate the age and metallicity designations as young (Y), intermediate (I), old (O), low (L), mid (M) and high (H), and the region designations as central (c), middle (m), and all (a).

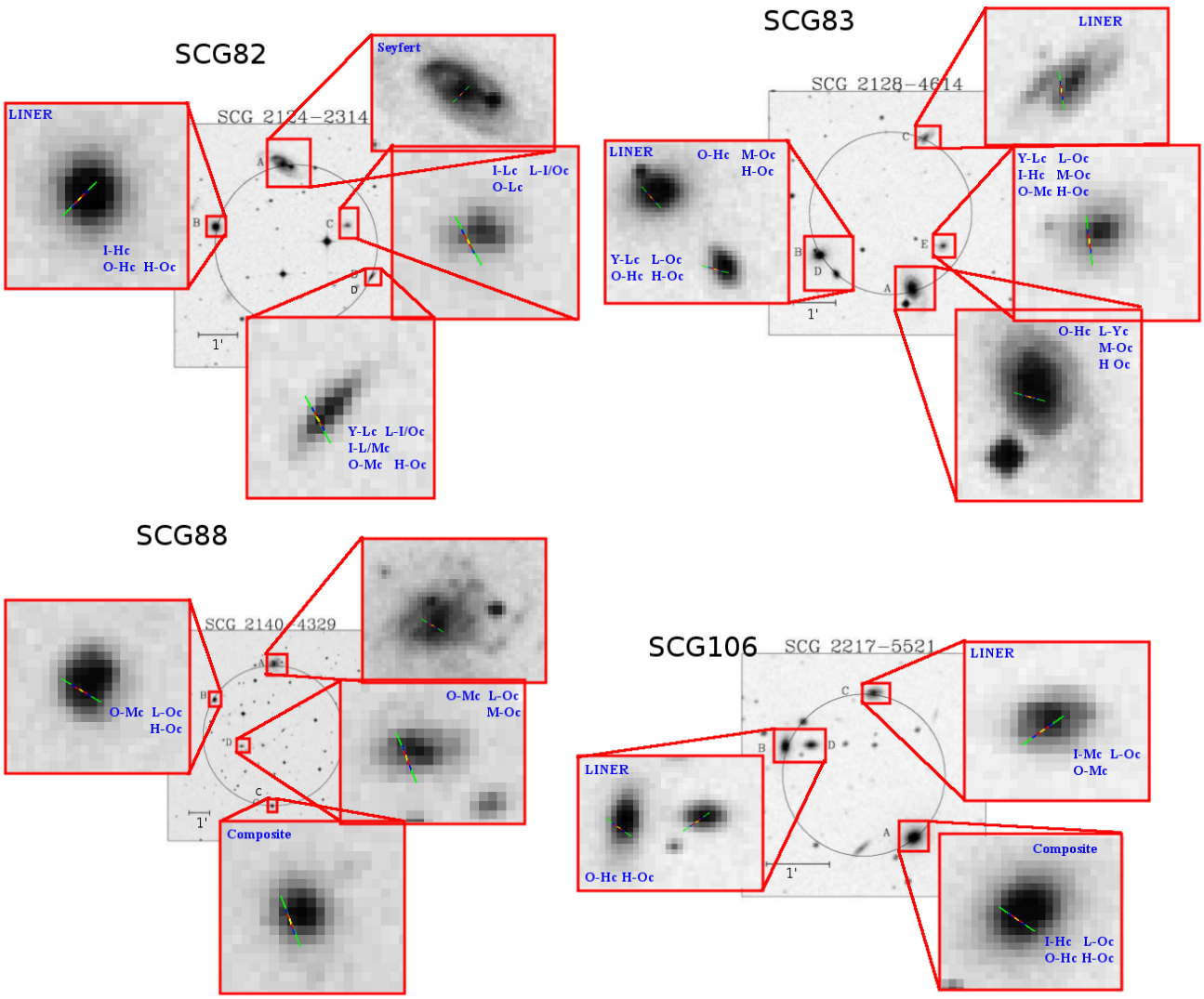

Figure 5.2: Summaries for group members continued.

My analysis shows that compact groups with late-type galaxies have much to tell about their SFH through their stellar populations. Many have high metallicities for their SPs indicating rapid processing of gas via SF. Most either still have their cold gas supplies or had it shut-off recently, supported by the low-metallicity young SPs. Every galaxy I observed shows SF or AGN activity. Half of the groups where I observed all members had at least four accordant members, versus $\sim 70\%$ found in the HCGs.

More observations are needed to fully understand these groups. Many of the galaxies did not meet my S/N criteria and all analyzed did not have high enough S/N in their edges. There are ways to verify the SP properties I measure with STARLIGHT. One method would involve taking narrow-band images of the galaxies. In contrast to the age/metallicity/reddening degeneracy of broad-band colors, narrow-band filters

focus on specific wavelength regions that are dominated by a single population of stars. Another way to verify ages and metallicities would be to measure the absorption lines found in the composite model spectrum fit by STARLIGHT. Instead of looking at the properties of the templates that make up the spectrum, I would attempt the more perilous exercise of analyzing the spectrum as if I did not know the underlying populations. The model spectrum can also be used to determine stellar masses by looking at the $D_n(4000)$ and $H\delta_A$ absorption features[5, 6]. Deep photometry in broad-band filters would enable fits to the surface brightness profiles to the galaxies. Unfortunately, galaxies are too sparse in groups to identify the dynamical center without X-ray maps.

Much work is needed to understand the SFHs of compact group galaxies. I summarize future work below.

1. Use the $H\alpha$ and $H\beta$ emission lines to estimate reddening. This would give us an idea of how much gas is still present.

2. Narrow-band photometry would be useful to verify the SPs I am measuring with STARLIGHT.

3. Fitting the absorption lines directly in the model spectrum would give us another measure of metallicity and ages for the SPs.

4. The $D_n(4000)$ and $H\delta_A$ absorption features in the extracted model spectrum will give us estimates of the M_*.

5. Narrow-band $H\alpha$ imaging combined with measurements from $H\alpha$ and $H\beta$ line fluxes will provide an estimate of the mass of ionized Hydrogen.

6. Environmental information for the discordant members. If they are isolated, use them for comparison.

7. We need to do a similar analysis to isolated and cluster galaxies to see how compact groups fit into galaxy evolution. 950 isolated galaxies can be found in the Catalog of Isolated Galaxies (CIG)[155]. A galaxy with diameter D is considered isolated when none of its neighbors with diameters d lie closer than $20d$ of the considered galaxy. The Analysis of the interstellar Medium of Isolated GAlaxies (AMIGA) survey further defined the isolation criteria and found 666 galaxies. They analyzed POSS-IE images of the CIGs and excluded any with neighbors that fell within a minimum radius of 0.5Mpc[156]. Once we have mass and morphology classifications for our SCG sample, we can define a comparable sample of CIGs to use in our analysis. The SDSS has spectra of the CIGs and we can find galaxies with similar S/N to our 3" bins.

8. We also need deeper spectroscopy to get adequate S/N at the edges of these galaxies. The edges are most likely to be affected by interactions and gas removal by ram pressure stripping as a galaxy enters

a dense environment.

9. It may be possible to get stellar kinematic information.

10. Deep surface photometry would allow us to fit surface brightness profiles to the galaxies. This would reveal if a galaxy has a disturbed morphology indicating a past interaction. I am currently working with undergraduate students to take deep photometry of the observed groups using the PROMPT array to look for visible signs of interactions. These observations use the Sloan filters and maximum exposure times of the telescopes. The resulting images are bias subtracted, flat fielded, sky subtracted and stacked to increase the signal in the faint edges of the galaxies. We rely on SExtractor background estimation to remove the sky. An example of before and after stacked images using dithered and non-dithered observations are provided. It is clear that dithering the images is superior at removing the sky background.

Figure 5.3: Examples of stacked PROMPT images. The left images are a single bias subtracted and flat fielded image and the images on the right are stacked. The top two images are for SCG15 and use the dithering method to remove the sky background. The bottom two images are for SCG68 and use SExtractor.

Using an IFS would help with this work. The SAMI survey may have observed some of these galaxies and our galaxies would fit nicely in their FOV.

This dissertation showed that the SPs of compact groups can provide insight into the SFHs of galaxies in these intermediate density environments. Fully understanding this important stage in galaxy evolution requires high S/N spectra combined with deep photometry. Combined with the spectra discussed here, a much clearer picture of how compact groups fit in the transition from isolated to cluster galaxy should emerge.

A: STARLIGHT Analysis Results

A.1: Age and Z Single Population Bracket Analysis

A.1.1: Young Age Bracket Analysis

Young	$< \log t_* >_L$			$< \log t_* >_M$		
	Average	Stddev	Noise [10,20,30]	Average	Stddev	Noise [10,20,30]
$T < 0.1$	0.07	0.06	$[0.07, 0.08, 0.08]$	0.07	0.06	$[0.07, 0.08, 0.08]$
$T < 0.2$	0.25	0.16	$[0.25, 0.25, 0.25]$	0.25	0.16	$[0.25, 0.25, 0.25]$
$T < 0.3$	0.32	0.2	$[0.32, 0.33, 0.33]$	0.32	0.2	$[0.32, 0.33, 0.33]$
$T < 0.4$	0.4	0.25	$[0.4, 0.4, 0.4]$	0.4	0.25	$[0.4, 0.4, 0.4]$
$T < 0.5$	0.42	0.26	$[0.42, 0.43, 0.43]$	0.42	0.26	$[0.42, 0.43, 0.43]$
$T < 0.6$	0.47	0.29	$[0.47, 0.48, 0.48]$	0.47	0.29	$[0.47, 0.48, 0.48]$
$T < 0.7$	0.5	0.3	$[0.5, 0.5, 0.5]$	0.5	0.3	$[0.5, 0.5, 0.5]$
$T < 0.8$	0.55	0.33	$[0.55, 0.55, 0.55]$	0.55	0.33	$[0.55, 0.55, 0.55]$
$T < 0.9$	0.57	0.35	$[0.57, 0.58, 0.58]$	0.57	0.35	$[0.57, 0.58, 0.58]$
$T < 1.0$	0.57	0.35	$[0.57, 0.58, 0.58]$	0.57	0.35	$[0.57, 0.58, 0.58]$
$T < 1.1$	0.6	0.36	$[0.6, 0.6, 0.6]$	0.6	0.36	$[0.6, 0.6, 0.6]$
$T < 1.3$	0.65	0.39	$[0.65, 0.65, 0.65]$	0.65	0.39	$[0.65, 0.65, 0.65]$
$T < 1.4$	0.65	0.39	$[0.65, 0.65, 0.65]$	0.65	0.39	$[0.65, 0.65, 0.65]$
$T < 1.5$	0.67	0.4	$[0.67, 0.68, 0.68]$	0.67	0.4	$[0.67, 0.68, 0.68]$

Table A.1: Age residuals for young age brackets. Values are in dex.

A.1.2: Intermediate Age Bracket Analysis

	$< \log t_* >_L$			$< \log t_* >_M$		
Intermediate	Average	Stddev	Noise [10,20,30]	Average	Stddev	Noise [10,20,30]
$0.1 < T < 1.7$	0.32	0.4	$[0.29, 0.33, 0.33]$	-0.65	0.85	$[-0.44, -0.63, -0.87]$
$0.1 < T < 1.9$	0.33	0.42	$[0.3, 0.35, 0.35]$	-0.62	0.86	$[-0.42, -0.6, -0.85]$
$0.1 < T < 2.2$	0.34	0.45	$[0.31, 0.36, 0.36]$	-0.6	0.86	$[-0.39, -0.58, -0.83]$
$0.1 < T < 2.5$	0.34	0.49	$[0.29, 0.36, 0.36]$	-0.59	0.85	$[-0.38, -0.57, -0.8]$
$0.1 < T < 3.2$	0.29	0.59	$[0.22, 0.3, 0.34]$	-0.57	0.83	$[-0.4, -0.55, -0.75]$
$0.1 < T < 3.5$	0.29	0.59	$[0.22, 0.3, 0.34]$	-0.57	0.83	$[-0.4, -0.55, -0.75]$
$0.1 < T < 4.0$	-0.08	0.76	$[-0.18, -0.06, -0.01]$	-0.67	0.7	$[-0.61, -0.64, -0.74]$

Table A.2: Age residuals for intermediate age brackets. Values are in dex.

A.1.3: Old Age Bracket Analysis

	$< \log t_* >_L$			$< \log t_* >_M$		
Old	Average	Stddev	Noise [10,20,30]	Average	Stddev	Noise [10,20,30]
$T > 4.0$	-0.06	0.41	$[0.01, -0.07, -0.1]$	-0.06	0.41	$[0., -0.08, -0.1]$

Table A.3: Age residuals for old age bracket. Values are in Gyrs.

A.1.4: Low Z Bracket Analysis

Low	Average	Stddev	Noise [10,20,30]	Average	Stddev	Noise [10,20,30]
	$< Z_* >_L$			$< Z_* >_M$		
$Z \leq -1.7$	0.3	0.31	$[0.3, 0.3, 0.3]$	0.3	0.3	$[0.3, 0.3, 0.3]$
$Z \leq -1.3$	0.54	0.42	$[0.53, 0.54, 0.54]$	0.52	0.42	$[0.5, 0.53, 0.54]$

Table A.4: Z residuals for low Z brackets. Values are in [M/H].

A.1.5: Mid Z Bracket Analysis

	$< Z_* >_L$			$< Z_* >_M$		
Mid	Average	Stddev	Noise [10,20,30]	Average	Stddev	Noise [10,20,30]
$-1.3 < Z \leq -0.7$	-0.12	0.26	$[-0.19, -0.14, -0.03]$	-0.11	0.26	$[-0.19, -0.13, -0.03]$
$-1.3 < Z \leq -0.4$	-0.02	0.21	$[-0.02, -0.01, -0.02]$	-0.03	0.21	$[-0.03, -0.02, -0.03]$
$-1.3 < Z \leq 0.0$	0.14	0.32	$[0.12, 0.14, 0.15]$	0.12	0.33	$[0.11, 0.12, 0.13]$

Table A.5: Z residuals for mid Z brackets. Values are in [M/H].

A.1.6: High Z Bracket Analysis

	$< Z_* >_L$			$< Z_* >_M$		
High	Average	Stddev	Noise [10,20,30]	Average	Stddev	Noise [10,20,30]
$Z \geq 0.0$	0.06	0.14	$[0.07, 0.06, 0.05]$	0.06	0.14	$[0.06, 0.06, 0.05]$

Table A.6: Z residuals for high Z bracket. Values are in [M/H].

A.2: Single and Mixed Population Analysis

A.2.1: Single Population All Age and Z Residuals

	294	24	56
Age	$< \log t_* >_L$		
Average	0.56	0.58	0.56
Stddev	0.64	0.64	0.64
Noise Average	$[0.54, 0.56, 0.56]$	$[0.58, 0.58, 0.58]$	$[0.56, 0.56, 0.56]$
Noise Stddev	$[0.64, 0.64, 0.64]$	$[0.64, 0.64, 0.64]$	$[0.64, 0.64, 0.64]$
	$< \log t_* >_M$		
Average	-1.01	-1.09	-1.08
Stddev	0.65	0.64	0.64
Noise Average	$[-0.97, -1.02, -1.02]$	$[-1.09, -1.09, -1.09]$	$[-1.08, -1.08, -1.08]$
Noise Stddev	$[0.65, 0.64, 0.64]$	$[0.64, 0.64, 0.64]$	$[0.64, 0.64, 0.64]$
Z	$< Z_* >_L$		
Average	1.03	0.54	1.03
Stddev	0.86	0.86	0.86
Noise Average	$[1.03, 1.02, 1.03]$	$[0.54, 0.54, 0.54]$	$[1.03, 1.03, 1.03]$
Noise Stddev	$[0.86, 0.86, 0.86]$	$[0.86, 0.86, 0.86]$	$[0.86, 0.86, 0.86]$
	$< Z_* >_M$		
Average	-0.34	-0.46	-0.36
Stddev	0.89	0.86	0.87
Noise Average	$[-0.30, -0.36, -0.35]$	$[-0.46, -0.46 - 0.46]$	$[-0.37, -0.36, -0.36]$
Noise Stddev	$[0.92, 0.88, 0.86]$	$[0.86, 0.86, 0.86]$	$[0.87, 0.87, 0.87]$

Table A.7: Residuals for single populations. Ages are reported as $Log(t)$, Z is in [M/H].

A.2.2: Two Population All Age and Z Residuals

	294	24	56
Age	$< \log t_* >_L$		
Average	0.33	0.32	0.27
Stddev	0.46	0.47	0.48
Noise Average	$[0.32, 0.34, 0.34]$	$[0.32, 0.32, 0.33]$	$[0.28, 0.27, 0.27]$
Noise Stddev	$[0.46, 0.46, 0.46]$	$[0.47, 0.47, 0.47]$	$[0.49, 0.48, 0.48]$
	$< \log t_* >_M$		
Average	-1.24	-1.35	-1.37
Stddev	0.46	0.47	0.48
Noise Average	$[-1.19, -1.24, -1.27]$	$[-1.35, -1.35, -1.34]$	$[-1.37, -1.37, -1.37]$
Noise Stddev	$[0.46, 0.45, 0.46]$	$[0.47, 0.47, 0.47]$	$[0.48, 0.48, 0.48]$
Z	$< Z_* >_L$		
Average	1.01	0.5	0.96
Stddev	0.88	0.89	0.91
Noise Average	$[1.02, 1.01, 1.01]$	$[0.49, 0.5, 0.5]$	$[0.96, 0.96, 0.96]$
Noise Stddev	$[0.88, 0.87, 0.88]$	$[0.89, 0.89, 0.89]$	$[0.91, 0.91, 0.91]$
	$< Z_* >_M$		
Average	-0.35	-0.51	-0.44
Stddev	0.91	0.9	0.91
Noise Average	$[-0.32, -0.37, -0.36]$	$[-0.52, -0.5, -0.5]$	$[-0.47, -0.43, -0.42]$
Noise Stddev	$[0.95, 0.89, 0.88]$	$[0.90, 0.90, 0.89]$	$[0.90, 0.92, 0.91]$

Table A.8: Residuals for two populations. Ages are reported as $Log(t)$, Z is in [M/H].

A.2.3: Three Population All Age and Z Residuals

	294	24	56
Age	$< \log t_* >_L$		
Average	0.59	0.53	0.45
Stddev	0.59	0.61	0.62
Noise Average	$[0.58, 0.59, 0.59]$	$[0.53, 0.53, 0.53]$	$[0.45, 0.45, 0.45]$
Noise Stddev	$[0.60, 0.58, 0.59]$	$[0.61, 0.61, 0.61]$	$[0.62, 0.62, 0.62]$
	$< \log t_* >_M$		
Average	-0.99	-1.14	-1.19
Stddev	0.59	0.61	0.62
Noise Average	$[-0.95, -0.99, -1.02]$	$[-1.13, -1.14, -1.14]$	$[-1.19, -1.19, -1.19]$
Noise Stddev	$[0.59, 0.58, 0.59]$	$[0.61, 0.61, 0.61]$	$[0.62, 0.62, 0.62]$
Z	$< Z_* >_L$		
Average	1.03	0.55	1.04
Stddev	0.86	0.86	0.85
Noise Average	$[1.04, 1.03, 1.03]$	$[0.55, 0.55, 0.55]$	$[1.04, 1.04, 1.04]$
Noise Stddev	$[0.85, 0.86, 0.86]$	$[0.86, 0.86, 0.86]$	$[0.85, 0.86, 0.86]$
	$< Z_* >_M$		
Average	-0.34	-0.45	-0.36
Stddev	0.88	0.86	0.86
Noise Average	$[-0.33, -0.36, -0.34]$	$[-0.46, -0.45, -0.45]$	$[-0.38, -0.35, -0.34]$
Noise Stddev	$[0.91, 0.88, 0.86]$	$[0.86, 0.86, 0.86]$	$[0.86, 0.86, 0.86]$

Table A.9: Residuals for three populations. Ages are reported as $Log(t)$, Z is in [M/H].

A.3: Number of Base Templates Analysis

A.3.1: Age Residuals

Young	294	24	56
	$< \log t_* >_L$		
Average	0.07	0.07	0.07
Stddev	0.05	0.05	0.05
Noise Average	$[0.07, 0.07, 0.07]$	$[0.07, 0.07, 0.07]$	$[0.07, 0.07, 0.07]$
Noise Stddev	$[0.06, 0.05, 0.05]$	$[0.05, 0.05, 0.05]$	$[0.05, 0.05, 0.05]$
	$< \log t_* >_M$		
Average	0.07	0.07	0.07
Stddev	0.05	0.05	0.05
Noise Average	$[0.07, 0.07, 0.07]$	$[0.07, 0.07, 0.07]$	$[0.07, 0.07, 0.07]$
Noise Stddev	$[0.06, 0.05, 0.05]$	$[0.05, 0.05, 0.05]$	$[0.05, 0.05, 0.05]$

Table A.10: Residuals for all young populations. Ages are reported as $Log(t)$.

Intermediate	294	24	56
	$< \log t_* >_L$		
Average	-0.1	0.49	0.47
Stddev	0.77	0.48	0.48
Noise Average	$[-0.2, -0.08, -0.03]$	$[0.49, 0.49, 0.49]$	$[0.47, 0.48, 0.47]$
Noise Stddev	$[0.76, 0.76, 0.78]$	$[0.48, 0.48, 0.48]$	$[0.48, 0.48, 0.48]$
	$< \log t_* >_M$		
Average	-0.68	-1.17	-1.16
Stddev	0.71	0.48	0.48
Noise Average	$[-0.62, -0.66, -0.78]$	$[-1.17, -1.18, -1.18]$	$[-1.16, -1.17, -1.17]$
Noise Stddev	$[0.72, 0.72, 0.69]$	$[0.48, 0.48, 0.48]$	$[0.48, 0.48, 0.48]$

Table A.11: Residuals for all intermediate populations. Ages are reported as $Log(t)$.

Old	294	24	56
	$< \log t_* >_L$		
Average	-0.07	-0.13	-0.14
Stddev	0.37	0.1	0.1
Noise Average	$[-0.02, -0.09, -0.11]$	$[-0.13, -0.13, -0.13]$	$[-0.13, -0.14, -0.14]$
Noise Stddev	$[0.61, 0.1, 0.1]$	$[0.1, 0.1, 0.1]$	$[0.1, 0.1, 0.09]$
	$< \log t_* >_M$		
Average	-0.08	-0.13	-0.14
Stddev	0.36	0.1	0.1
Noise Average	$[-0.02, -0.09, -0.11]$	$[-0.13, -0.13, -0.13]$	$[-0.14, -0.14, -0.14]$
Noise Stddev	$[0.61, 0.1, 0.1]$	$[0.1, 0.1, 0.1]$	$[0.1, 0.1, 0.09]$

Table A.12: Residuals for all old populations. Ages are reported as $Log(t)$.

A.3.2: Z Residuals

Low	294	24	56
	$< Z_* >_L$		
Average	0.54	-0.07	0.54
Stddev	0.42	0.42	0.42
Noise Average	$[0.53, 0.54, 0.54]$	$[-0.07, -0.07, -0.07]$	$[0.54, 0.54, 0.54]$
Noise Stddev	$[0.42, 0.42, 0.42]$	$[0.42, 0.42, 0.42]$	$[0.42, 0.42, 0.42]$
	$< Z_* >_M$		
Average	0.52	-0.07	0.54
Stddev	0.43	0.42	0.42
Noise Average	$[0.5, 0.53, 0.54]$	$[-0.07, -0.07, -0.07]$	$[0.54, 0.54, 0.54]$
Noise Stddev	$[0.44, 0.42, 0.42]$	$[0.42, 0.42, 0.42]$	$[0.42, 0.42, 0.42]$

Table A.13: Residuals for all low Z populations. Zs are in [M/H].

Mid	294	24	56
	$< Z_* >_L$		
Average	-0.02	-0.15	-0.02
Stddev	0.21	0.15	0.17
Noise Average	$[-0.03, -0.01, -0.01]$	$[-0.15, -0.15, -0.15]$	$[-0.02, -0.02, -0.02]$
Noise Stddev	$[0.24, 0.21, 0.17]$	$[0.15, 0.15, 0.15]$	$[0.18, 0.17, 0.16]$
	$< Z_* >_M$		
Average	-0.03	-0.15	-0.04
Stddev	0.21	0.15	0.17
Noise Average	$[-0.03, -0.02, -0.03]$	$[-0.15, -0.15, -0.15]$	$[-0.04, -0.04, -0.04]$
Noise Stddev	$[0.24, 0.21, 0.17]$	$[0.15, 0.15, 0.15]$	$[0.18, 0.17, 0.16]$

Table A.14: Residuals for all mid Z populations. Zs are in [M/H].

High	294	24	56
	$< Z_* >_L$		
Average	0.06	0.1	0.07
Stddev	0.14	0.12	0.14
Noise Average	$[0.07, 0.06, 0.05]$	$[0.09, 0.1, 0.1]$	$[0.07, 0.07, 0.06]$
Noise Stddev	$[0.14, 0.14, 0.14]$	$[0.13, 0.12, 0.12]$	$[0.14, 0.14, 0.14]$
	$< Z_* >_M$		
Average	0.06	0.1	0.07
Stddev	0.14	0.12	0.14
Noise Average	$[0.06, 0.06, 0.04]$	$[0.09, 0.1, 0.1]$	$[0.07, 0.07, 0.06]$
Noise Stddev	$[0.14, 0.14, 0.14]$	$[0.13, 0.12, 0.12]$	$[0.14, 0.14, 0.14]$

Table A.15: Residuals for all high Z populations. Zs are in [M/H].

B: CINDERS Observations

Table B.1: First pass of observations

Field	Exposure time (min) (bright,grey,dark)	Month to observe	If need bundle for sky
SCG2114-2301	ACF –,–,82 EDB –,–,95	Jul 20 - Aug 30	AD –,–,98 CB –,114,73 EF –,–,82
SCG2200-2241	AB –,–,105 CD –,–,120	Aug 1 - Sep 15	
SCG0007-4642	DAB –,–118 DCB –,–,118	Sep 10 - Oct 10	AB –,–,118 DC –,–,118
SCG0018-4854	CDA –,–,101 CBA –,–,86	Sep 15 - Oct 1	DA –,–,120 CB –,–,101
SCG0030-2553	DAB –,111,72 DCB –,111,72	Sept 5 - Oct 15	AB –,–,1156 DC –,111,71
SCG0141-3429	BAC –,–,94 ED –,–,111	Sept 25 - Nov 5	BA –,–,112 BC –,–,94 ED –,–,111
SCG0301-5041	ACB –,101,65 CD –,–,115	Oct 1 - Nov 30	BA –,–,120 CD –,–,115
SCG0316-5433	ABC –,–,115 ADC –,108,70	Oct 10 - Dec 1	AB –,117,76 DC –,108,69
SCG0537-2925	DAB –,108,69 DCB –,108,69	Nov 20 - Jan 20	AB –,–,117 DC –,108,69
SCG0540-2610	CBA 120,59,38 CDA –,105,67	December	BA –,86,56 CD –,105,67
Total hours	dark: 2790-4185 grey: 1204-1806		
Total exposures	dark: 28-42 grey: 12-18		
Total galaxies	43		

Table B.2: Second pass of observations

Field	Exposure time (min) (bright,grey,dark)	Month to observe	If need bundle for sky
SCG2128-4614 A B C D E	CAB –,–,119 CED –,–,116	Jul 25 - Aug 25	AB –,115,74 CB –,–,119 ED –,–,115
SCG2159-2241 A B C D E	BA –,–,103 CA –,88,57 DA –,–,101 EA –,–,111	Aug 1 - Sep 10	
SCG0031-2143 A B C D E	AB –,–,104 CD –,–,107 ED –,–,106	Sept 5 - Oct 15	
SCG0131-3851 A B C D E	BA –,–,109 CD –,–,107 ED –,–,112	Sept 20 - Oct 31	
SCG0154-2020 A B C D	ABC –,–,81 DBC –,–,108	Sept 30 - Oct 2	AB –,–,83 DC –,–,108
SCG0319-5426 A B C D E	CA –,–,114 DE –,89,57 DB –,–,111	Oct 10 - Dec 1	
SCG0533-5057 A B C D	AB –,82,53 CD –,–,117	December	
SCG0609-4458 A B C D	BA –,–,92 DC–,–,118	Dec 1 - Jan 15	
Total hours	dark: 4206-6309		
Total exposures	dark: 42-63		
Total galaxies	37		

Table B.3: Remaining observations.

Field	Exposure time (min) (bright, grey, dark)	Month to observe	If need a bundle for sky
SCG2101-3536	ACB –,–,110	Jul 15 - Aug 30	AD –,–,110
A B C D	BCD –,–,110		BC –,–,110
SCG2104-2539	BA 97,47,31	Jul 15 - Aug 30	
A B C D	CD –,–,118		
SCG2110-3806	AB –,–,113	Jul 20 - Aug 30	
A B C D	DC –,–,92		
SCG2123-2159	CBA –,–,116	Jul 25 - Aug 30	DA –,–,106
A B C D	BAD–,–,106		CB –,–,96
SCG2124-2314	DAB –,–,103	Jul 25 - Sep 1	DA –,–,103
A B C D	CAB –,–,115		CB –,–,115
SCG2136-5854	AC –,–,103	August	
A B C D	BD –,–,88		
SCG2140-4329	ABD –,–,102	Aug 1 - Sep 5	AB –,–,82
A B C D	ADC –,–,102		CD –,–,102
SCG2147-4631	CB –,–,89	Aug 5 - Sep 5	
A B C D	DA –,–,96		
SCG2203-2812	ADB –,–,119	Aug 1 - Sep 15	AB–,–,87
A B C D	CDB –,–,119		
SCG2217-5521	AB –,–,116	Aug 1 - Sep 15	
A B C D	CD –,115,73		
SCG2226-3546	EDB –,–,95	Aug 5 - Sep 15	AB –,–,103
A B C D E	CA –,99,64		CB –,99,64
			ED –,–,95
SCG2254-4301	BDA –,–,120	Aug 15 - Sep 20	BA –,–,114
A B C D	CBD –,–,120		CD –,–,120
SCG2315-2125	DBA –,–,113	Aug 20 - Sep 25	BA –,–,119
A B C D	DCA –,–,113		DC –,–,113

SCG2316-2259 A B C D	DAC –,–,103 BA –,109,70	Aug 20 - Sep 30	BA –,109,70 DC –,–,120
SCG2345-2824 A B C D	AB –,97,63 DC –,–,98	Aug 20 - Oct 5	
SCG2358-4339 A B C D E	ACB –,–,81 DBE –,–,114	Sep 1 - Oct 5	AB –,–,88 CB –,–,81 DE –,–,114
SCG0002-3558 A B C D	CDA –,–,95 CBA –,–,117	Sep 1 - Oct 10	BA –,–,113 CD –,–,117
SCG0007-3753 A B C D	ACD –,–,119 ADB –,–,119	Sep 1 - Oct 10	AB –,–,98 CD –,–,119
SCG0009-5713 A B C D	BCA –,–,110 BCD –,–,81	Sep 1 - Oct 10	AB –,–,85 CD –,–,110
SCG0012-2421 A B C D	BCD –,–,105 BAD –,–,105	Sep 1 - Oct 10	BA –,–,104 CD –,–,99
SCG0028-2254 A B C D	CA –,–,115 BD –,–,115	Sept 5 - Oct 15	
SCG0045-2043 A B C D E	BCA –,–,99 EDC –,–,96	Sept 15 - Oct 15	BA –,–,102 BC –,–,99 ED –,–,95
SCG0045-4831 A B C D	BA –,–,80 BC –,–,106 BD –,–,110	Sept 15 - Oct 5	
SCG0048-3242 A B C D	ADB –,–,113 CDB –,–,113	Sept 5 - Oct 25	AB –,–,110 CD –,–,113
SCG0050-3517 A B C D E	ABE –,–,109 DC –,–,113	Sept 10 - Oct 25	AB –,–,120 DC –,–,113 BE –,–,109
SCG0100-2208 A B C D	DCA –,–,112 BC –,–,116	Sept 15 - Oct 25	BA –,–,107 DC –,–,112

SCG0102-4714 A B C D E	BC –,115,74 BE –,–,98 CA –,115,74	Sept 20 - Oct 15	
SCG0105-1747 A B C D	BAD –,–,107 CBA –,–,107	Sept 20 - Oct 20	BD –,–,107 CA –,–,107
SCG0106-4722 A B C D	DAB –,–115 DAC –,–,115	Sept 20 - Oct 15	AB 107,52,34 DC –,–,115
SCG0121-3521 A B C D	BA –,69,45 CD –,–,101	Sept 15 - Oct 31	
SCG0147-2506 A B C D E	BCA –,–,117 DEA –,–,120	Sept 25 - Nov 5	BA –,75,49 CD –,–,113 ED –,–,115
SCG0156-5629 A B C D	BA –,–,85 CD –,112,72	October	
SCG0549-3447 A B C D	CA –,111,71 DB –,–,94	Nov 20 - Jan 20	
SCG0608-4734 A B C D E F	CAD –,–,104 CBD –,–,104 CFE –,–,107	Dec 10 - Jan 10	CA –,–,114 CB –,–,114 DE –,–,112 FE –,–,107

REFERENCES

[1] A. Toomre and J. Toomre. Galactic Bridges and Tails. *Astrophysical Journal*, 178:623–666, December 1972.

[2] I. Shlosman. Induced starburst and nuclear activity: Faith, facts, and theory. In J. W. Sulentic, W. C. Keel, and C. M. Telesco, editors, *NASA Conference Publication*, volume 3098 of *NASA Conference Publication*, November 1990.

[3] R. C. Kennicutt, Jr., K. A. Roettiger, W. C. Keel, J. M. van der Hulst, and E. Hummel. The effects of interactions on spiral galaxies. II - Disk star-formation rates. *Astronomical Journal*, 93:1011–1023, May 1987.

[4] S. D. Friedman, R. D. Cohen, B. Jones, H. E. Smith, and W. A. Stein. Imaging and spectroscopic studies of the interacting system Markarian 171. *Astronomical Journal*, 94:1480–1486, December 1987.

[5] G. Kauffmann, T. M. Heckman, S. D. M. White, S. Charlot, C. Tremonti, J. Brinchmann, G. Bruzual, E. W. Peng, M. Seibert, M. Bernardi, M. Blanton, J. Brinkmann, F. Castander, I. Csábai, M. Fukugita, Z. Ivezic, J. A. Munn, R. C. Nichol, N. Padmanabhan, A. R. Thakar, D. H. Weinberg, and D. York. Stellar masses and star formation histories for 10^5 galaxies from the Sloan Digital Sky Survey. *Monthly Notices of the Royal Astronomical Society*, 341:33–53, May 2003.

[6] G. Kauffmann, T. M. Heckman, S. D. M. White, S. Charlot, C. Tremonti, E. W. Peng, M. Seibert, J. Brinkmann, R. C. Nichol, M. SubbaRao, and D. York. The dependence of star formation history and internal structure on stellar mass for 10^5 low-redshift galaxies. *Monthly Notices of the Royal Astronomical Society*, 341:54–69, May 2003.

[7] G. Kauffmann, T. M. Heckman, C. Tremonti, J. Brinchmann, S. Charlot, S. D. M. White, S. E. Ridgway, J. Brinkmann, M. Fukugita, P. B. Hall, Ž. Ivezić, G. T. Richards, and D. P. Schneider. The host galaxies of active galactic nuclei. *Monthly Notices of the Royal Astronomical Society*, 346:1055–1077, December 2003.

[8] G. Kauffmann, S. D. M. White, T. M. Heckman, B. Ménard, J. Brinchmann, S. Charlot, C. Tremonti, and J. Brinkmann. The environmental dependence of the relations between stellar mass, structure, star formation and nuclear activity in galaxies. *Monthly Notices of the Royal Astronomical Society*, 353:713–731, September 2004.

[9] M. Stephan. Nebulæ (new) discovered and observed at the observatory of Marseilles, 1876 and 1877, M. Stephan. *Monthly Notices of the Royal Astronomical Society*, 37:334, April 1877.

[10] C. K. Seyfert. Five thousand external galaxies and a new dense group. *Astronomical Journal*, 53:203, 1948.

[11] B. A. Vorontsov-Velyaminov. Atlas and catalog of interacting galaxies. 1959, Sternberg Institute, Moscow State University. In *Atlas and catalog of interacting galaxies (1959)*, 1959.

[12] B. A. Vorontsov-Velyaminov. Atlas of interacting galaxies, part II and the concept of fragmentation of galaxies. *Astronomy and Astrophysics Supplemental Series*, 28:1–117, April 1977.

[13] H. Arp. Atlas of Peculiar Galaxies. *Astrophysical Journal Supplemental*, 14:1, November 1966.

[14] G. O. Abell. The National Geographic Society-Palomar Observatory Sky Survey. *Leaflet of the Astronomical Society of the Pacific*, 8:121, 1959.

[15] R. K. Shakhbazyan. Compact groups of compact galaxies. *Astrophysics*, 9:296–304, October 1973.

[16] R. K. Shakhbazian. VizieR Online Data Catalog: Compact groups of compact galaxies (Shakhbazian+ 1973-1979). *VizieR Online Data Catalog*, 7089, September 1996.

[17] A. J. Wesselink. Report on the Yale-Columbia Southern Proper Motion Program. In W. Gliese, C. A. Murray, and R. H. Tucker, editors, *IAU Symp. 61: New Problems in Astrometry*, volume 61 of *IAU Symposium*, page 201, 1974.

[18] J. A. Rose. A survey of compact groups of galaxies. *Astrophysical Journal*, 211:311–318, January 1977.

[19] J. A. Rose. The dynamical nature of compact groups of galaxies. *Astrophysical Journal*, 231:10–22, July 1979.

[20] P. Hickson. Systematic properties of compact groups of galaxies. *Astrophysical Journal*, 255:382–391, April 1982.

[21] I. Prandoni, A. Iovino, and H. T. MacGillivray. Automated search for compact groups of galaxies in the southern sky. *Astronomical Journal*, 107:1235–1244, April 1994.

[22] N. C. Hambly, H. T. MacGillivray, M. A. Read, S. B. Tritton, E. B. Thomson, B. D. Kelly, D. H. Morgan, R. E. Smith, S. P. Driver, J. Williamson, Q. A. Parker, M. R. S. Hawkins, P. M. Williams, and A. Lawrence. The SuperCOSMOS Sky Survey - I. Introduction and description. *Monthly Notices of the Royal Astronomical Society*, 326:1279–1294, October 2001.

[23] A. Iovino. Detecting Fainter Compact Groups: Results from a New Automated Algorithm. *Astrophysical Journal*, 124:2471–2489, November 2002.

[24] E. Barton, M. Geller, M. Ramella, R. O. Marzke, and L. N. da Costa. Compact Group selection From Redshift Surveys. *Astronomical Journal*, 112:871, September 1996.

[25] A. W. McConnachie, D. R. Patton, S. L. Ellison, and L. Simard. Compact groups in theory and practice - III. Compact groups of galaxies in the Sixth Data Release of the Sloan Digital Sky Survey. *Monthly Notices of the Royal Astronomical Society*, 395:255–268, May 2009.

[26] E. Díaz-Giménez, G. A. Mamon, M. Pacheco, C. Mendes de Oliveira, and M. V. Alonso. Compact groups of galaxies selected by stellar mass: the 2MASS compact group catalogue. *Monthly Notices of the Royal Astronomical Society*, 426:296–316, October 2012.

[27] J. Sohn, H. S. Hwang, M. J. Geller, A. Diaferio, K. J. Rines, M. G. Lee, and G.-H. Lee. Compact Groups of Galaxies with Complete Spectroscopic Redshifts in the Local Universe. *Journal of Korean Astronomical Society*, 48:381–398, December 2015.

[28] J. C. Clemens, J. A. Crain, and R. Anderson. The Goodman spectrograph. In A. F. M. Moorwood and M. Iye, editors, *Ground-based Instrumentation for Astronomy*, volume 5492 of *Proceedings of the Society of Photo-Optical Instrumentation Engineers*, pages 331–340, September 2004.

[29] P. Hickson, C. Mendes de Oliveira, J. P. Huchra, and G. G. Palumbo. Dynamical properties of compact groups of galaxies. *Astrophysical Journal*, 399:353–367, November 1992.

[30] J. W. Sulentic and J. B. Smith. A fresh look at discordant redshift galaxies in compact groups. *Astrophysics and Space Science*, 244:23–28, March 1996.

[31] J. W. Sulentic. The Twin Paradoxes of Compact Groups: Discordant Excess Muted But the Dynamical Puzzle Persists. *Astrophysical Journal*, 482:640–647, June 1997.

[32] C. Mendes de Oliveira. The nature of discordant redshift galaxies in compact groups. *Monthly Notices of the Royal Astronomical Society*, 273:139–145, March 1995.

[33] A. Iovino and P. Hickson. Discordant redshifts in compact groups. *Monthly Notices of the Royal Astronomical Society*, 287:21–25, May 1997.

[34] V. C. Rubin, D. A. Hunter, and W. K. Ford, Jr. Optical properties and dynamics of galaxies in the Hickson compact groups. *Astrophysical Journal Supplement Series*, 76:153–183, May 1991.

[35] A. L. B. Ribeiro, R. R. de Carvalho, H. V. Capelato, and S. E. Zepf. Structural and Dynamical Analysis of the Hickson Compact Groups. *Astrophysical Journal*, 497:72–88, April 1998.

[36] S. Nishiura, M. Shimada, Y. Ohyama, T. Murayama, and Y. Taniguchi. A Dynamical Study of Galaxies in the Hickson Compact Groups. *Astronomical Journal*, 120:1691–1712, October 2000.

[37] H. Plana, P. Amram, C. Mendes de Oliveira, C. Balkowski, and J. Boulesteix. Gas Kinematics in Three Hickson Compact Groups: The Data. *Astronomical Journal*, 125:1736–1755, April 2003.

[38] P. Amram, H. Plana, C. Mendes de Oliveira, C. Balkowski, and J. Boulesteix. Gas kinematics of a sample of five Hickson Compact Groups. The data. *Astronomy and Astrophysics*, 402:865–877, May 2003.

[39] S. Torres-Flores, C. Mendes de Oliveira, P. Amram, H. Plana, B. Epinat, C. Carignan, and C. Balkowski. Kinematics of galaxies in compact groups. Studying the B-band Tully-Fischer relation. *Astronomy and Astrophysics*, 521:A59, October 2010.

[40] P. Hickson, E. Kindl, and J. P. Huchra. Discordant redshifts in compact groups of galaxies. *Astrophysical Journal Letters*, 329:L65–L67, June 1988.

[41] R. Coziol, E. Brinks, and H. Bravo-Alfaro. The Relation between Galaxy Activity and the Dynamics of Compact Groups of Galaxies. *Astronomical Journal*, 128:68–88, July 2004.

[42] S. Torres-Flores, C. Mendes de Oliveira, D. F. de Mello, P. Amram, H. Plana, B. Epinat, and J. Iglesias-Páramo. Star formation in the intragroup medium and other diagnostics of the evolutionary stages of compact groups of galaxies. *Astronomy and Astrophysics*, 507:723–746, November 2009.

[43] H. Tovmassian, M. Plionis, and J. P. Torres-Papaqui. Physical properties of Hickson compact groups and of the loose groups within which they are embedded. *Astronomy and Astrophysics*, 456:839–846, September 2006.

[44] R. Coziol, A. L. B. Ribeiro, R. R. de Carvalho, and H. V. Capelato. The Nature of the Activity in Hickson Compact Groups of Galaxies. *Astrophysical Journal*, 493:563–570, January 1998.

[45] R. Coziol, R. R. de Carvalho, H. V. Capelato, and A. L. B. Ribeiro. The Evolution of Galaxies in Compact Groups. *Astrophysical Journal*, 506:545–556, October 1998.

[46] R. N. Proctor, D. A. Forbes, G. K. T. Hau, M. A. Beasley, G. M. De Silva, R. Contreras, and A. I. Terlevich. Ages and metallicities of Hickson compact group galaxies. *Monthly Notices of the Royal Astronomical Society*, 349:1381–1396, April 2004.

[47] C. Mendes de Oliveira, P. Coelho, J. J. González, and B. Barbuy. Ages, Metallicities, and α-Element Enhancement for Galaxies in Hickson Compact Groups. *Astronomical Journal*, 130:55–64, July 2005.

[48] I. G. de la Rosa, R. R. de Carvalho, A. Vazdekis, and B. Barbuy. Truncated Star Formation in Compact Groups of Galaxies: A Stellar Population Study. *Astronomical Journal*, 133:330–346, January 2007.

[49] T. Bitsakis, V. Charmandaris, E. da Cunha, T. Díaz-Santos, E. Le Floc'h, and G. Magdis. A mid-IR study of Hickson compact groups. II. Multiwavelength analysis of the complete GALEX-Spitzer sample. *Astronomy and Astrophysics*, 533:A142, September 2011.

[50] M. A. Martínez, A. Del Olmo, R. Coziol, and J. Perea. AGN Population in Hickson Compact Groups. I. Data and Nuclear Activity Classification. *Astronomical Journal*, 139:1199–1211, March 2010.

[51] K. E. Johnson, J. E. Hibbard, S. C. Gallagher, J. C. Charlton, A. E. Hornschemeier, T. H. Jarrett, and A. E. Reines. The Infrared Properties of Hickson Compact Groups. *Astronomical Journal*, 134:1522–1543, October 2007.

[52] L. M. Walker, K. E. Johnson, S. C. Gallagher, J. C. Charlton, A. E. Hornschemeier, and J. E. Hibbard. Examining the Role of Environment in a Comprehensive Sample of Compact Groups. *Astronomical Journal*, 143:69, March 2012.

[53] M. E. Cluver, P. N. Appleton, P. Ogle, T. H. Jarrett, J. Rasmussen, U. Lisenfeld, P. Guillard, L. Verdes-Montenegro, R. Antonucci, T. Bitsakis, V. Charmandaris, F. Boulanger, E. Egami, C. K. Xu, and M. S. Yun. Enhanced Warm H_2 Emission in the Compact Group Mid-infrared "Green Valley". *Astrophysical Journal*, 765:93, March 2013.

[54] T. D. Desjardins, S. C. Gallagher, P. Tzanavaris, J. S. Mulchaey, W. N. Brandt, J. C. Charlton, G. P. Garmire, C. Gronwall, A. E. Hornschemeier, K. E. Johnson, I. S. Konstantopoulos, and A. I. Zabludoff. Intragroup and Galaxy-linked Diffuse X-Ray Emission in Hickson Compact Groups. *Astrophysical Journal*, 763:121, February 2013.

[55] J. Iglesias-Páramo and J. M. Vílchez. On the Influence of the Environment on the Star Formation Rates of a Sample of Galaxies in Nearby Compact Groups. *Astrophysical Journal*, 518:94–102, June 1999.

[56] M. Shimada, Y. Ohyama, S. Nishiura, T. Murayama, and Y. Taniguchi. The Nuclear Activity of Galaxies in the Hickson Compact Groups. *Astronomical Journal*, 119:2664–2685, June 2000.

[57] J. Iglesias-Páramo and J. M. Vílchez. Star-forming Objects in the Tidal Tails of Compact Groups. *Astrophysical Journal*, 550:204–211, March 2001.

[58] P. Hickson, T. K. Menon, G. G. C. Palumbo, and M. Persic. Infrared emission from compact groups of galaxies. *Astrophysical Journal*, 341:679–684, June 1989.

[59] J. W. Sulentic and D. F. de Mello Rabaca. Searching for a far-infrared enhancement in compact groups of galaxies. *Astrophysical Journal*, 410:520–525, June 1993.

[60] M. Moles, A. del Olmo, J. Perea, J. Masegosa, I. Marquez, and V. Costa. Star formation and merging in compact groups of galaxies. *Astronomy and Astrophysics*, 285, May 1994.

[61] V. R. Venugopal. Hickson's compact groups of galaxies: far-infrared enhancement. *Monthly Notices of the Royal Astronomical Society*, 277:455–457, November 1995.

[62] S. Leon, F. Combes, and T. K. Menon. Molecular gas in galaxies of Hickson compact groups. *Astronomy and Astrophysics*, 330:37–56, February 1998.

[63] L. Verdes-Montenegro, M. S. Yun, J. Perea, A. del Olmo, and P. T. P. Ho. Effects of Interaction-induced Activities in Hickson Compact Groups: CO and Far-Infrared Study. *Astrophysical Journal*, 497:89–107, April 1998.

[64] T. Bitsakis, V. Charmandaris, E. Le Floc'h, T. Díaz-Santos, S. K. Slater, E. Xilouris, and M. P. Haynes. A mid-IR study of Hickson compact groups. I. Probing the effects of environment in galaxy interactions. *Astronomy and Astrophysics*, 517:A75, July 2010.

[65] V. Martinez-Badenes, U. Lisenfeld, D. Espada, L. Verdes-Montenegro, S. García-Burillo, S. Leon, J. Sulentic, and M. S. Yun. Molecular gas content and SFR in Hickson compact groups: enhanced

or deficient? *Astronomy and Astrophysics*, 540:A96, April 2012.

[66] G. A. Mamon. Are compact groups of galaxies physically dense? *Astrophysical Journal*, 307:426–430, August 1986.

[67] P. Hickson and H. J. Rood. The nature of compact groups of galaxies. *Astrophysical Journal Letters*, 331:L69–L72, August 1988.

[68] D. G. Walke and G. A. Mamon. The frequency of chance alignments of galaxies in loose groups. *Astronomy and Astrophysics*, 225:291–302, November 1989.

[69] E. Díaz-Giménez and G. A. Mamon. Compact groups from the Millennium Simulations - I. Their nature and the completeness of the Hickson sample. *Monthly Notices of the Royal Astronomical Society*, 409:1227–1243, December 2010.

[70] G. A. Mamon. The dynamics of small groups of galaxies. I - Virialized groups. *Astrophysical Journal*, 321:622–644, October 1987.

[71] F. Governato, R. Bhatia, and G. Chincarini. A long-lasting compact group. *Astrophysical Journal Letters*, 371:L15–L18, April 1991.

[72] P. W. Bode, H. N. Cohn, and P. M. Lugger. Simulations of Compact Groups of Galaxies: The Effect of the Dark Matter Distribution. *Astrophysical Journal*, 416:17, October 1993.

[73] A. Diaferio, M. J. Geller, and M. Ramella. The formation of compact groups of galaxies. I: Optical properties. *Astronomical Journal*, 107:868–879, March 1994.

[74] L. Hernquist, N. Katz, and D. H. Weinberg. Physically detached 'compact groups'. *Astrophysical Journal*, 442:57–66, March 1995.

[75] F. Governato, P. Tozzi, and A. Cavaliere. Small Groups of Galaxies: A Clue to a Critical Universe. *Astrophysical Journal*, 458:18, February 1996.

[76] R. A. Pildis, A. E. Evrard, and J. N. Bregman. Properties of Simulated Compact Groups of Galaxies. *Astronomical Journal*, 112:378, August 1996.

[77] H. Aceves and H. Velázquez. N-Body Simulations of Small Galaxy Groups. *Revista Mexicana de Astronomía y Astrofísica*, 38:199–214, October 2002.

[78] H. J. Rood and B. A. Williams. The neighborhood of a compact group of galaxies. *Astrophysical Journal*, 339:772–782, April 1989.

[79] M. Ramella, A. Diaferio, M. J. Geller, and J. P. Huchra. The birthplace of compact groups of galaxies. *Astronomical Journal*, 107:1623–1628, May 1994.

[80] H. J. Rood and M. F. Struble. Spatial coincidence between a number of Hickson compact groups and loose groups or clusters. *Publications of the Astronomical Society of the Pacific*, 106:413–416, April 1994.

[81] G. G. C. Palumbo, P. Saracco, P. Hickson, and C. Mendes de Oliveira. Environment of compact groups of galaxies. *Astronomical Journal*, 109:1476–1484, April 1995.

[82] G. G. C. Palumbo, P. Saracco, C. Mendes de Oliveira, P. Hickson, V. Tornatore, and G. C. Baiesi-Pillastrini. Compact groups of galaxies and large-scale structure. *Astrophysical Journal*, 405:413–418, March 1993.

[83] H. M. Tovmassian, O. Yam, and H. Tiersch. Hickson Compact Groups: The Cores of Elongated Loose

Groups. *Revista Mexicana de Astronomía y Astrofísica*, 37:173–177, October 2001.

[84] P. Hickson. Compact Groups of Galaxies. *Annual Review of Astronomy and Astrophysics*, 35:357–388, 1997.

[85] V. Coenda, H. Muriel, and H. J. Martínez. Comparing galaxy populations in compact and loose groups of galaxies. *Astronomy and Astrophysics*, 543:A119, July 2012.

[86] H. J. Martínez, V. Coenda, and H. Muriel. Comparing galaxy populations in compact and loose groups of galaxies. II. Brightest group galaxies. *Astronomy and Astrophysics*, 557:A61, September 2013.

[87] J. T. Mendel, S. L. Ellison, L. Simard, D. R. Patton, and A. W. McConnachie. Compact groups in theory and practice - IV. The connection to large-scale structure. *Monthly Notices of the Royal Astronomical Society*, 418:1409–1422, December 2011.

[88] M. F. Skrutskie, R. M. Cutri, R. Stiening, M. D. Weinberg, S. Schneider, J. M. Carpenter, C. Beichman, R. Capps, T. Chester, J. Elias, J. Huchra, J. Liebert, C. Lonsdale, D. G. Monet, S. Price, P. Seitzer, T. Jarrett, J. D. Kirkpatrick, J. E. Gizis, E. Howard, T. Evans, J. Fowler, L. Fullmer, R. Hurt, R. Light, E. L. Kopan, K. A. Marsh, H. L. McCallon, R. Tam, S. Van Dyk, and S. Wheelock. The Two Micron All Sky Survey (2MASS). *Astronomical Journal*, 131:1163–1183, February 2006.

[89] E. Díaz-Giménez and A. Zandivarez. Where are compact groups in the local Universe? *Astronomy and Astrophysics*, 578:A61, June 2015.

[90] R. Coziol, A. Iovino, and R. R. de Carvalho. The Relation between Activity and Environment in Compact Groups of Galaxies. *Astronomical Journal*, 120:47–67, July 2000.

[91] R. C. Kennicutt, Jr., W. C. Keel, and C. A. Blaha. A comparison of the physical conditions in nuclear, hotspot, and disk H II regions. *Astronomical Journal*, 97:1022–1035, April 1989.

[92] J. B. Stevens, R. L. Webster, D. G. Barnes, D. J. Pisano, and M. J. Drinkwater. The HI Content of Compact Groups of Galaxies. *Publications of the Astronomical Society of Australia*, 21:318–333, 2004.

[93] E. Pompei, M. Dahlem, and A. Iovino. Optical and radio survey of southern compact groups of galaxies. I. Pilot study of six groups. *Astronomy and Astrophysics*, 473:399–409, October 2007.

[94] R. Bacon, Y. Copin, G. Monnet, B. W. Miller, J. R. Allington-Smith, M. Bureau, C. M. Carollo, R. L. Davies, E. Emsellem, H. Kuntschner, R. F. Peletier, E. K. Verolme, and P. T. de Zeeuw. The SAURON project - I. The panoramic integral-field spectrograph. *Monthly Notices of the Royal Astronomical Society*, 326:23–35, September 2001.

[95] G. A. Blanc, K. Gebhardt, A. Heiderman, N. J. Evans, II, S. Jogee, R. van den Bosch, I. Marinova, T. Weinzirl, P. Yoachim, N. Drory, M. Fabricius, D. Fisher, L. Hao, P. J. MacQueen, J. Shen, G. J. Hill, and J. Kormendy. The VIRUS-P Exploration of Nearby Galaxies (VENGA): Survey Design and First Results. In L. M. Stanford, J. D. Green, L. Hao, and Y. Mao, editors, *New Horizons in Astronomy: Frank N. Bash Symposium 2009*, volume 432 of *Astronomical Society of the Pacific Conference Series*, page 180, October 2010.

[96] M. A. Bershady, M. A. W. Verheijen, R. A. Swaters, D. R. Andersen, K. B. Westfall, and T. Martinsson. The DiskMass Survey. I. Overview. *Astrophysical Journal*, 716:198–233, June 2010.

[97] F. F. Rosales-Ortega, R. C. Kennicutt, S. F. Sánchez, A. I. Díaz, A. Pasquali, B. D. Johnson, and C. N. Hao. PINGS: the PPAK IFS Nearby Galaxies Survey. *Monthly Notices of the Royal Astronomical Society*, 405:735–758, June 2010.

[98] M. A. Strauss, D. H. Weinberg, R. H. Lupton, V. K. Narayanan, J. Annis, M. Bernardi, M. Blanton, S. Burles, A. J. Connolly, J. Dalcanton, M. Doi, D. Eisenstein, J. A. Frieman, M. Fukugita, J. E. Gunn, Ž. Ivezić, S. Kent, R. S. J. Kim, G. R. Knapp, R. G. Kron, J. A. Munn, H. J. Newberg, R. C. Nichol, S. Okamura, T. R. Quinn, M. W. Richmond, D. J. Schlegel, K. Shimasaku, M. SubbaRao, A. S. Szalay, D. Vanden Berk, M. S. Vogeley, B. Yanny, N. Yasuda, D. G. York, and I. Zehavi. Spectroscopic Target Selection in the Sloan Digital Sky Survey: The Main Galaxy Sample. *Astronomical Journal*, 534:A8, October 2011.

[99] E. Mármol-Queraltó, S. F. Sánchez, R. A. Marino, D. Mast, K. Viironen, A. Gil de Paz, J. Iglesias-Páramo, F. F. Rosales-Ortega, and J. M. Vilchez. Integral field spectroscopy of a sample of nearby galaxies. I. Sample, observations, and data reduction. *Astronomy and Astrophysics*, 534:A8, October 2011.

[100] S. M. Croom, J. S. Lawrence, J. Bland-Hawthorn, J. J. Bryant, L. Fogarty, S. Richards, M. Goodwin, T. Farrell, S. Miziarski, R. Heald, D. H. Jones, S. Lee, M. Colless, S. Brough, A. M. Hopkins, A. E. Bauer, M. N. Birchall, S. Ellis, A. Horton, S. Leon-Saval, G. Lewis, Á. R. López-Sánchez, S.-S. Min, C. Trinh, and H. Trowland. The Sydney-AAO Multi-object Integral field spectrograph. *Monthly Notices of the Royal Astronomical Society*, 421:872–893, March 2012.

[101] J. Bland-Hawthorn. The Hector Survey: integral field spectroscopy of 100,000 galaxies. In B. L. Ziegler, F. Combes, H. Dannerbauer, and M. Verdugo, editors, *IAU Symposium*, volume 309 of *IAU Symposium*, pages 21–28, February 2015.

[102] G. Raskin, H. van Winckel, H. Hensberge, A. Jorissen, H. Lehmann, C. Waelkens, G. Avila, J.-P. de Cuyper, P. Degroote, R. Dubosson, L. Dumortier, Y. Frémat, U. Laux, B. Michaud, J. Morren, J. Perez Padilla, W. Pessemier, S. Prins, K. Smolders, S. van Eck, and J. Winkler. HERMES: a high-resolution fibre-fed spectrograph for the Mercator telescope. *Astronomy and Astrophysics*, 526:A69, February 2011.

[103] H. Flores, M. Puech, F. Hammer, O. Garrido, and O. Hernandez. GIRAFFE multiple integral field units at VLT: A unique tool to recover velocity fields of distant galaxies. *Astronomy and Astrophysics*, 420:L31–L34, June 2004.

[104] K. Bundy, M. A. Bershady, D. R. Law, R. Yan, N. Drory, N. MacDonald, D. A. Wake, B. Cherinka, J. R. Sánchez-Gallego, A.-M. Weijmans, D. Thomas, C. Tremonti, K. Masters, L. Coccato, A. M. Diamond-Stanic, A. Aragón-Salamanca, V. Avila-Reese, C. Badenes, J. Falcón-Barroso, F. Belfiore, D. Bizyaev, G. A. Blanc, J. Bland-Hawthorn, M. R. Blanton, J. R. Brownstein, N. Byler, M. Cappellari, C. Conroy, A. A. Dutton, E. Emsellem, J. Etherington, P. M. Frinchaboy, H. Fu, J. E. Gunn, P. Harding, E. J. Johnston, G. Kauffmann, K. Kinemuchi, M. A. Klaene, J. H. Knapen, A. Leauthaud, C. Li, L. Lin, R. Maiolino, V. Malanushenko, E. Malanushenko, S. Mao, C. Maraston, R. M. McDermid, M. R. Merrifield, R. C. Nichol, D. Oravetz, K. Pan, J. K. Parejko, S. F. Sanchez, D. Schlegel, A. Simmons, O. Steele, M. Steinmetz, K. Thanjavur, B. A. Thompson, J. L. Tinker, R. C. E. van den Bosch, K. B. Westfall, D. Wilkinson, S. Wright, T. Xiao, and K. Zhang. Overview of the SDSS-IV MaNGA Survey: Mapping nearby Galaxies at Apache Point Observatory. *Astrophysical Journal*, 798:7, January 2015.

[105] G.N. Cecil, A.J. Moffett, Y. Cui, K.D. Eckert, J. McBride, S. Kannappan, K. Keller, B.N. Barlow, B. Dunlap, and J. Bland-Hawthorn. Deployable Integral Field Units, Multislits, and Image Slicer for the Goodman Imaging Spectrograph on the SOAR Telescope. In *American Astronomical Society Meeting Abstracts #215*, volume 42 of *Bulletin of the American Astronomical Society*, page 403, January 2010.

[106] M. Salaris and S. Cassisi. *Evolution of Stars and Stellar Populations*. 2006.

[107] L. Girardi, A. Bressan, C. Chiosi, G. Bertelli, and E. Nasi. Evolutionary sequences of stellar models

with new radiative opacities. VI. Z=0.0001. *Astronomy and Astrophysics Supplement*, 117:113–125, May 1996.

[108] G. Schaller, D. Schaerer, G. Meynet, and A. Maeder. New grids of stellar models from 0.8 to 120 solar masses at Z = 0.020 and Z = 0.001. *Astronomy and Astrophysics Supplement Series*, 96:269–331, December 1992.

[109] M. Alongi, G. Bertelli, A. Bressan, C. Chiosi, F. Fagotto, L. Greggio, and E. Nasi. Evolutionary sequences of stellar models with semiconvection and convective overshoot. I - Z = 0.008. *Astronomy and Astrophysics Supplement Series*, 97:851–871, March 1993.

[110] A. Bressan, F. Fagotto, G. Bertelli, and C. Chiosi. Evolutionary sequences of stellar models with new radiative opacities. II - Z = 0.02. *Astronomy and Astrophysics Supplement Series*, 100:647–664, September 1993.

[111] F. Fagotto, A. Bressan, G. Bertelli, and C. Chiosi. Evolutionary sequences of stellar models with new radiative opacities. IV. Z=0.004 and Z=0.008. *Astronomy and Astrophysics Supplement Series*, 105, May 1994.

[112] F. Fagotto, A. Bressan, G. Bertelli, and C. Chiosi. Evolutionary sequences of stellar models with very high metallicity. V. Z=0.1. *Astronomy and Astrophysics Supplement Series*, 105, May 1994.

[113] C. Charbonnel, G. Meynet, A. Maeder, and D. Schaerer. Grids of stellar models. VI. Horizontal branch and early asymptotic giant branch for low mass stars (Z=0.020, 0.001). *Astronomy and Astrophysics Supplement Series*, 115:339, February 1996.

[114] C. Charbonnel and S. Talon. The hot side of the lithium dip - LiBeB abundances beyond the main sequence. *Astronomy and Astrophysics*, 351:635–643, November 1999.

[115] L. Girardi, G. Bertelli, A. Bressan, C. Chiosi, M. A. T. Groenewegen, P. Marigo, B. Salasnich, and A. Weiss. Theoretical isochrones in several photometric systems. I. Johnson-Cousins-Glass, HST/WFPC2, HST/NICMOS, Washington, and ESO Imaging Survey filter sets. *Astronomy and Astrophysics*, 391:195–212, August 2002.

[116] A. Vazdekis, P. Sánchez-Blázquez, J. Falcón-Barroso, A. J. Cenarro, M. A. Beasley, N. Cardiel, J. Gorgas, and R. F. Peletier. Evolutionary stellar population synthesis with MILES - I. The base models and a new line index system. *Monthly Notices of the Royal Astronomical Society*, 404:1639–1671, June 2010.

[117] E. E. Salpeter. The Luminosity Function and Stellar Evolution. *Astrophysical Journal*, 121:161, January 1955.

[118] J. M. Scalo. The initial mass function of massive stars in galaxies Empirical evidence. In C. W. H. De Loore, A. J. Willis, and P. Laskarides, editors, *Luminous Stars and Associations in Galaxies*, volume 116 of *IAU Symposium*, pages 451–466, 1986.

[119] P. Kroupa, C. A. Tout, and G. Gilmore. The distribution of low-mass stars in the Galactic disc. *Monthly Notice of the Royal Astronomical Society*, 262:545–587, June 1993.

[120] P. Kroupa. The Local Stellar Initial Mass Function. In S. Deiters, B. Fuchs, A. Just, R. Spurzem, and R. Wielen, editors, *Dynamics of Star Clusters and the Milky Way*, volume 228 of *Astronomical Society of the Pacific Conference Series*, page 187, 2001.

[121] P. Kroupa. On the variation of the initial mass function. *Monthly Notice of the Royal Astronomical Society*, 322:231–246, April 2001.

[122] G. Bruzual and S. Charlot. Stellar population synthesis at the resolution of 2003. *Monthly Notices of the Royal Astronomical Society*, 344:1000–1028, October 2003.

[123] P. Sánchez-Blázquez, R. F. Peletier, J. Jiménez-Vicente, N. Cardiel, A. J. Cenarro, J. Falcón-Barroso, J. Gorgas, S. Selam, and A. Vazdekis. Medium-resolution Isaac Newton Telescope library of empirical spectra. *Monthly Notices of the Royal Astronomical Society*, 371:703–718, September 2006.

[124] D. Burstein, S. M. Faber, C. M. Gaskell, and N. Krumm. Old stellar populations. I - A spectroscopic comparison of galactic globular clusters, M31 globular clusters, and elliptical galaxies. *Astrophysical Journal*, 287:586–609, December 1984.

[125] J. Gorgas, S. M. Faber, D. Burstein, J. J. Gonzalez, S. Courteau, and C. Prosser. Old stellar populations. IV - Empirical functions for features in the spectra of G and K stars. *Astrophysical Journal Supplement Series*, 86:153–198, May 1993.

[126] G. Worthey, S. M. Faber, J. J. Gonzalez, and D. Burstein. Old stellar populations. 5: Absorption feature indices for the complete LICK/IDS sample of stars. *Astrophysical Journal Supplement Series*, 94:687–722, October 1994.

[127] G. Worthey and D. L. Ottaviani. Hγ and Hδ Absorption Features in Stars and Stellar Populations. *Astrophysical Journal Supplement Series*, 111:377–386, August 1997.

[128] S. C. Trager, G. Worthey, S. M. Faber, D. Burstein, and J. J. González. Old Stellar Populations. VI. Absorption-Line Spectra of Galaxy Nuclei and Globular Clusters. *Astrophysical Journal Supplement Series*, 116:1–28, 1998.

[129] B. Panter, A. F. Heavens, and R. Jimenez. Star formation and metallicity history of the SDSS galaxy survey: unlocking the fossil record. *Monthly Notice of the Royal Astronomical Society*, 343:1145–1154, August 2003.

[130] R. Cid Fernandes, A. Mateus, L. Sodré, G. Stasińska, and J. M. Gomes. Semi-empirical analysis of Sloan Digital Sky Survey galaxies - I. Spectral synthesis method. *Monthly Notices of the Royal Astronomical Society*, 358:363–378, April 2005.

[131] P. Ocvirk, C. Pichon, A. Lançon, and E. Thiébaut. STECMAP: STEllar Content from high-resolution galactic spectra via Maximum A Posteriori. *Monthly Notice of the Royal Astronomical Society*, 365:46–73, January 2006.

[132] P. Ocvirk, C. Pichon, A. Lançon, and E. Thiébaut. STECKMAP: STEllar Content and Kinematics from high resolution galactic spectra via Maximum A Posteriori. *Monthly Notice of the Royal Astronomical Society*, 365:74–84, January 2006.

[133] M. Koleva, P. Prugniel, P. Ocvirk, D. Le Borgne, and C. Soubiran. Spectroscopic ages and metallicities of stellar populations: validation of full spectrum fitting. *Monthly Notice of the Royal Astronomical Society*, 385:1998–2010, April 2008.

[134] R. R. de Carvalho and R. Coziol. HCG 16 Revisited: Clues about Galaxy Evolution in Groups. *Astronomical Journal*, 117:1657–1667, April 1999.

[135] I. Plauchu-Frayn, A. Del Olmo, R. Coziol, and J. P. Torres-Papaqui. The star formation histories of Hickson compact group galaxies. *Astronomy and Astrophysics*, 546:A48, October 2012.

[136] I. Ferreras, A. Pasquali, R. R. de Carvalho, I. G. de la Rosa, and O. Lahav. A principal component analysis approach to the star formation history of elliptical galaxies in compact groups. *Monthly Notice of the Royal Astronomical Society*, 370:828–836, August 2006.

[137] V. Coenda, H. Muriel, and H. J. Martínez. Comparing galaxy populations in compact and loose groups of galaxies. III. Effects of environment on star formation. *Astronomy and Astrophysics*, 573:A96, January 2015.

[138] A. Vazdekis, E. Casuso, R. F. Peletier, and J. E. Beckman. A New Chemo-evolutionary Population Synthesis Model for Early-Type Galaxies. I. Theoretical Basis. *Astrophysical Journal Supplemental*, 106:307, October 1996.

[139] C. Conroy. Modeling the Panchromatic Spectral Energy Distributions of Galaxies. *Annual Review of Astronomy and Astrophysics*, 51:393–455, August 2013.

[140] R. Cid Fernandes, R. M. González Delgado, H. Schmitt, T. Storchi-Bergmann, L. P. Martins, E. Pérez, T. Heckman, C. Leitherer, and D. Schaerer. The Stellar Populations of Low-Luminosity Active Galactic Nuclei. I. Ground-based Observations. *Astrophysical Journal*, 605:105–126, April 2004.

[141] L. J. Kewley, B. Groves, G. Kauffmann, and T. Heckman. The host galaxies and classification of active galactic nuclei. *Monthly Notices of the Royal Astronomical Society*, 372:961–976, November 2006.

[142] J. A. Baldwin, M. M. Phillips, and R. Terlevich. Classification parameters for the emission-line spectra of extragalactic objects. *Publications Astronomical Society of the Pacific*, 93:5–19, February 1981.

[143] D. E. Osterbrock and R. W. Pogge. The spectra of narrow-line Seyfert 1 galaxies. *Astrophysical Journal*, 297:166–176, October 1985.

[144] S. Veilleux and D. E. Osterbrock. Spectral classification of emission-line galaxies. *Astrophysical Journal Supplement Series*, 63:295–310, February 1987.

[145] L. J. Kewley, M. A. Dopita, R. S. Sutherland, C. A. Heisler, and J. Trevena. Theoretical Modeling of Starburst Galaxies. *The Astrophysical Journal*, 556:121–140, July 2001.

[146] D. E. Osterbrock and G. J. Ferland. *Astrophysics of gaseous nebulae and active galactic nuclei*. 2006.

[147] A. L. B. Ribeiro, R. R. de Carvalho, R. Coziol, H. V. Capelato, and S. E. Zepf. HCG 16: A High Concentration of Active Galaxies in the Nearby Universe. *Astrophysical Journal Letters*, 463:L5, May 1996.

[148] V. C. Rubin, D. A. Hunter, and W. K. Ford, Jr. One galaxy from several - The Hickson compact group H31. *Astrophysical Journal*, 365:86–92, December 1990.

[149] C. Xu, J. W. Sulentic, and R. Tuffs. Starburst in the Intragroup Medium of Stephan's Quintet. *Astrophysical Journal*, 512:178–183, February 1999.

[150] L. Cortese, G. Gavazzi, A. Boselli, P. Franzetti, R. C. Kennicutt, K. O'Neil, and S. Sakai. Witnessing galaxy preprocessing in the local Universe: the case of a star-bursting group falling into Abell 1367. *Astronomy and Astrophysics*, 453:847–861, July 2006.

[151] A. Ginsburg and J. Mirocha. PySpecKit: Python Spectroscopic Toolkit. Astrophysics Source Code Library, September 2011.

[152] W. A. Baum. Photosensitive Detectors. *Annual Review of Astronomy and Astrophysics*, 2:165, 1964.

[153] S. C. Barden, J. A. Arns, W. S. Colburn, and J. B. Williams. Volume-Phase Holographic Gratings and the Efficiency of Three Simple Volume-Phase Holographic Gratings. *Publications of the Astronomical Society of the Pacific*, 112:809–820, June 2000.

[154] P. G. van Dokkum. Cosmic-Ray Rejection by Laplacian Edge Detection. *The Publications of the Astronomical Society of the Pacific*, 113:1420–1427, November 2001.

[155] V. E. Karachentseva. Catalogue of isolated galaxies. *Soobshcheniya Spetsial'noj Astrofizicheskoj Observatorii*, 8, 1973.

[156] S. Verley, S. C. Odewahn, L. Verdes-Montenegro, S. Leon, F. Combes, J. Sulentic, G. Bergond, D. Espada, E. García, U. Lisenfeld, and J. Sabater. The AMIGA sample of isolated galaxies. IV. A catalogue of neighbours around isolated galaxies. *Astronomy and Astrophysics*, 470:505–513, August 2007.